

**IMPROVING PLATELET STORAGE BAGS: ANTIFOULING POLYMER COATINGS,
ANTIMICROBIAL PEPTIDES AND SURFACE TOPOGRAPHY**

by

Narges Hadjesfandiari

Pharm.D., Tehran University of Medical Sciences, 2007

A THESIS SUBMITTED IN PARTIAL FULFILLMENT OF
THE REQUIREMENTS FOR THE DEGREE OF

DOCTOR OF PHILOSOPHY

in

THE FACULTY OF GRADUATE AND POSTDOCTORAL STUDIES
(Chemistry)

THE UNIVERSITY OF BRITISH COLUMBIA
(Vancouver)

June 2017

© Narges Hadjesfandiari, 2017

ABSTRACT

This thesis is aimed at developing an antibacterial and biocompatible coating for platelet storage bags. Platelets are blood cells that play an essential role in stopping bleeding. Stored platelets for transfusion have a limited shelf life due to the loss of platelet quality upon storage and the risk of bacterial growth in the storage bags. The hydrophobic surface of plasticized polyvinyl chloride platelet storage bags is conducive to bacterial adhesion, biofilm formation and platelet adhesion.

In Chapter 1 platelet transfusion and the associated challenges as well as biomaterials' surface characteristics and biocompatibility are introduced. In Chapter 2 some hydrophilic polymer brushes are developed on platelet bag surfaces and characterized. Polymer coatings made of poly(*N,N*-dimethylacrylamide) (PDMA) and a copolymer of DMA and *N*-(3-aminopropyl)methacrylamide hydrochloride (APMA) (DMA/APMA: 5/1) could inhibit bacterial adhesion on platelet bag surfaces under growth conditions by 95 % and 70 % respectively. These coated surfaces also showed decreased platelet adhesion.

To add bactericidal activity to the coating, antimicrobial peptides (AMPs) are then conjugated to polymer brushes and characterized in Chapter 3. These coated substrates increased the level of platelet adhesion and activation, however. Tuning the amount of peptide on bag surfaces and reproducing coated surface characteristics (with or without peptides) were both challenging.

Taking another approach in Chapter 4, mussel-inspired chemistry is used to coat platelet bags as well as gold and silicon wafers with the antifouling polymeric system. The optimum polymer coating could resist fibrinogen adsorption, bacterial and platelet adhesion. An AMP-

containing bactericidal coating was also synthesized and coated on silicon wafers using this approach. AMPs were mapped on the modified surfaces and they showed bactericidal activity *in vitro*.

A significance of the applied methods in this thesis is their compatibility with commercial biomaterials containing leachable plasticizers.

The chemical composition and morphology of some platelet bags used in Canada are studied in Chapter 5. Evaluation of bacterial and platelet adhesion on their surfaces suggests fabricating bags with only one textured surface inside and positioning it above a non-textured surface. Potential commercial application of the coatings developed here has been a perspective of this project.

LAY SUMMARY

Platelets are a cellular component of whole blood that play an essential role in blood clotting. The introduction of platelet storage and transfusion has had a significant impact on the treatment and prevention of bleeding in patients. Currently, the storage of platelets is limited to 4 to 7 days due to platelet quality loss and the risk of microbial growth in the bags. This thesis focuses on the interaction of bag material with platelets and bacteria. Studies on the topography of the platelet bag surfaces demonstrated that smoothing the material is one approach to reducing bacterial and platelet adhesion on the bag surfaces.

More generally, using two different approaches, a biocompatible polymer coating was developed for the bag material that reduced the adhesion of bacteria and platelets on the bag surfaces. Some nature-inspired antimicrobial agents, antimicrobial peptides, were also conjugated to the polymer coating in order to kill bacteria.

PREFACE

This thesis was conducted under the supervision of Professor Donald E. Brooks at the UBC Centre for Blood Research, Vancouver.

Ethics approval was received for studies conducted with platelets: UBC Ethics approval number H07-02067.

The clinically isolated *S. epidermidis* strains were provided by Dr. Sandra Ramirez, Canadian Blood services, Ottawa, Canada.

For all the data in this thesis including the synthesis of small organic molecules, their purification, surface modifications of substrates, their characterization, platelet and bacterial adhesion tests and their imaging, and identification of blood bags components and surface morphology, Narges Hadjesfandiari was responsible except:

Figure 5.13: Evaluation of platelet quality during 7 days of storage was performed by the Devine lab, Dr. Peter Schubert, Dr. Zhongming Chen, and Brankica Culibrk.

Figure 2.20 and 2.21: The program to convert the AFM raw data (collected by NH) to force versus tip-sample separation was written by Dr. Johan Janzen. X-ray photoelectron spectroscopy, time of flight second ion mass spectroscopy and gel permeation chromatography data were collected by Dr. Ken Wong, Dr. Tae Kyong John Kim, and Ms. Irina Chafeeva, respectively. NH did the analyses of these data.

Part of the Chapter 2 introduction was published in a book chapter. NH was responsible for the literature review and writing all parts used in this thesis:

Hadjesfandiari, N.; Bajgai, M. P.; Yu, K.; Brooks, D. E.; Kizhakkedathu, J. N. Polymer Brushes: General Characteristics, Synthesis and Biomedical Applications. *Encyclopedia of Polymer Science and Technology*, Rigoberto C. Advincula, John Wiley and Sons, 12 JUL 2013. Reproduced by permission of John Wiley & Sons, Inc.

Part of the Chapter 3 introduction was published in a review paper. NH was responsible for the literature review and writing all parts used in this thesis:

Hadjesfandiari, N.; Yu, K.; Mei, Y.; Kizhakkedathu, J. N. Polymer brush-based approaches for the development of infection-resistant surfaces. *J. Mater. Chem. B*, 2014, 2, 4968-4978. Reproduced by permission of the Royal Society of Chemistry.

Chapter 4 has been submitted. NH was responsible for the design of the polymeric systems, their synthesis and optimization, surfaces modification, *in vitro* evaluation of fibrinogen adsorption, bacterial and platelet adhesion, and writing the manuscript. Part of this work involving quartz crystal microbalance measurements was performed in Professor Haag's and Dr. Weinhart's labs, Freie Universität Berlin, by NH.

Hadjesfandiari, N.; Weinhart, M.; Kizhakkedathu, J. N.; Haag, R.; Brooks, D. E. Development of an antifouling and bactericidal coating for platelet storage bags using mussel-inspired chemistry.

Part of Chapter 5 was published in a research paper. NH was responsible for the design of experiments, surfaces characterization, performing all bacterial tests and writing the manuscript. Professor Devine's lab, Dr. Peter Schubert, Dr. Zhongming Chen, and Brankica Culibrk, performed evaluation of platelet quality during a 7-day storage. Mrs. Salma Fallah Toosi helped with the optical profilometry data collection.

Hadjesfandiari, N.; Schubert, P.; Toosi, S.; Chen, Z.; Culibrk, B.; Ramirez-Arcos, S.; Devine, D. V.; Brooks, D. E. Effect of texture of platelet bags on bacterial and platelet adhesion. *Transfusion*, 2016, 56, 2808-2818. Reproduced by permission of John Wiley & Sons, Inc.

TABLE OF CONTENTS

ABSTRACT	ii
LAY SUMMARY	iv
PREFACE	v
TABLE OF CONTENTS	vii
LIST OF TABLES	xii
LIST OF FIGURES	xiii
LIST OF SYMBOLS AND ABBREVIATIONS	xix
ACKNOWLEDGEMENTS	xxiii
CHAPTER 1: Introduction	1
1.1 Platelet Transfusion	1
1.1.1 Platelets	1
1.1.2 Indications for platelet transfusion	3
1.1.3 Challenges associated with platelet transfusion	3
1.1.3.1 Preventive measures to decrease the risk of transfusing contaminated platelets ..	5
1.1.3.2 <i>Staphylococcus epidermidis</i>	7
1.2 Platelet Storage Bag Material	8
1.2.1 Requirements for platelet storage bag material	8
1.2.1.1 Plasticizer and its safety	9
1.2.1.2 Biocompatibility	12
1.3 General Material Surface Characteristics and Biocompatibility	15
1.3.1 Chemical properties	15
1.3.2 Morphology	18
1.4 Goal of the Project	19
1.5 Outline of Thesis	19
CHAPTER 2: Development of Antifouling Polymer Brushes for Platelet Storage Bags	22
2.1 Introduction	22
2.1.1 General characteristics of polymer brushes	22
2.1.2 Synthesis of polymer brushes	24

2.1.2.1 Physical adsorption	24
2.1.2.2 Covalent grafting or chemical bonding	26
2.1.3 Antifouling polymer brushes	29
2.1.4 Antifouling coatings reported for the medical grade PVC	34
2.1.5 Development of polymer brushes on platelet storage bags	36
2.2 Results and Discussion: Synthesis and Characterization of Hydrophilic Polymer Brushes on pPVC	37
2.2.1 The pPVC substrate	38
2.2.2 Amination of pPVC: synthesis and characterization	41
2.2.3 Immobilization of initiators on surfaces and their characterization	44
2.2.4 Surface-initiated ATRP	47
2.2.5 Characterization of polymer brush-grafted surfaces	51
2.2.5.1 Molecular weight of the polymer brushes	63
2.2.5.2 Graft density and thickness of the polymer brushes	67
2.3 Results and Discussion: <i>In Vitro</i> Evaluation of the Modified pPVC Samples	72
2.3.1 Bacterial adhesion	72
2.3.2 Platelet adhesion	75
2.4 Conclusions	77
2.5 Methods and Materials	78
2.5.1 Development of polymer brushes on platelet storage bags	80
2.5.1.1 Amination of substrates	80
2.5.1.2 Synthesis of initiators	82
2.5.1.3 Immobilization of initiators	84
2.5.1.4 Surface-initiated ATRP	84
2.5.1.5 Cleavage of polymer brushes	87
2.5.2 <i>In vitro</i> evaluation of the modified surfaces	87
2.5.2.1 Bacterial adhesion	87
2.5.2.2 Platelet adhesion	89
CHAPTER 3: Development of Bactericidal Polymer Brushes for Platelet Storage Bags	90
3.1 Introduction	90

3.1.1 Antimicrobial peptides	90
3.1.2 Different classes of immobilized bactericidal agents on surfaces	92
3.1.3 Polymer brushes incorporating AMPs	94
3.1.4 AMPs in platelet storage bags	100
3.2 Results and Discussion: Synthesis and Characterization of AMP-Containing Polymer Brushes on pPVC	101
3.2.1 Synthesis of AMP-containing polymer brushes on pPVC	101
3.2.2 Characterization of AMP on surfaces	102
3.2.2.1 Determination of surface concentration of antimicrobial peptides on pPVC by fluorometry	102
3.3 Results and Discussion: <i>In Vitro</i> Evaluation of the Modified pPVC Samples	110
3.4 Conclusions	112
3.5 Methods and Materials	113
3.5.1 Synthesis of AMP-containing polymer brushes on pPVC	113
3.5.2 Synthesis of AMP-containing polymer brushes on silicon wafers	114
3.5.3 Determination of surface concentration of AMPs on pPVC by fluorometry	114
3.5.3.1 Preparation of calibration curves	114
3.5.3.2 Reaction of PAQ with pPVC-DA51-AMP	115
3.5.4 <i>In vitro</i> evaluation of the modified surfaces	116
CHAPTER 4: Development of Antifouling and Bactericidal Coatings for Platelet Storage Bags Using Mussel-Inspired Chemistry	117
4.1 Introduction	117
4.1.1 Marine mussel adhesion	118
4.1.2 Mussel-inspired building blocks	121
4.2 Results and Discussion: Antifouling Coatings	122
4.2.1 Synthesis of DA51 and DA51-cat	122
4.2.2 Coating of DA51-cat	125
4.2.3 Fibrinogen adsorption	130
4.2.4 Bacterial resistance	132
4.2.5 Biocompatibility with platelets	136

4.3 Results and Discussion: Bactericidal Coating	139
4.3.1 DA51-E6-cat: synthesis, coating, and characterization	139
4.3.2 DA51-E6-cat: bactericidal activity	148
4.4 Conclusion	151
4.5 Methods and Materials	152
4.5.1 Development of antifouling coating on platelet bag surfaces	153
4.5.1.1 Synthesis of the hydrophilic polymer system (DA51)	153
4.5.1.2 Functionalization of the polymers with catecholic groups (DA51-cat)	153
4.5.1.3 Coating of the mussel-inspired polymeric system on substrates	154
4.5.1.4 Characterization	154
4.5.2 <i>In vitro</i> evaluation of the modified surfaces	155
4.5.2.1 Fibrinogen adsorption on the samples	155
4.5.2.2 Evaluation of bacterial adhesion	155
4.5.2.3 Evaluation of platelet adhesion	157
4.5.3 Development of bactericidal coating	158
4.5.3.1 Synthesis and coating of the bactericidal polymers (DA51-E6-cat)	158
4.5.3.2. Imaging of live/dead bacteria on the surfaces	159
CHAPTER 5: Effect of Texture of Platelet Bags on Bacterial and Platelet Adhesion	161
5.1 Introduction	161
5.2 Results and Discussion	162
5.2.1 Topography of platelet bag surfaces	162
5.2.2 Chemical composition of platelet bags	166
5.2.3 Bacterial adhesion	171
5.2.4 Platelet adhesion and quality	177
5.3 Conclusions	183
5.4 Methods and Materials	183
5.4.1 Topography of platelet bag surfaces	183
5.4.2 Bacterial adhesion	184
5.4.3 Platelet quality	185
5.4.3.1 Platelet concentrate preparation	185

5.4.3.2 Platelet quality in the A15 bags under blood bank storage conditions	186
5.4.4 Platelet adhesion	186
CHAPTER 6: Conclusions and Future Work	188
6.1 Conclusions and Summary	188
6.2 Future Work	191
REFERENCES	193
APPENDICES	214
Appendix A CHAPTER 2 Additional Data	214
Appendix B CHAPTER 3 Additional Data	217
Appendix C CHAPTER 4 Additional Data	218
Appendix D CHAPTER 5 Additional Data	221

LIST OF TABLES

Table 1.1 Outline of thesis chapters	20
Table 2.1 Surface characterization of the pPVC and the silicon wafer surfaces treated with allylamine	42
Table 2.2 Characteristics of the polymers formed in solution during surface-initiated polymerization	49
Table 2.3 Comparison of the incorporation ratio of the monomers in the DA copolymers with the feeding ratio	51
Table 2.4 Comparison of the incorporation ratio of the monomers in the MA copolymers with the feeding ratio	52
Table 2.5 Control experiments for studying polymer brush synthesis on pPVC surfaces	57
Table 2.6 Comparison of the molecular weight and polydispersity of the grafted polymer versus the polymer formed in solution.	66
Table 2.7 Polymerization conditions for different samples.....	86
Table 3.1 Three cationic AMPs and their amino acid sequence.	101
Table 4.1 The structures of amino acids present in E6.....	141
Table 5.1 Some physicochemical characteristics of the platelet storage bags studied in Chapter 5.	163

LIST OF FIGURES

Figure 1.1 Platelets morphology.....	1
Figure 1.2 Platelet's role in coagulation.....	2
Figure 1.3 Storage of platelet bags in blood banks.....	4
Figure 1.4 BacT/ALERT 3D culture system.....	7
Figure 1.5 Structures of common plasticizers in blood bags.....	10
Figure 2.1 Polymer chains tethered to a surface.....	23
Figure 2.2 Different approaches to prepare polymer brushes.....	25
Figure 2.3 Polymer brushes grown from a substrate by ATRP.....	28
Figure 2.4 Chemical structures of different hydrophilic neutral (A) and zwitterionic (B) polymers with antifouling properties.....	31
Figure 2.5 The general scheme of grafting polymer brushes from pPVC.....	38
Figure 2.6 ¹ H NMR spectra of pPVC in d8-THF (A) and the hexane extract of pPVC in CDCl ₃ (B).....	39
Figure 2.7 Dechlorination of PVC as a result of heating.....	40
Figure 2.8 Positive ion TOF-SIMS spectrum of pPVC.....	41
Figure 2.9 Amination of silicon wafer surfaces using a wet chemical method.....	43
Figure 2.10 A proposed scheme for plasma polymerization of allylamine.....	44
Figure 2.11 The synthesized initiators for SI-ATRP on pPVC surfaces.....	45
Figure 2.12 The synthetic scheme for the SI-ATRP initiators.....	45
Figure 2.13 ¹ H NMR spectra of the synthesized SI-ATRP initiators: NCI (A), CI (B) and EG-CI (C).....	46
Figure 2.14 ¹ H NMR spectrum of DA51 in D ₂ O.....	50
Figure 2.15 Static water contact angle on the control and modified pPVC surfaces.....	52
Figure 2.16 ATR-FTIR spectra of the control pPVC and the pPVC modified with PDMA polymer brushes.....	53
Figure 2.17 ATR-FTIR spectra of the pPVC samples modified with DA (poly(DMA/APMA)) copolymers (A) and MA (poly(MPDSA/HPMA)) copolymers (B).....	55
Figure 2.18 An AFM tip on the end of a cantilever deflects when the tip encounters features of the surface.....	60

Figure 2.19 AFM force curve when a silicon nitride tip interacted with pPVC surface in 0.5 M NaCl solution.....	61
Figure 2.20 Approach and retraction force curves for the pPVC surfaces modified with PDMA (A) and PMPDSAH (B and C).	62
Figure 2.21 Approach and retraction force curves for the pPVC surfaces modified with DA51. 63	
Figure 2.22 ATR-FTIR spectra of the pPVC-DA51 samples before (blue) and after (red) hydrolysis.....	64
Figure 2.23 ¹ H NMR spectrum of the “cleaved” mixture from pPVC-DA51 in D ₂ O	65
Figure 2.24 GPC-MALLS/RI profiles of the cleaved DA51 from pPVC.....	66
Figure 2.25 AFM force profile of the pPVC surfaces modified with PDMA	70
Figure 2.26 Adhesion of <i>S. aureus</i> on the samples after 4 h (A) and 8 h (B and C) incubation at 37 °C.....	73
Figure 2.27 Level of <i>S. aureus</i> adhesion on pPVC surfaces modified with DA51 and PDMA in comparison with the control pPVC.	74
Figure 2.28 pPVC has one textured face (A) and one non-textured face (B).....	74
Figure 2.29 Platelet adhesion on pPVC (i), pPVC-PDMA (ii) and pPVC-DA51 (iii) after 4 h incubation at 37 °C.	75
Figure 2.30 Platelet adhesion on pPVC (i) and pPVC-PDMA (ii) after 7 days of storage under blood bank conditions.....	77
Figure 2.31 Opening the platelet storage bag (A) and exposing it to allylamine plasma (B).	81
Figure 3.1 After the adsorption of AMPs on a bacterial cytoplasmic membrane, one or multiple events can lead to membrane disruption and bacterial death.	91
Figure 3.2 Cationic AMPs show higher affinity to bacterial membrane versus mammalian membranes.....	92
Figure 3.3 AMPs covalently conjugated to polymer brushes have enough freedom for interaction with the bacteria.....	95
Figure 3.4 Some reported strategies for conjugating antimicrobial peptides to substrates via polymer brushes.....	98
Figure 3.5 The chemical structures of two water-soluble crosslinkers: sulfo-SMCC and sulfo-SIAB.	101

Figure 3.6 The general scheme of conjugating AMPs to polymer brushes through the sulfo-SMCC linker.....	102
Figure 3.7 PAQ reacts with arginine under basic conditions. The product hydrolyzes to a fluorescent compound under acidic conditions.	103
Figure 3.8 The amount of immobilized AMPs on the pPVC surfaces can be determined by PAQ fluorometry.	104
Figure 3.9 The fluorescence emission peak at $\lambda_{em} = 392$ nm was used for measuring the amount of peptide at pPVC-DA51-AMP surfaces (Tet-26 here).	105
Figure 3.10 The general scheme of development of DA51-1010cys on silicon wafers.....	106
Figure 3.11 The change in thickness (bars) and static water contact angle (line) after modification of silicon wafer with APTES, DA51, and DA51-AMP (1010cys here).	107
Figure 3.12 Comparison of ATR- FTIR spectra of pPVC-DA51 samples before and after conjugation with AMP in samples with a high surface concentration of AMPs (7-10 $\mu\text{g}/\text{cm}^2$ of Tet-26 here) confirming the presence of the peptide.....	110
Figure 3.13 Platelet adhesion on pPVC (i), pPVC-DA51 (ii) and pPVC-DA51-AMP (iii) after 4 h incubation at 37 °C observed by SEM.	111
Figure 3.14 Level of <i>S. aureus</i> adhesion on pPVC surfaces modified with PDMA, DA51 and DA51-Tet20 in comparison with the control pPVC.....	111
Figure 4.1 <i>Mytilus edulis</i> mussel and its byssus (A). The structural formula of mussel foot protein 1, Mefp1, containing aminoacids lysine (K) and DOPA (Y) (B).	119
Figure 4.2 Catechol oxidative chemistry.....	120
Figure 4.3 Catechol can participate in hydrogen bonding, metal coordination complexes and π - π interactions.....	120
Figure 4.4 Chemical structure of dopamine (A) and a proposed structure of polydopamine (PDA).	121
Figure 4.5 Some recent examples of antifouling coatings with mussel-inspired functionalities	122
Figure 4.6 A) ^1H NMR spectra of DA51 (in D_2O) and DA51-cat (in d_4 -methanol). B) DA51-cat can coat silicon and gold substrates successfully under basic and oxidative conditions. For pPVC, a two-layer coating consisting of PDA and DA51-cat was required to introduce antifouling properties.....	123

Figure 4.7 A) Static water contact angle on the bare and coated substrates. B) Thickness of PDA, DA51-cat and PDA-DA51-cat coatings on silicon and gold surfaces.....	126
Figure 4.8 Both textured (A) and non-textured (B) surfaces of the pPVC substrate used in this chapter have a large scale of roughness.....	127
Figure 4.9 PDA aggregates were sporadically observed on pPVC surfaces (A). Shaking the samples during coating increased the amount of aggregates (B).	128
Figure 4.10 DA51-cat (black trace) could deposit on pPVC-coated sensors (~1300 ng/cm ²) within 1 h of flow under basic conditions (MOPS buffer, pH 8.5) while DA51 (red trace) did not show any interaction with the surfaces.....	129
Figure 4.11 Static water contact angles on the bare and coated substrates	130
Figure 4.12 QCM traces (the third overtones) showing the shift in frequency (Δf) of the quartz crystal versus time in response to fibrinogen adsorption on untreated or treated pPVC-coated sensors	131
Figure 4.13 Fluorescent 3D confocal images (left-hand panels) and SEM images of control pPVC (A) and pPVC-PDA-DA51-cat (B) after 32-h incubation with SE11002, a biofilm-positive <i>S. epidermidis</i> strain, at 37 °C showed less bacterial adhesion and biofilm formation on the modified samples.....	134
Figure 4.14 A) A cluster of SE10002, a biofilm-positive <i>S. epidermidis</i> strain, on the untreated pPVC samples with appearance of extracellular matrix (marked with arrows). B) Number of the released bacteria from pPVC coupons (CFUs/cm ²) after 4-h incubation with SE11003, a biofilm-negative <i>S. epidermidis</i> strain.....	135
Figure 4.15 Fluorescent images (A) and SEM images (B) of the surfaces of the minibags made of pPVC (i and ii) and pPVC-PDA-DA51-cat (iii) after incubation with platelet-rich plasma for 1 day at 22 °C.	137
Figure 4.16 A) The scheme of conjugation of DA51-cat to an amine-to-sulfhydryl crosslinker, BMPS. B) ¹ H NMR spectrum of DA51-L-cat in d4-methanol	140
Figure 4.17 A) The scheme of conjugation of DA51-L-cat to a cysteine-containing AMP, E6. B) ¹ H NMR spectrum of DA51-E6-cat in d4-methanol.....	141
Figure 4.18 The negative ion TOF-SIMS spectra of the silicon wafer samples coated with PDA-DA51-E6-cat (A) and PDA-DA51-cat (B). The theoretical positions of two most abundant sulfur isotopes (³² S and ³⁴ S) are marked with turquoise lines by the software.....	143

Figure 4.19 TOF-SIMS ion maps of ^{32}S on silicon wafers coated with PDA-DA51-E6-cat (Ai) and PDA-DA51- cat (Bi).....	144
Figure 4.20 The positive ion TOF-SIMS spectra of the silicon wafer samples coated with PDA-DA51-E6-cat (A) and PDA-DA51-cat (B). The characteristic peak of arginine at 43.0290 was detected in the PDA-DA51-E6-cat samples	145
Figure 4.21 The positive ion TOF-SIMS spectra of the silicon wafer samples coated with PDA-DA51-E6-cat (A) and PDA-DA51-cat (B). The characteristic peaks of arginine at 73.0624 and 127.0985 were detected in the PDA-DA51-E6-cat samples.	146
Figure 4.22 The positive ion TOF-SIMS spectra of the silicon wafer samples coated with PDA-DA51-E6-cat (A) and PDA-DA51-cat (B). The characteristic peak of isoleucine at 86.0965 was detected in the PDA-DA51-E6-cat samples	147
Figure 4.23 Fluorescent images of the untreated silicon wafer (i), silicon wafer coated with PDA-DA51-cat (ii) and silicon wafer coated with PDA-DA51-E6-cat (iii) with green filter (A) and red filter (B)	150
Figure 5.1 A15 bag has one textured (<i>rough</i>) face (A) and one <i>smooth</i> face (B) while both inside faces of P15 (C) and F1 (D) are <i>rough</i>	163
Figure 5.2 Optical profilometry of A15-rough (A), P15 (B) and F1 (C) showed a micrometer-scale of roughness of these surfaces.....	164
Figure 5.3 For comparison, the same surface areas ($111 \times 148 \mu\text{m}$) of central part of the diamond in A15-rough (Ai) and A15-smooth (Bi) were studied by optical profilometer	165
Figure 5.4 Surface topography of $10 \times 10 \mu\text{m}$ (A) and $40 \times 40 \mu\text{m}$ (B) of A15-smooth obtained by atomic force microscopy	166
Figure 5.5 ^1H NMR (A) and ^{13}C NMR (B) spectra of the hexane extract of P15	167
Figure 5.6 ^1H NMR spectrum of P15 in d8-THF	168
Figure 5.7 ATR-FTIR spectra of F1 (A) and P15 (B).....	169
Figure 5.8 ^1H NMR spectrum of F1	170
Figure 5.9 Fluorescent 3D confocal images of A15-rough (Ai), P15 (Aii) and F1 (Aiii), and fluorescent images of A15-rough (Bi) and A15-smooth (Bii) after 24-h incubation with SE10002	172

Figure 5.10 SEM images of A15-rough (i) and A15-smooth (ii) after 24-h incubation with biofilm-negative SE11003 (A) and biofilm-positive SE10002 (B) revealed less bacterial adhesion and biofilm formation on A15-smooth..... 173

Figure 5.11 Number of the released bacteria from platelet bag cuts (CFU number/cm²)..... 174

Figure 5.12 SEM images of A15-rough (A), A15-smooth (B), P15 (C) and F1 (D) after 7 days of incubation with pooled platelets under blood bank storage conditions revealed less platelet adhesion on A15-smooth compared to all the *rough* surfaces..... 178

Figure 5.13 Evaluation of platelet quality after 2, 5, and 7 days of storage in the A15 bags under blood bank storage conditions 179

Figure 5.14 SEM imaging (A) and optical profilometry (B) of the pouch bag of P15 revealed roughness of the surfaces of this bag to be in micrometer scale 182

LIST OF SYMBOLS AND ABBREVIATIONS

δ	Bending vibration in IR spectroscopy
Δf	Shift in the frequency of quartz crystal
Δm	Change in mass
ν	Stretching vibration in IR spectroscopy
ρ	density
σ	Graft density of polymer chains
A	Surface area
A15	Terumo 80440 platelet storage bag
ADP	Adenosine diphosphate
AFM	Atomic force microscopy
AMP	Antimicrobial peptide
APMA	<i>N</i> -(3-Aminopropyl)methacrylamide hydrochloride
APTES	(3-Aminopropyl)triethoxysilane
ATR-FTIR	Attenuated total reflectance Fourier transform infrared
ATRP	Atom transfer radical polymerization
AVG	Average
BHT	Butylated hydroxyl toluene
BMPS	<i>N</i> -(β -Maleimidopropoxy)succinimide ester
BTHC	Butyryl trihexyl citrate
CFU	Colony forming unit
CI	Cleavable initiator
CLRP	Controlled/living radical polymerization
CP-MAS	Cross polarization-magic-angle spinning
CuAAC	Cu(I)-catalyzed azide-alkyne cycloaddition
D	Distance between the grafting points
DA51	Poly(DMA/APMA) (5/1)
DA51-cat	DA51 modified with some catechol groups
DA51-L-cat	DA51-cat modified with some linkers
DA51-E6-cat	DA51-cat modified with some E6

DCM	Dichloromethane
DEHP	Di-2-ethylhexyl phthalate
DHHA	3,4-Dihydroxyhydrocinnamic acid
DMA	<i>N,N</i> -Dimethylacrylamide
DMF	<i>N,N</i> -Dimethylformamide
DMSO	Dimethyl sulfoxide
DOPA	3,4-Dihydroxyphenyl-L-alanine
EDC	1-Ethyl-3-(3-dimethylaminopropyl)carbodiimide hydrochloride
EG-CI	Ethylene glycol cleavable initiator
F1	Fenwal PL2410 platelet storage bag
FDA	Food and Drug Administration
GPC	Gel permeation chromatography
HMTETA	1,1,4,7,10,10-Hexamethyltriethylenetetramine
l	Monomer unit length
L_c	Contour length
L_e	Equilibrium thickness
LB	Luria broth
M_n	Number average molecular weight
M_w	Weight average molecular weight
MA51	Poly(MPDSAH/APMA) (5/1)
MALLS	Multi angle laser light scattering
MDR	Multi drug resistant
Mefp	<i>Mytilus edulis</i> foot protein
MES	2-(<i>N</i> -Morpholino)ethanesulfonic acid
MOPS	3-(<i>N</i> -Morpholino)propanesulfonic acid
MPDSAH	3-(Methacryloylamino)propyl)-dimethyl(3-sulfopropyl)ammonium hydroxide
mPEG	Monomethoxy-terminated PEG
MWCO	Molecular weight cut-off
N	Degree of polymerization
N_A	Avogadro's number
NCI	Non-cleavable initiator

NetCad	Canadian Blood Services Network Centre for Applied Development
NMP	Nitroxide-mediated polymerization
NMR	Nuclear magnetic resonance
OEG	Oligoethylene glycol
P15	MacoPharma TDV8006XU platelet storage bag
PAAm	Polyacrylamide
PAGE	Poly(allyl glycidyl ether)
PAQ	9,10-Phenanthrenequinone
PBS	Phosphate-buffered saline
PCBMA	Poly(carboxybetaine methacrylate)
PDA	Polydopamine
PDMS	Poly(dimethylsiloxane)
PEG	Polyethylene glycol
PEO	Polyethylene oxide
PF4	Platelet factor 4
PI	Propidium iodide
PMOXA	Poly(2-methyl-2-oxazoline)
PMP	Platelet microbicidal protein
PMPC	Poly(2-methacryloyloxyethyl phosphorylcholine)
pPVC	Plasticized PVC
PSBMA	Poly(<i>N</i> -(3-sulfopropyl)- <i>N</i> -(methacryloxyethyl)- <i>N,N</i> -dimethyl ammonium betaine)
PSL	Platelet storage lesion
PVC	Polyvinyl chloride
QA	Quaternary ammonium
QCM	Quartz crystal microbalance
QCM-D	QCM with dissipation monitoring
R _a	Average roughness
R _g	Radius of gyration
R _{max}	The largest peak-to-valley height
RAFT	Reversible addition-fragmentation chain transfer

RBC	Red blood cells
RI	Refractive index
SD	Standard deviation
SEM	Scanning electron microscopy
SI-ATRP	Surface-initiated atom transfer radical polymerization
Sulfo-SIAB	Sulfosuccinimidyl (4-iodoacetyl)aminobenzoate
Sulfo-SMCC	Sulfosuccinimidyl 4-(<i>N</i> -maleimidomethyl)cyclohexane-1-carboxylate
T _g	Glass transition temperature
TCEP	Tris(2-carboxyethyl)phosphine
TEHTM	Tri(2-ethylhexyl)trimellitate
THF	Tetrahydrofuran
TOF-SIMS	Time of flight second ion mass spectroscopy
TSB	Tryptic soy broth
TSBG	TSB enriched with glucose
uPVC	Unplasticized PVC
UV	Ultraviolet
v/v	Volume/ volume
W	Weight
w/v	Weight/volume
XPS	X-ray photoelectron spectroscopy

ACKNOWLEDGEMENTS

First, I would like to thank my supervisor, Professor Donald Brooks. He gave me significant freedom and encouraged me to explore and learn different methods and instruments. Don was patient with my investigations and even in his busiest days he always made time for a meeting; I am wholeheartedly grateful to him for all the support and I appreciate the opportunity of working in his lab. I would like to thank Professors Derek Gates and Hongbin Li for accepting to be in my PhD committee and reading my thesis.

I was fortunate to collaborate with the Devine lab; my special thanks to Professor Dana Devine, Dr. Peter Schubert, Dr. Zhongming Chen, and Mrs. Brankica Culibrk. I am sincerely grateful to Professor Rainer Haag and Dr. Marie Weinhart for the opportunity of working in their laboratories. I enjoyed every minute of my research and stay in Berlin.

I am grateful to all present and previous members of the Brooks and Kizhakkedathu laboratories for their friendship and always being supportive when I had a talk or exam. I would like to especially thank Dr. Johan Janzen and Dr. Rajesh Shenoj who always made time to provide help and guidance. Much appreciation to all knowledgeable staff at UBC who gave me trainings and answered my many questions: Dr. Fred Rossel (Center for Blood Research), Dr. Paul Xia and Dr. Maria Ezhova (Dept. of Chemistry), Drs. John Kim, Philip Wong, and Mario Beaudoin (AMPEL) and Mr. Jacob Kabel (Materials Engineering). I thank UBC Center for Blood Research administrative team, Professor Edward Conway and Mrs. Anna Sinova for providing a dynamic learning environment and for all the great seminars and facilities. Many thanks to Dr. Sandra Ramirez for providing clinically isolated *S. epidermidis* strains.

My sincere thanks to Professor Cedric Carter for all the encouragement and for making PhD challenges fade away by crosswords and his sophisticated English words. I am grateful to all generous blood donors and NetCad who made the studies on platelets possible. I also would like to acknowledge financial support from Canadian Blood Services/Health Canada Graduate Fellowship, Gladys Estella Laird Fellowship and UBC.

Canada: I am indebted to you for giving me the chance to come here and explore new sides of life and research.

Mother, Father, Bahareh, Behnaz and Naeimeh: Your honesty and hard work have always inspired me. Thank you for being my role models.

Babak: This thesis is dedicated to you for your love and the sacrifices you made to be with me here.

CHAPTER 1: Introduction

1.1 Platelet Transfusion

1.1.1 Platelets

Platelets are 2-3 μm non-nucleated disc-shaped cells (**Figure 1.1**) in mammalian blood and their main function is in haemostasis. Haemostasis is the body's physiologic response aimed at stopping bleeding or haemorrhage. Around 2 to 4 $\times 10^8$ / mL of platelets circulate in human blood with a half-life of 8 to 12 days.



Figure 1.1 Platelets morphology. From left to right, scanning electron microscope images (with pseudo colors) of resting platelets, partially activated platelets, and fully activated platelets. Reproduced with permission from *J. Biol. Chem.* 2003, 278 (51), cover page.

A coat of glycoproteins on the platelet membrane prevents their adherence to normal vascular endothelium which lines the blood vessels and yet helps them attach to damaged endothelial cells and exposed collagen. After adhering to a damaged vessel, platelets become activated and undergo some biochemical and physical changes. They release granules containing biologically active compounds such as platelet factor 4 (PF4) and adenosine diphosphate (ADP) that make platelets more sticky to the proteins present on the damaged tissue such as von Willebrand factor, which rapidly binds to exposed collagen in the damaged vessel wall. They

also activate other nearby platelets. P selectin, a glycoprotein that mediates adhesion of platelets to other cells, is also released and expressed on platelet surfaces.¹ (Figure 1.2)

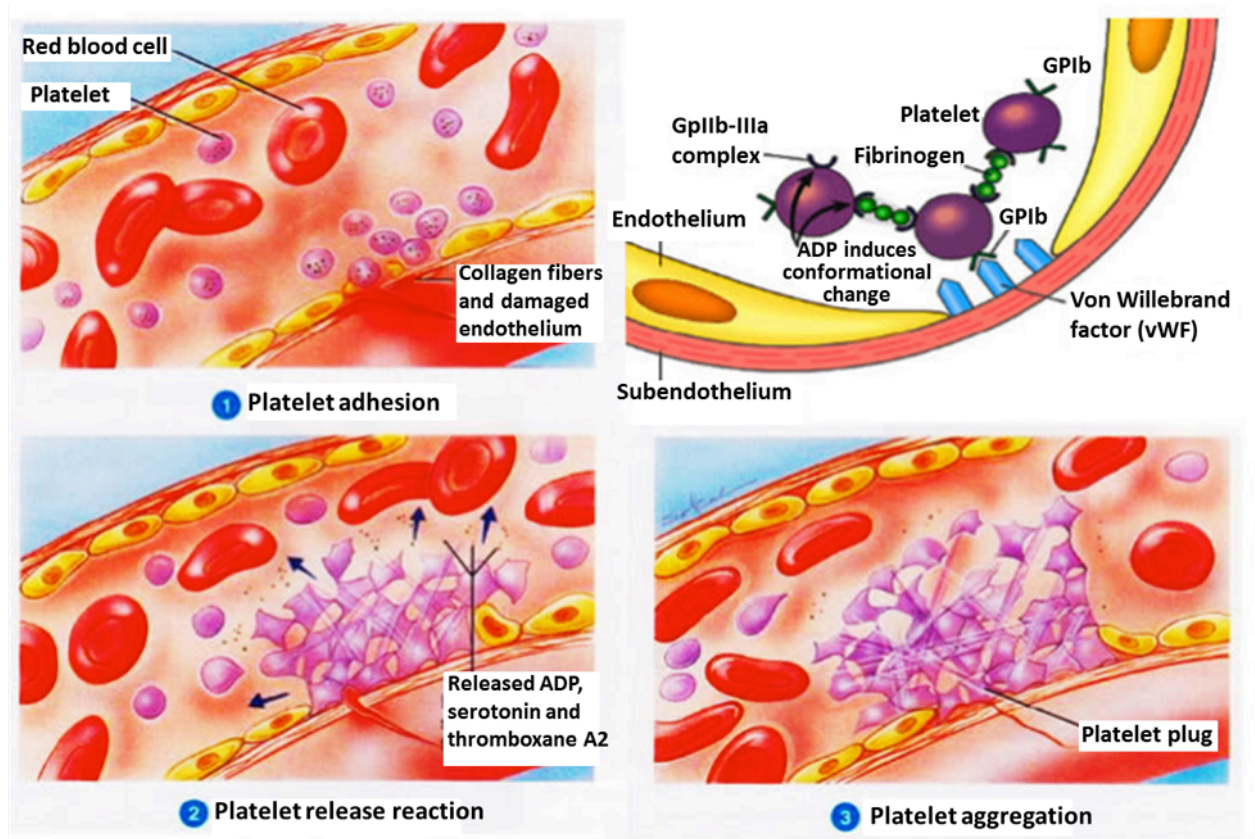


Figure 1.2 Platelet's role in coagulation. Circulating platelets are activated by exposed collagen at sites of vascular injury and also by locally generated thrombin. Platelets adhere to the injured endothelium, spread out, form a monolayer and recruit more platelets by secretion of active molecules such as ADP. As more and more platelets get activated, they aggregate and form a platelet plug at the site of injury. The figure was retrieved with some modifications from the Ternopil State Medical University website, December 2, 2016.

Platelet activation is characterized by a drastic shape change including swelling and developing pseudopods (Figure 1.1). All the biochemical and shape changes lead to aggregation of platelets and formation of a platelet plug on the damaged endothelium. Active molecules released from the platelets further play a role in the formation of the fibrin fibers and consequently of a blood clot, which completes the haemostasis process, particularly essential in big ruptures.¹

1.1.2 Indications for platelet transfusion

Considering the vital role of platelets in haemostasis, platelet transfusion is used to prevent or treat bleeding in patients with thrombocytopenia (not enough platelets) or with platelet function defects. According to the American Red Cross, around 7000 units of platelets are needed daily in the US. Platelet transfusion is required, for example, in the cases of active bleeding, preparation for invasive surgeries, for the support of leukemia patients, and for cancer patients who undergo chemotherapy or radiotherapy.² In all these cases, patients suffer from bleeding or they are at risk of bleeding because of low numbers or dysfunctional platelets.

In Canada, platelet concentrates are prepared by two different methods: the single-donor apheresis method and the buffy coat production method. In apheresis platelets, whole blood is removed from the donor, anticoagulated, and platelets are separated from it by centrifugation. The remaining blood components are then returned to the donor. For buffy coat production, whole blood is removed from a donor, anticoagulated and spun. Red blood cells (RBC) from the bottom and plasma from the top are isolated and used for other purposes. The middle buffy coat part (it contains platelets) is pooled with three other buffy coats from other donors and suspended in an autologous plasma unit. The four buffy coats must have matched blood type.³

1.1.3 Challenges associated with platelet transfusion

Unlike other major blood products, i.e. plasma and RBC, platelets cannot be stored at cold temperatures. Plasma can be frozen and used up to 1 year. RBCs are stored at 4 °C for up to 42 days. Platelets, however, undergo some changes under cold storage, namely, clustering of von Willebrand factor receptors on the platelet surface and morphological changes.⁴ When transfused to the recipient, these platelets are cleared rapidly from the blood circulation by hepatic

macrophages. Platelets form micro aggregates at 4 °C that can block lung capillaries in the recipients and this blocking may be clinically important in massive transfusions.⁴

Because of the above issues, platelets are stored in incubators at 22 °C under continuous side-to-side agitation (**Figure 1.3**). Continuous agitation of platelet bags contributes to a balanced gas and metabolite distribution and preservation of the quality of platelets.



Figure 1.3 Storage of platelet bags in blood banks. Platelet storage bags are stored in platelet incubators at 22 °C on agitators that provide side-to-side motion.

Compared to the cold conditions, room temperature supports the growth of bacteria and makes microbial infection a major complication associated with platelet transfusion.^{5,6} Even a few bacteria that have found their way to the platelet unit can grow to a deadly dose after some time at room temperature. Many platelet recipients (e.g. cancer patients) are immunocompromised and may receive multiple doses of platelet units, both of which can put them at higher risk. Fatalities resulting from the transfusion of contaminated platelets have been reported.⁷⁻⁹ A recent case was detected in Ottawa in 2014 where a splenectomized patient suffering from leukemia passed away as a result of sepsis caused by receiving a tainted platelet

unit.⁸ Sepsis resulting from transfusion of bacterial contaminated platelet is the second most prevalent cause of death from blood transfusion.⁵

Further, platelets undergo some changes *in vitro* during storage known as the platelet storage lesion (PSL).¹⁰ These changes are reflected in some platelet functions such as platelet adhesion, aggregation, platelet-dependent coagulation, and *in vivo* recovery and survival after transfusion. Loss of quality upon storage calls into question the efficacy of transfusion of an older platelet unit. Old platelets with storage-related deterioration will undergo an accelerated clearance from circulation.¹⁰

PSL and the risk of bacterial contamination are the main causes of the limited shelf life of stored platelets, which is 4-7 days in different countries. After this period, the units must be discarded and this is estimated to be 30% of the platelet units in countries with a 5-day storage limit such as Canada.¹⁰

1.1.3.1 Preventive measures to decrease the risk of transfusing contaminated platelets

Over the past decade, preventive interventions in blood collection and processing and application of bacterial screening methods have considerably decreased the risk of bacterial contamination of platelet units and septic transfusion reactions.

Collection: To avoid collecting potentially contaminated blood, donors are screened by questions related to their general health and also for signs of infection. Body temperature is also determined before phlebotomy.

The majority of bacteria isolated from contaminated platelet bags are part of our normal skin flora. Therefore, efficient disinfection at the site of phlebotomy can reduce the risk of introducing these bacteria into the blood unit and its products.¹¹ Further, the first 30-50 mL of

drawn blood is known to contain most of the contaminating bacteria from the external source. Diversion of this portion into a separate pouch decreases the risk of transfusing a contaminated unit.¹¹

Storage: Pathogen reduction technologies have been introduced to blood banks to improve blood safety.¹² Irradiation of collected blood with ultraviolet (UV) light can target the nucleic acids of pathogens and inhibit their proliferation. One such system, Mirasol (Terumo Inc.) has been shown to reduce infectivity of blood products contaminated by various viruses¹³, bacterial strains^{13,14}, and parasites¹⁵ by using UV light in the presence of a photosensitizer, riboflavin. However, this system has its limitations in inactivation of bacterial spores, high titres of bacteria and also endotoxins. Further, treatment of platelets by Mirasol affects the quality of platelets, which leads to reduced platelet survival *in vivo*.¹⁶

Different bacterial screening methods are available for blood products. Canadian Blood Services currently use the BacT/ALERT 3D culture system (bioMérieux Inc.) to screen every platelet unit for any bacterial contamination. This system provides bottles containing aerobic culture medium equipped with colorimetric sensors in the bottom. (Some countries use both aerobic and anaerobic bottles to allow a wider range of screening). A 10 mL sample is taken from the platelet bags 24-48 hours after the donation. The sample is transferred into the medium bottle. The bottles are incubated in the instrument for 6 days after the blood collection time (**Figure 1.4**). As the bacteria (if any) grow in the bottle, the CO₂ level increases and leads to a decrease in the pH. This change in pH results in a color change in the sensor at the bottom of the bottle, which is detected by the instrument and will alert the blood bank for recalling the platelet unit and its discard.¹⁷

The preventive measures during collection and processing as well as screening the platelet units by BacT/ALERT have improved the safety of platelet transfusion dramatically. However, cases of missed detection have still been reported.^{6,18,19} The risk of bacterial contamination of platelet units is estimated to be 1 per every 1000 to 5000 (depending on the method of production) and risk of subsequent septic transfusion reactions is 1 per every 70,000 to 118,000 platelet units in the US.²⁰



Figure 1.4 BacT/ALERT 3D culture system. BacT/ALERT 3D culture system is used in Canada to test a sample of every platelet unit for possible bacterial contamination. The image was retrieved from the bioMérieux webpage, <http://www.biomerieux-usa.com/industry/bact-alert-3d-product-safety?dest=view>, December 3, 2016.

1.1.3.2 *Staphylococcus epidermidis*

Coagulase negative staphylococci and propionibacteria are the predominant bacterial contaminants of platelet units.⁶ Coagulase negative staphylococci were deemed harmless, as they are part of our normal flora on tissues like skin, upper respiratory tract and vagina. However, sepsis resulting from these bacteria, particularly in immunocompromised patients, has become one of the hospital-acquired infectious challenges.²¹

Staphylococcus epidermidis, a normal skin flora microorganism, is the most commonly isolated coagulase negative staphylococci from platelet units. Transfusion of such units has led to fatal cases.^{8,22} *S. epidermidis* forms biofilms in platelet concentrates. It has been observed that *S. epidermidis* strains that did not carry *icaD* genes (genes associated with biofilm formation) and

therefore did not produce slime and did not form biofilms in culture media were nonetheless able to form biofilms in platelet concentrates.²³ Biofilm formation and the slow growth rate of this bacterium can be contributing factors to its missed detection.^{23,24}

S. epidermidis is well known for biofilm formation on surgical implants and interestingly was not considered an opportunistic pathogen until the widespread use of medical devices occurred in recent decades.

1.2 Platelet Storage Bag Material

1.2.1 Requirements for platelet storage bag material

There are different performance requirements for the material used to fabricate platelet storage bags:²⁵

Mechanical strength: Similar to any liquid containers, platelet bags must resist the stresses during handling and transportation and further, centrifugation.

Flexibility: Flexibility of the bags lets them fill and empty completely during blood collection and transfusion without a need to vent the bag.

Clarity: Platelet units are visually inspected before platelet transfusion for any aggregates or discoloration, so the plastic bag must be clear.

Temperature resistance: One of the sterilization methods used for platelet bags is to autoclave. Bags must resist the high temperature (~ 121 °C).

Bag fabrication considerations: Platelet bags are fabricated by welding two sheets of plastic. To weld the plastics using radio frequency welding, the material must have a certain degree of polarity. Platelet transfusion bag sets have different components e.g. satellite bags, tubing and

ports. The plastic material must be easy to work with under different processes (e.g. molding and calendaring) to give the final product.

Gas permeability: The containers should provide an optimum gas permeability to maintain the aerobic metabolism of the platelets. The level of adenosine triphosphate (ATP) generation lowers if there is inadequate oxygen level in the bag. As compensation, glycolysis and therefore lactic acid production increases, which in turn leads to falling pH. Platelets stop glycolysis and oxygen intake at pH around 6, which leads to their activation. The platelets under the low pH release the activation marker α -granular PF4, while platelets under sufficient oxygen do not.²⁶

Platelet bags should also allow most of the generated carbon dioxide to diffuse out of the bag while a partial pressure remains to make a bicarbonate buffer and help maintain the pH.

Safety and biocompatibility: These features of platelet bags that are required generally for any biomaterials will be discussed in the following sections.

1.2.1.1 Plasticizer and its safety

According to US Food and Drug Administration (FDA) regulations on empty containers for the collection and processing of blood and blood components, “the materials used in the construction of the device should not, either directly or indirectly through the release of their material constituents, (1) produce unreasonable risk of adverse local or systemic effects; (2) be carcinogenic; or (3) cause adverse reproductive and developmental effects.”²⁷

Polyvinyl chloride (PVC) is the most widely used material for platelet storage bags. PVC has a glass transition temperature (T_g) of 80 °C and plasticizers are used to make it flexible for different biomedical applications.

Phthalate esters are a large class of plasticizers. Di-2-ethylhexyl phthalate (DEHP) (**Figure**

1.5) has been used in blood storage bags for decades, but its use has been declining since increasing data on its toxicity became available. DEHP and its metabolite mono-2-ethylhexyl phthalate have been associated with reproductive and developmental defects, endocrine disruption, immaturity of the male reproductive tract, and peroxisome proliferation in the liver and thereby an increase in the incidence of liver cancer (liver cancer data only from rodents).²⁸ In 1998, US toy manufacturers voluntarily agreed to stop using phthalates in pacifiers and rattlers. The European Union put a ban on phthalate plasticizers in toys in 2006 as they may leach out when children chew soft toys containing them.²⁹

Blood bags with phthalate-based plasticizers are approved by the FDA. However, the FDA has encouraged use of DEHP-free devices wherever possible, in particular for in-danger groups.³⁰ The Health Canada Expert Advisory Panel suggests that medical DEHP-plasticized devices should not be used for pregnant or lactating women, newborns, pre-pubertal males, double-volume exchange transfusions and for administering lipophilic formulations.³¹

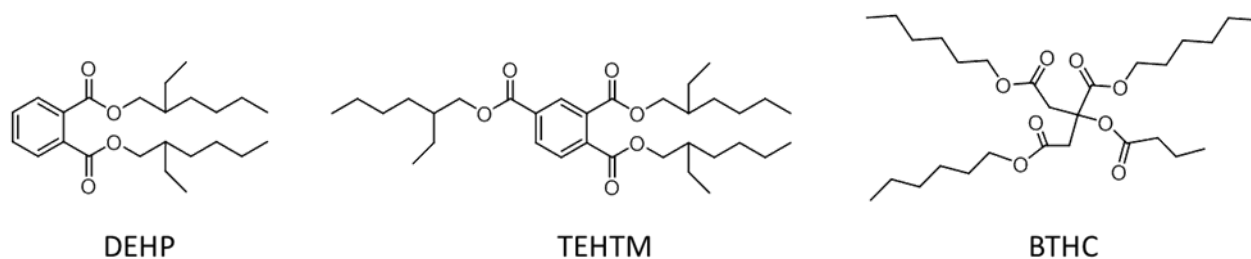


Figure 1.5 Structures of common plasticizers in blood bags.

DEHP can leach out into the contained liquid and the rate of leaching depends on the temperature of the fluid, content of fluids, the amount of fluid in contact with the PVC, storage time and the extent of shaking or flow rate of fluid. In particular, DEHP can leach out into the blood, plasma or a drug solution. However, its dose and the consequent safety concerns are more

critical, as stated above, in the cases involving neonates, pregnant or lactating women. Massive infusion of blood to trauma patients and total parental nutrition where the presence of lipid in the bag enhances the leakage of plasticizer are other cases of concern.

DEHP has been replaced by tri(2-ethylhexyl) trimellitate (TEHTM or TOTM) (**Figure 1.5**) in some PVC formulations such as platelet storage bags. TEHTM leaches out at slower rate because of its higher molecular weight and its steric hindrance.³² Further, TEHTM provides higher gas permeability compared to similar formulations with DEHP.²⁵ Compared to DEHP, TEHTM has shown less hepatotoxicity *in vitro*³³, however like other phthalates ester, it exerts estrogenic activity.³⁴ To obtain similar flexibility to that provided by DEHP, a higher amount of TEHTM is required. This might have an effect on biocompatibility of the bags as will be seen in Section 1.2.1.2.

Because of the higher cost of TEHTM and also the beneficial effect of DEHP on RBCs, DEHP is still the most widely used plasticizer in red blood cell bags and other medical devices. DEHP has been shown to stabilize RBC membranes; improve stored RBC morphology, osmotic fragility and microvesicle release.^{35,36} RBCs stored beyond 21 days in the absence of DEHP have shown considerable hemolysis while they can be preserved in DEHP-containing bags for up to 42 days.³⁷ On the other hand, DEHP has some negative effects on platelets. By decreasing the activity of phospholipase A2, DEHP exerts an inhibitory effect on the normal response of platelets to physiological stimuli, *in vitro* and *in vivo*.³⁷

Considering the safety concerns over phthalate ester plasticizers, citrate-based plasticizers such as butyryl trihexyl citrate (BTHC) (**Figure 1.5**) have found their place in platelet bag manufacturing.³⁸ BTHC is also an expensive plasticizer. It has an unpleasant smell, has high leachability into blood plasma, and cases of allergy to it have been reported.³⁹ Both acute and

repeated dose toxicity tests on BTHC have proved a low order of toxicity. However, lifetime bioassay data on BTHC is not available but it has been reported to be neither genotoxic nor a peroxisome proliferating agent.²⁸

Plastic bags based on a polyolefin system have been also developed.³¹ Such bags do not need plasticizers and eliminate the issues with plasticizer leaching, however, to our knowledge they have a very limited share of the market.

1.2.1.2 Biocompatibility

Besides different physical and mechanical requirements for platelet bags, the material of the bag must be compatible with platelets. That is, it should not cause aggregation, activation and in general should not contribute to their loss of quality upon storage. To provide sufficient gas exchange, platelet bags have relatively large surface to volume ratios, which means extensive surface area for interaction with platelets. Further, as noted earlier, platelet bags are continuously agitated during storage thus increasing platelet-substrate interaction. This emphasizes the importance of biocompatibility of bag surfaces with platelets.

As stated above, the majority of platelet bag brands are fabricated from plasticized PVC (pPVC). PVC is widely used in biomedical devices but the tendency of bacteria to adhere on PVC surfaces and form biofilms has been reported in the literature.⁴⁰ Bacteria that grow in multicellular biofilms and attach to a surface by exopolymeric substances or their glycocalyx are resistant to antimicrobial agents that kill planktonic (suspended) bacteria of the same strains.⁴⁰

Microscopic studies have shown that microbial biofilms can form in the inner side of PVC endotracheal tubes and cause nosocomial pneumonia.⁴⁰ Ventilator-associated pneumonia is known to be resistant to common antibiotic therapies. For instance, Gorman *et al.* observed that

Staphylococcus aureus and *Pseudomonas aeruginosa* on PVC surfaces exhibited greater resistance to ceftazidime and hexetidine compared to planktonic bacteria. This resistance increased significantly during aging of the biofilm, from 24 h to 4 days. Interestingly, and of clinical importance, even newly colonised bacteria (1 h) showed higher resistance to antibiotics compared to planktonic bacteria.⁴⁰

Triandafillu *et al.* studied interactions of various *P. aeruginosa* strains with PVC endotracheal tubes *in vitro*.⁴¹ Briefly, they observed that bacterial cells with more hydrophilic surfaces had a reduced adhesion on the hydrophobic PVC surfaces compared to bacteria with hydrophobic surfaces (water contact angles of the bacteria used in their study were within a range of 21° to 84°). The hydrophilic bacteria had more surface C=O and C-(O, N) and less C-(C, H) (analyzed by X-ray photoelectron spectroscopy (XPS)). Strains that had flagella adhered to PVC at higher rates compared to the mutants without flagella, which showed that active movement of bacteria increased the contact frequencies with PVC. However, the mutant strains' adhesion level was considerable, too. The zeta potential of PVC and bacterial strains seemed to have low importance as the electrostatic interactions were screened in the ionic surroundings.⁴¹

Thrombin generation and complement activation on PVC surfaces have also been reported.⁴² Hong *et al.* observed that after 60-minute incubation of heparinized whole blood with PVC at 37 °C, complement proteins, coagulation proteins, leukocytes, and platelets adsorbed on PVC surfaces. They observed that coagulation activation was dependent on the presence of leukocytes and RBCs.⁴²

Lamba *et al.* evaluated interaction of medical-grade PVC/DEHP with whole blood.⁴³ They observed that compared to two other medical devices, regenerated cellulose (Cuprophane) and an acrylonitrile-allyl sulphamate copolymer (AN69S), PVC/DEHP was a high complement

activator. The FXII-like activity was also higher on the surfaces of the PVC/DEHP than the other two polymers.⁴³ The adsorption of factor VIII from infusion solution to the surfaces of PVC containers has been also reported to be clinically important.⁴⁴

Yin *et al.* studied two medical-grade PVC tubings plasticized with either DEHP or TEHTM.⁴⁵ In PVC/DEHP, 68% of molecules at the surface, as measured by XPS, were DEHP while TEHTM accounted for 85% of the molecules at the surface of PVC/TEHTM. The fibrinogen adsorption level and thrombin-antithrombin III complex formation were higher on PVC/TEHTM compared to PVC/DEHP. Complement C3a generation by PVC/TEHTM was also higher. Considering the similar chemical identity of these plasticizers, they attributed this difference to the higher distribution of TEHTM on surfaces.⁴⁵ An early work in this field also showed that bioincompatibility of pPVC decreased after the extraction of plasticizer.⁴⁶ In this study, pPVC samples were treated with methanol to remove the plasticizer. The resulting “cleaned” surfaces were less hydrophobic than the original samples. Lower levels of fibrinogen, γ -globulin, and platelets adhesion were observed on these surfaces compared to the original samples while the level of albumin adsorption was higher.⁴⁶ Another study also showed that fibrinogen adsorption on PVC surfaces increased linearly with an increase in DEHP or TEHTM level on the surface of the materials.⁴⁷

Interactions between biomaterials and blood take place on the outermost few molecular layers. Studying surface properties that influence these interactions can guide modification approaches for improving the biocompatibility of the materials. In Section 1.3, we review some literature about these general surface properties.

1.3 General Material Surface Characteristics and Biocompatibility

Biocompatibility of materials depends largely on their surface properties and the reactions that occur when the material comes in contact with the biological system. The materials that are in contact with blood *in vivo* (e.g. haemodialysis tubing, vascular grafts and catheters) or *ex vivo* (e.g. blood storage bags) should not activate the complement, coagulation and kallikrein systems.⁴⁸⁻⁵¹ They should not cause any damage or activity change in the blood components, for example, RBC lysis or platelet activation and aggregation. Many biomaterials that have been in the market for decades for biomedical applications were not initially designed for these purposes. Instead, they were evaluated for biocompatibility because they were available for other uses.

Material surface characteristics including chemical composition of the material, wettability and surface morphology influence the interaction of the materials with proteins and cells.⁵² Modification of these properties has been the subject of several studies to control the adhesion of proteins, bacteria and cells on material surfaces. Besides biomaterial applications such as orthopaedic and dental implants, urinary and respiratory catheters, dialysis tubing, peritoneal dialysis catheters, and nano drug carriers, modification of material surfaces is actively under investigation in other fields as well. Unwanted adsorption of bacteria and other microorganisms on surfaces has been a long lasting problem in industries related to marine applications and wastewater treatment.^{53,54}

1.3.1 Chemical properties

Many studies have tried to gain an understanding of bioactivity of various functional groups to provide an easy recipe for rational engineering of materials. However, preparation of well-defined samples and also attributing complex protein/cell-material interactions to a

particular functionality is challenging. We briefly describe some observations about the effect of chemical properties of materials on their biocompatibility.

Protein adhesion: Adsorption of protein to substrate surfaces is believed to be the first step in the interaction of materials with biofluids.^{55,56} Plasma proteins, such as albumin, fibrinogen, IgG, and von Willebrand factor have a tendency to adhere to artificial surfaces, probably via hydrophobic interactions.⁵⁷⁻⁵⁹ Fibrinogen extensively adsorbs on methyl-functionalized surfaces through hydrophobic interactions.⁶⁰ Methyl groups are common in the chemical composition of many substrates. Fibrinogen can also bind tightly to exposed hydroxyl groups⁶¹ and amine groups.⁵²

Surface chemistry of biomaterials also plays a role in interaction with complement proteins and hence recruitment and activation of phagocytes and leukocytes.⁵² IgG adsorbs strongly on hydrophobic surfaces and undergoes a conformation change that exposes the active sites for binding to complement proteins.⁶² Hydroxyl functionalized surfaces also selectively adsorb IgG from serum, which in turn leads to complement protein adsorption.⁶³ Interaction of hydroxyl groups with complement proteins triggers leukocyte adhesion and activation on such surfaces. Amine groups in contrast have demonstrated slight complement activation.⁶⁴

In comparing a limited series of derivatized surfaces it was found that neutral hydrophilic surfaces with hydrogen-bond acceptor (but not donor) functionalities constituted the most non-fouling surfaces.⁶⁵ The strong interaction of hydrophilic surfaces with water molecules provides a barrier against protein adsorption, cell adhesion, and enhances the biocompatibility of surfaces, as potential binding materials must replace some of the water molecules to adhere to the substrates.

Similar to fibrinogen, platelets and leukocytes also adhere less to hydrophilic surfaces,^{52,66} and addition of hydrophobic methyl groups has been shown to enhance cell adhesion on surfaces.⁶⁷

Platelet adhesion: Studying platelet adhesion on surfaces is usually inseparable from protein adsorption. As stated above, adsorption of protein on surfaces can trigger a series of unwanted biological reactions. The adsorbed proteins undergo some conformational change and expose their hydrophobic domains to strengthen their contact with the surface. This surface-mediated conformation can expose some previously buried sequences (when it was in solution) and initiate adverse reactions such as inflammation and coagulation.⁵²

Adhered fibrinogen, fibronectin, and von Willebrand factor lead to subsequent platelet adhesion, which plays a role in thrombogenesis on foreign surfaces. These proteins interact with platelet receptors such as GPIIb/IIIa, and consequently mediate platelet aggregation and adhesion on material surfaces.⁶⁸⁻⁷¹

Fibrinogen is known to play the main role in mediating platelet adhesion to synthetic materials. A study on the interaction of polystyrene (as a hydrophobic substrate) with human plasma fibrinogen and platelets showed that platelets did not adhere to the surfaces pretreated with afibrinogenemic plasma.⁷¹ When polystyrene was treated with fibrinogen-replenished afibrinogenemic plasma, platelets could adhere on the polymer surfaces.

Bacterial adhesion: Adhered fibrinogen and platelets both promote bacterial adhesion to materials. Glycoprotein (GP)IIb-IIIa, GPIba, FcγRIIa, complement receptors, and Toll-like receptors are the main platelet receptors that interact with bacteria.⁷² This can be a direct interaction with bacterial proteins and receptors, or through proteins such as fibrinogen, von Willebrand factor, and complements.⁷²

Independent of the presence of plasma, bacteria have a strong tendency to adhere to hydrophobic surfaces. Attempts have been made to understand the mechanism of initial bacteria adsorption on substrates by physicochemical properties of the bacteria and material surfaces. Using Derjaguin-Landau-Verwey-Overbeek (DLVO) theory, a total sum of van der Waals forces, electrostatic forces and acid-base (arises from the Lewis electron-acceptor/electron-donor groups) contributes to bacteria-substrate interaction at large distances.^{73,74} The strong irreversible interaction at small distances between bacteria and substrate is then governed by hydrophobic forces and specific biochemical interactions (e.g. carbohydrate-lectin interaction). Some bacteria have fimbriae, hair-like polypeptide-based structures on their membranes, that can also interact with surfaces through both specific (biochemical receptor-ligand) interactions and/or non-specific physicochemical forces.⁷⁵

1.3.2 Morphology

Besides chemical properties of substrates, surface morphology and roughness play a role in surface-cell interactions.^{76,77} Bacterial and platelet adhesion is less likely to happen on ultra smooth materials with grooves or scratches that are too small for the cell to fit in.⁷⁸⁻⁸⁰ For example, Medilanski *et al.* observed that bacterial adhesion was minimal on surfaces with the average roughness (R_a) of $0.16 \mu\text{m}$.⁸¹

On the other hand, irregularities on materials of the order of bacterial size have been shown to promote bacterial adhesion and biofilm formation by providing more contact area and therefore promoting stronger interaction with the bacteria.⁸² Bacteria tend to colonize and form biofilms in the depressions of surfaces, as they are protected from shear forces.⁸²

Tsunoda *et al.* observed that smoother surfaces had lower platelet adhesion and better hemocompatibility.⁸³ Under a flow condition, platelet adhesion increased on a rough hydrophobic surface when compared with the same material but with smooth surfaces.⁸⁴

The above observations imply that surface characteristics of biomaterials, including chemistry and morphology, can be modified in order to improve the biocompatibility of the materials.

1.4 Goal of the Project

As discussed in Sections 1.1.2 and 1.1.3, platelets are a heavily used resource in blood transfusion yet have a shelf life roughly half of their lifetime in the circulation because of the platelet storage lesion and risk of microbial infections. Attempts to overcome these challenges to extend the shelf life of platelets have largely ignored the storage container material except to guarantee sufficient gas exchange.⁸⁵ In this thesis, the development of coatings for platelet storage bags to improve biocompatibility of platelet storage bags and decrease the risk of transfusion of bacterial contaminated platelet units is studied. Any effect of topography and roughness of platelet storage bag surfaces on their interactions with bacteria and platelets is also investigated.

1.5 Outline of Thesis

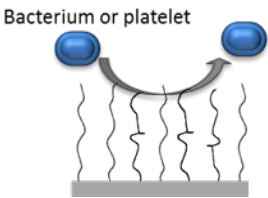
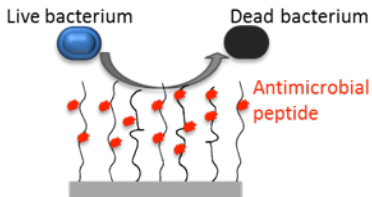
The outline of thesis is shown in **Table 1.1**. In the first three chapters, two different approaches are used to develop antifouling and bactericidal coating for platelet storage bags. In Chapter 2, hydrophilic polymer brushes are grown from platelet storage bags to decrease platelet

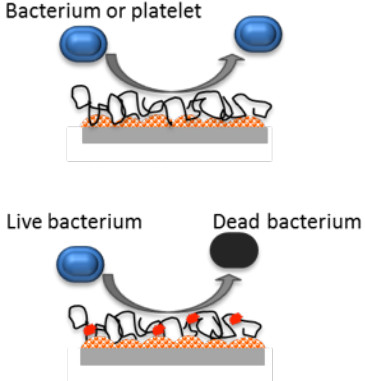
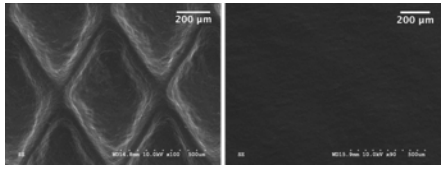
and bacterial adhesion on the bag surfaces. In Chapter 3, antimicrobial peptides (AMPs) are conjugated to the developed polymer brush system on platelet storage bags.

Considering some challenges discussed in the first two chapters, mussel-inspired chemistry is used to modify surface properties of platelet storage bags in Chapter 4.

In Chapter 5, the chemical compositions and morphology of some platelet storage bags that have been used by Canadian Blood Services are compared. Bacterial and platelet adhesion on the surfaces of these materials are assessed in this light.

Table 1.1 Outline of thesis chapters

<p>Chapter 2</p> 	<ul style="list-style-type: none"> - Introduction to polymer brushes and their synthesis - Introduction to antifouling polymer brushes - Development of antifouling polymer brush coatings for platelet storage bags - Characterization and <i>in vitro</i> evaluation of the developed surfaces.
<p>Chapter 3</p> 	<ul style="list-style-type: none"> - Introduction to antimicrobial peptides (AMPs) - Introduction to polymer brushes incorporating AMPs - Development of bactericidal polymer brush coating for platelet storage bags - Characterization and <i>in vitro</i> evaluation of the developed surfaces.

<p>Chapter 4</p>  <p>Bacterium or platelet</p> <p>Live bacterium Dead bacterium</p>	<ul style="list-style-type: none"> - Introduction to mussel-inspired chemistry - Development of an antifouling coating for platelet storage bags using mussel-inspired chemistry and its characterization and <i>in vitro</i> evaluation. - Development of a bactericidal coating using mussel-inspired chemistry and AMPs, and its characterization and <i>in vitro</i> evaluation - Mapping of the peptides on silicon wafers coated with this bactericidal coating.
<p>Chapter 5</p> 	<ul style="list-style-type: none"> - Effect of texture of platelet bags on bacterial and platelet adhesion.
<p>Chapter 6</p>	<ul style="list-style-type: none"> - Conclusions and future work

CHAPTER 2: Development of Antifouling Polymer Brushes for Platelet Storage Bags

This chapter starts with the definition of polymer brushes and general approaches for their synthesis. Among different methods, the literatures that used atom transfer radical polymerization (ATRP) for grafting polymer brushes from various substrates are reviewed. Then different groups of antifouling polymer brushes that showed resistance against bacterial or platelet adhesion are introduced.

Sections 2.2 to 2.5 focus on the development of antifouling polymer brushes coating for platelet storage bags; their synthesis, characterization, and *in vitro* evaluation. Results and Discussion are presented first (Section 2.2 and 2.3), followed by Conclusions (Section 2.4) and Methods and materials at the end (Section 2.5).

2.1 Introduction

2.1.1 General characteristics of polymer brushes

Polymer brushes are assemblies of one end tethered polymer chains at high graft density on a surface or interface. Mechanical stability and functional versatility of polymer brushes resulted in a wide range of applications in various technological fields such as corrosion resistance, colloidal stabilization, catalysis, smart materials, lithography, nanotechnology, and biomaterials over the past 50 years.

Polymer molecules tethered to a surface or an interface can be categorized into two regimes based on the average distance between the grafting points (D) in relation to the radius of gyration (R_g) of the polymer chains in solution (**Figure 2.1**).^{86,87} At low grafting densities (σ), polymer chains adopt a mushroom conformation where the thickness of the grafted layer will be

close to the R_g of the polymer. However, at high density polymer chains will stretch away from the surface to minimize overlapping and steric interactions, and they adopt a brush like conformation; the formal distinction is made when $D < 2 R_g$. The properties of polymer brushes are quite different from grafted layers in the mushroom regime and free polymer chains in solution due to the steric crowding of the chains.

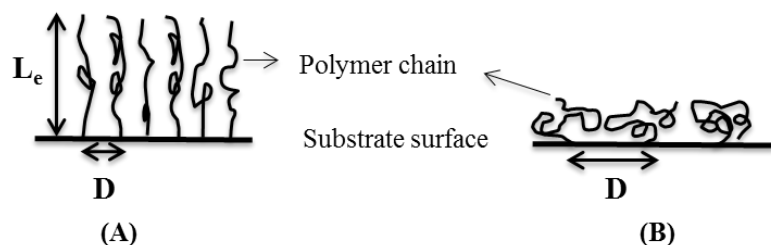


Figure 2.1 Polymer chains tethered to a surface. Polymer chains tethered to a surface in brush regime (A) and in mushroom regime (B). ‘D’ is the distance between grafting points and ‘ L_e ’ is the equilibrium thickness of the brush.

Alexander theory explains that the free energy of a polymer chain in the brush regime is the sum of the chain stretching energy and the excluded volume interactions.⁸⁸ The equilibrium thickness (L_e) of the brush is derived when the free energy of the chain is minimized, and in good solvents it is linearly dependent on the degree of polymerization (N) and $1/3$ power of graft density ($L_e \propto N\sigma^{1/3}$).^{89,90} It is assumed that the polymer chain free ends are located at the outer edge of the grafted polymer layer and there is a constant concentration profile within the brush.

Another model that uses self-consistent field arguments predicts that the polymer chain concentration decreases monotonically away from the surface.⁹¹ Solvent quality and polydispersity of polymer chains have large effect on chain end distribution.

Extensive research has been performed to study theoretical models for polymer brushes and establish the relation between their thickness and graft density of polymer brushes.⁹²

Experimental studies on poly(methyl methacrylate) brushes⁹³ have demonstrated that in a good solvent system, the relationship between the thickness and the graft density of chains in the brush regime has a typical exponent of 0.33 ($L_e \propto \sigma^{1/3}$) when the graft density is equal to or less than 0.4 chains/nm². The power of dependency changes to around 0.6 ($L_e \propto \sigma^{0.6}$) for the grafting densities between 0.4 and 0.7 chains/nm². If graft density is even higher than 0.7 chains/nm², the power of dependency can be between 0.8 and 1.3. However in a poor solvent system, the scaling has been found to be independent of graft density with an exponent of 0.8 ($L_e \propto N\sigma^{0.8}$) over the studied range of graft densities from 0.1 to 0.8 chains/nm².⁹³

Understanding of the variables in a polymer brush system, particularly the influence of graft density is highly relevant to various applications associated with polymer brushes.⁸⁶

2.1.2 Synthesis of polymer brushes

Polymer chains can be tethered to a surface through either physical adsorption or chemical bonding.

2.1.2.1 Physical adsorption

One of the first and easiest methods for the preparation of polymer brushes is by the physical adsorption or physisorption of end-functionalized homopolymers or block copolymers with some anchors on solid surfaces via non covalent interactions, such as electrostatic forces or hydrophobic interactions (**Figure 2.2A**). In the case of block copolymers, different studies have shown that the polymer adsorption can be performed both from selective solvents (solvents which solvate only one block of block copolymer) and from non-selective solvents (good solvents for both/all blocks of the copolymer). Some examples of physisorption that have been

studied thoroughly are the adsorption of block copolymer of polyethylene oxide/polystyrene⁹⁴, copolymer of poly(2-vinylpyridine)/polystyrene.⁹⁵

Although the process is simple, physisorption is less common than tethering of polymer chains through covalent bonding, due to the reversible nature of adsorption and instability of physical bonding. Another limitation of using the physisorption method for the synthesis of polymer brushes is that densely grafted brushes are rarely achieved.

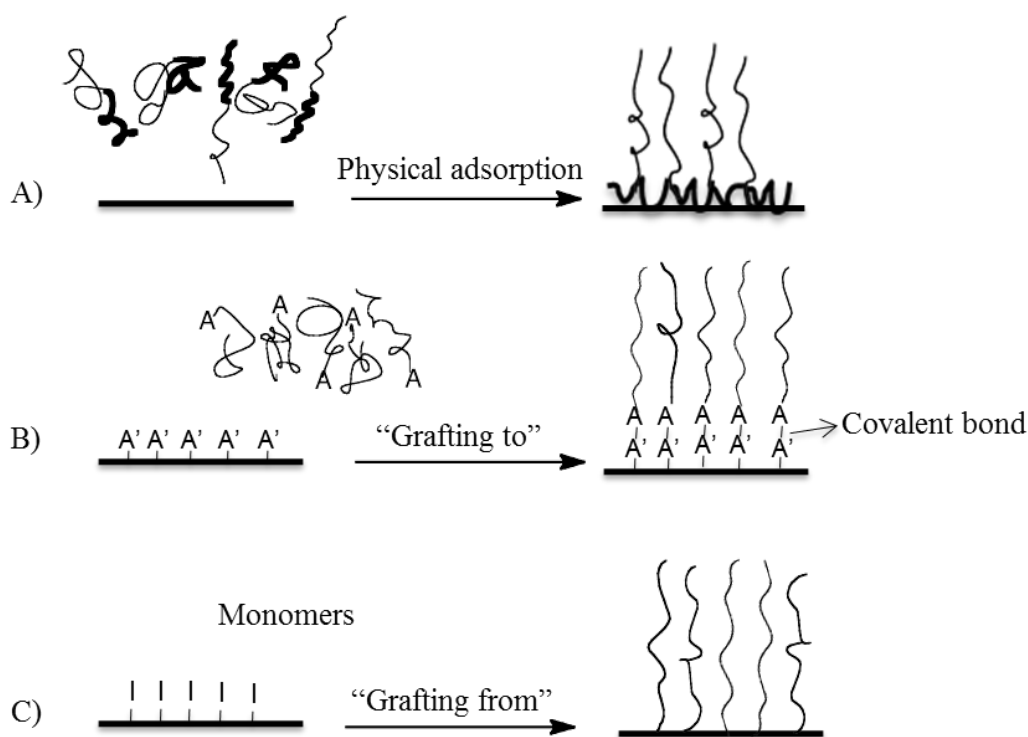


Figure 2.2 Different approaches to prepare polymer brushes. A) Preformed polymer chains adsorb from one end to a surface via physical bonding. B) The functional group on one end of the preformed polymer molecules makes a covalent bond with the complementary group on the substrate. C) surface-immobilized initiator molecules start polymerization of monomers.

2.1.2.2 Covalent grafting or chemical bonding

Two common methods used for the covalent attachment of polymer chains to the surface are “grafting to” and “grafting from” approaches.

“Grafting to” approach: In this method, the functional group on one end of the preformed polymer molecules will bind to the complementary groups on the substrate to form the grafted layer (**Figure 2.2B**). One important advantage of this method is that the polymer molecules in solution can be fully characterized before tethering, and the grafting chemistry is relatively simple compared to the “grafting from” method. Achieving a high graft density of polymer brushes, especially for high molecular weight polymer chains is challenging by this method, however. The chains that are already grafted limit further chain attachment to the substrate.

Different strategies have been used to tether pre-functionalized polymer chains to surfaces.⁹⁶ Different groups of polymers such as polystyrene⁹⁷, polyacrylamide⁹⁸, and polyethylene oxide polymers⁹⁹ were functionalized with a thiol group on one end of each chain and then attached to gold surfaces or gold-coated surfaces via the sulfur. In another example, a copolymer of styrene/methyl methacrylate was end functionalized with a hydroxyl group and tethered to a silicon oxide surface through the hydroxyl group.¹⁰⁰

In a third approach, an anchoring layer of poly(glycidyl methacrylate) (PGMA) was made on the substrate through adsorption, spin coating or dip coating to generate an epoxide functionalized surface which was further reacted with hydroxyl or amine end functionalized polymers.¹⁰¹ Flexibility of the epoxide groups and formation of an interpenetrating zone at the substrate/PGMA interface led to obtaining higher graft density by this method compared to other “grafting to” methods.¹⁰¹

“Grafting from” approach: Currently the “grafting from” or surface-initiated polymerization is widely used for the synthesis of various polymer brush systems. In this method polymer chains are grown from the surface, and unlike the ‘grafting to’ approach it provides better control over graft density (higher graft densities) and thickness of the polymer brushes. In this approach, initiator molecules are densely tethered to the surface followed by the polymerization of monomers from the anchored initiators (**Figure 2.2C**). Different surface initiated polymerization techniques have been used including cationic or anionic polymerizations, ring opening polymerization, ring opening metathesis polymerization, conventional free radical polymerization, and controlled/living radical polymerizations (CLRP). Three main categories of CLRP used for the synthesis of polymer brushes are nitroxide-mediated polymerization (NMP), reversible addition-fragmentation chain transfer (RAFT), and ATRP. The main advantage of CLRP over conventional radical polymerization is the control over the molecular weight and polydispersity of polymer chains. Both high molecular weight and block copolymer brushes are feasible by these methods.^{102,103} This introduction is limited to surface-initiated ATRP (SI-ATRP) since, as will be seen in the following, it meets the requirements for growing hydrophilic polymer chains from platelet bag surfaces.

Surface-initiated atom transfer radical polymerization (SI-ATRP)

SI-ATRP is the most common controlled living radical polymerization technique that has been used to grow polymer brushes from various substrates.¹⁰² In this technique, the initiator is a halogen-containing (mostly chlorine or bromine-containing) molecule that can form a stable radical after homolytic cleavage of carbon-halogen bond in the presence of a metal catalyst (**Figure 2.3**).¹⁰⁴ The cleavage of the bond and equilibrium between the active and dormant

species is aided by the transition metal based catalyst (often copper salts).¹⁰⁴

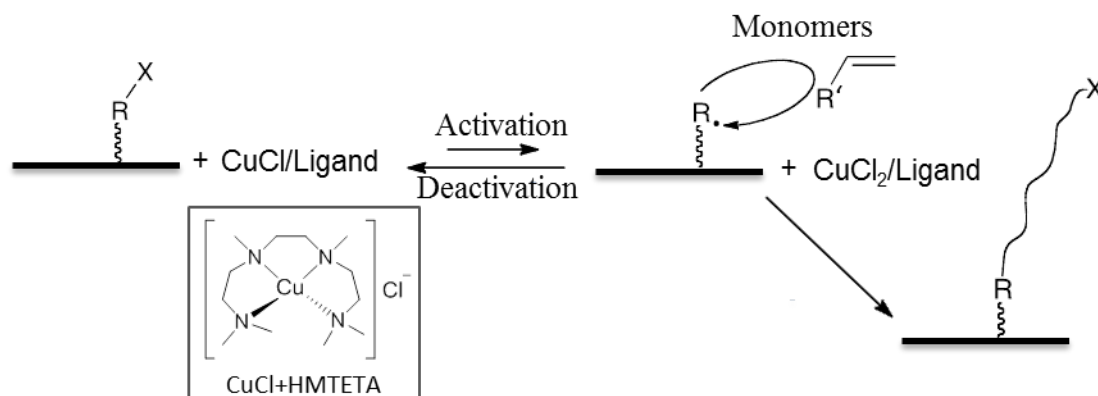


Figure 2.3 Polymer brushes grown from a substrate by ATRP.

ATRP is applicable to a variety of monomers with different functional groups. However, the carboxylic acid group can poison the catalyst and the RAFT method is a more suitable technique for the polymerization of monomers containing such groups (e.g. acrylic acid).¹⁰⁴ ATRP can be performed in various solvent systems and at different temperatures; it has been used to develop multi-block copolymers and can provide a uniform polymer brush system on a surface with controlled molecular weights without requiring extreme experimental conditions.¹⁰⁴

In a typical SI-ATRP, the organic halide initiator e.g. an α -haloesters or α -haloamides is immobilized on a surface at high density and then polymerization starts in the presence of an activator catalyst (e.g. $CuCl/HMTETA$ (1,1,4,7,10,10-hexamethyltriethylene tetramine as the ligand) (**Figure 2.3**), and monomers. Some deactivator species (e.g. $CuCl_2$ /ligand) are usually added to this solution in order to control the molecular weight and polydispersity. Similar to all other surface initiated polymerization techniques, high surface concentration of initiator is important to generate a dense polymer brush system.¹⁰⁵ Some approaches taken to generate high density of ATRP initiators on a surface include the Langmuir-Blodgett technique¹⁰⁶ or by applying an appropriate gas plasma.¹⁰⁷

In ATRP, good control of the properties of the polymer brush system can be achieved by controlling different variables including the solvent system, catalyst, the concentration of the catalyst (and the ratio of the activator to the deactivator), and the concentration of monomer and surface initiators.^{104,105,108} A drawback of ATRP is the relative sensitivity of the activator species (CuCl) to the air, however, new generation ATRP greatly avoids this problem.^{102,109} The use of metal catalyst and the possibility of its presence on the surface after the modification is another disadvantage of ATRP that has been minimized by the introduction of activator generated/regenerated by electron transfer ATRP.¹⁰²

A more recent method used to graft polymer chains from the surface is “reverse” ATRP, where catalyst is added to the polymerization medium in the higher state of oxidation (e.g. CuCl₂/ligand), and activator species will be formed in the solution as a result of the cleavage of a conventional free radical initiator. However, compared to the direct ATRP, the graft density obtained in “reverse ATRP” was low and more studies using this technique are predicted.

2.1.3 Antifouling polymer brushes

As noted in the first chapter, control of protein adsorption and cell adhesion on material surfaces is of great concern for a variety of applications. One of the most explored features of hydrophilic polymer brushes is their antifouling character. A densely grafted hydrophilic polymer brush functions as an inert shielding layer or barrier to reduce the undesirable interactions between the surface and components in biological fluid. When protein molecules or cells compress the hydrated polymer brush layer on material surfaces, the decrease in the conformational entropy of the grafted polymer chains as well as an increase in osmotic pressure within the brush makes them repulsive against the adhesion of proteins and cells.^{110,111} The

decrease in the entropy of system contributes to an increase in the free energy of the system and makes the protein or cell adhesion unfavourable.¹¹²

Protein adsorption generally decreases with an increase in brush graft density. However, as the graft density increases, secondary interactions between the protein and polymer chains (weak enthalpic contribution) might contribute to the adsorption or rejection of proteins.¹¹³ Such enthalpic interactions between protein and polymer are influenced by the chemistry of the polymers. Various neutral and zwitterionic hydrophilic polymer brushes have been used extensively as antifouling brushes. Some examples of these polymer brush systems (**Figure 2.4**) developed on various materials are summarized here, with a focus on their resistance against bacterial and platelet adhesion, as these are the properties need to be introduced to the platelet storage bag surfaces.

Unsworth *et al.* reported that polyethylene oxide (PEO) or polyethylene glycol (PEG) brushes (**Figure 2.4**) provide optimum protein repellent properties at the density of 0.5 chains/nm².¹¹⁴ Roosjen *et al.* synthesized covalently-bound PEO brushes on glass surfaces, and observed a decrease in adhesion of staphylococci and *Escherichia coli* by 98%, compared to the uncoated surfaces. However, for more hydrophobic bacteria such as *Pseudomonas aeruginosa* and also for large sized microorganisms such as yeasts, the extent of decrease in adhesion was smaller.^{115,116} These researchers also showed that PEO brushes with molecular weight of 526, 2000 and 9800 Da could decrease the adhesion of *S. epidermidis* and *Candida albicans* on glass surfaces, however, for *P. aeruginosa* and *C. tropicalis* only higher molecular weight polymer brushes (2000 and 9800 Da) could inhibit the adhesion because of the higher hydrophobic character of these microorganisms.¹¹⁷

Nejadnik *et al.* immobilized Pluronic F-127 (PEO-polypropylene oxide-PEO tri-block copolymer) on hydrophobic silicone rubber via physical adsorption.¹¹⁸ The developed PEO brush coating reduced staphylococci attachment on the surface and decreased the rate of biofilm growth. Viability of the biofilms on brush coatings was higher than their viability on pristine silicone but biofilms could be removed by fluid shear contrary to the biofilms on bare surfaces. For *P. aeruginosa*, a PEO brush coating did not decrease initial adhesion or rate of biofilm formation significantly.¹¹⁸ Pluronic with an optimized ratio of propylene oxide to ethylene oxide also decreased the level of platelet adhesion and enhanced surfaces hemocompatibility.¹¹⁹ In an *in vivo* model, silicone rubber discs with a biofilm of *S. aureus* were implanted in mice. After the infection was induced in the mice, the infected discs were removed and replaced with either PEO brush coated discs or control discs. The PEO brush coated discs resisted infection development compared to the bare silicone rubber discs.¹²⁰ Although the PEG brush coatings demonstrated the proof-of-concept and are biocompatible, there have been some reports on the poor stability of PEG due to their oxidative degradation *in vivo*^{121,122} and also generation of antibodies against PEG¹²³, thus the search for alternatives has grown.

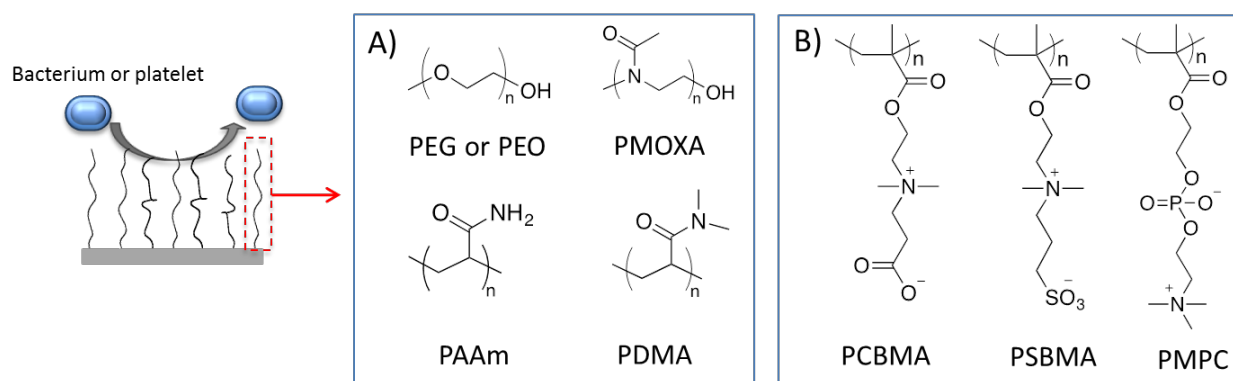


Figure 2.4 Chemical structures of different hydrophilic neutral (A) and zwitterionic (B) polymers with antifouling properties.

Poly(2-alkyl-2-oxazoline) is another neutral hydrophilic polymer with antifouling properties studied for inhibiting bacterial adhesion.^{124,125} Poly(2-methyl-2-oxazoline) (PMOXA) (**Figure 2.4**) brushes immobilized on a silicon surface via a poly(L-lysine) (PLL) backbone reduced protein adsorption from undiluted human plasma; the performance of PMOXA and PEG brushes (on the similar substrate and backbone) against protein adsorption was found to be similar in this study.¹²⁶ Pidhatika *et al.* developed PLL-graft-PMOXA on niobia (Nb₂O₅) surfaces with different graft density and evaluated them against two different strains of *E. coli*, with or without fimbriae. A comparative study using modified surfaces, niobia and niobia-PLL-graft-PMOXA surfaces showed that surface characteristics such as interfacial charge, density and homogeneity of the surface-grafted polymer chains affected the bacterial adhesion on the surface. Surfaces modified with PMOXA brushes with high graft density and with overall surface potential close to zero efficiently inhibited the adhesion of both *E. coli* strains (with and without fimbriae).⁷⁵ Biocompatibility of PMOXA and Poly(2-ethyl-2-oxazoline) (PEtOXA) has been demonstrated in soluble form (intravenous injection in mice) and surface-immobilized form (on polyurethane films and glass surfaces) and was comparable to the properties of PEO.¹²⁵ However, possibility of enzymatic degradation of the amide bond of poly (2-alkyl-2-oxazoline) and formation of imine residues are the reported concerns about using these polymers.¹²⁷

Polyacrylamide (PAAm) (**Figure 2.4**) brushes have been developed on silicon wafers and hydrophobic silicone rubbers in order to make the surfaces non-adherent to bacteria.^{128,129} Adhesion of *S. aureus*, *S. salivarius*, and *C. albicans* was reduced on PAAm brushes, compared to uncoated samples.^{128,129} PAAm brushes also showed good stability under storage conditions (in phosphate- buffered saline (PBS) or reconstituted freeze-dried saliva at 37 °C for one month).¹³⁰ Liu *et al.* grafted PAAm from gold surfaces and observed that the developed surfaces

were resistant to the adhesion of *S. epidermidis* and *P. aeruginosa*. They also evaluated the adhesion of proteins from a wide range of media on PAAm brushes and observed that the antifouling properties of this coating were equivalent to PEG brushes (if not better).¹³¹ Poly(*N,N*-dimethylacrylamide) (PDMA) brushes (**Figure 2.4**) grown from unplasticized PVC¹³² and polystyrene¹³³ were shown to decrease platelet adhesion significantly. Compared to molecular weight, graft densities of the PDMA brushes played a more important role in controlling interfacial properties.¹³² Amphiphilic block copolymers composed of hydrophobic (poly(2-methoxyethyl acrylate)) and hydrophilic PDMA showed good adhesion to various substrates (e.g. polystyrene, titanium, and glass).¹³⁴ The coated substrates showed high protein resistance. Considering the biocompatibility of polyacrylamides, they have been suggested as a promising alternative to PEG-based antifouling materials.

Zwitterionic poly(carboxybetaine methacrylate) (PCBMA) brushes (**Figure 2.4**) grafted from glass inhibited the formation of *P. aeruginosa* biofilm on the surfaces.¹³⁵ This coating sustained its resistance to the biofilm formation for 64 h at 37 °C and for 240 h at 25 °C, by 93% and 95%, respectively, compared to the bare glass surfaces.¹³⁵ Another excellent example of zwitterionic polymer brushes is poly(*N*-(3-sulfopropyl)-*N*-methacryloxyethyl-*N,N*-dimethyl ammonium betaine (PSBMA) brushes (**Figure 2.4**).^{136,137} PSBMA brush coating on polyurethane vascular catheters gave 97 to 99.9% reduction in the adhesion of a broad range of microorganisms including *S. aureus* and *C. albicans* compared to the bare catheters and also resisted biofilm formation (tested against *E. coli* and *S. aureus*). When implanted in rabbits, PSBMA-coated catheters showed 50% less inflammation and 97% fewer adhered bacteria. In this study, Smith *et al.* also showed that PSBMA brushes could reduce the activation of platelets and accumulation of thrombotic material on the catheters.¹³⁷ PSBMA brush coating could reduce

attachment and activation of platelets, lymphocytes, monocytes, and neutrophils on vascular catheters *in vitro* more than 98%. Device-associated thrombus *in vivo* was also inhibited by the brush coating.¹³⁷

Coatings made of poly(2-methacryloyloxyethyl phosphorylcholine) (PMPC) (**Figure 2.4**), a well-studied zwitterionic polymer, have also been reported (not all defined in brush regime) to inhibit biomaterial-associated infections.¹³⁸⁻¹⁴⁰ An example is PMPC grafted on an acrylic resin denture base material to prevent denture plaque-associated infections.¹⁴¹ PMPC coating inhibited adhesion of *Streptococcus* bacteria and biofilm formation, and could sustain their antifouling properties after repetitive mechanical stress.¹⁴¹

Zwitterionic polymers have received increased attention lately to prevent biomaterial-associated infections. The biocompatibility and non-thrombogenic properties of these coatings are particularly beneficial for this purpose.¹⁴²⁻¹⁴⁵ Although zwitterionic and neutral hydrophilic polymer brushes have been proved to be successful in inhibiting bacterial adhesion, they do not necessarily kill the adhered bacteria and further, the activity of the surfaces varies depending on microbial species.

The chemistry (functionality and nature of the polymer backbone) and the physical structure (graft density, molecular weight and branching) of the brushes can be modified to achieve optimal broad-spectrum bacterial adhesion resistance.

2.1.4 Antifouling coatings reported for the medical grade PVC

PVC tubing plasticized with diisooctyl phthalate was coated with alternate layers of iron (III) and either heparin or dextran sulfate through electrostatic interactions.¹⁴⁶ Compared to the

control PVC, these hydrophilic polysaccharide-iron coated PVC surfaces significantly reduced adhesion of platelets, polymorphonuclear neutrophils and peripheral blood mononuclear cells.¹⁴⁶

In another study, a heparin coating on PVC tubing could also improve the hemocompatibility of these surfaces.¹⁴⁷ Some of this effect was correlated to differences in adsorption or cleavage of plasma proteins on these surfaces.¹⁴⁷

Coating biomaterials with biomacromolecules such as albumin and heparin has been a leading approach for enhancing wettability and biocompatibility of biomaterial surfaces. However, biomacromolecules do not necessarily retain their original and active conformation when immobilized on the surface. Besides, they are labile to enzymatic degradation. Therefore, a synthetic polymer coating appears to be a more promising option.¹⁰⁸

In another study PEO-entrapped PVC films were fabricated.¹⁴⁸ The authors were interested to see if PEO could act as a nontoxic plasticizer and also if it could improve the biocompatibility of PVC. They found that the added PEO was surface active and a 10% addition of PEO (as a PEO-polypropylene oxide -PEO triblock copolymers) could suppress platelet adhesion.¹⁴⁸

pPVC films were treated with oxygen plasma in another study.¹⁴⁹ The treated surfaces had lower water contact angle (57°) compared to the control samples (102°). Less attachment of fibroblast L929 cells on the treated samples was observed.¹⁴⁹ However, as discussed in Chapter 1, hydroxylated groups generally promote complement activation and do not show proper biocompatibility.

Some active radicals were formed on pPVC surfaces via plasma treatment in air, and poly acrylic acid brushes were grown from these activated surfaces.¹⁵⁰ Irgasan, a potent antimicrobial agent, was then coupled to the polymer brushes to introduce bactericidal activity to the substrate.¹⁵⁰ However, this study used organic solvent for the surface reactions that extracts some

of the plasticizers and changes the material properties.

2.1.5 Development of polymer brushes on platelet storage bags

The majority of platelet storage bag brands are made from pPVC; PVC in a mixture with either TEHTM or BTHC. TEHTM and BTHC tend to leach out of the material in the presence of organic solvents and/or high temperature. Leakage of plasticizer changes the mechanical properties and the gas permeability of the bags. It also challenges their safety and biocompatibility if more plasticizer has migrated to the interface as discussed in Chapter 1. Therefore, the methods that require organic solvent and high temperature should be avoided for the development of the polymer brushes on these surfaces. Another consideration is compatibility of the method with the monomers. Our laboratory's experience has led us to polymeric systems composed of acrylamide-based monomers^{108,132,151,152}, and radical polymerization has been widely used for these monomers in research and industrial scales.

Considering the limitations of working with pPVC, a 'grafting to' method sounds a better option for this material. In this method the polymer system can be prepared and purified without any consideration of the temperature and the solvent. Then it can be grafted to the pPVC surfaces that are equipped with some groups for coupling with the polymer chains. However, achieving a high density of grafted polymer chains using this method is challenging.

ATRP in water at controlled temperatures has been successfully used by our lab and other research groups for 'grafting from' PAAm brushes from poly(dimethylsiloxane) (PDMS) surfaces¹⁵³ and silicone rubber¹²⁸, PDMA brushes from unplasticized PVC¹³², pPVC¹⁵⁴, and polystyrene particles¹³³, copolymer of *N,N*-dimethylacrylamide and *N*-(3-aminopropyl)methacrylamide hydrochloride (poly(DMA/APMA)) from titanium¹⁵²,

poly(oligo(ethylene glycol)acrylamide) brushes from polystyrene particles¹⁵⁵, and poly *N*-substituted acrylamide monomers containing carbohydrate residues from silicon substrates.¹⁵⁶

Considering the physical properties of pPVC and the need for mild and aqueous conditions, ATRP was used to graft the polymer brushes from this substrate.

2.2 Results and Discussion: Synthesis and Characterization of Hydrophilic Polymer Brushes on pPVC

A general scheme of polymer brush synthesis on platelet bag surfaces is shown in **Figure 2.5**. The platelet bag material used for all these experiments was Solmed EH-222 provided by the American Renolit Corporation, denoted here pPVC for plasticized PVC. Briefly, the pPVC surface was initially functionalized with amine groups via allylamine plasma modification. A water-soluble ATRP initiator was synthesized and reacted with the amine groups on the surface. Polymerization of hydrophilic monomers proceeded from the surface in water at room temperature. These hydrophilic monomers were DMA, APMA and MPDSAH (3-(methacryloylamino)propyl)-dimethyl(3-sulfopropyl)ammonium hydroxide) (**Figure 2.5**).

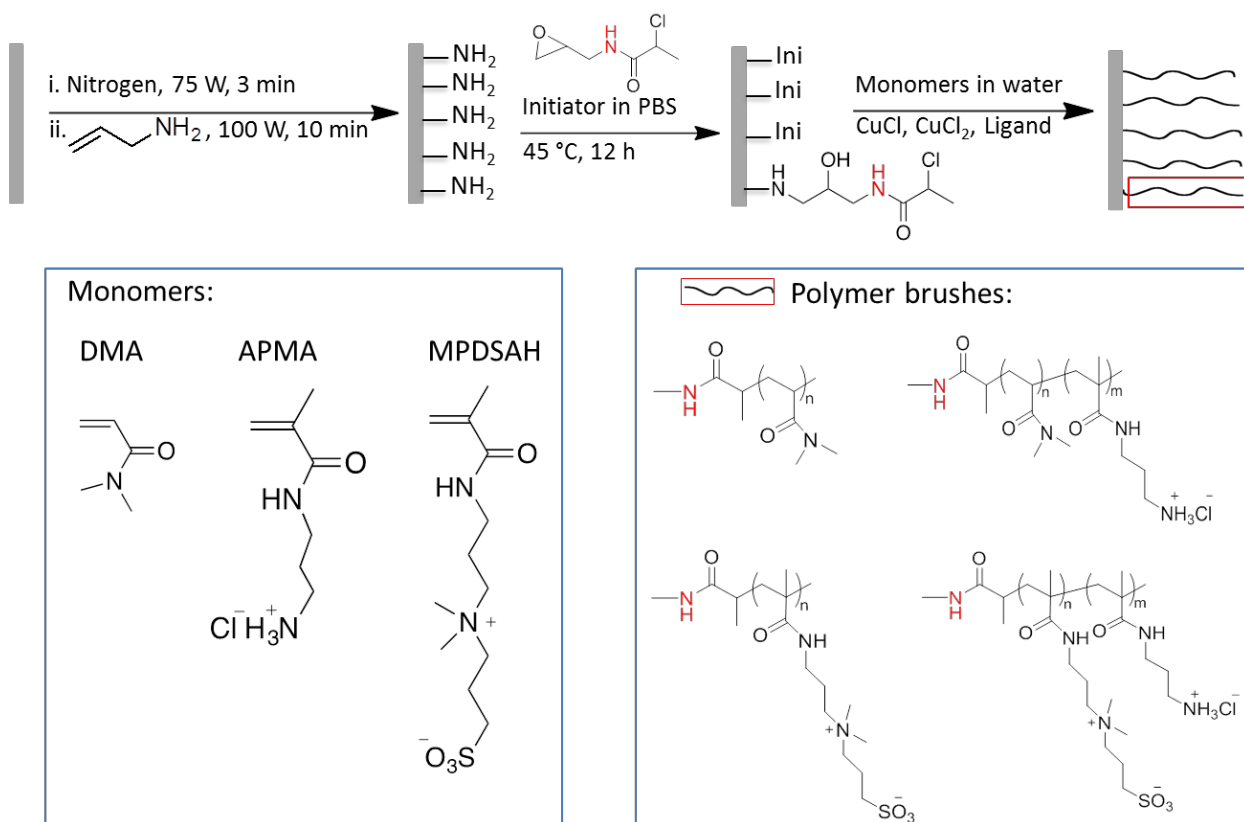


Figure 2.5 The general scheme of grafting polymer brushes from pPVC. The homopolymers and copolymers were composed of three hydrophilic monomers: DMA, APMA and MPDSA.

2.2.1 The pPVC substrate

The main components of this material are PVC and TEHTM. ^1H nuclear magnetic resonance (NMR) spectroscopy of pPVC dissolved in deuterated THF (tetrahydrofuran) is shown in **Figure 2.6A**. Peak assignment and structure elucidation were performed based on the chemical shifts and coupling constants.

Forty percent of the mass of the pPVC was extracted during 7 days of its immersion in hexane at room temperature. **Figure 2.6B** shows the ^1H NMR spectrum of the clear liquid extracted from pPVC in hexane that matched TEHTM.

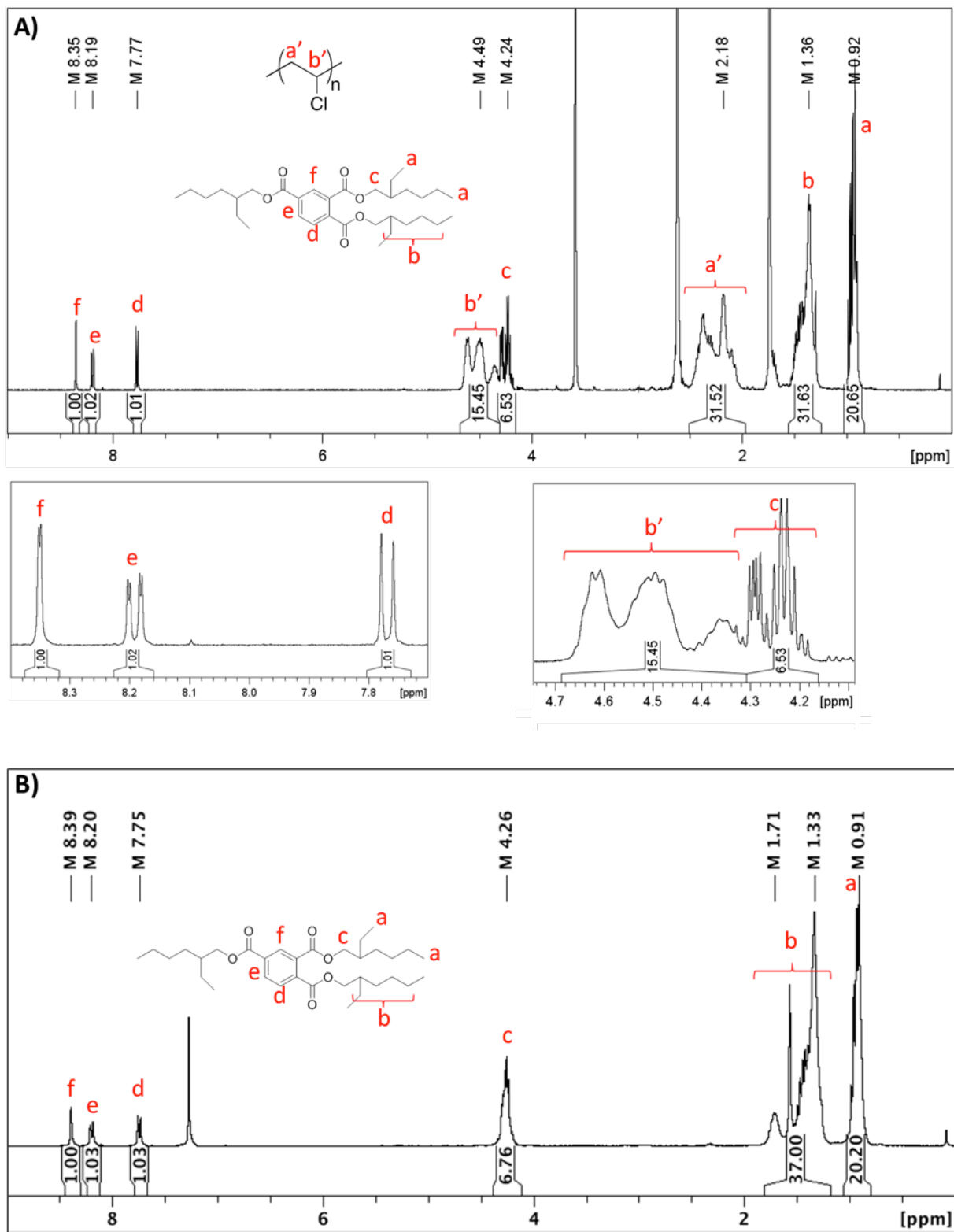


Figure 2.6 ^1H NMR spectra of pPVC in $d_8\text{-THF}$ (A) and the hexane extract of pPVC in CDCl_3 (B).

XPS spectrum of pPVC showed the presence of calcium and silicon on the surface of pPVC. It is known that one or more thermal stabilizers must be present in pPVC formulations because of the poor thermal stability of PVC.¹⁵⁷ When heated to 100 °C, PVC undergoes dechlorination and releases HCl (**Figure 2.7**). This reaction can propagate along the chain. A group of widely used thermal stabilizers are metal soaps such as zinc stearate or calcium stearate. So the thermal stabilizer could be the source of calcium observed on the XPS spectrum of pPVC.

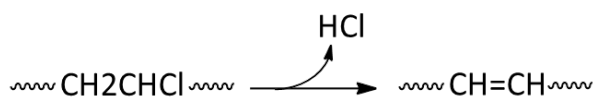


Figure 2.7 Dechlorination of PVC as a result of heating

More detailed study of pPVC by time of flight second ion mass spectroscopy (TOF-SIMS) (**Figure 2.8**) showed characteristic ionic fragments of PDMS in the positive ion mass spectrum, which confirmed the silicon peak in the XPS spectrum. The characteristic peaks of PDMS are 73, 147, 207, 221 m/z with a 74 Da OSi(CH₃)₂ repeating unit.^{158,159}

It is not known at this stage if PDMS had been used in the fabrication of pPVC, e.g. on the molds or if it had been introduced by contact between another material and pPVC during shipping or storage in the laboratory. However it was not washed off by a wash using 1% Extran detergent.

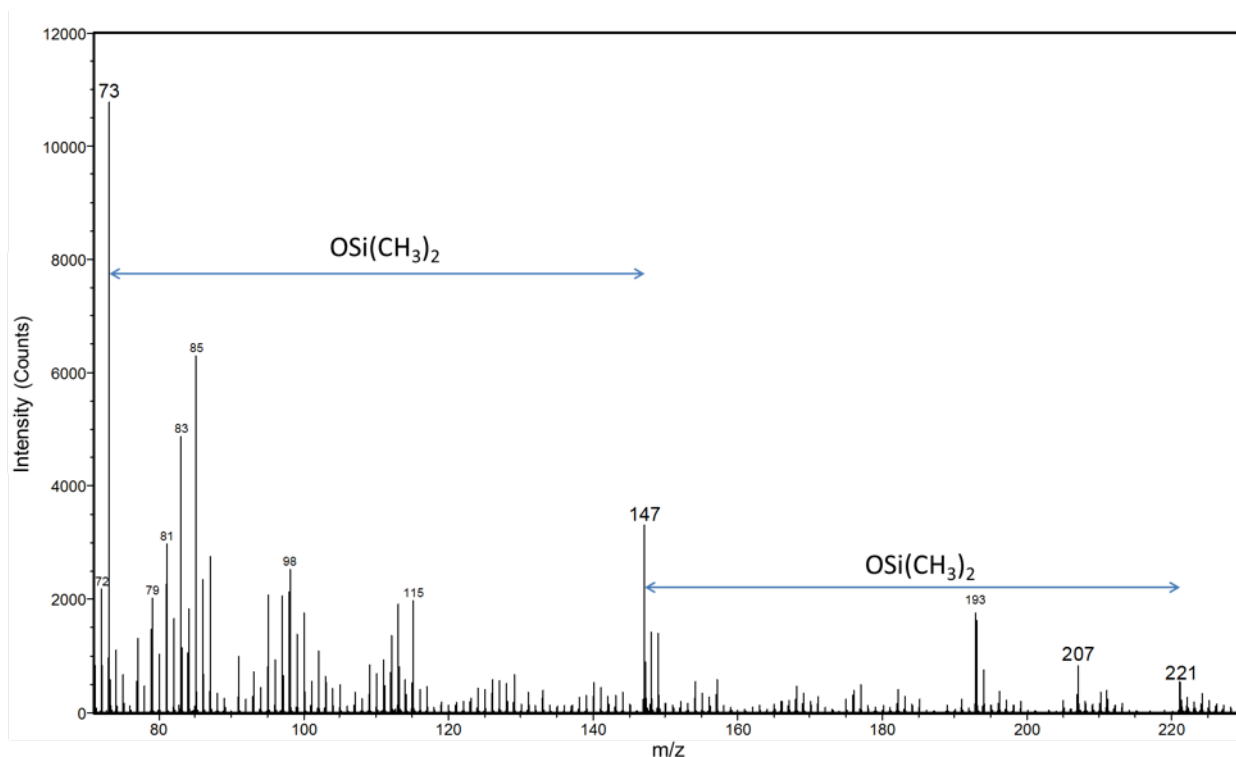


Figure 2.8 Positive ion TOF-SIMS spectrum of pPVC. Characteristic peaks of PDMS; 73, 147, 207, 221 m/z were detected on the pPVC surfaces. The 74 Da difference was attributed to $\text{OSi}(\text{CH}_3)_2$.

2.2.2 Amination of pPVC: synthesis and characterization

Allylamine plasma or the “dry method” versus “wet method”

The plastic surfaces need to be functionalized to covalently graft polymer brushes from them. A conventional method would be to use a chemical reaction or wet method. For example, some pPVC samples have been reacted with aminothiophenol in a mixture of water and DMF (dimethylformamide) at around 55 °C.^{132,160} The thiol groups substituted the chloride on PVC backbone, and the amine group could be used for further modification. However, as shown by these studies too, using DMF and heat caused leaching out of the plasticizer and also swelling of the material.

The dry method, or plasma enhanced chemical vapour deposition, is a promising alternative for the functionalization of plastic materials. This method can provide a homogenous

coating over curved or patterned surfaces and can be performed at room temperature without exposing samples to any solvent.¹⁶¹ Previous studies have shown that allylamine plasma can generate 5-12 NH₂ groups/nm².¹⁶² The polyallylamine layer generated by the plasma on the substrates form a continuous film (no islands) via a layer by layer mechanism.¹⁰⁷

Plasma polymerization of allylamine was used to generate amine groups on pPVC surfaces. Silicon wafers were treated in parallel with pPVC films to allow more characterization. **Table 2.1** shows the summary of the results. After allylamine plasma treatment, the water contact angle on pPVC surfaces changed from $102 \pm 4^\circ$ on control pPVC to $57 \pm 5^\circ$ on pPVC-NH₂.

Table 2.1 Surface characterization of the pPVC and the silicon wafer surfaces treated with allylamine plasma. Water contact angles and thickness are reported as AVG \pm SD of at least three substrates and the value for each substrate is the average value of measurements on three locations.

Sample	Water contact angle ($^\circ$) ^a	Molar ratio of N on surface in percentage ^b	Thickness of the developed layer (nm) ^c
pPVC	$102 \pm 4^\circ$	0.9 and 1.56 % (Two coupons)	N.A.
pPVC-NH ₂	$57 \pm 5^\circ$	1.9 %	N.A.
Silicon wafer (Si)	$8 \pm 1^\circ$	Zero	N.A.
Si-NH ₂ via Allylamine plasma	$62 \pm 4^\circ$	5.2 %	8.1 ± 1.2 nm
Si-NH ₂ via APTES reaction	$55 \pm 3^\circ$	3.9 %	2.7 ± 1.6 nm

^a Determined by placing a water droplet of 3 μ L on the surface and measuring the interior angle.

^b Measured by XPS. ^c Measured by ellipsometry.

Water contact angle on the silicon wafers treated under the same condition changed from $8 \pm 1^\circ$ (on the control silicon wafer) to $62 \pm 4^\circ$. Thickness of the layer was 8.1 ± 1.2 nm measured by ellipsometry. Survey scan XPS showed that the concentration of nitrogen was 5.2 % on these

surfaces. The corresponding value on the control silicon wafer was zero. For comparison, a wet chemical process commonly used for amination of pretreated titanium and silicon oxide surfaces^{163,164} was also used (**Figure 2.9**).

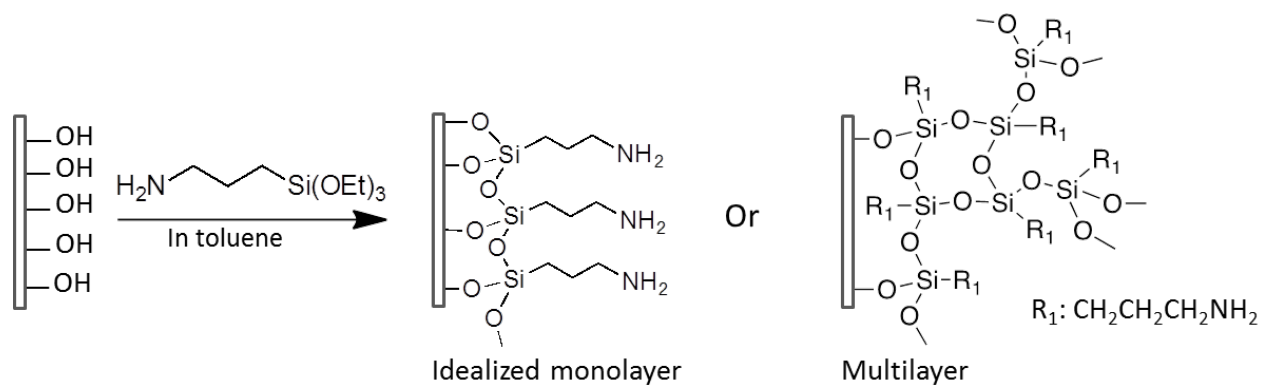


Figure 2.9 Amination of silicon wafer surfaces using a wet chemical method. Silanization of silicon wafer surfaces with APTES is an efficient method of amination of these surfaces.

In this method, silanization of a silicon wafer surface with (3-aminopropyl)triethoxysilane (APTES) in toluene at room temperature generated the amine groups. The resulting water contact angle on these surfaces was $48 \pm 3^\circ$. The concentration of nitrogen using the wet method was 3.9 % found by XPS and the thickness of the layer was 2.7 ± 1.6 nm measured by ellipsometry. This thickness matched the presence of a multilayered APTES (**Figure 2.9**).

The results of XPS analysis on two control pPVC coupons showed some variations in concentration of C, N and O (N percentage is shown in **Table 2.1**) probably due to the nonuniformity of chemical composition on surfaces or contribution from organic contaminants. Therefore, the concentration of these elements was not used for making comparisons during the progress of modification.

Figure 2.10 shows a proposed mechanism for plasma polymerization of allylamine from the literature.¹⁰⁷

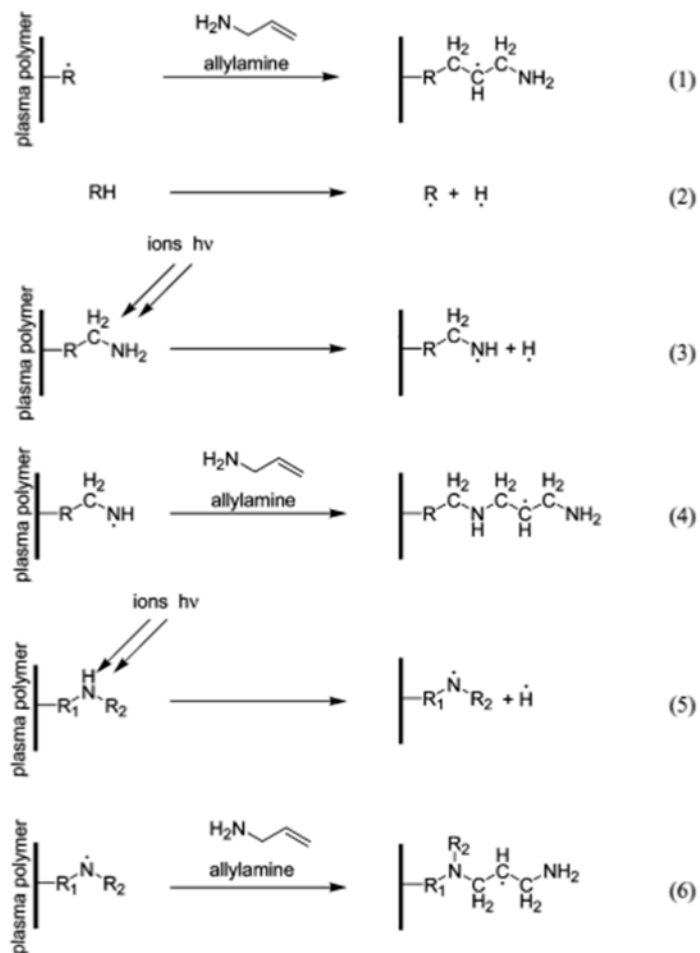


Figure 2.10 A proposed scheme for plasma polymerization of allylamine. Reproduced with permission from *J. Phys. Chem. B* 2005, 109, 23093.

2.2.3 Immobilization of initiators on surfaces and their characterization

To be able to implement the next steps of the surface modification in water, water-soluble ATRP initiators were synthesized. These molecules had the labile halogen required for ATRP initiation on one side and on the other side had epoxy groups for reacting with the immobilized amine groups. As will be explained later, different structures were prepared for different purposes (**Figure 2.11**). **Figure 2.12** shows the synthesis of different initiators. The initiators' structures were confirmed by ^1H NMR (**Figure 2.13**). The NMR spectra of the intermediates are provided in Appendix A1.

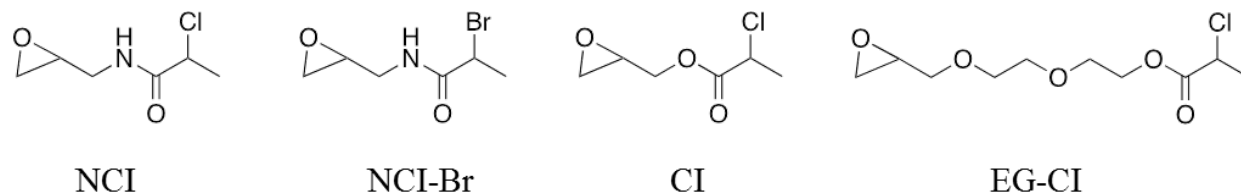


Figure 2.11 The synthesized initiators for SI-ATRP on pPVC surfaces. The initiators carry the labile halogen required for ATRP initiation on one side and epoxy group for reacting to the immobilized amine groups on the other side.

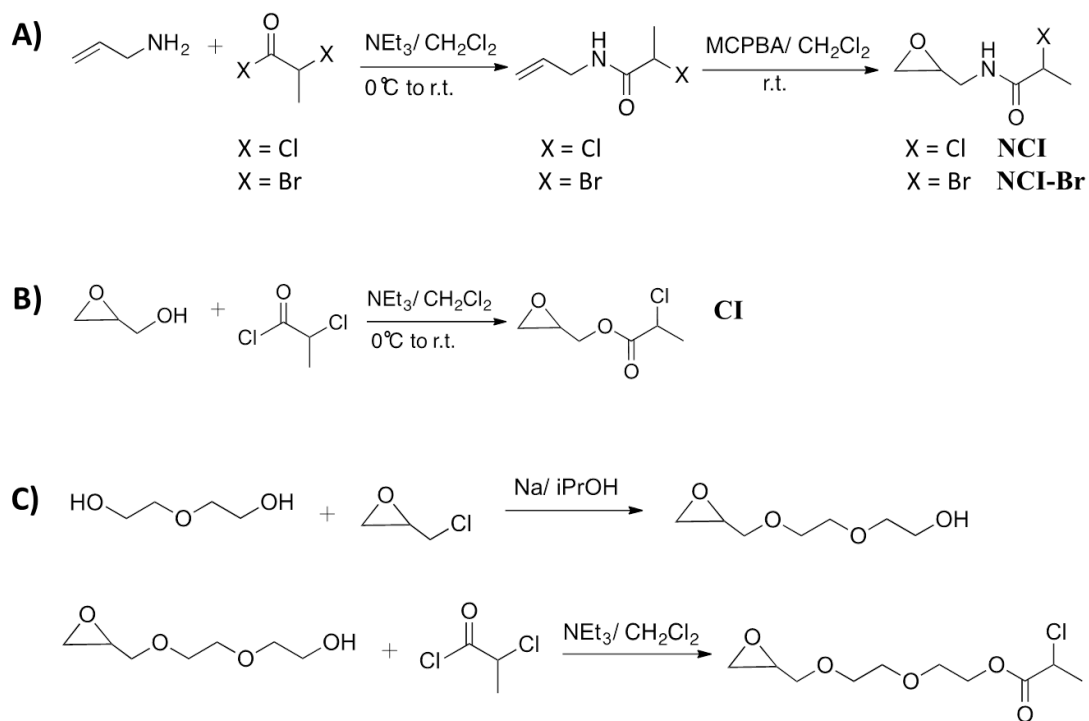


Figure 2.12 The synthetic scheme for the SI-ATRP initiators: NCI and NCI-Br (A), CI (B), and EG-CI (C)

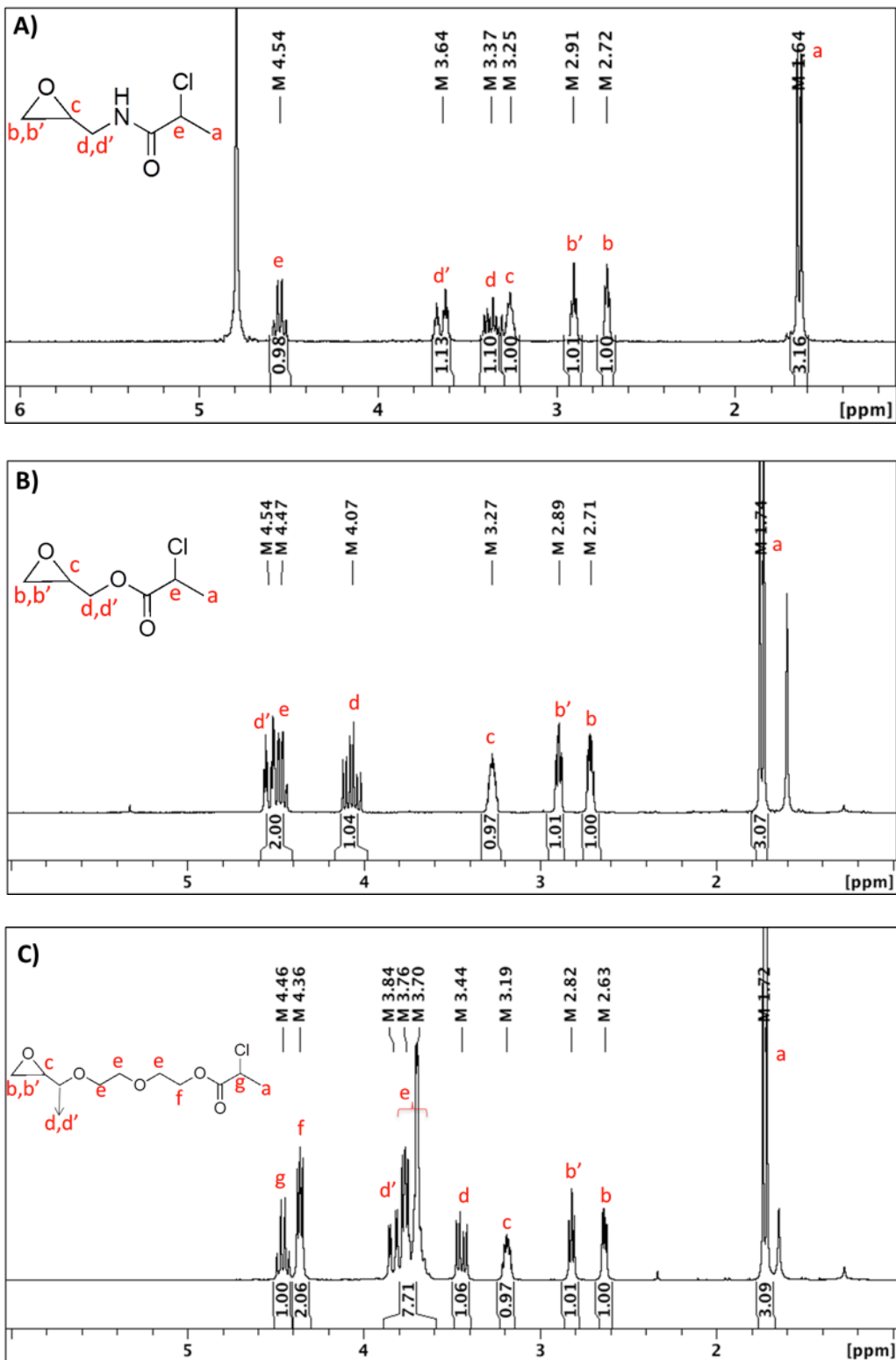


Figure 2.13 ¹H NMR spectra of the synthesized SI-ATRP initiators: NCI in D₂O (A), CI in CDCl₃ (B) and EG-CI in CDCl₃ (C)

Aminated pPVC surfaces were reacted with the initiator in phosphate buffer solution pH 7.5 at 45 °C.

Backbiting and self-termination have been reported for ATRP of acrylamide monomers and bromine is more labile, which makes these events more likely.¹⁶⁵ Therefore a chlorine-containing initiator, named NCI for the non-cleavable initiator was used (**Figure 2.11**). The water contact angle on surfaces changed slightly to $61 \pm 4^\circ$ after initiator immobilization.

As chlorine atoms from PVC overlap with those of the initiator molecules, a bromine containing initiator (**Figure 2.11**, NCI-Br) was also synthesized in order to be able to use XPS for confirmation of the tethering of initiator to the surfaces. The concentration of bromine on the surface was 0.3 % after tethering NCI-Br.

Cleavable initiators containing an ester bond were also synthesized to allow cleavage of the grafted polymer chains for characterization purposes (**Figure 2.11**, CI for cleavable initiator and EG-CI for ethylene glycol cleavable initiator).

In parallel with pPVC, silicon wafer samples aminated with allylamine plasma were reacted with the initiators under similar conditions. There was no detectable change in water contact angle, however, XPS confirmed the presence of chlorine with 1.5 % molar ratio on the surface after tethering NCI. The chlorine peak concentration on Si-NH₂ was zero.

2.2.4 Surface-initiated ATRP

Polymerization of water-soluble monomers including DMA, MPDSAH, and APMA was initiated by the surface-immobilized initiators in the presence of CuCl (activator), CuCl₂ (deactivator), HMTETA (ligand), and water as the solvent. For homopolymerization and copolymerization involving MPDSAH, 0.2 M KCl was added to screen electrostatic interactions

that might limit polymerization and solubility of polymers. Our laboratory's experience over many types of aqueous ATRP homopolymerization and copolymerization led us to run the reaction for 24 h.^{108,152,166–168}

In SI-ATRP, the concentration of immobilized initiator is quite low. Therefore, the concentration of the deactivator (CuCl_2) generated after halogen atom transfer to CuCl may not be enough to reversibly trap the propagating radicals, which leads to an uncontrolled chain growth. To overcome this, some persistent radical (deactivator), or some “sacrificial initiator” can be added to the polymerization solution from the beginning of the reaction.^{102,105} This way, polydispersity of the grown polymers and their length will be better controlled.^{169,170}

In the present experiments, some CuCl_2 was added to the polymerization solution. Further, some sacrificial initiator was added to the solution to provide some solution polymers. Although kinetics of polymerization in solution and grafting from surfaces are not the same, characterization of the solution polymer can give some idea about the molecular weight and structure of the obtained polymer chains on the surfaces.^{169,171}

Table 2.2 shows the characteristics of the polymers formed in solution during surface initiated polymerization. Number average molecular weight (M_n) of the polymers and their polydispersity were determined by gel permeation chromatography (GPC) fitted with a multi angle laser light scattering (MALLS) detector and a refractive index (RI) detector. As expected from controlled polymerization characteristics of ATRP, the polydispersity of all polymers was limited.

Copolymerization of DMA and APMA with different ratios and copolymerization of MPDSAHA and APMA with different ratios were performed likewise via ATRP and yielded $\text{P}(\text{DMA}/\text{APMA})$ and $\text{P}(\text{MPDSAHA}/\text{APMA})$, named DA and MA, respectively. APMA

incorporation in the polymer brushes provided the required amine groups for conjugation of AMPs in the next step that will be discussed in Chapter 3.

As will be seen in the next section, in the case of copolymer brushes made of MPDSAH and APMA XPS was used to study if incorporation of the monomers was similar to the feeding ratio. For copolymers made of DMA and APMA, the solution polymers formed during polymer brush synthesis was studied because of the limitations mentioned above associated with determination of C and N concentrations on pPVC surfaces.

Table 2.2 Characteristics of the polymers formed in solution during surface-initiated polymerization.

Sample	Description	Number average Molecular Weight (M_n) (Da) ^a	Polydispersity (M_w/M_n) ^{b*}
PDMA	PDMA	1.82×10^5	1.30
DA51	P(DMA/APMA) (5/1)	1.23×10^5	1.28
DA41	P(DMA/APMA) (4/1)	1.29×10^5	1.29
DA21	P(DMA/APMA) (2/1)	1.13×10^5	1.32
DA11	P(DMA/APMA) (1/1)	1.33×10^5	1.26
PMPDSAH	PMPDSAH	5.28×10^5	1.18
MA51	P(MPDSAH/APMA) (5/1)	4.01×10^5	1.17
MA41	P(MPDSAH/APMA) (4/1)	3.84×10^5	1.15
MA21	P(MPDSAH/APMA) (2/1)	3.12×10^5	1.18
MA11	P(MPDSAH/APMA) (1/1)	2.54×10^5	1.22

^{a,b} Measured with a GPC-MALLS/RI system. * M_w : weight average molecular weight.

Figure 2.14 shows the NMR spectrum of P(DMA/APMA) (5/1), named DA51. NMR spectra of the PDMA homopolymer and PAPMA homopolymer are also shown for clarity of assignments (Appendix A2). Integrations of the signal of the methyl group of APMA at 0.93 ppm (**Figure 2.14, a**) and the signal of the proton on the backbone of PDMA at 2.62 ppm (**Figure 2.14, c**) were used to estimate the incorporation ratio of these monomers in the synthesized copolymer. Similar values were determined from the NMR spectra of P(DMA/APMA) (4/1), (2/1) and (1/1), named DA41, DA21 and DA11. **Table 2.3** summarizes these results.

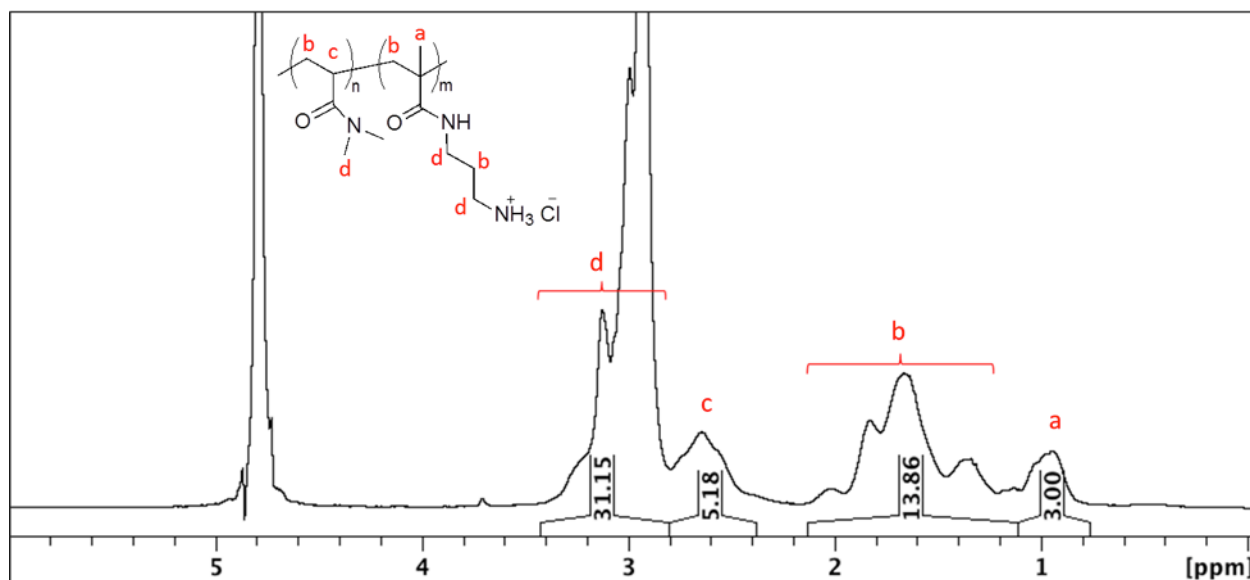


Figure 2.14 ^1H NMR spectrum of DA51 in D_2O . The ratio of DMA/APMA was determined by integration of the corresponding peaks; **a** represents 3 protons on the APMA methyl group and **c** represents one proton on the DMA backbone.

Table 2.3 Comparison of the incorporation ratio of the monomers in the DA copolymers with the feeding ratio.

Sample	Molar ratio of DMA to APMA	
	Theoretical	Experimental (Based on NMR data)
DA51	5	5.18
DA41	4	4.07
DA21	2	2.23
DA11	1	0.94

2.2.5 Characterization of the polymer brush-grafted surfaces

Water contact angle measurements: As shown above, pPVC samples have hydrophobic surfaces with water contact angle $102 \pm 4^\circ$. The water contact angles resulted from different polymer chains on pPVC are summarized in **Figure 2.15**. Grafted PDMA chains could decrease the water contact angle on these surfaces to as low as 37° . In the copolymer coatings, an increase in the ratio of the APMA monomer increased the water contact angle. This was attributed to the presence of the carbon side chain in APMA. PMPDSAH could decrease the water contact angle dramatically, too (**Figure 2.15**) and incorporation of more APMA in MA copolymers increased the water contact angle. Some studies have discussed that zwitterionic polymers provide better hydrophilic coatings as they interact with water through strong electrostatic interactions versus hydrogen bonding.¹⁷²

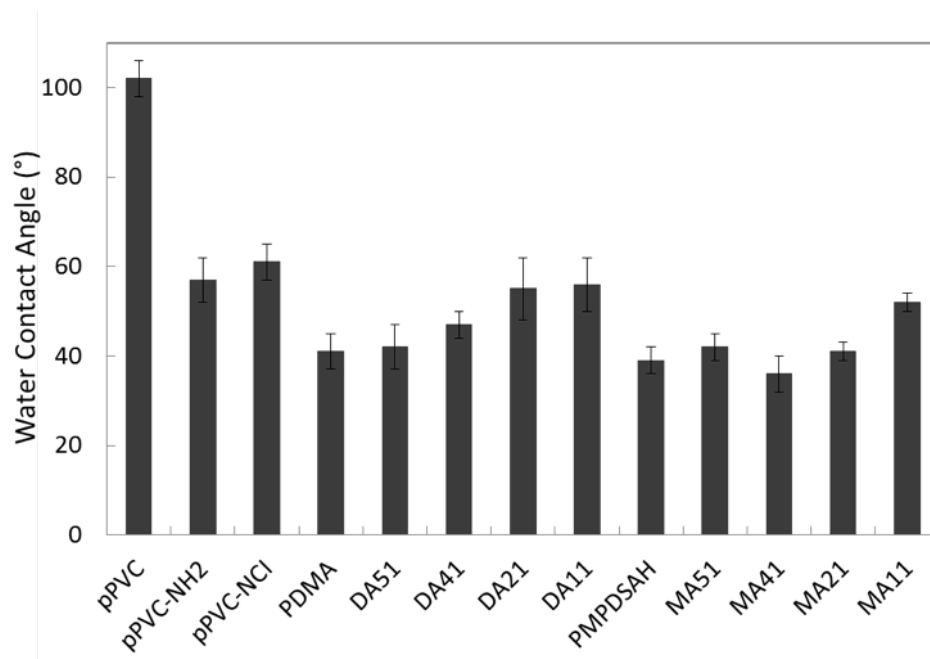


Figure 2.15 Static water contact angle on the control and modified pPVC surfaces. The water contact angle values are reported as AVG \pm SD of three different samples, 5 spots on each sample.

XPS: In the case of copolymer brushes made of MPDSAHA and APMA, XPS was used to study if incorporation of the monomers was similar to the feeding ratio. The theoretical ratio of Sulfur to Nitrogen (S/N) was calculated based on the feeding ratio. The experimental ratio of S/N was calculated from the XPS spectra, and was found to be close to the theoretical values (**Table 2.4**).

Table 2.4 Comparison of the incorporation ratio of the monomers in the MA copolymers with the feeding ratio.

Sample	Molar ratio of Sulfur to Nitrogen (S/N)	
	Theoretical	Experimental (Based on XPS data)
MA51	0.42	0.46
MA41	0.40	0.44
MA21	0.33	0.32
MA11	0.25	0.29

ATR-FTIR spectroscopy: Attenuated total reflectance Fourier transform infrared (ATR-FTIR) spectroscopy was used to characterize the surfaces. The strong peak at 1726 cm^{-1} was correlated with the ‘ester’ C=O stretch in the TEHTM plasticizer (**Figure 2.16**). A strong amide absorption band at 1630 cm^{-1} confirmed the growth of polymer chains containing amide bonds from the surface (amide C=O stretch) (**Figure 2.16**).

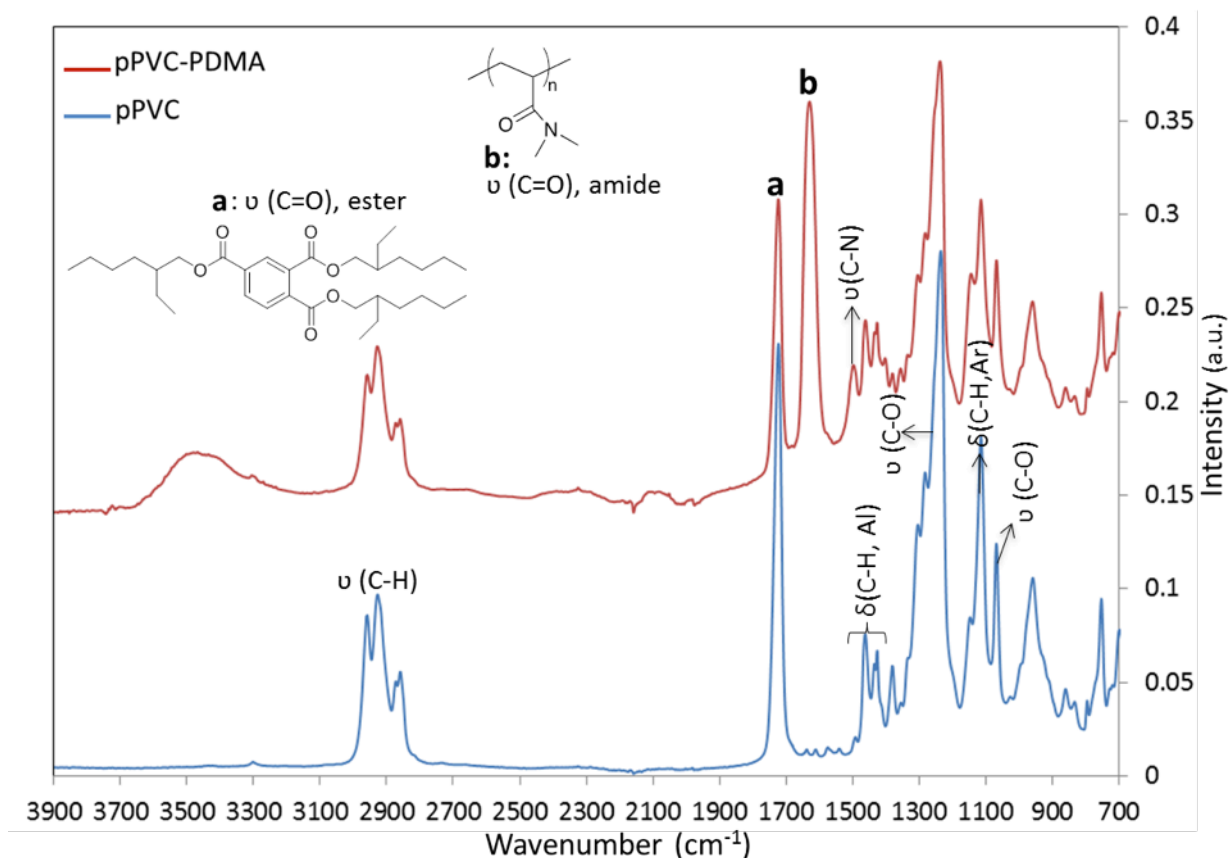


Figure 2.16 ATR-FTIR spectra of the control pPVC and the pPVC modified with PDMA polymer brushes. The PDMA amide peak at 1630 cm^{-1} and TEHTM ester peak at 1726 cm^{-1} are the characteristic peaks focused on in the study. Stretching (ν) and bending (δ) vibrations of some bonds of PDMA and pPVC are marked in the spectra. Al and Ar stand for aliphatic and aromatic, respectively.

The intensity of IR peaks has been used as a semi quantitative marker to compare the amount of polymers on surfaces.^{128,173} As shown in **Figure 2.16**, the intensity of the PDMA amide peak (at 1630 cm^{-1}) is greater than the plasticizer ester peak (at 1726 cm^{-1}). The intensity

of the amide peak decreases as the ratio of DMA/APMA decreases in the copolymers (**Figure 2.17A**). The peak intensity of MPDSAH and its copolymers with APMA are less than 20 % of the amide peaks in DMA (**Figure 2.17B**). The peak at 1426 cm^{-1} corresponds to the CH_2 vibration of PVC and it was used as a reference band for normalizing the data. As the results did not change after normalization, reporting the intensity of amide peaks as they were collected was continued.

The molecular masses of MPDSAH and APMA are higher than DMA, which means the same thickness of these polymers characterized by IR would contain fewer amide groups and therefore provide a lower intensity of amide peaks. However the significant difference between PMPDSAH and PDMA cannot be explained solely by the difference in the molar masses (molecular weight of DMA, APMA and MPDSAH are 99, 178.5, 292, respectively).

The penetration depth of IR in our experimental setup was around $2\ \mu\text{m}$. Given that TEHTM is more than 45 % of pPVC and that it is distributed in the bulk as well as on the surfaces, an amide peak equivalent or more intense than the plasticizer does not match an expected one-layer polymer brush on the surfaces with a thickness of a few hundred nanometers.

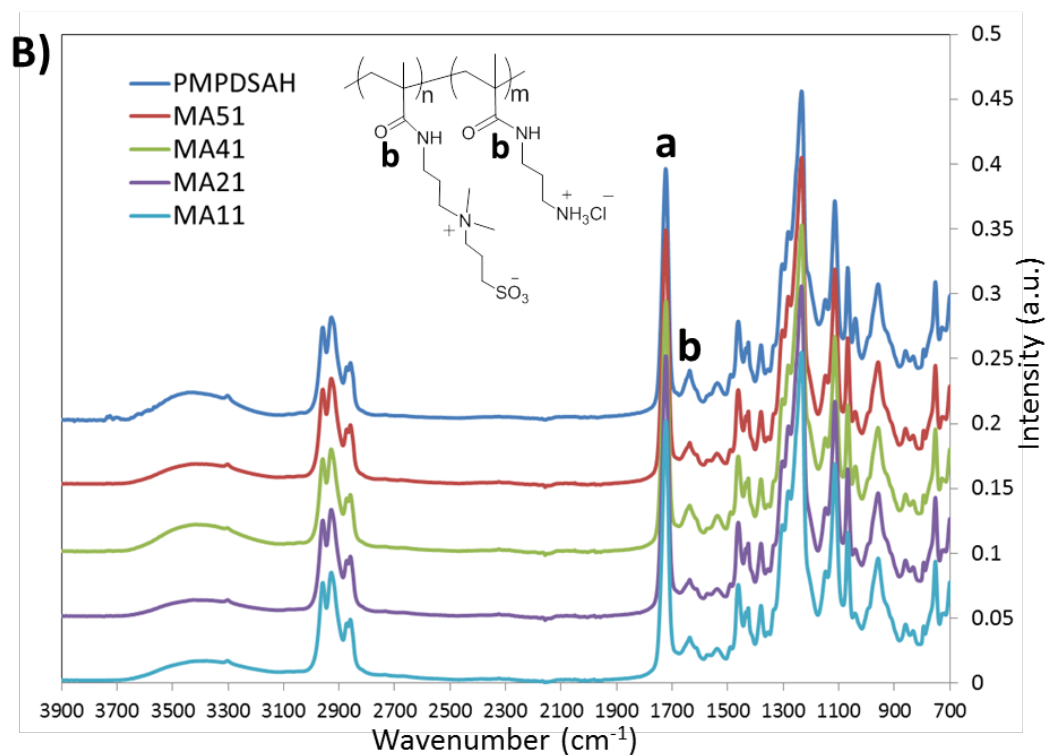
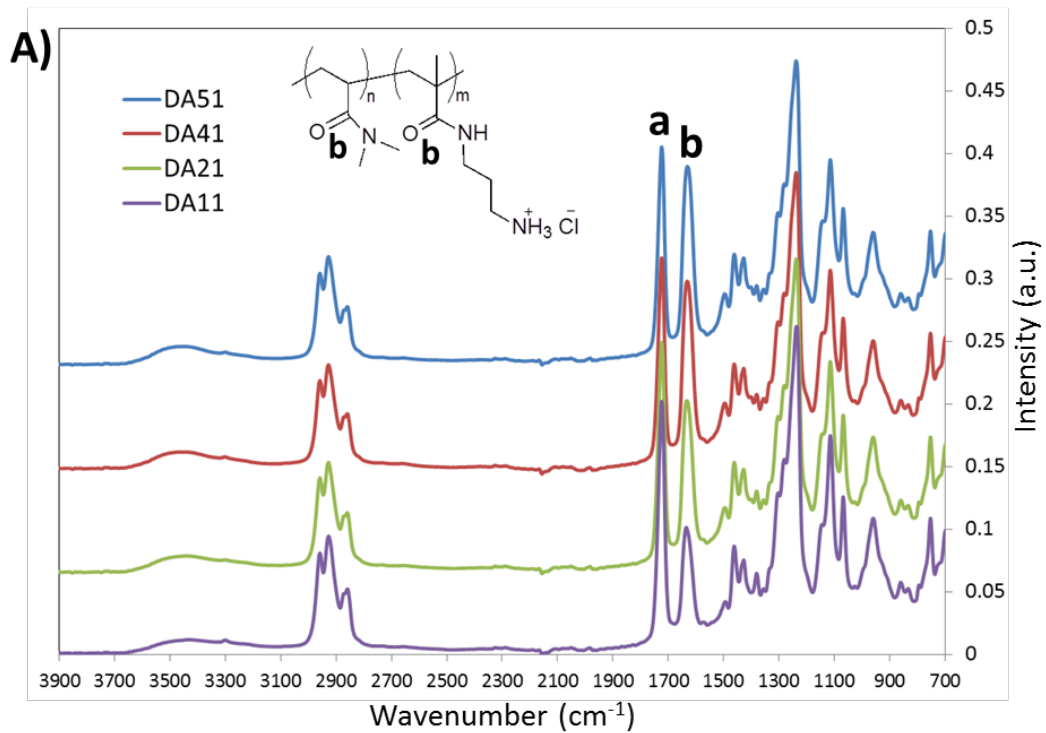


Figure 2.17 ATR-FTIR spectra of the pPVC samples modified with DA (poly(DMA/APMA)) copolymers (A) and MA (poly(MPDSAHA/APMA)) copolymers (B). “a” marks the characteristic ester peak of TEHTM as shown in Figure 2.16 .

A set of experiments was performed to get a better understanding of the polymer brush grafting from surfaces. A summary of these experiments is presented in **Table 2.5**. In each experiment, one or more required elements for the polymer brush synthesis were omitted. The polymerization solution included DMA and APMA (5 to 1), CuCl, CuCl₂ and HMTETA.

Experiment 1. pPVC surfaces were treated using the complete recipe including allylamine plasma treatment and initiator immobilization followed by ATRP. The intensity of the amide peak was 0.15 a.u. and the water contact angle on the modified surfaces was around 42°.

Experiment 2. pPVC surfaces were not exposed to allylamine plasma treatment and initiator coupling. The samples without any treatment were put in the ATRP solution. Surprisingly, the presence of polymer on pPVC was confirmed with ATR-FTIR with intensity comparable to the complete recipe. pPVC surfaces, however, remained hydrophobic and water contact angle on these surfaces was only slightly lower than on the control pPVC surfaces.

Experiment 3. pPVC surfaces were treated by the complete recipe including allylamine treatment and initiator immobilization followed by ATRP, however without any sacrificial initiator in the solution. The presence of polymer was confirmed with ATR-FTIR with intensity comparable to that of the complete recipe. The water contact angle was similar to the samples treated under a complete recipe (44°).

Experiment 4. pPVC surfaces were not exposed to allylamine plasma and initiator coupling, and the sacrificial initiator was not added to the polymer solution. An amide peak with lower intensity (0.11) was still observed. Water contact angle on the substrate did not change, however.

Table 2.5 Control experiments for studying polymer brush synthesis on pPVC surfaces

Experiment Number	Allylamine plasma	Initiator coupling	Sacrificial initiator in ATRP solution	Intensity of amide C=O peak (a.u.) ^a ($\pm 5\%$)	Water contact angle ($^{\circ}$) ($\pm \sim 7\%$)
1 pPVC	+	+	+	0.15	42 $^{\circ}$
2 pPVC	-	-	+	0.135	85 $^{\circ}$
3 pPVC	+	+	-	0.14	44 $^{\circ}$
4 pPVC	-	-	-	0.11	98 $^{\circ}$
5 uPVC	+	+	+	0.05	40 $^{\circ}$
6 uPVC	-	-	+	0	84 $^{\circ}$
7 pPVC	-	-	No sacrificial initiator and no metal catalyst	0	101 $^{\circ}$

^aThe amide C=O stretch at 1630 cm^{-1} was used as a marker of the presence of DA51 polymer chains. The peak at 1426 cm^{-1} corresponding to the CH_2 vibration of PVC was used as a reference.

It has been reported that there are some labile chlorines in commercial PVC that can act as initiators for ATRP.¹⁷⁴ These labile chlorines are tertiary or allylic chlorines, which are generated as a result of branching and chain transfers during PVC production. Initiated by the labile chlorines in PVC, 2-ethyl hexyl acrylate and n-butyl acrylate have been grafted from commercial PVC by ATRP.¹⁷⁴ Detection of some amide bonds without the presence of any initiator on the surfaces or in solution can be explained by the labile chlorines in the PVC backbone. The amount of labile chlorine has been reported to be 1 to 4 % depending on the manufacturing method.¹⁷⁴ The slight change in water contact angle in Experiment #2 and #4 implies that these labile chlorines are not abundant on the surfaces of PVC.

Detection of a strong peak associated with amide bond on the pPVC surface region sampled by ATR-FTIR without any change in water contact angles can be explained by the presence of the polymer in the pPVC bulk phase. PVC and TEHTM are not chemically bound.

TEHTM lowers the T_g of PVC by increasing the free volume; low molecular weight plasticizers such as TEHTM create free space between the PVC chains and themselves. It seems that this space can also accept polymer molecules between the PVC molecules. Hydrogen bonding between the carbonyl groups of the synthesized polymer chains and HCl of PVC could be a contributing factor to the penetration of monomers and possibly the solution polymer chains into pPVC bulk. Miscibility of PVC with poly(methyl methacrylate) has been explained in the literature by such interactions.¹⁷⁵

For confirmation, in Experiment #5 a rigid PVC film that contained little plasticizer, here called unplasticized PVC (uPVC), was coated using the exact same step by step reactions. The resulting amide peak from DA51 on uPVC was only 0.05 a.u. compared to 0.15 a.u. on pPVC (Appendix A3). This can be explained by the lack of free space for the penetration of the polymers inside the bulk. Further, without any immobilized initiator on uPVC surfaces (Experiment #6), ATRP did not lead to detectable amide bonds on uPVC.

It should also be noted that pPVC has very rough surfaces compared to the unplasticized PVC. Hence, per unit macroscopic area, the total micro-scale interfacial area of pPVC is higher than uPVC, which implies more intense amide peaks are expected on pPVC surfaces than on uPVC. However, as will be shown later, the two faces of pPVC films have a significant difference in roughness (Section 2.3) but gave the same intensity of amide peaks, which further supports the notion that the polymers in the bulk contributes to the majority of the peak.

In experiment #8, only monomers were present in the polymerization solution. No CuCl, CuCl₂, or ligand was added. No amide peak was observed in this experiment, which confirmed the ATRP nature of the polymerizations carried out.

The observations summarized in **Table 2.5** lead to the conclusion that some sources of ATRP initiation exist in pPVC structures that caused polymer growth in the bulk phase, and the data obtained by ATR-FTIR did not represent the polymer chains on the surfaces, but included polymer on the surface and in the pPVC bulk phase together. The growing polymer chains in solution may penetrate into the bulk of pPVC, as well. A set of experiments was performed using only DMA to exclude if amine groups on APMA played some roles; a similar trend was observed for DMA, but not for the zwitterionic monomer, MPDSAH. A stronger interaction of zwitterionic polymer with water can be a possible reason for this observation.

Therefore, ATR-FTIR data was not used as a method for comparing different polymer system coverage on the surfaces.

Atomic force microscopy (AFM): To get an understanding about the barrier capacity of the developed hydrophilic coatings against hydrophobic interactions, some force measurements were done by atomic force microscopy on substrates immersed in aqueous solutions.

Generally in these experiments, a cantilever holding a silicon nitride (Si_3N_4) tip approaches and is retracted from the pPVC surfaces and the interactions between the tip and pPVC surfaces are recorded (in the AFM instrument used here, the sample moves not the cantilever). During approach and retraction the cantilever bends toward or away from the pPVC surfaces depending if the interaction is attractive or repulsive. This deflection changes the position of a laser beam reflected from the backside of the cantilever on to a position-sensitive photodiode (**Figure 2.18**). The deflection of the laser at the photodiode is directly correlated with the deflection of the cantilever.

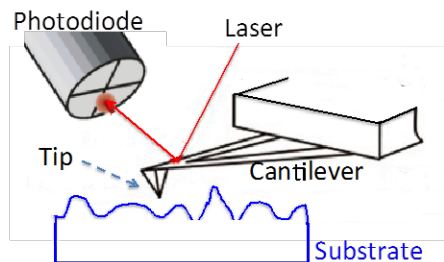


Figure 2.18 A tip on the end of a cantilever deflects when the tip encounters features of the surface. A laser beam constantly reflects off the cantilever onto a position-sensitive photodiode. The deflection of the laser at the photodiode is directly correlated with the deflection of the cantilever.

As seen in **Figure 2.19A**, when the AFM tip was far from the pPVC sample, there was no interaction between them, hence no deflection of the tip (A). As the AFM tip got closer to the unmodified control pPVC surfaces, a strong attraction between the tip and the pPVC surfaces caused the jump-to-contact of the cantilever (B). When the tip moved even further toward the surface, the deflection of the tip became equivalent to the sample movement (slope of the line is equal to one). This is called a constant compliance (C).

During retraction, the silicon nitride tip adhered to pPVC for a distance past the point where the first contact was made during the approach (D). The deflection increased (more negative) up to a critical point where it abruptly reached zero (E).

Figure 2.19A is an example of the raw data collected from an AFM study which recorded the cantilever deflection versus the sample position. This raw data has been converted and reported as force versus tip-sample separation in all other figures following a program written by Dr. Johan Janzen in our lab and used widely by our group for several years.^{132,166,181} This program uses a rigorous criterion for statistically defining the constant compliance region and hence the zero separation location. Determination of “zero separation” is challenging for deformable materials, however.¹⁷⁶ Immediately after the jump-to-contact where the tip and the

surface come in contact, adhesion forces set in and draw the tip even more into contact. Adhesion forces plus the force exerted by the tip movement can cause an indentation. Therefore, “zero separation” for the deformable surfaces with surface forces becomes practically difficult.¹⁷⁶

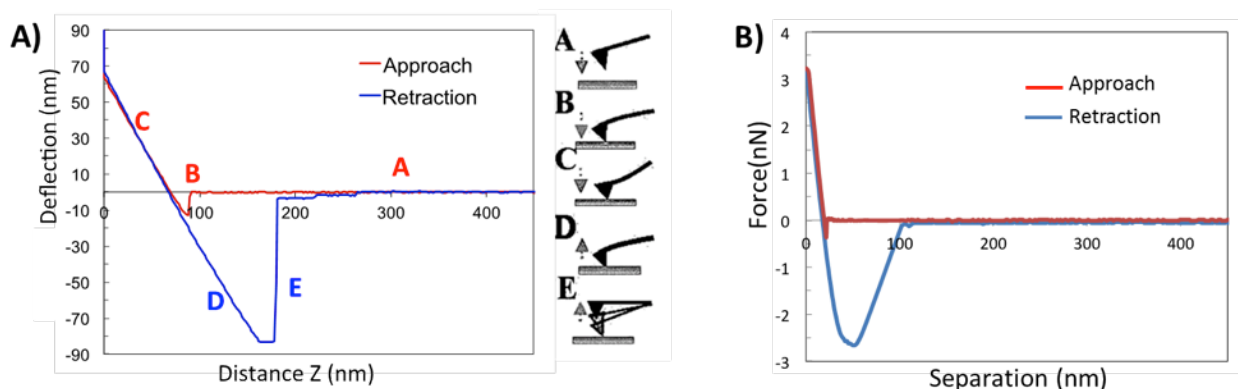


Figure 2.19 AFM force curve when a silicon nitride tip interacted with pPVC surface in 0.5 M NaCl solution. Original data collected by AFM (A) was converted to a curve presenting the force versus tip-sample separation (B).

Each silicon nitride substrate carries four cantilevers with different spring constants. The force between the tip and pPVC surfaces is calculated based on Hooke’s law by multiplying the measured deflection by the spring constant. The cantilever should be selected depending on the substrate. For example, if the cantilever is too stiff compared to the substrate, it will not respond to the forces associated with the samples. On the other hand, if it is too soft, the force curve represents the properties of the cantilever instead of the substrate. The cantilever with spring constant 0.24 N/m was used in the experiments reported here.

Figure 2.19B shows the data of **Figure 2.19A** after conversion. Maximum attractive (negative) force is called pull-off or rupture force and represents the interfacial energy between the tip and sample in that particular medium (here 0.5 M aqueous NaCl). Similar force curves to what were observed for the pPVC-Si₃N₄ tip interaction have been reported for the interactions of other hydrophobic surfaces with the silicon nitride tips.¹⁷⁷ **Figure 2.20** represents force measurements for pPVC surfaces modified with PDMA and PMPDSA. Contrary to the

unmodified pPVC, the interactions between the silicon nitride tip and these polymer brush-modified surfaces were repulsive, both in the approach and retract traces. The tip-polymer brush interactions reflect various contributing factors: a combination of electrostatic and van der Waals interactions described by DLVO theory, and the steric repulsion from the polymer brushes (non-DLVO force). Generally if the charge density is low and/or the solution contains high concentrations of electrolytes, electrostatic interactions are screened and dominated by the van der Waals force. To minimize electrostatic effects, the AFM experiments were performed in 0.5 M NaCl solution. The samples were in equilibrium with 0.5 M NaCl solution for at least half an hour prior to AFM analysis.

Force curves for PDMA (**Figure 2.20A**) and MPDSAH (**Figure 2.20B and 2.20C**) both demonstrated that the overall interaction between the hydrophobic AFM tip and the modified hydrophilic surfaces was repulsive. Any possible attractive DLVO forces between the tip and the polymers were dominated by the steric force. The repulsive steric forces exerted by the polymer brushes are a consequence of excluded volume interactions. In 20 % of the studied PMPDSAH samples, a weak adhesive interaction was observed in the retraction curve (**Figure 2.20C**). This could be attributed to the interaction of the alkyl side chain of PMPDSAH with the tip.

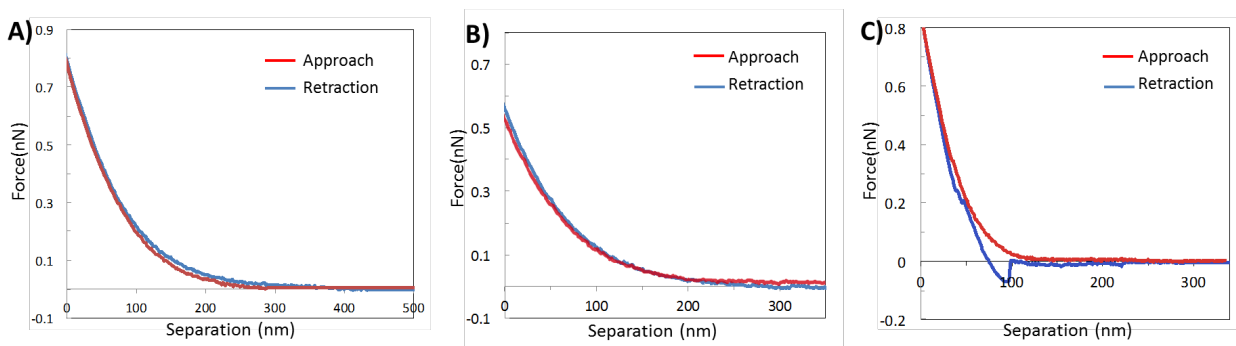


Figure 2.20 Approach and retraction force curves for the pPVC surfaces modified with PDMA (A) and PMPDSAH (B and C).

For DA51 brushes, although the approach curve was repulsive, a weak adhesive force during retraction was observed (**Figure 2.21**) that can be attributed to the interaction of the alkyl side chains of APMA with the tip, which is felt until the polymers are extended to their maximum length (**Figure 2.21B**).

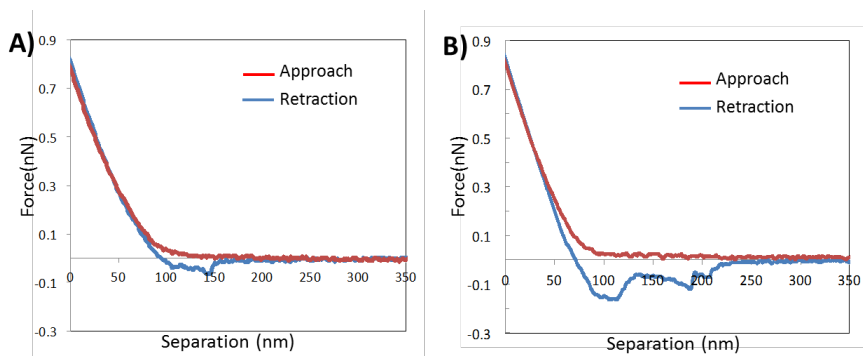


Figure 2.21 Examples of approach and retraction force curves for the pPVC surfaces modified with DA51.

Obtaining repulsive interactions in approach curves of all the modified samples as well as different spots on the same sample proved that all polymeric systems (PDMA, DA51 and PMPDSA) could efficiently cover the pPVC substrate and no bare pPVC was exposed to the AFM tip. This implies that the polymer chains were densely grafted on the surfaces.

AFM force curves and the graft density of polymer brushes will be discussed further in Section 2.2.5.2.

2.2.5.1 Molecular weight of the polymer brushes

As discussed in Section 2.2.4, one approach for estimating the molecular weight of the grafted polymer brushes is the use of sacrificial initiator in the solution and analysis of the solution polymer with a GPC-MALLS/RI system. Although this is a common practice, it is not always valid.¹⁷⁸

A method that can give a direct and more accurate measure of the polymer brush molecular weight is based on the cleavage of the polymer chains from the surfaces, then their analysis. In this method, the immobilized initiator on substrates must contain a cleavable bond. For the present experiments an initiator was synthesized with a similar structure as the main initiator (NCI), except with an ester bond instead of the amide bond (**Figure 2.11, CI**). The initiator was immobilized on pPVC surfaces as before, followed by the SI-ATRP of the monomers. The coated surfaces were washed thoroughly to get rid of (any) adsorbed polymer on their surfaces, then immersed in a 1 M aqueous sodium hydroxide solution for 4 days for the hydrolysis. Comparing ATR-FTIR spectra before and after hydrolysis (**Figure 2.22**), there was not a significant change in the intensity of amide bond. The peaks were normalized using the peak at 1426 cm^{-1} (CH_2 vibration of PVC) for comparison. The plasticizer ester peak at 1726 cm^{-1} showed some decrease while the amide peak showed no change or some insignificant increase.

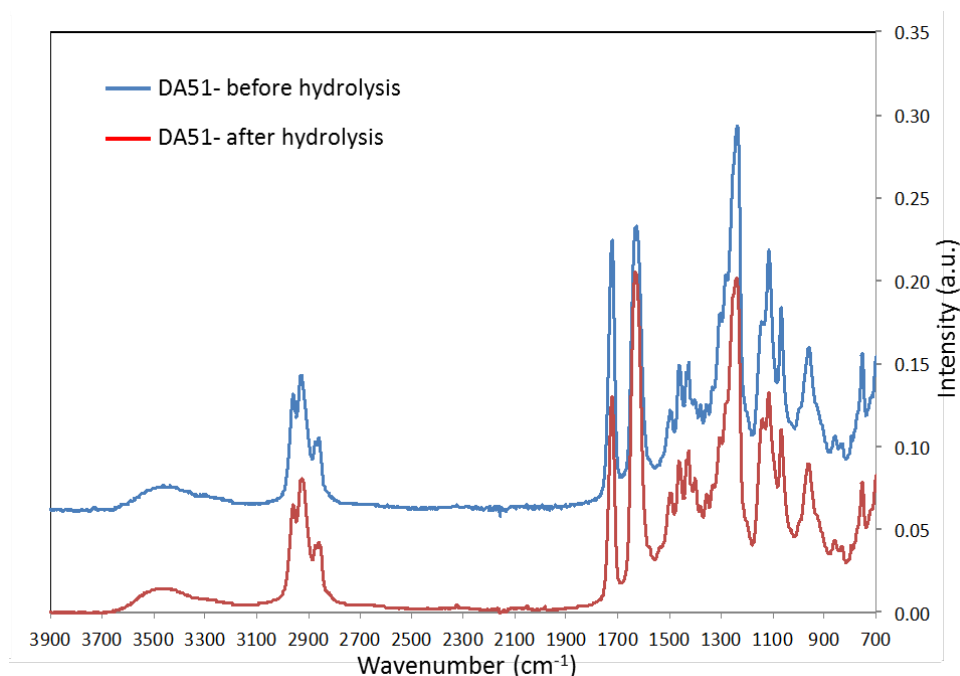


Figure 2.22 ATR-FTIR spectra of the pPVC-DA51 samples before (blue) and after (red) hydrolysis. The peak was normalized based on the PVC backbone CH_2 peak at 1426 cm^{-1} for comparison.

The water solubility of the cleavable initiator (CI) was low and its penetration in the bulk of pPVC was under question. A short ethylene glycol-containing cleavable initiator with high water solubility (**Figure 2.11, EG-CI**) was synthesized and immobilized on the surface. However a similar result to CI was observed by ATR-FTIR analysis. The product hydrolyzed from pPVC surfaces was cloudy. The solution was filtered and diluted with 20 mL of water then dialyzed against water and recovered by lyophilisation. ATR-FTIR (**Figure 2.22**) and NMR (**Figure 2.23**) spectra both confirmed that TEHTM was extracted (probably hydrolyzed to some extent) from pPVC under the hydrolysis condition. The total recovered precipitate from 25 cm² of pPVC was dissolved in D₂O for NMR analysis. The solution was filtered before running the NMR experiment to get rid of some insoluble particles, most likely the plasticizer.

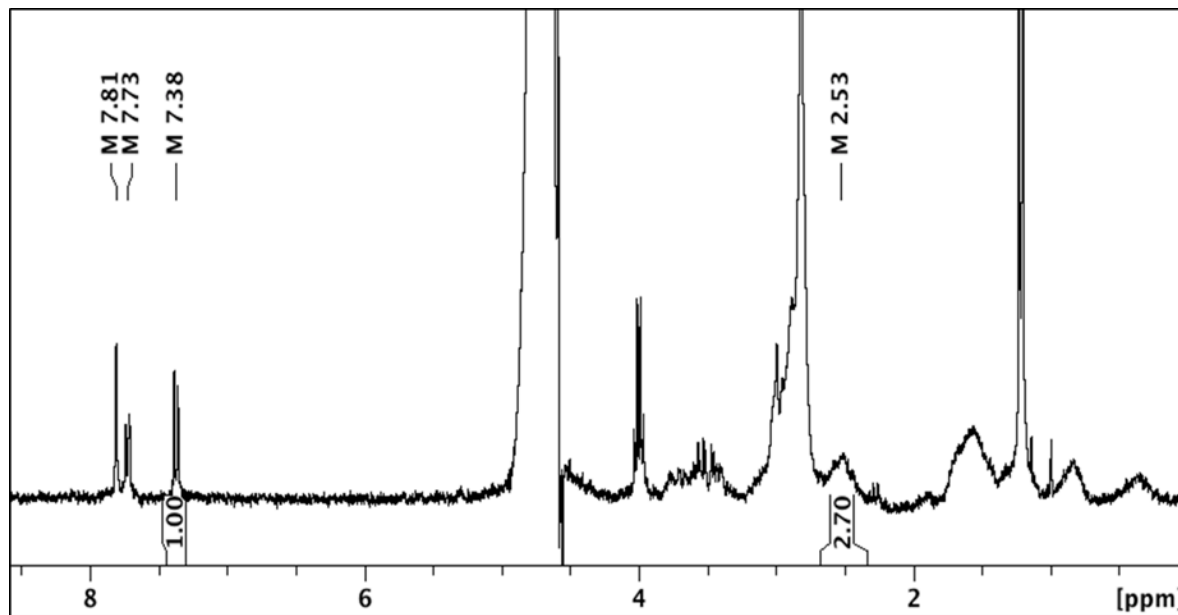
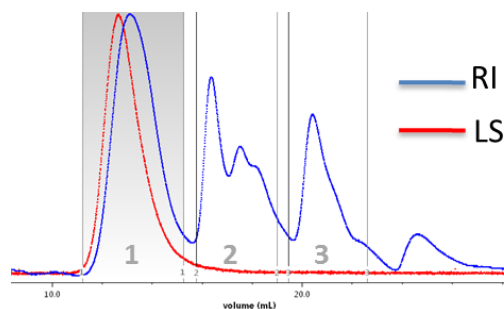


Figure 2.23 ¹H NMR spectrum of the “cleaved” mixture from pPVC-DA51 in D₂O. The peaks in the aromatic region are characteristic peaks of TEHTM (see **Figure 2.6B**). The broad peaks at 2.2-3.2 ppm are characteristic peaks of DA51 (see **Figure 2.14**).

The ¹H NMR spectrum demonstrated the presence of DA51 as well as TEHTM in the “cleaved” mixture (**Figure 2.23**). The same sample was recovered for molecular weight

determination. A GPC chromatogram also showed the presence of the plasticizer (low molecular weight) and DA51 (Peak 1) (**Figure 2.24**). The reported molecular weights for peak 2 and 3 are not precise using this setup.



	Peak 1	Peak 2	Peak 3
M_n (Da)	1.26×10^5	3.48×10^3	1.58×10^2
Polydispersity (M_w/M_n)	1.33	1.55	2.10

Figure 2.24 GPC-MALLS/RI profiles of the cleaved DA51 from pPVC.

Table 2.6 compares the molecular weight and polydispersity of the cleaved polymer with the corresponding polymer formed in solution in the presence of sacrificial initiator, and shows that solution polymers were the same order of magnitude as the grafted polymers but differed by 20-30 %.

Table 2.6 Comparison of the molecular weight and polydispersity of the grafted polymer versus the polymer formed in solution.

DA51	Cleaved from the pPVC	Formed in solution during graft polymerization
Sample 1, M_n (Polydispersity) ^a	12.6×10^4 (1.33)	9.59×10^4 (1.24)
Sample 2, M_n (Polydispersity)	9.44×10^4 (1.42)	7.77×10^4 (1.15)

^a M_n and polydispersity were measured by GPC-MALLS/RI system.

The grafted polymers showed higher molecular weight relative to the solution polymers, which was not consistent with the trend reported recently in the literature. The polymers grown from substrates generally have smaller molecular weight relative to those formed in solution

(data from organic solvents).^{178,179} Polymerization from the surface can be limited by mass transfer, particularly when the graft density and/or propagation rate is high. The termination rate is higher on surfaces and different experiments have shown that the thickness of polymer brushes reaches a plateau and does not necessarily increase by extending the reaction time.^{178,179}

Koylu and Carter reported a lower molecular weight for the solution polymers compared to the grafted one, however. Interestingly their substrate was a penetrable substrate, too.¹⁸⁰ It has been suggested that the distribution of the initiators in a three-dimensional arrangement instead of being confined to a two-dimensional plane may play a role in the distance between the brushes and the diffusion of the monomers into the layer.^{178,180} However, the reason behind the higher molecular weight has not been clarified.

In the present experiments, besides the permeability of the material, bulk PVC can also act as the initiator. It is likely but unclear if the acrylamide compatibility with PVC could increase the local concentration of monomers in the interface, which could contribute to the higher molecular weight on pPVC.

2.2.5.2 Graft density and thickness of the polymer brushes

Graft density of polymer chains is a determining factor in the barrier capacity of polymer brushes. Graft density has been shown to have a more important role than the molecular weight in introducing antifouling properties to a surface.¹³² As it was discussed earlier, penetration/growth of the polymer chains into the bulk of pPVC was an unexpected outcome of the modification method. These events challenge control over tuning the molecular weight and graft density of the polymer system, and compromise the reproducibility of the system. It should be also considered if the presence of a considerable amount of polymer in the bulk could affect

the properties of platelet bag material and its safety, e.g. by PDMA release during platelet storage. Having such limitations of the system in mind, some effort was made to obtain information about the properties of the polymer chains that were externally accessible on some of the modified surfaces for a proof of concept. To calculate the graft density of the polymer brushes on pPVC surfaces, two different approaches were taken:

i. Using the cleaved polymer chains

By obtaining molecular weight and mass of the cleaved polymer using GPC-MALLS/RI, the brush density can be measured with the following equation¹³²,

$$\sigma = \frac{W \times N_A}{M_n \times A}$$

where σ = graft density (chains/nm²), W = mass of cleaved polymer (g), N_A = Avogadro's number (mol⁻¹), M_n = number average molecular weight (g/mol), and A = surface area (nm²).

This method has been applied in our laboratory for finding the graft density of PDMA grafted from uPVC¹⁷³, and poly((methoxypolyethyleneglycol) acrylamide) grafted from polystyrene particles.¹⁵⁵

As shown in Section 2.2.5.1, TEHTM was hydrolyzed and mixed with the polymer cleaved from the pPVC surfaces. Further, as the ATR-FTIR spectra could not represent the changes on the surfaces of pPVC, it was not confirmed if all polymers on the surface were cleaved off and similarly if all the 'cleaved' polymers were sourced from the surface, not from some trapped polymers in the bulk.

Having all these limitations in mind, here is an example of the calculation of DA51 graft density using the cleavable initiator:

$$W = 228 \times 10^{-6} \text{ g}$$

The recovered 'cleaved' solid was dissolved in 300 μ L of 0.5 M NaNO₃ solution, and 200 μ L of this solution was injected in the GPC system after filtration. The calculated mass of the polymer

(peak 1 in **Figure 2.24**) by the system (RI detector) was 152 μg (equivalent to 228 μg in 300 μL).

$$N_A = 6.02 \times 10^{23} \text{ mol}^{-1}$$

$$M_n = 1.26 \times 10^5 \text{ g/mol}$$

$$A = 24.9 \times 10^{14} \text{ nm}^2$$

The actual micro surface area of pPVC must be higher than the measured surface area (24.9 cm^2) due to the roughness of the material.

$$\rightarrow \sigma = 0.43 \text{ chains/nm}^2$$

ii) Using AFM measurements

As explained in Section 2.1.1, the equilibrium thickness (L_e) of the brush in good solvents is linearly dependent on the degree of polymerization (N) and on the 1/3 power of graft density.

$$L_e = k \times N \times \sigma^{\frac{1}{3}}$$

To calculate graft density of polymer chains on pPVC using this equation, N can be calculated from the M_n of the solution polymers or better the cleaved polymers. L_e can be measured by AFM analysis.

Equilibrium thickness of the polymer brushes: Dr. Diane Goodman, a previous PhD student in our lab, developed the measurement of the thickness of PDMA brushes with different graft densities on latex particles by AFM, and her method is used here.¹⁶⁶

In the collected AFM force curve, the separation at which the interaction went into a constant compliance regime was set to be the separation = 0. This is where the tip has reached the substrate. Goodman *et al.* showed that the possible offset distance created by the incompressible polymer between the sharp tip and the latex was negligible.^{166,181}

Using the approach force curve, the equilibrium thickness was taken as the biggest separation at which the tip deviates from the baseline significantly; repulsion around 0.02 nN (**Figure 2.25**). The L_e of PDMA chains grown from pPVC found by this method was 205 ± 53 nm.

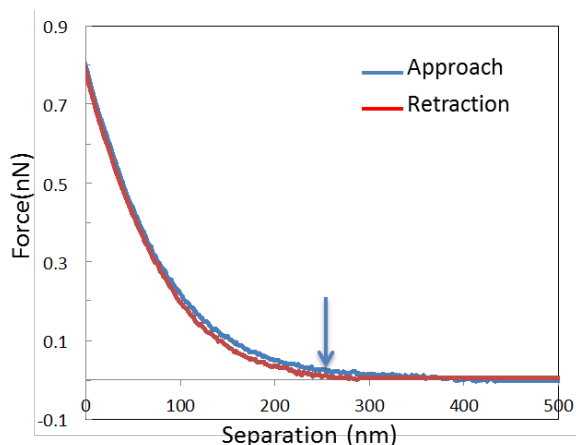


Figure 2.25 AFM force profile of the pPVC surfaces modified with PDMA. Arrow marks onset of repulsion corresponding to L_e of the PDMA.

Goodman *et al.* showed that at high graft density, L_e approached the contour length (L_c) of the polymer chains.¹⁶⁶ L_c is the length of a polymer chain at its maximum possible extension.

The L_c of PDMA chains was calculated using the M_n of the solution PDMA formed during SI-ATRP. Each monomer unit length is equivalent to two projected C-C bonds i.e. 0.25 nm. PDMA with M_n of 1.82×10^5 has around 1838 repeating units, which makes the L_c of PDMA around 460 nm, around twice the L_e calculated by AFM. The value of L_e/L_c (~ 0.5) corresponds in literature to the polymer brushes with a high graft density.¹⁶⁶

Graft density of the polymer brushes: Having the N (degree of polymerization) and L_e (brush thickness), graft density can be calculated according to the equation $L_e = k \times N \times \sigma^{\frac{1}{3}}$ if k is known.

An example for PDMA brushes:

$L_e = 265 \text{ nm}$
Found by AFM

$$k = 0.51 \text{ nm}^{5/3} \text{ }^{182}$$

This value has been calculated in the referred literature for a monomer with a bigger side chain than DMA side chain. The k value for DMA could be slightly lower than this value.

$$N = 1840$$

→ $\sigma = 0.02 \text{ chains/nm}^2$ by using the equation that $L_e \propto \sigma^{1/3}$.

To understand if the polymer chains with a graft density of 0.02 chains/nm^2 are in a polymer brush regime or not, the $D < 2 R_g$ was tested. As shown in Section 2.1.1, D is the distance between the grafting points and R_g is radius of gyration.

$$^{86} D = \frac{1}{\sqrt{\sigma}} = 7 \text{ nm}$$

$$^{183} R_g^2 = \frac{N \times l^2}{6} = \frac{1840 \times (0.25 \text{ nm})^2}{6}$$

Where N is the degree of polymerization and l is the monomer unit length.

$$R_g = 4.4 \text{ nm}$$

→ $D < 2 R_g$ or the grafted polymer chains are in brush regime.

As discussed in section 2.1.1, the power of dependency of L_e on graft density changes with a change in graft density. For example, the power of dependency was reported to be 0.6 ($L_e \propto \sigma^{0.6}$) for poly(methyl methacrylate) with a graft density between 0.4 and 0.7 chains/nm² ($0.4 < \sigma < 0.7$) in a good solvent system.⁹³ The solvent system in that example was not water so their findings are not necessarily valid in our polymer system. However, considering the high graft density obtained from the “cleaving” method, 0.43 chains/nm^2 , the graft density was recalculated using the equation $L_e = k \times N \times \sigma^{0.6}$, which gave $\sigma = 0.12 \text{ chains/nm}^2$; again confirming that the configuration of the chains was in the polymer brush regime.

2.3 Results and Discussion: *In Vitro* Evaluation of the Modified pPVC Samples

2.3.1 Bacterial adhesion

Bacterial adhesion is the first step in biofilm formation on biomaterials. Inhibition of the physicochemical interactions between bacteria and substrate can prevent the bacterial adhesion hence biofilm formation. Less bacterial adhesion on platelet bag surfaces implies that more bacteria stay in a planktonic state and have a chance to be sampled during sample withdrawal for bacterial screening.

Some of the pPVC samples modified with the hydrophilic polymer brush system were challenged with a high concentration of a coagulase negative *Staphylococcus* strain, *S. aureus*. As discussed in the Chapter 1, staphylococci are among the common sources of platelet contamination.

Copper and copper salts have some bactericidal activity. To make sure there is no copper left on pPVC surfaces, pPVC samples were thoroughly washed with water after ATRP and immersed in water for at least two hours. Samples were rinsed again with water. XPS survey screening did not detect any copper on the surfaces. The washing was kept consistent for all the samples.

Each 0.4×0.9 cm piece of control pPVC or modified pPVC was vertically immersed in 1×10^6 CFU/mL (colony forming units/mL) of *S. aureus* in Luria broth (LB). After 4 h of incubation at 37 °C without shaking, samples were gently washed in sterile PBS pH 7.4 to get rid of loosely adhered bacteria, then fixed for scanning electron microscopy (SEM) experiments. **Figure 2.26** shows the representative images of the surfaces after 4 h (**Figure 2.26A**) and 8 h (**Figure 2.26B, 2.26C**) of incubation, respectively. The pPVC surfaces modified with PDMA and DA51 polymer could inhibit bacterial adhesion efficiently during 4 and 8 h of incubation.

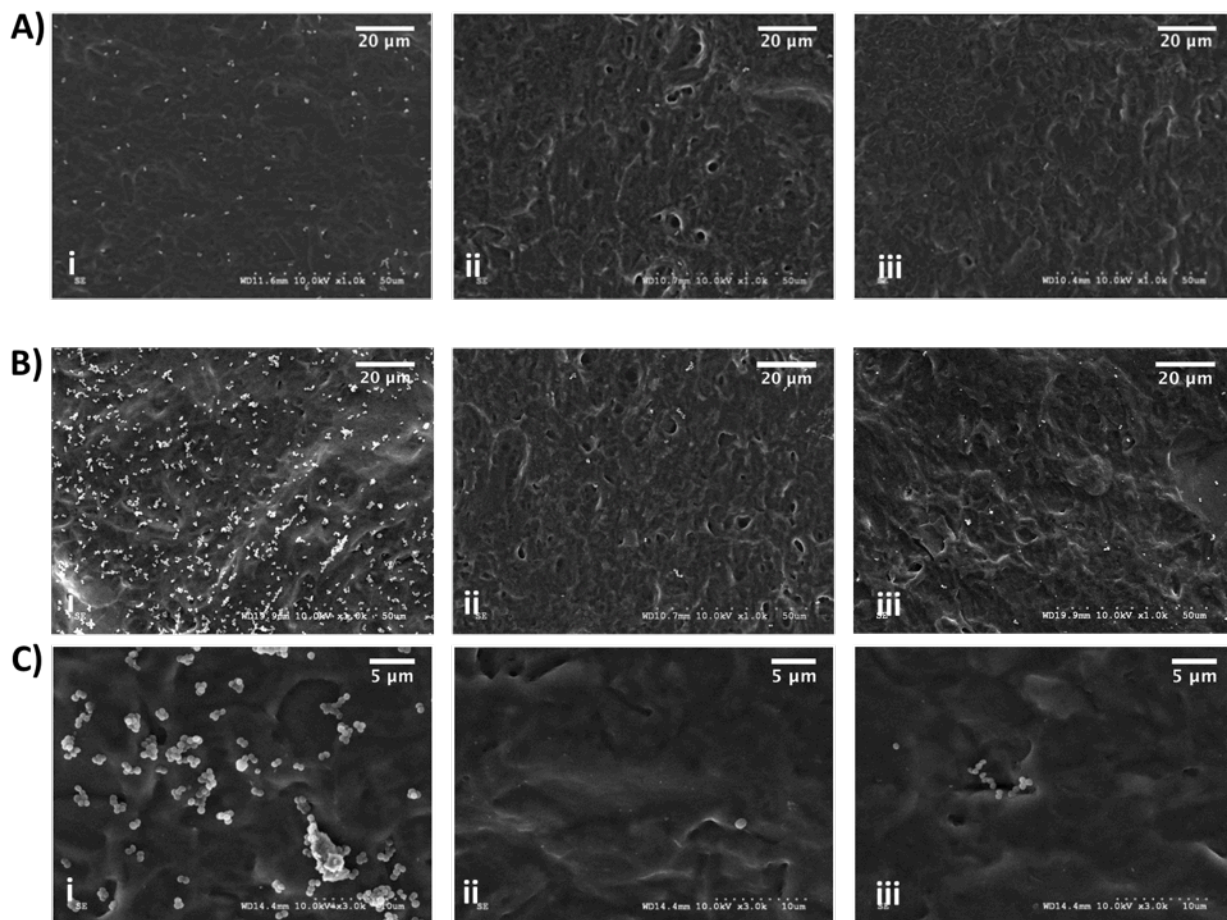


Figure 2.26 Adhesion of *S. aureus* on the samples after 4 h (A) and 8 h (B and C) incubation at 37 °C. Higher number of bacteria adhered on control pPVC samples (i) than on the modified pPVC samples with PDMA (ii) and DA51 (iii) polymer brushes. Ci-Ciii were imaged at higher magnification.

To quantify the differences between the samples, the samples incubated with the bacteria for 4 h were first washed with sterile PBS. Then the adhered bacteria on the surfaces were dislodged with sonication, cultured on LB agar plates and counted. **Figure 2.27** compares the number of adhered bacteria on the modified surfaces versus control pPVC (set as 100 %) using the dislodging method. PDMA coating in particular showed high resistance against bacterial adhesion and could decrease the adhesion of *S. aureus* to as low as 5 % of the control. Variation among the control pPVC samples was observed (around ± 15 %). The zwitterionic polymers and

DA21 and DA11 showed less efficiency in the resistance against bacterial adhesion. Their results are not included in **Figure 2.27** because not enough repeats of experiments were performed to give significant results.

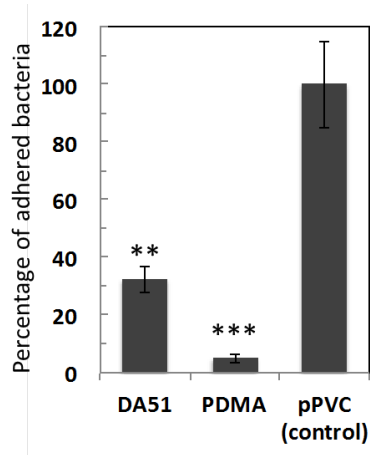


Figure 2.27 Level of *S. aureus* adhesion on pPVC surfaces modified with DA51 and PDMA in comparison with the control pPVC. ** P<0.01 and *** P<0.005

It should be noted that pPVC has one textured face and one non-textured face (**Figure 2.28**). All reported characterizations such as water contact angle measurement, AFM, and SEM were performed on the non-textured faces of pPVC. The dislodging method, however, provides bacteria detached from both faces of pPVC.

Platelets are stored at 22 °C in blood banks and the applied experimental conditions here (37 °C, bacteria culture media instead of platelet concentrate, and high concentration of bacteria (10⁶ CFU/mL)) are significantly more challenging.

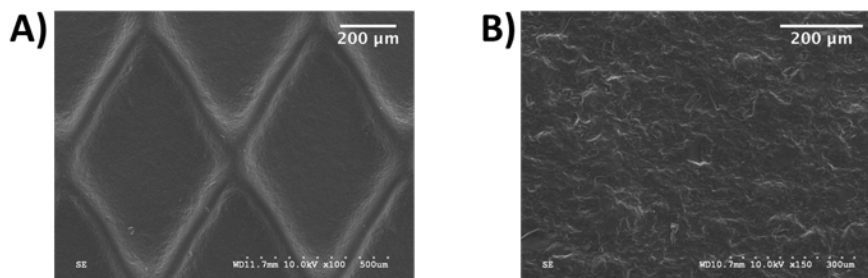


Figure 2.28 pPVC has one textured face (A) and one non-textured face (B).

2.3.2 Platelet adhesion

To evaluate if the developed polymer brushes on surfaces could decrease platelet adhesion and activation on surfaces, control and modified pPVC samples were immersed vertically in platelet-rich plasma in a 96-well plate for 4 h at 37 °C. The samples were gently rinsed in sterile PBS and fixed.

Figure 2.29 shows the platelet adhesion on control pPVC samples and the modified samples. As explained in Chapter 1, activated platelets form some pseudopods. Such structures can be seen on the control samples while the platelets on the modified samples could preserve the normal round discoid shape.

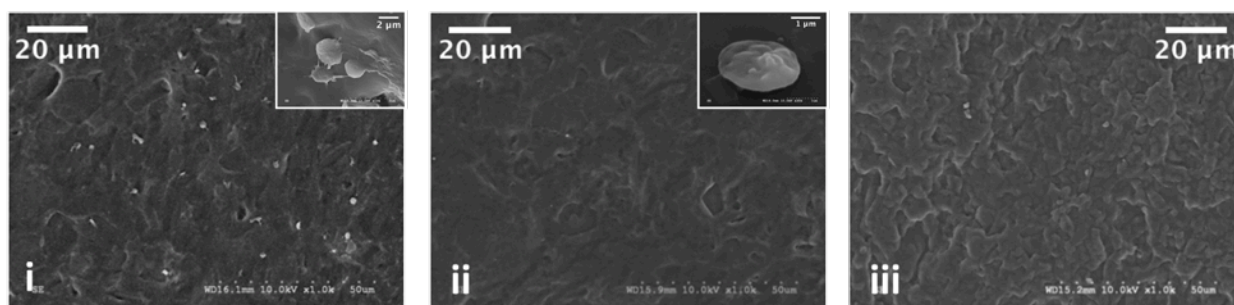


Figure 2.29 Platelet adhesion on pPVC (i), pPVC-PDMA (ii) and pPVC-DA51 (iii) after 4 h incubation at 37 °C. Inset: higher magnification.

The experiment conditions here were different from blood bank storage conditions. In addition to the difference in temperature (22 °C in blood banks), platelets were in constant contact with the 96-well plate material, polystyrene, which could stimulate platelet activation. Another difference in the conditions of platelet adhesion experiments as well as bacterial adhesion experiments was the vertical orientation of the samples. As shown in Chapter 1 platelet bags are positioned horizontally in the platelet incubator. To accelerate activation and adhesion of platelets within the short incubation time of 4 h, platelets were stored at 37 °C.

To evaluate platelet adhesion on the modified pPVC samples under conditions similar to blood banks and in particular, omitting the interaction of 96-well plate material with the platelets, platelet evaluation tests must be performed in the platelet bags. However, platelet storage bags are filled with around 200 mL of platelets which makes this scale of platelet tests unjustifiable.

As a proof of concept in a batch experiment, two commercial platelet bags were modified with PDMA. These bags had smaller size (13×16 cm) compared to the currently used Canadian Blood Services platelet bags (22×16 cm). The bags' main composition was PVC and TEHTM, the same as the main components of the pPVC material used so far in this thesis, but had a different topography. The details of the bags' modification are reported in the Methods and Materials Section. Briefly, bags were cut and opened to be exposed to the allylamine plasma. They were resealed after the amination and other steps including initiator coupling and ATRP were performed inside the bags. The modified and control bags were sterilized using gamma irradiation and filled with 50 mL of platelet-rich plasma. After 7 days of storage under blood bank conditions ($22\text{ }^{\circ}\text{C}$, horizontally positioned on platelet agitators), the bags were cut and opened. Five pieces from the lower face of each bag were imaged by SEM. The inner surfaces of these bags were textured. As seen in **Figure 2.30**, more platelets adhered on the control bags and most of them looked fully activated. The number of adhered platelets even after 7 days of storage is small enough that it is unlikely to have a significant effect on the number of transfused platelets. However activated platelets release activating factors that might compromise the quality of the bulk platelets. Adhered platelets also promote bacterial adhesion on surfaces. **Figure 2.30** shows that fewer platelets adhered on the surfaces of the platelet bags modified with PDMA compared to the control bags, and no aggregates of platelets were observed.

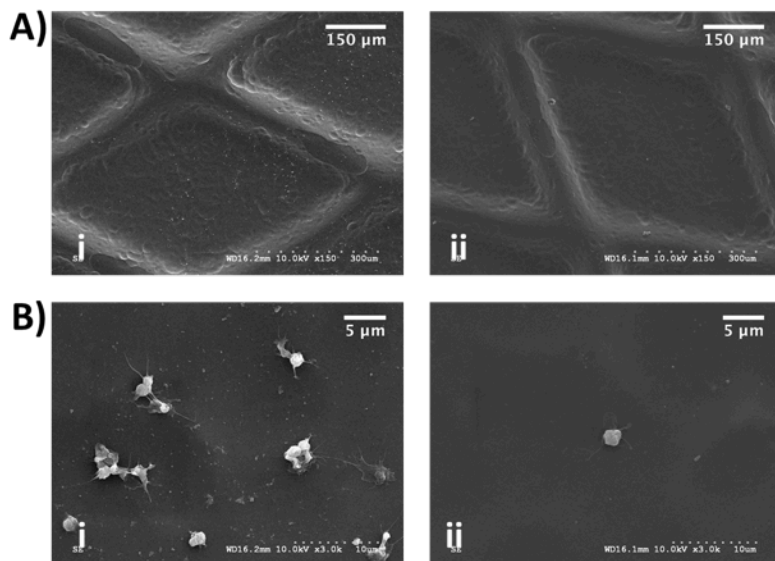


Figure 2.30 Platelet adhesion on pPVC (i) and pPVC-PDMA (ii) after 7 days of storage under blood bank conditions. Bi and Bii were imaged at higher magnification.

This experiment confirmed the biocompatibility of PDMA with platelets. Further, it showed that gamma sterilization was a compatible method for sterilization of the coated platelet bags.

2.4 Conclusions

SI-ATRP is a simple and efficient method to develop hydrophilic polymer brushes on pPVC. It provides the advantages of using water as the solvent, which is beneficial where the monomers are hydrophilic and the substrate, here pPVC, is not compatible with organic solvents. Allylamine plasma can coat pPVC surfaces uniformly and be a substitute for the conventional wet reactions that can disturb the properties of pPVC.

Water contact angle measurements, AFM and *in vitro* studies confirmed the formation of densely grafted hydrophilic polymer chains or hydrophilic polymer brushes on the surfaces. ATR-FTIR studies along with some control experiments showed the presence of PDMA or DA

polymers inside the bulk of pPVC material with a possible source of growth from labile chlorine in PVC and/or penetration of solution polymers into the bulk pPVC. Cleavage of the polymers from pPVC surfaces became complicated by leaching out of plasticizer and the limitations of ATR-FTIR in tracking the hydrolysis progress and completion.

AFM studies on the modified pPVC surfaces in comparison with control pPVC proved the barrier capacity of the developed hydrophilic PDMA, PMPDSAH and DA51 against hydrophobic interactions. PDMA and DA51 could inhibit bacterial and platelet adhesion on pPVC surfaces under accelerated growth (for bacteria) and activation (for platelets) conditions, which confirmed the barrier capacity of the developed hydrophilic coating.

The presence of polymer in the bulk of the material, limitations on characterization and lack of definitive control over the sources of polymer formation and consequently on the molecular weight and the graft density of the polymer chains on the surfaces were challenges with the development of polymer brush systems on pPVC surfaces.

2.5 Methods and Materials

Platelet bag material (Solmed EH-222) mainly composed of PVC and TEHTM was generously provided by the American Renolit Corporation and is denoted here as pPVC for plasticized PVC. All chemicals were purchased from Sigma-Aldrich and used as received unless stated otherwise. APMA (98 %) was from Polysciences. DMA (99 %) was distilled and stored in the refrigerator until use. Copper (I) chloride (1g) was purified by dissolving it in concentrated (37 %) hydrochloric acid (3 mL). Distilled water was added slowly to the black solution until no more white precipitate formed (around 12 mL of water). The precipitate was separated with suction filtration and washed with anhydrous ethanol then diethyl ether. The white powder was

stored in a vacuum desiccator.

Dialysis was performed in regenerated cellulose tubes from Sigma-Aldrich (D7884, molecular weight cut-off (MWCO) of 1000 Da). Deionized water was used for all the reactions, prepared by Milli-Q water purification system with a resistivity of 17.9 mΩ/cm. Distilled water was used for all other applications such as washing steps, dialysis and dilutions.

^1H and ^{13}C **NMR** spectra were recorded on either Bruker Avance 300MHz or 400 MHz NMR spectrometer. Peaks are reported in ppm referenced to the residual solvent signal.

TOF-SIMS analyses were performed using a TRIFT V nano TOF (Physical Electronics) instrument. Samples were transferred into the analytical chamber with a base pressure of $\sim 2 \times 10^{-9}$ Torr. A 30 keV Au⁺ pulsed primary ion source was used for all measurements. Mass calibration for the positive mode was carried out using H, CH₃ and C₂H₅. The data were analyzed using WincadenceN 1.8.1 software program from Physical Electronics.

A **M4L radio frequency gas plasma system** (PVA Tepla Inc.) was used for allylamine plasma treatment.

XPS was performed using a Leybold LH Max 200 surface analysis system equipped with Mg and AlK α sources at a power of 200 W. Elements were identified from survey spectra.

Thickness measurements were carried out on a variable angle spectroscopic **ellipsometer** (model VASE, J.A. Woollam Inc.) at incident angles of 55°, 65° and 75° in the wavelength range 480–900 nm. Data were processed using a Cauchy model in the WVASE32 software package. The refractive index of the polymer layers was set as 1.40 for the normal fit.¹⁸⁴

Static **water contact angles** were determined by placing a water droplet of 3 μL on the surface. A picture of the droplet was taken using a digital camera (Retiga 1300, Q-imaging Co.) and measured using Northern Eclipse software.

The absolute molecular weights of polymers were determined by **GPC** on a Waters 2695 separation module fitted with a DAWN EOS MALLS detector (laser wavelength $\lambda=690$ nm), coupled to an RI detector, both from Wyatt Technology Corp. Aqueous NaNO_3 (0.5 N, buffered at pH 7) was used as a mobile phase at a flow rate of 0.8 mL/min. The dn/dc value used for the molecular weight calculation of polymer was 0.15 mL/g.

ATR-FTIR spectra were recorded using a Thermo-Nicolet Nexus FTIR spectrometer with a MCT/A liquid nitrogen cooled detector, a KBr beam splitter and MKII Golden Gate single reflection ATR accessory.

AFM Measurements were performed on a Multimode, Nanoscope IIIa controller (Digital Instruments), equipped with a fluid cell. The rate of tip-sample approach was 500 nm/s.

S. aureus-Xen29 ATCC 12600 was from Perkin Elmer. LB powder was purchased from Thermo Fisher Scientific. The commercially available 25 % glutaraldehyde solution was diluted to 2.5 % using distilled water before use. The fixed samples were gold coated before **SEM** (S3000N Hitachi) imaging using an Edwards S150A sputter coater with gold deposition rate of 15 nm/minute for 30 seconds.

2.5.1 Development of polymer brushes on platelet storage bags

2.5.1.1 Amination of substrates

Allylamine plasma or the “dry method”: pPVC coupons were sonicated in distilled water and air dried overnight. Silicon wafers were washed with ethanol then flamed over a Bunsen burner until they became red. Substrates were positioned in the center of the middle tray of the M4L facing up for the treatment (the M4L carries five trays). Samples were pretreated with nitrogen plasma for three minutes at 75 watts, followed by allylamine plasma treatment for 10 minutes at

100 watts. Samples were sonicated in distilled water for 30 minutes. pPVC samples were air dried overnight before water contact angle measurements. Silicon wafers were dried with nitrogen flow before characterizations.

For the experiments that required both faces of pPVC to be modified with polymer brushes (quantitative bacterial adhesion tests as well as the growth (followed by hydrolysis) of the polymer brushes from the cleavable initiators), pPVC coupons were hung from the second tray (in the chamber space between trays 2 and 3) using some elastic bands.

For modification of platelet storage bags, the bags were cut open from the sides without a port (**Figure 2.31A**). The inner faces of the bags were faced up on the third tray of the M4L and treated with allylamine plasma (**Figure 2.31B**).

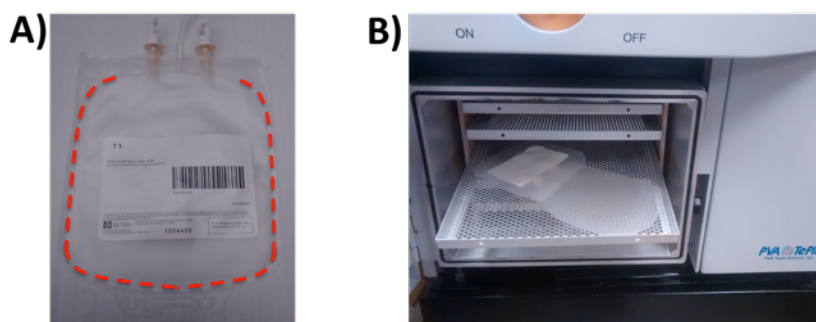


Figure 2.31 Opening the platelet storage bag (A) and exposing it to allylamine plasma (B).

The bags were washed with water and sonicated in water for 30 minutes. The bags were dried overnight and resealed using a heat sealer (American International Electronic Inc. AIE-305HD).

“Wet method”: Silicon wafers were first washed with ethanol then flamed over a Bunsen burner until they became red. The samples were immersed in a 25 % (v/v) solution of APTES in anhydrous toluene. In our setup, 2 × 2 cm silicon wafers were put in a 35 mL low form cylindrical weighing bottle with a ground glass stopper (Kimble 15165-5030) and filled with 12

mL of the reaction solution (3 mL APTES in 9 mL anhydrous toluene). Argon was purged on top of the solution, capped and kept for 3 h without shaking or stirring. The samples were consecutively washed with toluene, DMSO (dimethyl sulfoxide), acetone, and methanol. Samples were dried with a flow of nitrogen before characterization.

2.5.1.2 Synthesis of initiators

Synthesis of NCI: 2-Chloropropionyl chloride (12.3 mL, 0.126 mol) was added dropwise to a solution of allylamine (7.90 mL, 0.100 mol) and triethylamine (17.5 mL, 0.126 mol) in 150 mL anhydrous dichloromethane (CH_2Cl_2 or DCM) at 0 °C. After 40 minutes of stirring in an ice bath, the reaction was continued at room temperature for 20 h. The content was then filtered to remove the white precipitate (salts). The filtrate was washed with 20 mL of 2 M HCl solution, 30 mL of saturated sodium bicarbonate solution, and 20 mL of water consecutively. Then it was dried over anhydrous sodium sulfate. After removing the solvent a brown oily product was obtained. The crude product was purified by silica gel column chromatography (eluent: ethyl acetate/ hexane 10 %) to obtain the pure intermediate, *N*-allyl-2-chloropropanamide (13 g, yield ~ 85 %) (^1H NMR spectrum is shown in Appendix A1).

A solution of 6 grams (41 mmol) of the intermediate in 200 mL anhydrous DCM was treated with 12.7 grams (1.8 molar equivalent) of 3-chloroperoxybenzoic acid at room temperature. After stirring for 40 h, the mixture was filtered to separate the salt. The filtrate was kept in the fridge overnight and the formed precipitate was filtered again. The filtrate was washed with saturated aqueous sodium bisulfite (75 mL) and sodium bicarbonate (100 mL) solution successively, and finally with water (30 mL). The organic phase was dried over

anhydrous sodium sulfate, and purified by column chromatography (eluent: ethyl acetate/hexane 10 %) to give NCI (yellow solid) with a yield of 40 % (2.6 g).

Synthesis of NCI-Br: A similar procedure was used for the synthesis of the bromine containing non-cleavable initiator (NCI-Br). 2-Chloropropionyl chloride was substituted with 2-bromopropionyl bromide (caution: corrosive fumes) (13.2 mL, 0.126 mol). The final product was a yellow solid and the overall yield was 30 %.

Synthesis of CI: 2-Chloropropionyl chloride (12.3 mL, 0.126 mol) was added dropwise to a solution of glycidol (6.70 mL, 0.1 mol) and triethylamine (17.5 mL, 0.126 mol) in anhydrous DCM (200 mL) at 0 °C. After one hour mixing in an ice bath, stirring continued at room temperature for 20 h. The reaction mixture was filtered and the filtrate was washed with water. After drying over anhydrous sodium sulfate, the solution was concentrated to give a brown oily product. The crude product was purified by column chromatography (eluent: ethyl acetate/hexane 5 %) and gave a clear oil. (10 g, yield ~ 60 %)

Synthesis of EG-CI: A fresh cut of sodium (0.85 g, 0.04 mol) was washed in hexane and cut in small pieces. Sodium pieces were added to isopropanol (80 mL) and mildly refluxed for 3 h until completely dissolved. The solution was cooled to room temperature. Diethylene glycol (3.8 mL, 0.04 mol) was added slowly to the solution and stirred. Epichlorohydrin (31 mL, 0.4 mol) was added dropwise to the mixture. After 20 h of stirring at room temperature, the mixture was evaporated. The concentrate was dissolved in DCM (100 mL) and washed with 25 mL of water. The organic phase was dried over sodium sulfate and purified using column chromatography (Eluent: initially methanol/DCM 1 % was used then changed to methanol/DCM 2 %, under which the product was obtained).

2-Chloropropionyl chloride (0.84 mL, 8.5 mmol) was added dropwise to a solution of the synthesized intermediate (1.1 g, 6.8 mmol) and triethylamine (1.2 mL, 8.5 mmol) in 75 mL anhydrous DCM at 0 °C. After 40 minutes of stirring in an ice bath, the reaction was continued at room temperature for 24 h. The content was concentrated under vacuum. The oily crude product was dissolved in 50 mL DCM washed with 10 mL saturated sodium bicarbonate solution, and dried over anhydrous sodium sulfate. After solvent evaporation, a yellowish oily product was obtained which was purified using column chromatography (eluent: ethylacetate/hexane 20 %). The pure product (EG-CI) was a clear oil (overall yield ~ 20 %).

2.5.1.3 Immobilization of initiators

The aminated pPVC or silicon wafers were immersed in a 1 % w/v solution of the synthesized ATRP initiator in 10 mM PBS solution pH 7.5 for 12 h at 45 °C. The samples were washed with water then sonicated in water for 5 minutes. The samples were air dried overnight before characterization. Silicon wafers were dried by nitrogen flow.

For platelet bag modification, the bags were filled with a 1 % solution of the initiator and immersed in a water bath with a shaker at 30 rpm (reciprocal shaking bath, Thermo Scientific 2870) at 45 °C for 12 h. The bags were cut and opened as before, washed and sonicated in water for 5 minutes, and air dried overnight.

2.5.1.4 Surface-initiated ATRP

This step was carried out in a glove box filled with argon at room temperature. Milli-Q water was degassed with four cycles of freeze-vacuum-thaw and a DMA aliquot was degassed with argon flow for 20 minutes. The degassed water and DMA along with other chemicals were

transferred to a glove box filled with argon. **Table 2.7** shows the reactants used for different polymerizations.

For DA51, for example, DMA (500 mg, 5 mmol) and APMA·HCl (178 mg, 1 mmol) were dissolved in water (4 mL). CuCl (3.7 mg, 37 μ mol) was mixed with 1, 1, 4, 7, 10, 10-hexamethyl triethylene tetramine (HMTETA) (22 μ L, 80 μ mol) in water (0.5 mL) and added to the monomer solution along with CuCl₂ (0.5 mg, 3.7 μ mol). To add 0.5 mg of CuCl₂, 4 mg of CuCl₂ was transferred in the glove box and dissolved in 800 μ L of degassed water, and 100 μ L of this solution was added to the reaction mixture.

The final solution was shaken and filtered using a 0.45 μ m syringe filter into a new vial. The pPVC samples were immersed in the solution. In the reaction with the presence of sacrificial initiator, initiator was added to the reaction solution (3.7 μ mol) to produce polymer in the solution. For NCI, this is 0.6 mg, so 6 mg of NCI was dissolved in 100 μ L of water and 10 μ L of it was transferred to the polymerization solution.

The reaction was stopped after 24 h. pPVC samples were washed thoroughly in water and immersed in water at least for 2 h and washed again. Characterizations were performed after overnight air-drying. The solution was dialyzed (MWCO 1000 Da) against distilled water for 3 days with water changed every 12 h.

Table 2.7 Polymerization conditions for different samples

Sample	Description	Monomers	CuCl	*CuCl ₂	HMTETA	KCl
PDMA	PDMA	DMA 200 mg (2mmol)	3.7 mg	0.5 mg	22 μL	-
DA51	P(DMA/APMA) (5/1)	DMA 500 mg (5 mmol) APMA 180 mg (1 mmol)	3.7 mg	0.5 mg	22 μL	-
DA41	P(DMA/APMA) (4/1)	DMA 480 mg (4.8 mmol) APMA 216 mg (1.2 mg)	3.7 mg	0.5 mg	22 μL	-
DA21	P(DMA/APMA) (2/1)	DMA 400 mg (4 mmol) APMA 360 mg (2 mmol)	3.7 mg	0.5 mg	22 μL	-
DA11	P(DMA/APMA) (1/1)	DMA 300 mg (3 mmol) APMA 540 mg (3 mmol)	3.7 mg	0.5 mg	22 μL	-
PMPDSAH	PMPDSAH	MPDSAH 1.75 g (6 mmol)	3.7 mg	0.5 mg	22 μL	74.5 mg
MA51	P(MPDSAH/APMA) (5/1)	MPDSAH 1.46 g (5 mmol) APMA 180 mg (1 mmol)	3.7 mg	0.5 mg	22 μL	74.5 mg
MA41	P(MPDSAH/APMA) (4/1)	MPDSAH 1.40 g (4.8 mmol) APMA 216 mg (1.2 mmol)	3.7 mg	0.5 mg	22 μL	74.5 mg
MA21	P(MPDSAH/APMA) (2/1)	MPDSAH 1.17 g (4 mmol) APMA 360 mg (2 mmol)	3.7 mg	0.5 mg	22 μL	74.5 mg
MA11	P(MPDSAH/APMA) (1/1)	MPDSAH 876 mg (3 mmol) APMA 540 mg (3 mmol)	3.7 mg	0.5 mg	22 μL	74.5 mg

*CuCl₂ (4 mg) was dissolved in degassed water (800 μL), and 100 μL of this solution was transferred to the reaction solution.

Solvent was milli-Q water (5 mL) in all experiments.

For platelet bag modification, the bags modified with initiators were resealed after drying, and transferred to the glove box. For each bag 70 mL of polymerization solution was prepared. The reactants were transferred to the glove box and mixed as explained above: DMA (5.60 g, 56.0 mmol), CuCl (103 mg, 1.04 mmol), CuCl₂ (10.0 mg, 0.07 mmol), HMTETA (600 μL, 2.2 mmol) in ~ 140 mL water. The initiator NCI (17 mg) was added to the solution. The polymerization solution was filtered and divided between two bags and put on a shaker in the glove box for 24 h. The solution was removed after this period and the bags were washed with water 5 times (cycles of filling and emptying the bags). The bags were filled with water and put on the shaker overnight, then washed again with 5 cycles of water filling and emptying. Sterile

PBS (10 mL) was added to each modified and also control (untreated) bags and sent to the Canadian Blood Services' clinic in Oak Street, Vancouver for gamma sterilization.

2.5.1.5 Cleavage of polymer brushes

The modified surfaces were washed thoroughly to remove any adsorbed polymer on their surfaces. The sample (total double side surface area: 24.9 cm²) was cut in four pieces and immersed in 5 mL of 1 M sodium hydroxide solution for 4 days at room temperature. The samples were removed and washed with 2 mL of water, which was added to the hydrolysis solution. The mixture was filtered to remove insoluble particles. The filtrate was diluted with 20 mL of water then dialyzed against water and recovered by lyophilisation. Around 2 mg of a yellow powder was obtained from a 25 cm² pPVC sample. The solid was dissolved in 1 mL of D₂O. The insoluble particles were filtered out before NMR experiments. The sample was recovered after NMR experiment by lyophilisation and used for GPC-MALLS/RI analysis.

2.5.2 *In vitro* evaluation of the modified surfaces

2.5.2.1 Bacterial adhesion

LB medium was prepared by dissolving 25 g of the powder in 1 litre of distilled water. LB and PBS pH 7.4 (10 mM) were sterilized by autoclaving before use. *S. aureus* (20 µL) was transferred from the frozen stock into LB medium (4 mL) and incubated for 10 h at 37 °C without shaking. A 10 µL aliquot of this culture was subcultured again in LB (4 mL) and the optical density (OD) of the culture was measured at 595 nm after 8 h. Knowing that an OD of 0.1 represents 1×10^8 CFU/mL of *S. aureus*, a bacterial inoculum containing 1×10^6 CFU/mL was prepared. For example, to prepare a 10 mL suspension of 1×10^6 CFU/mL *S. aureus* from a

culture with an OD of 0.15 ($OD_{\text{culture}} - OD_{\text{LB}}$), 67 μL of this culture was transferred to 10 mL of LB. The final concentration was verified by serial dilution and spotting on LB agar plates.

Imaging of adhered bacteria: pPVC coupons, 0.4×0.9 cm, were immersed in 70 % ethanol for 10 minutes and washed five times with sterile PBS. Each coupon was vertically immersed in one well of a sterile 96-well plate. The bacterial inoculum ($310 \mu\text{L}$ of 1×10^6 CFU/mL) was added to each well and incubated at 37°C for either 4 h or 8 h without shaking. Each coupon was thoroughly rinsed by consecutive immersion in 5 sterile PBS vials, one minute in each. The coupons were fixed in a 2.5 % v/v glutaraldehyde solution for one hour, rinsed with water and dehydrated with graded ethanol concentrations (30, 60, 85, and 100 %), 10 minutes in each concentration. Coupons were stored in a desiccator. The non-textured faces of the pPVC samples were gold coated using an Edwards S150A sputter coater with gold deposition rate of 15 nm/minute for 30 seconds, and studied by SEM.

Dislodging and counting the released bacteria: pPVC coupons, 0.4×0.9 cm, were sterilized and incubated as above. After 4 h, each coupon was consecutively immersed in 5 sterile PBS vials. Each coupon was then transferred to a sterile 0.6 mL Eppendorf safe-lock tube containing 0.5 mL of sterile PBS and was sonicated for 10 minutes. The sonicator (Branson 3200) was filled with water up to 4 cm below the top and the samples were immersed in the water using a floating foam tube rack. The detached bacteria were subjected to 10-fold serial dilutions to give dilutions of 10^{-3} to 10^{-6} and 10 μL of each dilution was spotted on LB agar plates in triplicate and counted after incubation for about 15 h at 37°C .

To prepare LB agar plates, LB powder (25 g) and agar (15 g) were dissolved in 1 L of distilled water and autoclaved. When the solution cooled down enough to be handled, it was

divided among the agar plates in a sterile safety cabinet; ~20-25 mL of media was poured in each 10 cm plate.

2.5.2.2 Platelet adhesion

Platelet preparation: Fresh venous blood was collected from unmedicated healthy adult volunteers after obtaining their informed consent. The protocol was approved by the University of British Columbia Clinical Ethics Committee. Platelet-rich plasma was prepared by centrifuging citrate anticoagulated blood (using sodium citrate: blood 1:9) at 195xg (Allegra X-22R Centrifuge, Beckman Coulter) for 15 min at 22 °C.

Imaging of adhered platelets on coupons: Each pPVC sample, 0.4 × 0.9 cm, was rinsed with sterile PBS and put vertically in 310 µL of platelet-rich plasma (around 4×10⁸ platelets/mL) in a well of a 96-well plate and incubated for 4 h at 37 °C without shaking. The samples were gently rinsed in sterile PBS three times, fixed and gold coated as above. The non-textured faces of the pPVC samples were gold coated and studied by SEM.

Imaging of adhered platelets inside platelet bags: The sterile PBS (10 mL PBS had been added to each bag before gamma sterilization) was removed from the platelet bags in a safety cabinet. Platelet concentrate was provided by the Canadian Blood Services Network Centre for Applied Development (NetCad). Platelet bags were filled with 50 mL of the platelet concentrate and incubated in a 22 °C platelet incubator with agitation at 70 cycles per minute (Model 3606 and 4720, Forma Thermo Scientific). After 7 days of storage, the bags were emptied and cut. Pieces were cut from the lower face of the platelet bags and washed gently in PBS three times. Samples were fixed, dehydrated and gold coated as above. The inner surfaces of these bags were made of the textured material.

CHAPTER 3: Development of Bactericidal Polymer Brushes for Platelet Storage Bags

This chapter starts with an introduction to antimicrobial peptides (AMPs) and immobilization of bactericidal agents including AMPs on surfaces. Then it focuses on polymer brushes incorporating AMPs. Sections 3.2 to 3.5 focus on conjugation of AMPs to the polymer brushes; their synthesis, characterization, and *in vitro* evaluations. Results and Discussion are presented first (Section 3.2 and 3.3), followed by conclusions (Section 3.4) and Methods and Materials at the end (Section 3.5).

3.1 Introduction

3.1.1 Antimicrobial peptides

Resistance to the commonly used antibiotics for the treatment of community and hospital-acquired infections is an ever-growing problem. In particular, the big three Gram-positive species, staphylococci, enterococci, and streptococci, have all evolved resistant strains. With an increase in the incidence of multi drug resistant (MDR) pathogens, the search for new classes of antibiotics has been growing.

In 1987, Dr. Michael Zasloff isolated some peptides with antimicrobial activity from the skin of the African clawed frog *Xenopus leavis*.¹⁸⁵ These peptides were water soluble, amphiphilic and could kill different Gram-positive and negative bacteria, fungi and protozoa.¹⁸⁵ AMPs had been isolated from phagocytic cells of mammalians, too.¹⁸⁶⁻¹⁸⁸ Over the years, cationic AMPs have been discovered in a variety of vertebrates and invertebrates. Besides direct antimicrobial activity, these peptides promote host innate immunity.¹⁸⁹

Cationic AMPs have been extensively studied as a possible alternative for the treatment of

infections, particularly MDR bacterial infections.^{190,191} Natural cationic AMPs generally have 12 to 50 amino acids with an overall positive charge (+2 to +9) due to lysine or arginine residues. Up to 50 % of the peptide sequence is made of hydrophobic residues.¹⁸⁹ Cationic AMPs interact with negatively charged bacterial surfaces. Some can penetrate into the bacteria to reach a cytoplasmic target. The electrostatic interaction between the peptide and bacterial membranes leads to a high concentration of cationic peptides accumulating on bacterial membranes, which can in turn disturb the electrostatics of a bacterial membrane and cause its lysis.¹⁹² Although the mode of action of cationic AMPs is usually through disruption of the integrity of the bacterial cytoplasmic membrane (**Figure 3.1**), other mechanisms have been discovered which involve key cellular processes such as DNA and protein synthesis, enzymatic activity and cell wall synthesis.^{193–195}

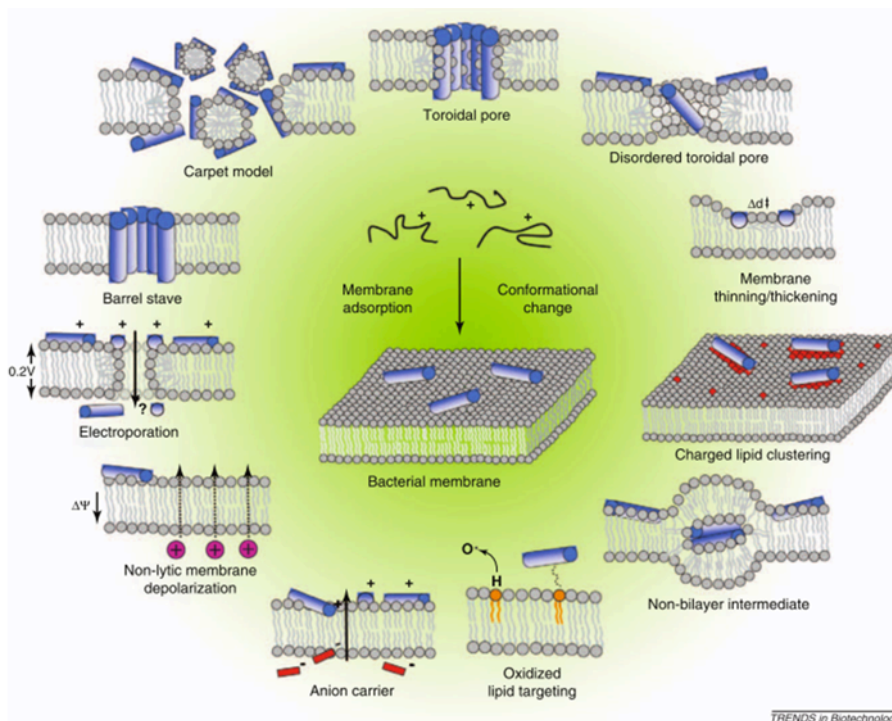


Figure 3.1 After the adsorption of AMPs on a bacterial cytoplasmic membrane, one or multiple events can lead to membrane disruption and bacterial death. Reproduced with permission from *Trends Biotechnol.* 2011, 29, 464–472.

As stated above, the presence of cationic and hydrophobic amino acid residues is a general characteristic of most AMPs. The positive charge helps the peptide to show selectivity to bacteria over the host cells; bacterial lipid bilayer are more negatively charged compared to zwitterionic lipids in mammalian cells.¹⁹⁶ Hydrophobicity, however, promotes interaction with fatty acids of both membranes.¹⁹⁵ Besides the lower negative charge of mammalian cell membrane lipids, the presence of cholesterol in mammalian membranes stabilizes them, providing protection against the AMP effect (**Figure 3.2**).¹⁹⁶ As can be expected, the interactions are concentration dependent and the therapeutic potential of a peptide should be evaluated with a consideration of its cell cytotoxic concentration.

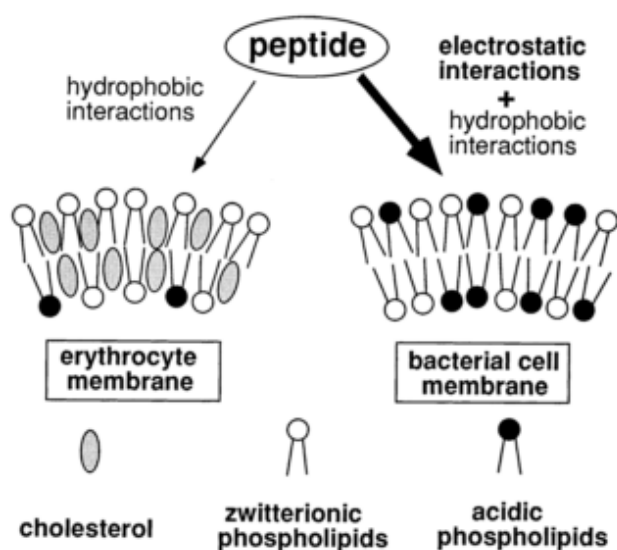


Figure 3.2 Cationic AMPs show higher affinity to bacterial membrane versus mammalian membranes. Abundant acidic phospholipids on bacterial membranes (versus zwitterionic phospholipids on mammalian membranes) make the electrostatic interactions with cationic AMPs favorable. Further the presence of cholesterol protects the mammalian membrane against AMPs. Reproduced with permission from *Biochim. Biophys. Acta* 1999, 1462, 1–10.

3.1.2 Different classes of immobilized bactericidal agents on surfaces

Immobilization of low molecular weight antibiotics, bacteriophages, lysozyme, chitosan, quaternary ammonium polymers, and cationic antimicrobial on different surfaces has been tested

to develop bactericidal surfaces. In this strategy, the bactericidal agents are covalently or physically immobilized on the surface and cause death of bacteria upon contact. Generally, the death of the bacteria results either from the bacterial membrane disruption or by a specific interaction between the immobilized antibacterial agent and a target biomolecule of the bacteria. Based on *in vitro* and *in vivo* studies, the immobilization of low molecular weight antibiotics such as penicillin, ampicillin and gentamycin have provided long-term antimicrobial activity, low risk of side effects and no drug accumulation in tissues.^{197,198} However, inducing bacterial resistance is the downside of this strategy.^{197,199}

Surface immobilization of bacteriophages, viruses that are able to infect bacteria with high specificity, has been reported to provide antibacterial activity for silicone catheters, silica particles and glass cover slides.^{200,201} However, the specificity of bacteriophages for one or a few bacterial strains prevents the broad use of this approach.²⁰² Other concerns include the development of phage-resistant bacteria and also toxicity to the host, especially where different types of bacteriophages are immobilized on a substrate.²⁰²

Lysozyme, a natural defense protein, has been immobilized on surfaces of polyvinyl alcohol and nylon 6/6, for example, to develop antimicrobial surfaces.²⁰³ Conjugation of proteins such as lysozyme (129 amino acids) to the surfaces has been reported to be challenging compared to the conjugation of relatively simple molecules. Further the activity of a protein can be affected by its environment and the possible altered orientation and conformation of the molecule after immobilization; in most cases the lysozyme completely lost its lytic properties after immobilization.²⁰⁴

Chitosan, a natural linear polysaccharide with bactericidal activity, has been tethered to different substrates such as polyethylene terephthalate, polypropylene, segmented polyurethane

and stainless steel surfaces.²⁰⁵ Although use of chitosan as a natural compounds is favorable as it is environmentally benign, bland bactericidal activity of chitosan which is influenced by pH causes some limitations.²⁰⁶

A large number of synthesized polymeric compounds with antimicrobial properties have been developed over the past years. Most of these compounds are known to be cheap, stable and easy to manufacture in large scale and modify large surface areas, however, their cytotoxicity and bioincompatibility are of great concern. The most widely explored synthesized polymeric agents are based on quaternary ammonium (QA) compounds. The possible working mechanism of antimicrobial polymers is generally through extremely high electrostatic forces in combination with hydrophobic interactions that disrupt the bacterial cell membranes and cause their death.²⁰⁴ This group of polymers can make potent antimicrobial coatings but because of their cytotoxicity and bioincompatibility, their applications have been mainly limited to the materials that do not come in direct contact with tissues and biofluids.²⁰⁷ Bacterial resistance to the QA system is another concern; there is increasing evidence that changes in bacterial cell membrane composition and altered gene expression after long exposure to QA coatings can occur.^{207,208}

AMPs are promising therapeutics for immobilization on surfaces. They have a broad spectrum of antibacterial activity, speed of action and low propensity for developing resistant mutants due to their different mechanisms of action. Further, they are generally non-toxic to host cells at the concentrations that kill the bacteria.

3.1.3 Polymer brushes incorporating AMPs

In immobilization of antimicrobial agents, the accessibility of the antimicrobial agent is an important factor for their optimal interaction with bacterial membrane. For example, in many

cases lysozyme was found to lose its lytic properties completely after immobilization,²⁰⁴ therefore spacers were incorporated to increase the freedom of lysozyme for interaction with bacterial membranes. Coatings based on polymer brushes offer key advantages on this front: i) a polymer brush system provides enough flexibility for the microbicidal agent to interact with the bacterial membrane due to the flexibility of the grafted chains, ii) the presence of a non-fouling polymer brush coating will reduce bacterial adhesion and also repel dead bacteria remnants from the surface (**Figure 3.3**) and iii) the hydrophilic polymer brush coating will improve the biocompatibility of the surfaces.

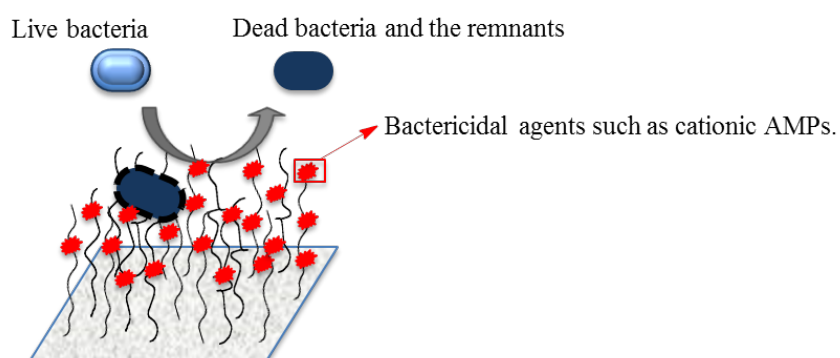


Figure 3.3 AMPs covalently conjugated to polymer brushes have enough freedom for interaction with the bacteria. The antifouling character of the polymer brushes repels the bacterial bodies and their remnants from the surfaces.

Earlier studies using direct immobilization (via short linkers, not polymer brushes) of short AMPs to polyamide resin, cellulose sheets and PEGylated TentaGel S and HypoGel resin beads showed that some of the AMPs retained their activity after immobilization.^{192,209,210} Some of these peptides were found to be highly active against bacteria and fungi and made the surfaces infection-resistant. Some studies controlled the orientation of the peptides on the surfaces and investigated the effect of the spacer on the activity of AMPs.^{197,210} Based on these studies, it is

important to acknowledge that only selected AMPs preserve their activity after surface immobilization and knowledge of the mode of action can help to identify suitable sequences of amino acids and the appropriate position of the sequence for tethering to the surface.²¹¹

One of the first studies utilizing polymer brushes to immobilize AMPs is from 2009 where Glinel *et al.* developed an antifouling coating on silicon wafer surfaces by the copolymerization of 2-(2-methoxyethoxy)ethyl methacrylate and hydroxyl-terminated oligo(ethylene glycol) methacrylate.²¹² Hydroxyl groups from the polymer chains reacted with a bi-functional reagent, which was further reacted with a sulfhydryl group of an AMP, magainin I (**Figure 3.4A**). A terminal cysteine moiety was incorporated in the original sequence of magainin I to provide the required sulfhydryl group for conjugation. Modified surfaces showed bactericidal activity against two tested Gram-positive bacteria. The authors explained that the flexible hydrophilic polymer brush system maintained magainin mobility to access the cell membrane of bacteria and permeabilize it, leading to the death of bacteria.²¹² Using a slightly different approach, a similar polymer brush system and AMP were developed on paramagnetic silica micro particles where antibacterial activity could be tuned by changing the concentration and size of particles.²¹³

Basu *et al.*²¹⁴ self-polymerized allyl glycidyl ether (AGE) under UV light on a plasma-activated silicon wafer surface and conjugated it with Polybia-MPI, an AMP separated from the venom of the social wasp *Polybia paulista* (**Figure 3.4B**). This coating showed bactericidal activity against *E. coli* and retained its activity after 3 days of incubation in artificial urine. Conjugation to the surface decreased the hemolytic activity of Polybia-MPI in comparison to the soluble peptides.²¹⁴ A similar polymer brush system, poly(allyl glycidyl ether) (PAGE), was developed on silicone urinary catheters and PDMS surfaces, and then conjugated to two new arginine/lysine/tryptophan-rich AMPs.²¹⁵ The modified surfaces showed strong bactericidal

activity in a bacterial medium, PBS and urine, suggesting that the presence of proteases and ions in urine and PBS did not affect the activity of the AMPs. Similar to the soluble AMPs, the peptides conjugated to the AGE polymer brushes caused bacterial membrane disruption, however, they showed a slower rate of killing. Reduced diffusivity and flexibility resulting from tethering has been proposed as a reason. PAGE-AMPs did not increase the cytotoxicity of the substrate toward smooth muscle cells.²¹⁵

Li *et al.* applied a different strategy for immobilization of AMPs on surfaces.²¹⁶ Initially a bifunctional oligoethylene glycol (OEG) containing an alkyne group (protected with trimethylgermanium (TMG) and an alkene group was immobilized on a silicon substrate (TMG-EG10). This was followed by the deprotection of TMG with Cu(I) and a Cu(I)-catalyzed azide–alkyne cycloaddition (CuAAC) reaction between an azide-bearing AMP and the alkyne group on the substrate in one pot (**Figure 3.4C**). The azide-bearing AMP was N₃-IG25, a truncated version of LL-37 linked to a long OEG linker as a spacer and functionalized with an azide group on one end. LL-37 is an extensively studied human AMP. No bacteria were observed on the silicon surfaces coated with OEG. On the contrary some bacteria adhered strongly on the surfaces coated with OEG-IG25 which showed the bacteria-peptide interaction. Cell membranes of these bacteria were damaged. Although the antimicrobial properties were achieved by the coating, the antifouling activity was not optimal for preventing the attachment of the bacteria or bacterial debris. A decrease in peptide concentration resulted in an increased antifouling character of the coating, however with a decreased bactericidal activity. Substrates with the highest concentration of IG25 showed 80 % survival of fibroblast cells (NIH3T3) adhered on this substrate after 24 h incubation suggesting that the attachment of the AMP on the surface did not increase the toxicity of the surface to this cell line.²¹⁶

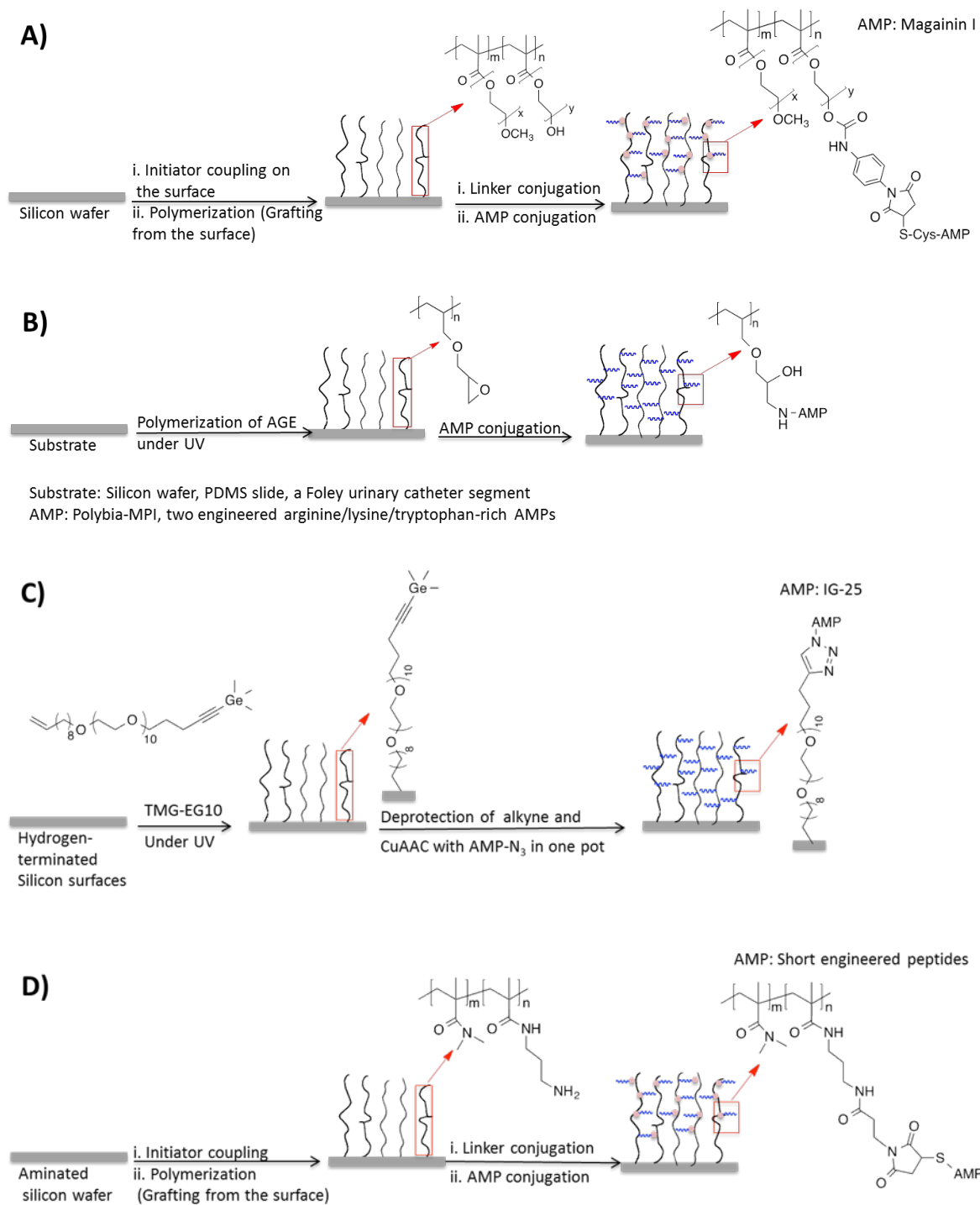


Figure 3.4 Some reported strategies for conjugating antimicrobial peptides to substrates via polymer brushes.

In a series of papers,^{152,217,218} our group developed hydrophilic polyacrylamide brushes conjugated with a series of short synthetic AMPs and evaluated the antibacterial activity and the biofilm resistance *in vitro* and *in vivo*. For their studies, Gao *et al.* used silicon wafers, silicon wafers coated with titanium and titanium implants. The grafting procedure started with amination of the surfaces followed by a reaction with initiator molecules and then surface-initiated copolymerization of DMA and APMA. The grafted polymers then reacted with a bi-functional reagent. Cysteine end-functionalized AMPs were finally conjugated to the polymer brushes via this linker (**Figure 3.4D**).¹⁵²

The modified titanium samples were implanted in rats to test their activity *in vivo*.¹⁵² An inoculum of 10^8 CFU of *S. aureus* was introduced to the implant site. After a 7-day implantation period, the antimicrobial activity of the immobilized AMPs was still preserved and further, they showed excellent anti-biofilm properties. The coated surfaces with AMPs showed no significant platelet activation and adhesion, no complement activation in human blood and no toxicity to osteoblast-like cells.¹⁵²

In the design of antibacterial surfaces based on polymer brushes and AMPs, a balance between the antifouling property and bactericidal activity is critical. As evident from the published results, a high surface concentration of AMPs will make the surfaces antimicrobial, however an increase in hydrophobicity and positive charge of the surfaces will increase the adsorption of bacterial debris and/or other present cells, and make the long-term application impossible, thus optimization is critical.

3.1.4. AMPs in platelet storage bags

AMPs have been reported to preserve bactericidal activity in complex matrices like blood with no concurrent host cytotoxicities.²¹⁹ Activated human platelets release various peptides, some of which have antimicrobial activity.²²⁰ Thrombin-induced platelet microbicidal protein-1 (tPMP-1) is a well-known example of such peptides. In a search for a cost-effective and easy-to-use method of pathogen inactivation in stored platelets, a few studies have inoculated AMPs in platelet storage bags.^{221–223} The inoculated peptides were either derived from platelet microbicidal proteins or they were arginine-tryptophan (RW) repeat peptides (1 to 5 repeats). RW3 (RWRWRW), in particular, showed bactericidal activity against *S. aureus*, *S. epidermidis*, *E. coli*, *P. aeruginosa*, and *K. pneumoniae*.²²¹ After 7 days of storage, platelets treated with RW3 showed similar *in vitro* quality measures as untreated platelets.²²² More importantly, treatment of human platelets with AMPs (RW3, RW4 or some PMP-derived peptides) did not affect their *in vivo* recovery and survival in mice. Further, these peptides did not induce any immunologic response in rabbits.²²³

The outcome of these preclinical studies encourages the development of an AMP-containing polymer coating for the platelet storage bags. As AMPs are immobilized onto the platelet bags and are not transfused to the patients, the unnecessary exposure of the patient to AMPs will be omitted in this approach. This is a desirable feature as a paper has recently shown that AMPs could lead to a selection for virulent mutants of a clinical *S. aureus* strain.²²⁴ These mutants were less susceptible to conventional antibiotics and further they showed cross-resistance to human innate immunity. These results raised awareness about the therapeutic use of AMPs and the associated risk of cross-resistance to human innate immunity and conventional antibiotic therapy.²²⁴

3.2 Results and Discussion: Synthesis and Characterization of AMP-containing Polymer Brushes on pPVC.

3.2.1 Synthesis of AMP-containing polymer brushes on pPVC

Cationic AMPs selected for this study are shown in **Table 3.1**. They were previously shown to preserve their bactericidal activity when tethered.¹⁵² All these AMPs have a cysteine (cysteine one letter code is C) on their C terminal to provide functionality for conjugation. DA51 seemed the best polymer system for the conjugation of peptide as it showed stronger antifouling properties compared to other copolymers with a higher ratio of APMA e.g. DA21 and DA11.

Table 3.1 Three cationic AMPs and their amino acid sequence.

Peptide	Sequence	Molecular weight
1010cys	IRWRIRVWVRRIC	1812 Da
Tet-20	KRWRIRVRVIRKC	1769 Da
Tet-26	WIVVIWRRKRRRC	1827 Da

To attach the AMPs to DA51 polymer brushes on pPVC, two water-soluble commercially available amine-to-sulfhydryl crosslinkers, sulfo-SMCC (sulfosuccinimidyl 4-(*N*-maleimidomethyl) cyclohexane-1-carboxylate) and sulfo-SIAB (sulfosuccinimidyl (4-iodoacetyl) aminobenzoate) were used (**Figure 3.5**).

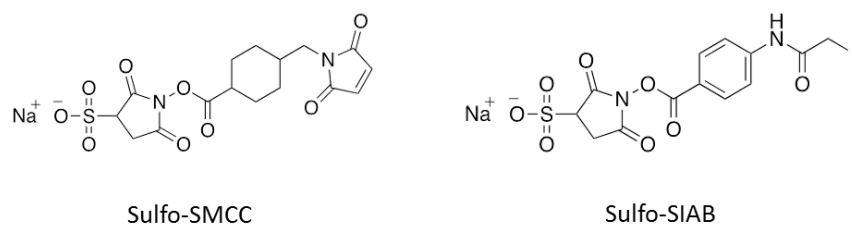


Figure 3.5 The chemical structures of two water-soluble crosslinkers: sulfo-SMCC and sulfo-SIAB.

pPVC-DA51 samples were first treated with triethylamine solution then immersed in the solution of either linker at pH 7.5. In the next step, AMPs were reduced with TCEP (tris(2-carboxyethyl)phosphine) and reacted with the pPVC-DA51-SIAB or pPVC-DA51-SMCC at pH 7.5 (**Figure 3.6** shows the reaction with SMCC). Any unreacted linker was quenched with 1-thioglycerol. Because of the photosensitivity of sulfo-SIAB, the rest of the experiments were performed with sulfo-SMCC.

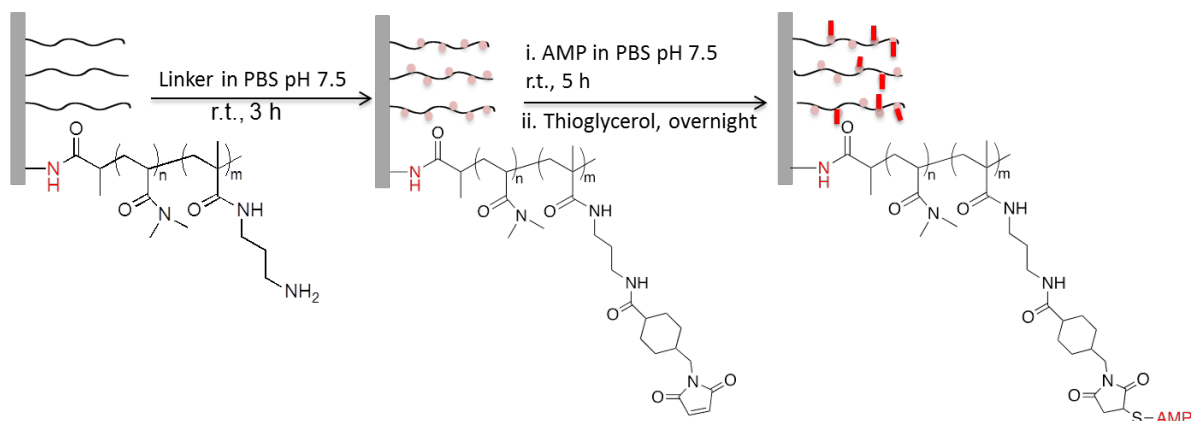


Figure 3.6 The general scheme of conjugating AMPs to polymer brushes through the sulfo-SMCC linker.

3.2.2 Characterization of AMP on surfaces

3.2.2.1 Determination of surface concentration of AMPs on pPVC by fluorometry

To estimate the density of AMPs on silicon wafer surfaces, Gao *et al.* in our lab had measured the increase in the polymer layer thickness after peptide conjugation and correlated this value to the amount of conjugated peptide.²¹⁷ Their method was not applicable to this measurement on the platelet bag surfaces, however, because of the inherent properties of pPVC (being rough and non-reflective).

To develop a method independent of the properties of the substrate, a sensitive fluorometric method was adapted that has been used for the determination of arginine concentration in solutions.^{225–227} This method is based on the reaction of 9,10-

phenanthrenequinone (PAQ) with arginine. PAQ reacts with arginine under basic conditions. The product undergoes a fast hydrolysis with HCl to give a fluorescent product ($\lambda_{\text{ex}} = 312 \text{ nm}$ / $\lambda_{\text{em}} = 392 \text{ nm}$), which can be used to quantitatively determine sub-microgram amounts of arginine (**Figure 3.7**). All AMPs used in this chapter carried 5 arginines in their sequence (**Table 3.1**, arginine one letter code is R). PAQ reacts with free arginine or arginine residues in proteins under a simple and convenient procedure. It has been shown that none of the common amino acids interfere with the assay and the reaction with PAQ is arginine-specific.²²⁵ The fluorescence remains a linear function of the amount of arginine in the presence of other amino acids, too.

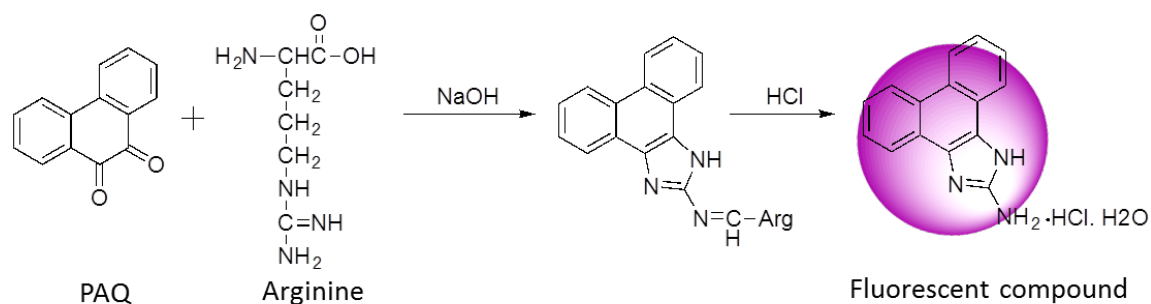


Figure 3.7 PAQ reacts with arginine under basic conditions. The product hydrolyzes to a fluorescent compound under acidic conditions.

In the general reaction, a basic aqueous solution of arginine or protein reacts with a solution of PAQ in ethanol. The reaction time has been shown to be dependent on temperature and the source of arginine (free arginine or a protein).²²⁵ Then this product undergoes a fast hydrolysis under acidic conditions and gives a fluorescent product.

Optimization of fluorometry technique for pPVC surfaces: To use this assay for measuring the amount of AMPs on pPVC surfaces, the assay conditions had to be modified. The original assay conditions seemed to extract the plasticizer (a cloudy solution after 3 h). Further, there was interference in fluorometry as some emission was collected for pPVC-DA51 samples (negative control). The conditions were optimized for pPVC to low temperature (35 °C), limited

concentration of ethanol (33 %) and a reaction time of 3 h. The effect of the initial PAQ concentration was also considered during the optimization. PAQ should not be too much in excess compared to the peptide. Using different concentrations of PAQ to determine the same amount of peptide, an uncertainty of $\pm 20\%$ of the measured value proved to be a conservative estimate of the uncertainty for concentrations below $6\ \mu\text{g/mL}$ of the peptide.

After a 3-h immersion of pPVC-DA51-AMP in PAQ solution under basic conditions, samples were treated with HCl solution to release the fluorescent moieties into the solution and quantify them by fluorescence spectrometry (**Figure 3.8**).

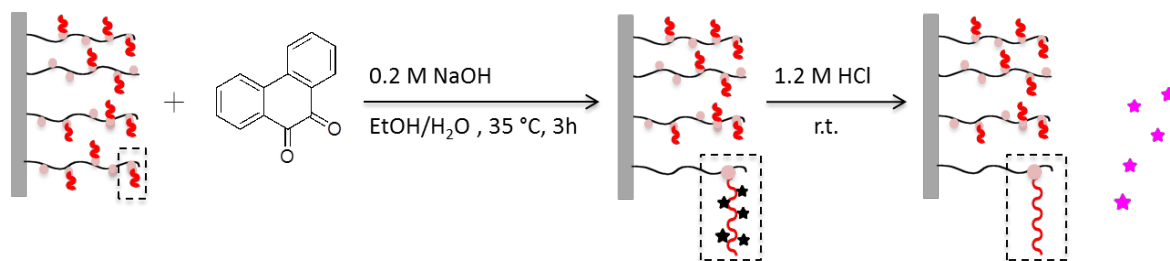


Figure 3.8 The amount of immobilized AMPs on the pPVC surfaces can be determined by PAQ fluorometry.

Unmodified pPVC and pPVC-DA51 were used as negative control substrates. The medium of the basic reaction was also tested before acidification for any fluorescent background (**Figure 3.9A**). The calibration curve for each AMP was prepared with a concentration range of 1.05 to $33.6\ \mu\text{g/mL}$ of the AMP in solution under the same conditions used for pPVC samples. These curves were then used to calculate the amount of peptide released from pPVC-DA51-AMPs samples. An example of the preparation of the Tet-26 calibration curve is shown in **Figure 3.9B and 3.9C**. After calculating the amount of released peptide from pPVC surfaces using the corresponding calibration curve, the total mass of AMP was divided by the surface area of the

pPVC to find its density ($\mu\text{g}/\text{cm}^2$). As mentioned in Chapter 2, pPVC has rough surfaces so the reported peptide amount is per unit macroscopic area.

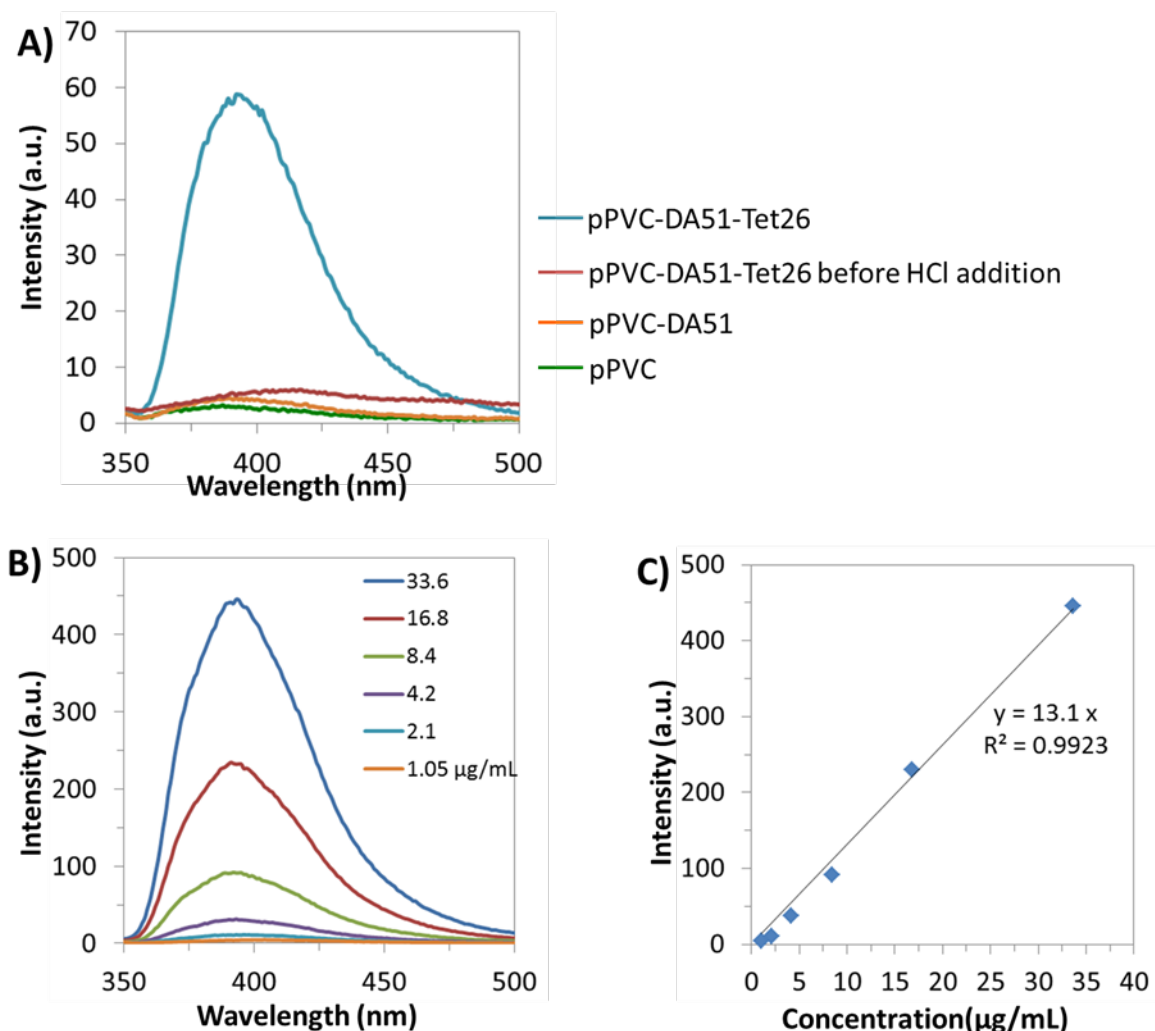


Figure 3.9 The fluorescence emission peak at $\lambda_{\text{em}} = 392 \text{ nm}$ was used for measuring the amount of peptide at pPVC-DA51-AMP surfaces (Tet-26 here). pPVC and pPVC-DA51 samples were used as negative controls. The solution of pPVC-DA51-AMP (Tet-26 here) was also tested before acidification (A). Calibration curves for aqueous solution of Tet-26 in the range of 1.05–33.6 $\mu\text{g}/\text{mL}$ (B and C). Similar curves were prepared for two other peptides and used for the calculation of the amount of peptides on pPVC surfaces.

Validating the fluorometry technique using the data obtained from silicon wafers: To check the accuracy of this method, silicon wafers were modified with the same polymer brush system and AMPs (**Figure 3.10**). The density of the tethered AMPs on the surfaces was estimated based

on dry thickness increase measured by ellipsometry and these results were compared to the AMP surface density calculated from the similar optimized fluorometric method used for pPVC.

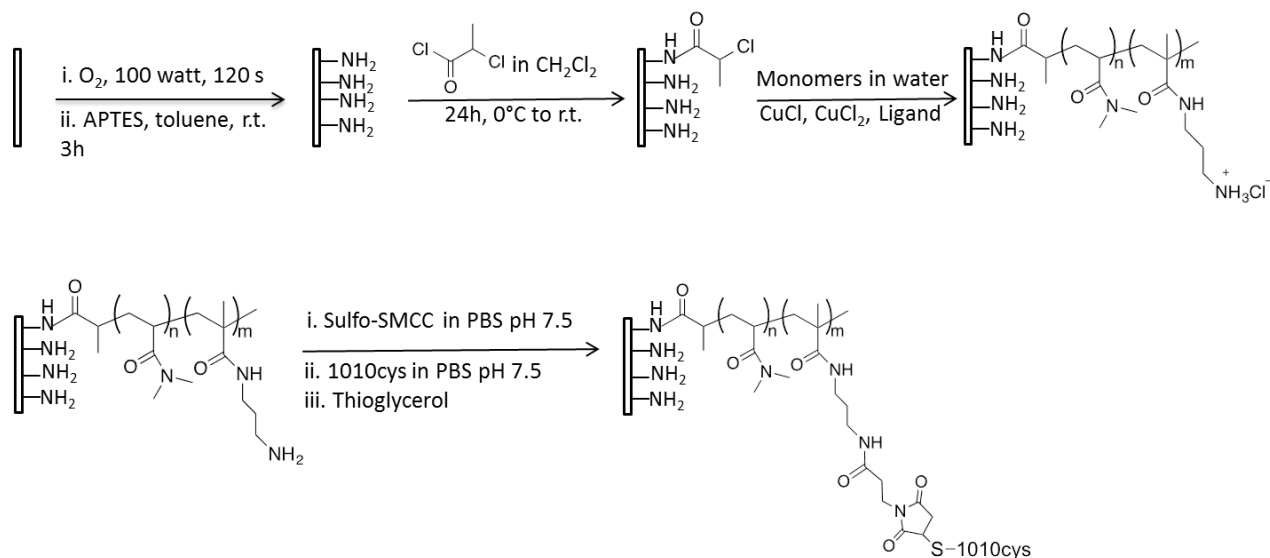


Figure 3.10 The general scheme of development of DA51-1010cys on silicon wafers.

Silicon wafers were first aminated via reaction with APTES as explained in Chapter 2. The amine groups were then reacted with 2-chloropropionyl chloride to provide the ATRP initiators on the surfaces. Polymer brushes were grown from the surfaces in water and treated in an aqueous triethylamine solution. The samples reacted with sulfo-SMCC in PBS pH 7.5. The maleimide group of the conjugated linker was in turn reacted with the AMP in PBS pH 7.5 (**Figure 3.10**). The water contact angle and thickness of the coating on silicon wafers are shown in **Figure 3.11**.

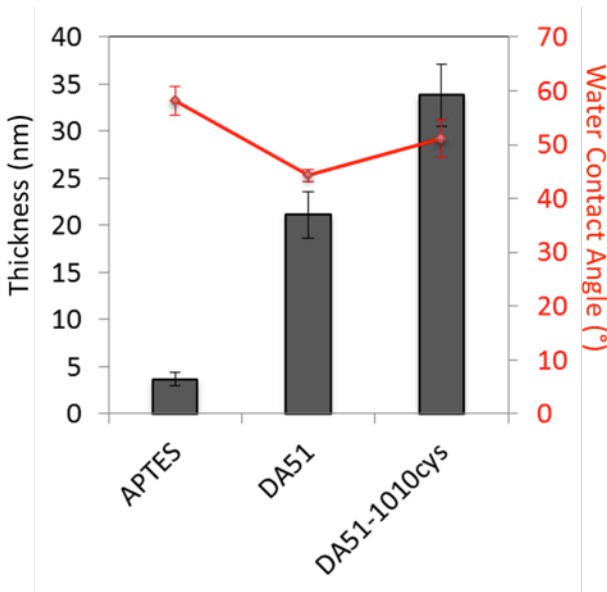


Figure 3.11 The change in thickness (bars) and static water contact angle (line) after modification of silicon wafer with APTES, DA51, and DA51-AMP (1010cys here). Values are reported as AVG \pm SD of three substrates.

The increase in the dry thickness of polymer coating after AMP conjugation was used to estimate the peptide density on surfaces. An example of the calculation of the peptide surface density (W_p , $\mu\text{g}/\text{cm}^2$) is shown in the following.

$$W_p = (h - h_b)\rho_b$$

$$h = 35 \text{ nm}$$

Dry thickness of the polymer chains conjugated with the peptide (DA51-1010cys) found by ellipsometry

$$h_b = 21 \text{ nm}$$

Dry thickness of polymer brush (DA51) layer found by ellipsometry

$$\rho_b = 1.2 \text{ g}/\text{cm}^3$$

Mass density of the polymeric system

$$\rightarrow W_p = 1.7 \mu\text{g}/\text{cm}^2$$

Surface density of 1010cys in $\mu\text{g}/\text{cm}^2$, equivalent to $9.4 \times 10^{-10} \text{ mol}/\text{cm}^2$.

The molar ratio of peptides to amines or peptide saturation (r_p) can be calculated knowing the surface density of APMA. An example of the calculation of the polymer chains surface density (σ_b , chains/nm²) is shown below. Once σ_b is known, the surface density of APMA can be calculated from that.

$$h_b = \frac{\sigma_b}{\rho_b N_A} M_n$$

$$h_b = 21 \text{ nm}$$

Dry thickness of polymer brush (DA51) layer found by ellipsometry

$$\rho_b = 1.2 \text{ g/mL}$$

Mass density of the polymeric system

$$N_A = 6.02 \times 10^{23} \text{ mol}^{-1}$$

Avogadro's number

$$M_n = 80,000 \text{ g/mol}$$

Number average molecular weight of polymer chains

$$\rightarrow \sigma_b = 0.19 \text{ chains/nm}^2 \text{ or } 2 \times 10^{13} \text{ chains/cm}^2$$

Surface density of polymer brushes in chains/cm², equivalent to $3.3 \times 10^{11} \text{ mol/cm}^2$

$$\rightarrow \sigma_{APMA} = 3.9 \times 10^{-9} \text{ mol/cm}^2 (\sigma_b \times 118)$$

Surface density of APMA in mol/cm². Each 80,000 Da polymer chain has around 118 APMA, determined from the molar ratio of DMA to APMA (5 to 1) in the polymer chain.

$$\rightarrow r_p = \frac{9.4 \times 10^{-10} \text{ peptide}}{3.9 \times 10^{-9} \text{ Amine}} = 0.24$$

The molar ratio of peptides to amines or peptide saturation was found to be 0.24, i.e. around 24 % of amine groups were conjugated to AMPs. As we will see in Chapter 4, the reaction of maleimide group with peptide is a highly efficient reaction. As the peptide was in excess compared to the tethered linkers, the low conversion could be attributed to the steric hindrance caused by the densely grafted polymer chains that limited the diffusion and access of the peptide to the inner parts of the polymer brushes.

After the thickness evaluation by ellipsometry, the same sample was reacted with PAQ for quantification of the peptide by fluorometry. Similar measurements were performed for two other samples, and they all confirmed the reliability of fluorometry for determination of peptide amount on the surfaces (Appendix B1), and this method was used for the estimation of peptide amounts on the coated pPVC surfaces.

The variations among pPVC surfaces modified with polymer brushes and AMP were considerable. In some samples, the concentration of AMP was measured to be low ($1-3 \mu\text{g}/\text{cm}^2$). The water contact angle on these surfaces did not change and the composition change on the surfaces was not traceable by ATR-FTIR spectroscopy. On the other hand some samples carried $7-10 \mu\text{g}/\text{cm}^2$ of AMP and the water contact angle increased by 5 to 10 degrees after the peptide conjugation. The peptide peaks could be also traced by ATR-FTIR spectroscopy (**Figure 3.12**). The ATR-FTIR spectrum of Tet-26 is shown in Appendix B2 for comparison. Generally, under the similar conditions and using the same pPVC-DA51 samples, a higher concentration of peptide was obtained using 1010cys while it was lower with Tet-20 or Tet-26. This might be attributed to the greater hydrophobic character of 1010cys (it showed less water solubility at the time of solution preparation, however it was soluble at the concentration used for conjugation) and suggested the possibility of physical adsorption. In some control experiments, the linker conjugation step was omitted and pPVC-DA51 was directly immersed in the AMP solution. AMPs were detected on these surfaces and they were not removed by washing and sonication in sodium dodecyl sulfate solution.

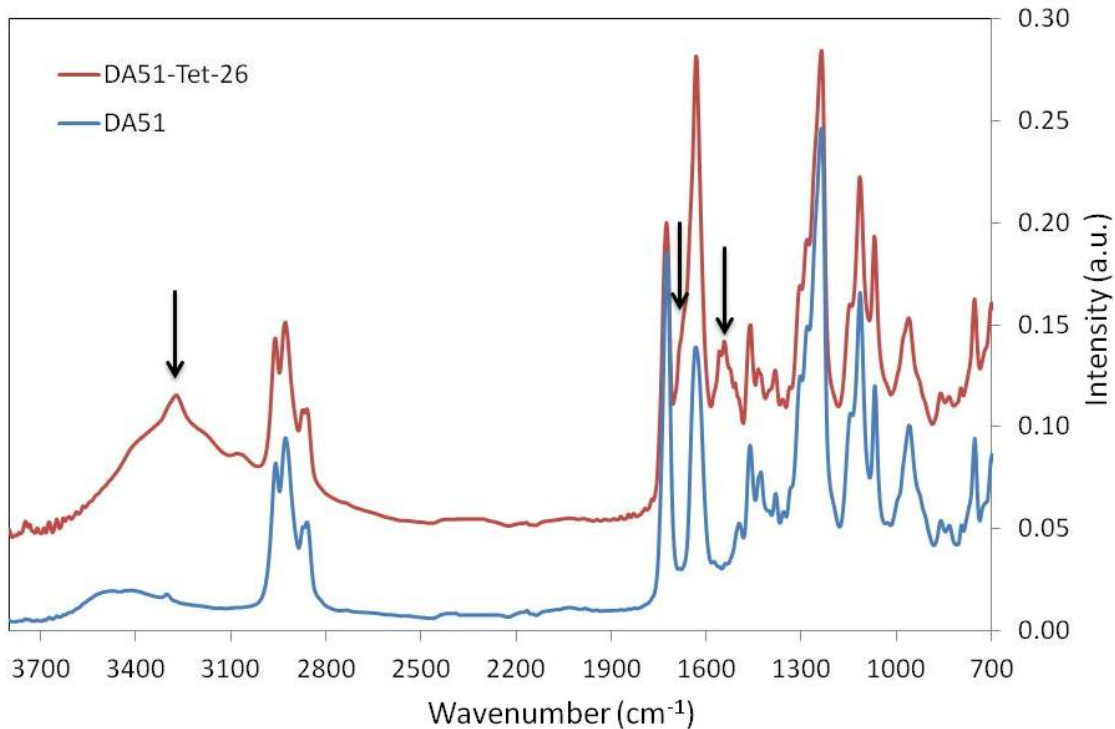


Figure 3.12 Comparison of ATR- FTIR spectra of pPVC-DA51 samples before and after conjugation with AMP in samples with a high surface concentration of AMPs (7-10 $\mu\text{g}/\text{cm}^2$ of Tet-26 here) confirming the presence of the peptide.

The effort to tune the amount of peptide on surfaces by changing the concentration of linker and peptide or polymer brush properties consistently failed and the variation among the samples was large. In Section 3.3, the *in vitro* evaluation of the samples will show the importance of tuning the amount of AMPs on the surfaces.

3.3 Results and Discussion: *In Vitro* Evaluation of the Modified pPVC Samples

In Chapter 2 it was shown that pPVC surfaces modified with PDMA and DA51 could resist bacterial and platelet adhesion. The pPVC samples coated with DA51-AMP were incubated with platelet concentrates at 37 °C for 4 h and the results were compared with untreated control pPVC samples and the pPVC-DA51 samples under the same conditions.

Contrary to the surfaces modified with DA51, the samples containing AMPs showed a high level of platelet adhesion and activation (**Figure 3.13**). The positively charged and hydrophobic character of the AMPs on the modified surfaces promoted platelet adhesion on surfaces and showed poor biocompatibility with them.

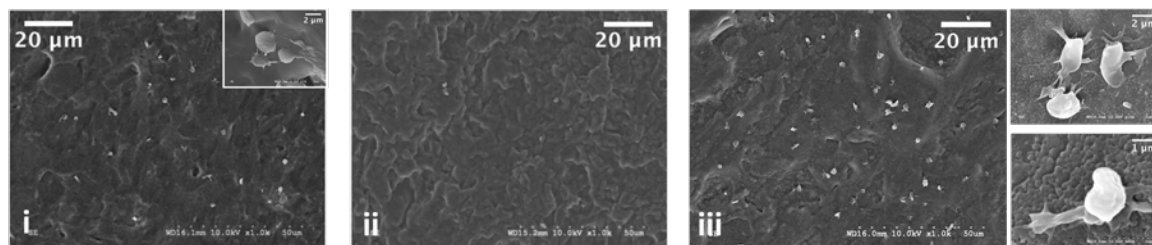


Figure 3.13 Platelet adhesion on pPVC (i), pPVC-DA51 (ii) and pPVC-DA51-AMP (iii) after 4 h incubation at 37 °C observed by SEM. (i) Higher magnification in the inset. (iii) Higher magnification in the right hand panels. Here, sample iii carried $8 \pm 1 \mu\text{g}/\text{cm}^2$ of 1010cys. The non-textured faces of pPVC were analyzed by SEM.

These samples did not show strong bactericidal activity (**Figure 3.14**). The difference between the level of live released bacteria from the surfaces of pPVC-DA51 and surfaces of pPVC-DA51-AMP (Tet-20 is shown in this graph) was not statistically significant.

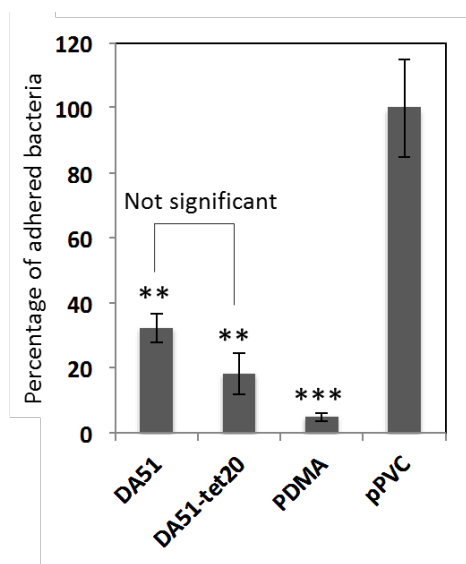


Figure 3.14 Level of *S. aureus* adhesion on pPVC surfaces modified with PDMA, DA51 and DA51-Tet20 in comparison with the control pPVC. ** $P < 0.01$ and *** $P < 0.005$. The difference between DA51 and DA51-Tet-20 was not statistically significant.

One reason could have been the method of evaluation of surfaces for antibacterial activity. The method described in Chapter 2 was used for these tests; briefly, each 0.4×0.9 cm control pPVC or modified pPVC was vertically immersed in 1×10^6 CFU/mL of *S. aureus* in LB for 4 h at 37 °C. The adhered bacteria on the surfaces were dislodged with sonication, serially diluted, cultured on LB agar plates and counted. The high concentration of bacteria relative to the amount of the bactericidal agents (AMPs on the surfaces) could be one reason. Further, the rich LB can help a bacterium with a partially disrupted membrane to survive. Such bacteria can also re-grow on agar plates (for counting) when there is no AMP available. Further, the *S. aureus* doubles in LB within roughly an hour, which is again another challenge for the bactericidal agents, especially if their concentration is low relative to the bacterial culture. In the next chapter these factors were considered in the experimental procedure and fixed by performing the tests in PBS instead of LB. The bacterial experiments were not repeated for this chapter because of the poor platelet biocompatibility of the surfaces.

3.4 Conclusions

Conjugation of AMPs to polymer brushes has been increasingly reported in the literature. In this chapter some short AMPs with cysteine in their C-terminal were conjugated onto the platelet bag surfaces coated with DA51 brushes using a water-soluble amine-to-sulfhydryl crosslinker. A fluorometric method based on the reaction of PAQ and arginine was optimized for estimating the amount of peptides on pPVC surfaces. This method showed that even in the absence of linker, AMPs were strongly attached to the surfaces. Another challenge was reproducing the coating properties on surfaces; as also discussed in Chapter 2, the thickness and density of the polymer chains on pPVC surfaces were difficult to tune and characterize. This problem persisted for

peptide conjugation. The tuning of polymeric system properties was critical as it was observed a high concentration of peptide on surfaces ($\sim 8 \mu\text{g}/\text{cm}^2$) increased platelet adhesion and activation on pPVC surfaces.

The presence of both polymer chains and peptide on surfaces from sources other than the designed synthetic pathway made the predictability of the coating characteristics difficult and was likely responsible for the poor reproducibility of the results.

3.5 Methods and Materials

All chemicals were purchased from Sigma-Aldrich and used as received unless stated otherwise. Sulfo-SIAB, sulfo-SMCC were purchased from Thermo Fisher Scientific. 1010cys (Sequence: IRWRIRVWVRRIC), Tet-20 (Sequence: KRWRIRVRVIRKC) and Tet-26 (Sequence: WIVVIWRRKRRRC) were synthesized by CanPeptide Inc. A Cary Eclipse fluorescence spectrophotometer (Agilent Technologies) was used for fluorometry. Deionized water was used for all the reactions, prepared by MilliQ water purification system with a resistivity of 17.9 m Ω /cm. Distilled water was used for all other applications such as washing steps.

3.5.1 Synthesis of AMP-containing polymer brushes on pPVC

pPVC-DA51 as prepared in Chapter 2 was first immersed in a 0.25 M aqueous solution of triethylamine (0.7 mL NEt₃ in 19.3 mL water) for 2 h. Then the samples were washed with PBS pH 7.5 and sonicated in the solution for 10 minutes. A 1 mg/mL solution of sulfo-SMCC or sulfo-SIAB was prepared in PBS pH 7.5 and each pPVC-DA51 sample was immersed in the solution for 3 h at room temperature. Solutions and samples containing an iodide group (from the

sulfo-SIAB structure) were protected from light. The samples were washed and sonicated in PBS pH for 15 minutes. A 5 mg/mL aqueous solution of TCEP was prepared and 20 μ L of this solution was added to a 1 mg/mL solution of AMP in PBS pH 7.5. The solution was mixed for 5 minutes. The pPVC-DA51-linker sample was then immersed in the AMP solution for 5 h at room temperature. 1-Thioglycerol (1 μ L) was then added to the solution and kept over night. The samples were finally washed and sonicated in water.

3.5.2 Synthesis of AMP-containing polymer brushes on silicon wafers

Silicon wafer pieces were first washed with ethanol then treated with oxygen plasma at 100 watt for 2 minutes. Amination of silicon wafers using APTES was as explained in Chapter 2, Section 2.5.1.1. The aminated silicon wafers were immersed in dichloromethane (3 mL) at 0 °C then triethylamine (310 μ L) was added to the solution. Chloropropionyl chloride (192 μ L) was next added slowly and mixed. The solution was kept in ice water for 4 h and then at room temperature. After a total of 24 h, samples were washed and sonicated in water. DA51 polymer brushes were grown under the conditions explained in Chapter 2, Section 2.5.1.4. Samples were treated with 0.2 M aqueous triethylamine as above and peptide conjugation was performed as explained above for pPVC surfaces.

3.5.3 Determination of surface concentration of AMPs on pPVC by fluorometry

3.5.3.1 Preparation of calibration curves

Peptide serial dilution: For each AMP, the peptide (2 mg) and mercaptoethanol (1 μ L) were dissolved in water (4 mL). To prepare a 134.4 μ g/mL solution of peptide, 537.6 μ L of this solution was mixed with 1462.4 μ L of water. One mL of this solution was transferred to 1 mL of

water (67.2 $\mu\text{g/mL}$). The serial dilution was continued to a concentration of 1.05 $\mu\text{g/mL}$. The solutions with concentrations from 33.6 to 1.05 $\mu\text{g/mL}$ were used for fluorometry.

PAQ Preparation: PAQ (2 mg) was dissolved in absolute ethanol (100 mL) to prepare a 100 μM solution.

Reaction of PAQ with Peptide: The content of each peptide vial is shown below. A 2 M solution of NaOH was used. The ratio of ethanol/water was kept equal to 1/2 in all concentrations. As mentioned before, PAQ should not be used in too much excess compared to the peptide and two different (final) concentrations of PAQ were used.

For the content of vials 1.05 to 4.2 $\mu\text{g/mL}$ AMP: 0.5 mL of PAQ solution, 1 mL of ethanol, 1 mL of peptide solution, 1.5 mL of water and 0.5 mL of NaOH solution.

For the content of vials 8.4 to 33.6 $\mu\text{g/mL}$: 1.5 mL of PAQ solution, 1 mL of peptide solution, 1.5 mL of water and 0.5 mL of NaOH solution.

The vials were put in a water bath at 35 $^{\circ}\text{C}$ and stirred. After 3 h, 1 mL of each vial was withdrawn and mixed with 1 mL of 1.2 M HCl. The solution was mixed and its fluorescence was recorded at $\lambda_{\text{ex}} = 312$ nm. The content of vial 1.05 $\mu\text{g/mL}$ without any peptide was used for collecting the background before running the samples.

3.5.3.2 Reaction of PAQ with pPVC-DA51-AMP

pPVC-DA51-AMP was added to a vial containing 0.5 mL of PAQ solution, 1 mL of ethanol, 2.5 mL of water and 0.5 mL of NaOH solution. The untreated pPVC and pPVC-DA51 were put in the vials with the same content. The samples were incubated at 35 $^{\circ}\text{C}$ and after 3 h 1.2 M HCl (4.5 mL) was added to the solution and mixed. The fluorescence of each solution was

recorded at $\lambda_{\text{ex}} = 312$ nm. An example of peptide calculation for the sample in **Figure 3.9** is shown below:

The fluorescence intensity of DA-51 (4 a.u.) as negative control was subtracted from the fluorescence intensity of DA-51-Tet-26 (58 a.u.) (**Figure 3.9A**)

The corrected fluorescence intensity of DA-51-Tet-26 was divided by 13.1 (**Figure 3.9C**) to give the amount of peptide. The result was divided by the surface area (0.72 cm^2 for a double side coated 0.4×0.9 cm sample) to estimate the density of peptide to be $5.7 \mu\text{g}/\text{cm}^2$. An uncertainty of ± 20 % of the measured value was considered.

3.5.4 *In vitro* evaluation of the modified surfaces

The protocols reported in Chapter 2 for evaluation of bacterial adhesion (2.5.2.1) and platelet adhesion on pPVC coupons (2.5.2.2) were used.

CHAPTER 4: Development of Antifouling and Bactericidal Coatings for Platelet Storage Bags Using Mussel-Inspired Chemistry

This chapter first introduces mussel adhesive proteins and dopamine building blocks for coating surfaces. Section 4.2 explains the synthesis of a hydrophilic polymer system containing mussel-inspired groups and its application and characterization on platelet bag surfaces as well as on some inorganic substrates. Following that, the coated platelet bag surfaces are evaluated *in vitro*. In Section 4.3, AMPs are added to the polymers to provide bactericidal activity and their detection on surfaces by TOF-SIMS is described. Conclusions will be presented in Section 4.4, followed by the Methods and Materials in Section 4.5.

4.1 Introduction

As discussed before, unwanted biological reactions such as activation of the complement system and the coagulation cascade can hamper biomaterials applications in many settings.⁴⁹⁻⁵¹ In Chapter 2, some polymer brushes composed solely or mainly of PDMA were developed for platelet bags. The applied “grafting from” method overcame some of the challenges associated with working with platelet bags. For example, no organic solvent was used and the use of allylamine plasma treatment was beneficial for the functionalization of pPVC with high density. However, some challenges were identified. A definitive design, tuning, and characterization of the polymer brushes properties (molecular weight, density and thickness) was not straightforward and easily reproducible. Modification of the commercial bags also needed some improvements in order to use smaller amounts of chemicals, to simplify the cutting and resealing of the bags as well as to work with them in the glove box.

In this chapter, the desired polymeric systems are prepared and characterized in solution,

then coated on platelet bag surfaces. The method is basically similar to the “grafting to” method. One of the challenges with “grafting to”, as explained in Chapter 2, is obtaining high grafting density since the already grafted chains limit further chain attachment to the substrate, particularly for rough surfaces such as those on platelet bags. Multiple anchoring points were incorporated in the developed polymeric system here to overcome this limitation. The resulting coating therefore will not be in the polymer brush regime.

Neutral hydrophilic polymer coatings as well as zwitterionic polymers have been widely investigated to improve the non-fouling character and biocompatibility of various materials. Such coatings provide a thermodynamic barrier to entrance of dissolved macromolecules into the surface region by limiting the configurations available to both the coating and impinging material, reducing the entropy and increasing the free energy of the system. In addition, the strong interaction of such coatings with water provides an additional barrier to biomolecules, as they must replace some of the water molecules to adhere to the substrates.^{111,228}

The method for coating the platelet bags in this chapter is based on mussel-inspired chemistry, which will be explained in next section.

4.1.1 Marine mussel adhesion

Blue marine mussels (*Mytilus edulis*) are known to stick to various surfaces under water such as rocks and boats and resist removal by waves.²²⁹ Mussels can adhere to a variety of surfaces, organic, inorganic, hydrophilic, hydrophobic, and even Teflon.²³⁰ *Mytilus edulis* foot proteins (Mefps) are secreted by an organ called the mussel foot and they solidify in water to form the mussel byssus that attaches strongly to a surface (**Figure 4.1A**).

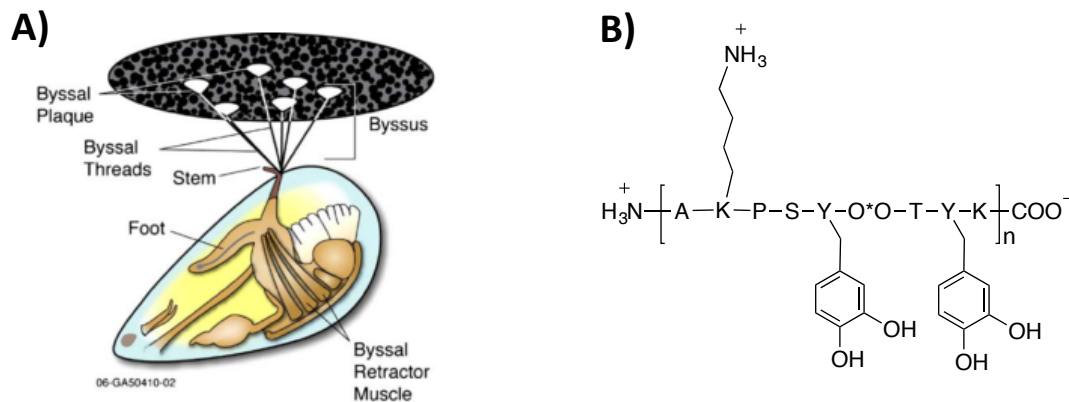


Figure 4.1 *Mytilus edulis* mussel and its byssus (A). The structural formula of mussel foot protein 1, Mefp1, containing aminoacids lysine (K) and DOPA (Y) (B). Reproduced with permission (Figure 4.1A) from *Mar. Biotechnol.* 2007, 9, 661–681.

Mefps, Mefp1 and Mefp5 in particular, are rich in an unusual amino acid, 3,4-dihydroxyphenyl-L-alanine (DOPA), and lysine (**Figure 4.1B**).^{231,232} DOPA contains the catechol functional group that undergoes oxidation triggered by catechol oxidase (an enzyme), leading to the formation of a hard cuticle.²³²

Catechol oxidation to *ortho*-quinone can occur in the presence of oxygen under alkaline conditions or can be triggered by catechol oxidase or oxidizing agents.²³³ *Ortho*-quinones are highly reactive and can react with another catechol (by quinone-phenol dismutation), with an amine or thiol functionality e.g. from a protein (by Michael addition), and/or with an amine group (by a Schiff base reaction) (**Figure 4.2**).²³³

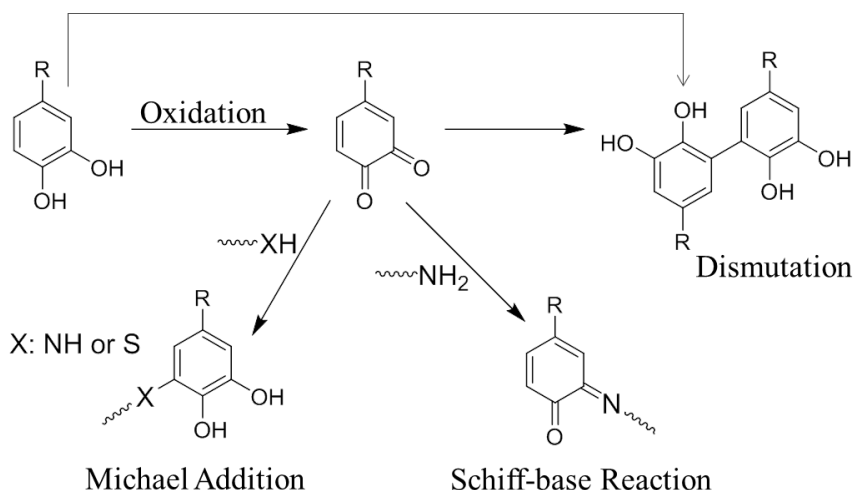


Figure 4.2 Catechol oxidative chemistry.

DOPA can also form strong metal coordination complexes and participate in hydrogen bonding (**Figure 4.3**) and π - π interactions. These interactions appear to contribute to both adhesive and cohesive properties in mussel adhesion. The success of polydopamine in coating all tested materials is not based on one particular kind of interaction with the substrate, but is due to a combination of different interactions with the substrate. For example, coordination complexes are dominant on coating a metal oxide surface while covalent cross linking occurs on aminated substrates and hydrogen bonding becomes important on polar polymeric substrates.

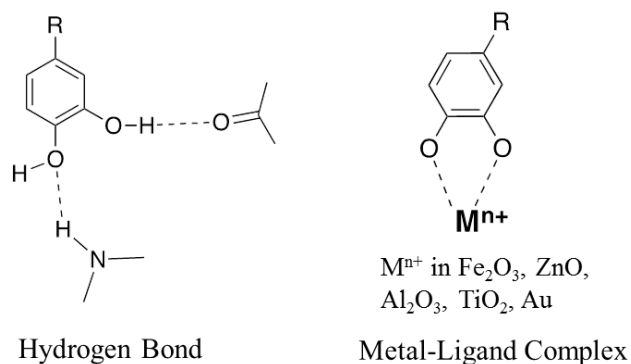


Figure 4.3 Catechol can participate in hydrogen bonding and metal coordination complexes. Modified figure from *Int. J. Adhes. Adhes.* 1987, 7, 9-14.

4.1.2 Mussel-inspired building blocks

Dopamine (**Figure 4.4A**) contains both amine and catechol functional groups found in Mefps and was introduced as a molecular building block for polymer coatings. A dilute aqueous solution of dopamine under basic conditions ($\text{pH} > 7.5$) self polymerizes and forms a thin surface-adherent film of polydopamine (PDA) on any type of substrates investigated so far.²³⁰ There have been different structures proposed for PDA; the most generally accepted proposal shows the PDA structure as an oligomer mixture (**Figure 4.4B**).²³⁴ Only one tautomer is shown in this Figure.

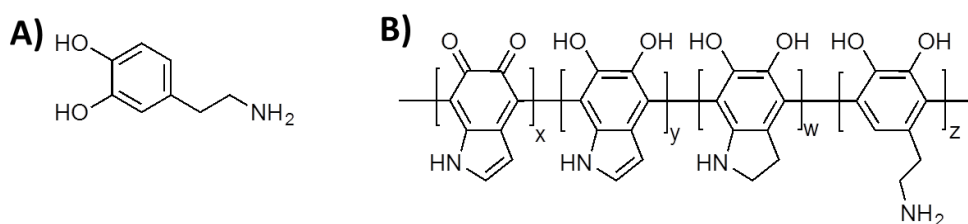


Figure 4.4 Chemical structure of dopamine (A) and a proposed structure of polydopamine (PDA) (B). There are different possible tautomers, one of which is shown here (B).

Mussel-inspired chemistry has been increasingly applied for the fabrication of antifouling coatings on various surfaces. In such systems, hydrophilic antifouling polymers anchor on substrates with mussel-inspired functionalities. Some recent examples (**Figure 4.5**) are a catechol (dopamine moiety) and zwitterion-bifunctionalized PEG coating for stainless steel, titanium and silicon wafer²³⁵ and poly(sulfobetaine methacrylate)-catechol conjugates for poly(L-lactic) acid films.²³⁶ Also, this concept was transferred to dendritic polyglycerol scaffolds with the success of fast and universal adhesion on material surfaces.^{237,238}

Synthesis of a hydrophilic polymer system equipped with mussel-inspired groups and its coating on the platelet bag surfaces will be explained in the next sections.

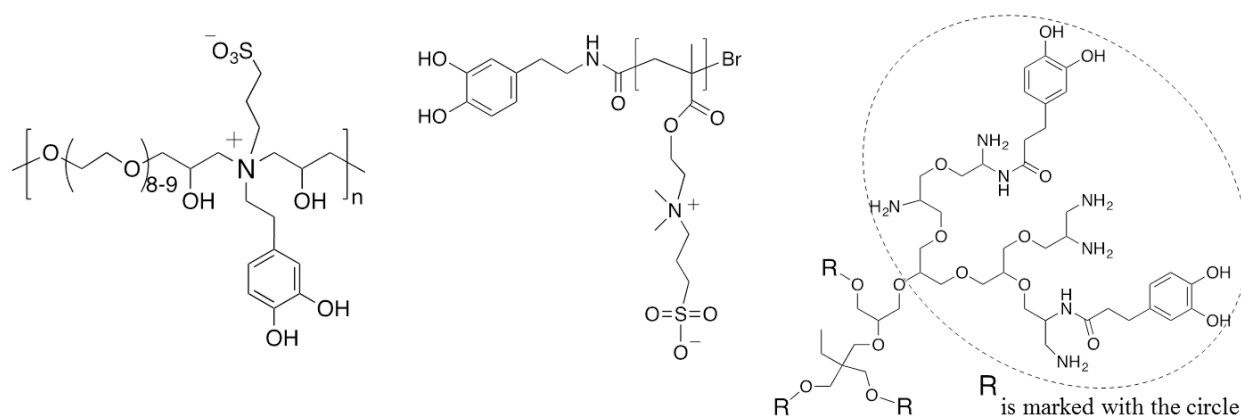


Figure 4.5 Some recent examples of antifouling coatings with mussel-inspired functionalities.^{235–238}

4.2 Results and Discussion: Antifouling Coating

4.2.1 Synthesis of DA51 and DA51-cat

A statistical copolymer of DMA and APMA with a ratio of 5 (DMA) to 1 (APMA) was synthesized using ATRP, called DA51 (**Figure 4.6A**). As explained in Chapter 2, ^1H NMR spectroscopy (**Figure 4.6A**) confirmed that incorporation of the monomers was similar to the feeding ratio (DMA:APMA, 5:1) through integration of the signal of the methyl group of APMA at 0.93 ppm (**Figure 4.6A, a**) and the signal of the proton on the backbone of PDMA at 2.62 ppm (**Figure 4.6A, b**). The M_n of the copolymers used for the coating was between 75 kDa and 110 kDa and the polydispersity of each batch was less than 1.2.

Amine groups on the copolymer were reacted with 3,4-dihydroxyhydrocinnamic acid (DHHA) in the presence of 1-ethyl-3-(3-dimethylaminopropyl)carbodiimide hydrochloride (EDC) to give DA51-cat. Around 25 to 30 % of the amine groups were converted to catechol groups, estimated from ^1H NMR spectra through integration of the signals of aromatic protons at 6.55 and 6.70 ppm (**Figure 4.6A, c,d**) and the methyl group of APMA at 0.93 ppm. ^1H NMR (**Figure 4.6A**) and ^{13}C NMR spectra (Appendix C1) of DA51-cat were obtained in deuterated methanol to avoid oxidation during the acquisition progress.

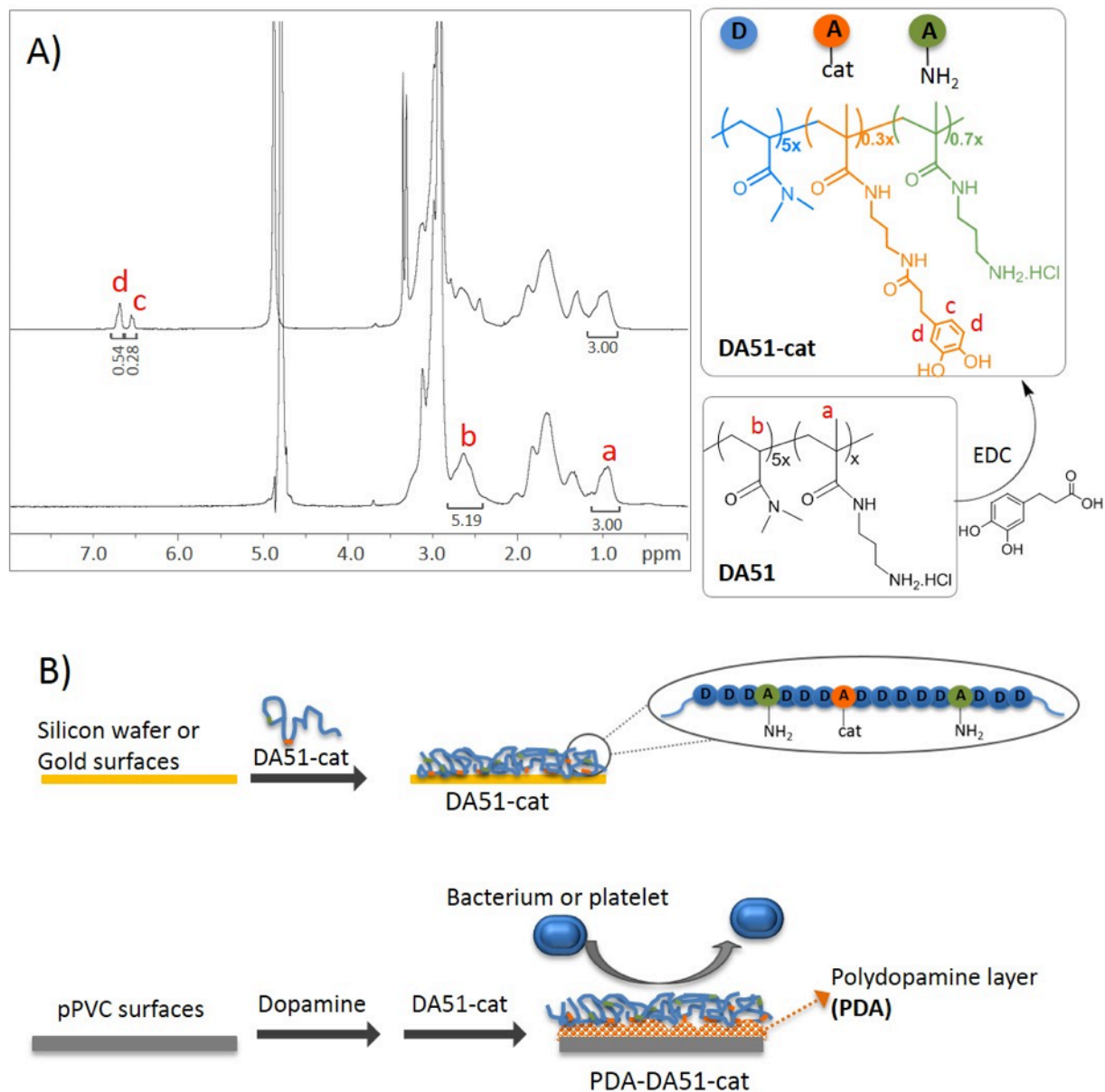


Figure 4.6 A) ^1H NMR spectra of DA51 (in D_2O) and DA51-cat (in d_4 -methanol). DA-51 was reacted with DHHA in the presence of EDC to yield DA51-cat. The percentages of amine and catechol groups in the polymer chains were calculated by integration of the corresponding peaks. B) DA51-cat can coat silicon and gold substrates successfully under basic and oxidative conditions. For pPVC, a two-layer coating consisting of PDA and DA51-cat was required to introduce antifouling properties.

With a molar ratio of 5:1 for DMA:APMA monomers and 25 to 30 % conversion of amines to catechol, the density of catechol on the polymer was around 5 mol %, equivalent to roughly 40 catechol groups per polymer chain (100 kDa).

The number of anchoring groups per molecule is a factor to be considered in order to get a stable and efficient coating. For example, it has been reported that coatings prepared from mPEG-DOPA₃ (mPEG is monomethoxy-terminated PEG polymers and DOPA is the anchoring catecholic group) with a molecular weight of 5 kDa yielded a higher deposited mass on titanium substrates compared to coatings prepared from a monocatechol functionalized mPEG-DOPA₁ (5 kDa).²³⁹

Increasing the density of catechol groups by converting 40 % of amines to catechol reduced the polymer's water solubility; however, it was still soluble at a concentration of 10 mg/mL, which was used for coating. Importantly, limiting the density of catechol groups preserves the desired antifouling character of the coating. Excess catechol groups that are not involved in the anchoring can promote biofouling by reacting with amine groups on proteins or other biomolecules.²⁴⁰ The molar ratio of catechol in the synthesized polymer system here is in the range of previously developed antifouling coatings, e.g. 6.7 % in a cell repellent dextran coating.²⁴⁰

It is known that multivalently presented catechol groups alone do not exhibit a robust surface anchoring capability²⁴¹, and the presence of amine groups is important.²³⁰ The ratio of free, unreacted amine groups remaining on the polymer system to catechol groups (ca. 2 to 1) is aligned with the value previously reported for some stable coatings.²³⁷ Some of the free amine groups can be also further conjugated to introduce new properties to the polymer and therefore to the substrate, e.g. conjugation of AMPs to introduce bactericidal activity as will be seen later in

this chapter or conjugation of RGD²⁴² to selectively enhance osteoblast adhesion on the substrates.

4.2.2 Coating of DA51-cat

To coat the samples with the DA51-cat, two approaches were taken (**Figure 4.6B**): (i) directly using the synthesized DA51-cat, and (ii) first coating the samples with a layer of PDA followed by the DA51-cat layer.

In the first approach, silicon wafers, gold-coated silicon wafers and pPVC coupons were immersed in a 10 mg/mL solution of DA51-cat in 3-(*N*-morpholino)propanesulfonic acid (MOPS) sodium buffer at pH 8.5 for 24 h. The water contact angle and thickness of the coated layers were evaluated after washing and overnight drying. **Figure 4.7** shows that the water contact angle and thickness of the coated layers are similar for gold and silicon wafer samples independent of their initial hydrophobic/-philic character, and the resulting water contact angle was 30° to 35° due to the single layer DA51-cat coating (**Figure 4.7A**, DA51-cat). However, the coating of the platelet bag material was obviously not as efficient and non-uniformity in water contact angle was observed across the same sample.

In the second approach, silicon wafers, gold-coated silicon wafers and pPVC coupons were first immersed in a 1 mg/mL solution of dopamine·HCl in phosphate buffer pH 8.5 for 10 h to get an 11 to 13 nm layer of PDA (**Figure 4.7B**, PDA). PDA-coated samples were then immersed in the 10 mg/mL solution of DA51-cat in MOPS buffer. This second layer added 3 to 4 nm on top of the PDA on both the gold and silicon substrates (**Figure 4.7B**, PDA-DA51-cat). Contrary to the single layer DA51-cat coating, using PDA layer followed by DA51-cat coated pPVC

samples uniformly and decreased the water contact angle to as low as 40°, which proved the efficiency of this approach for coating pPVC (**Figure 4.7A**).

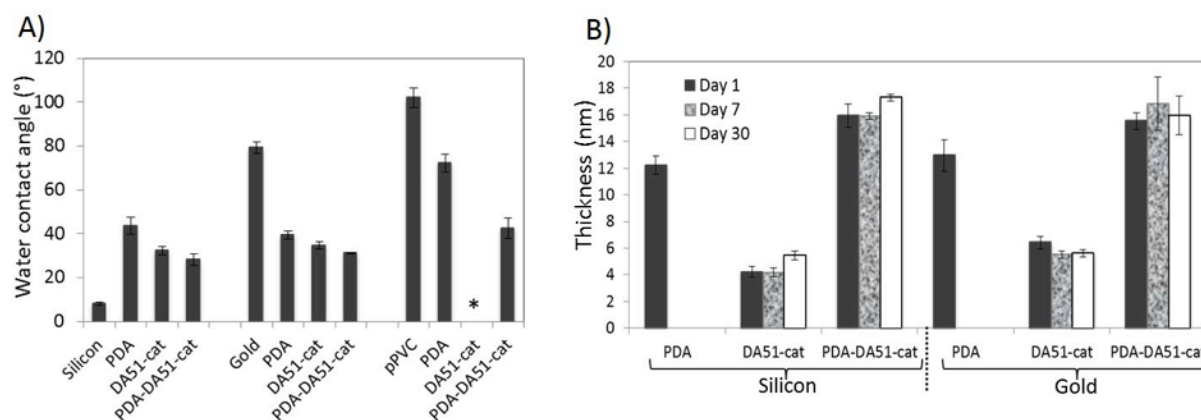


Figure 4.7 A) Static water contact angle on the bare and coated substrates. * DA51-cat failed to coat pPVC surfaces uniformly. **B) Thickness of PDA, DA51-cat and PDA-DA51-cat coatings on silicon and gold surfaces** after 1 day (black), 7 days (grey mosaic), and 30 days (white) of storage in sterile PBS measured by ellipsometry. The thickness and water contact angle values are reported as Avg \pm SD of at least three different samples.

The difficulty of coating a polymeric substrate (pPVC here) compared to the inorganic samples has been observed before. It has been reported that an active coating was required to coat polystyrene, while a less active coating (lower percentage of catechol) could be used directly to coat titanium oxide effectively.²³⁸ A simple dip coating of zwitterionic polymers onto hydrophobic surfaces has also been reported to be challenging because of the stronger interaction of the polymers with water.²⁴³ The lower efficiency of the single layer coating on pPVC samples can be related to the strong hydrophobic nature of pPVC, as well as the large scale of roughness and the presence of holes, grooves and defects on pPVC material (**Figure 4.8**). It is possible that the presence of the antioxidant BHT (butylated hydroxyl toluene) in the platelet bag material could also play a role.

It was also observed that under exactly the same conditions of coating, PDA coating changed the water contact angle on silicon wafers and gold to around 40° while it only changed it on pPVC to around 70° (**Figure 4.7A**). Previous studies have obtained water contact angles around 47° resulting from PDA coatings on various hydrophilic/phobic substrates.²³⁰

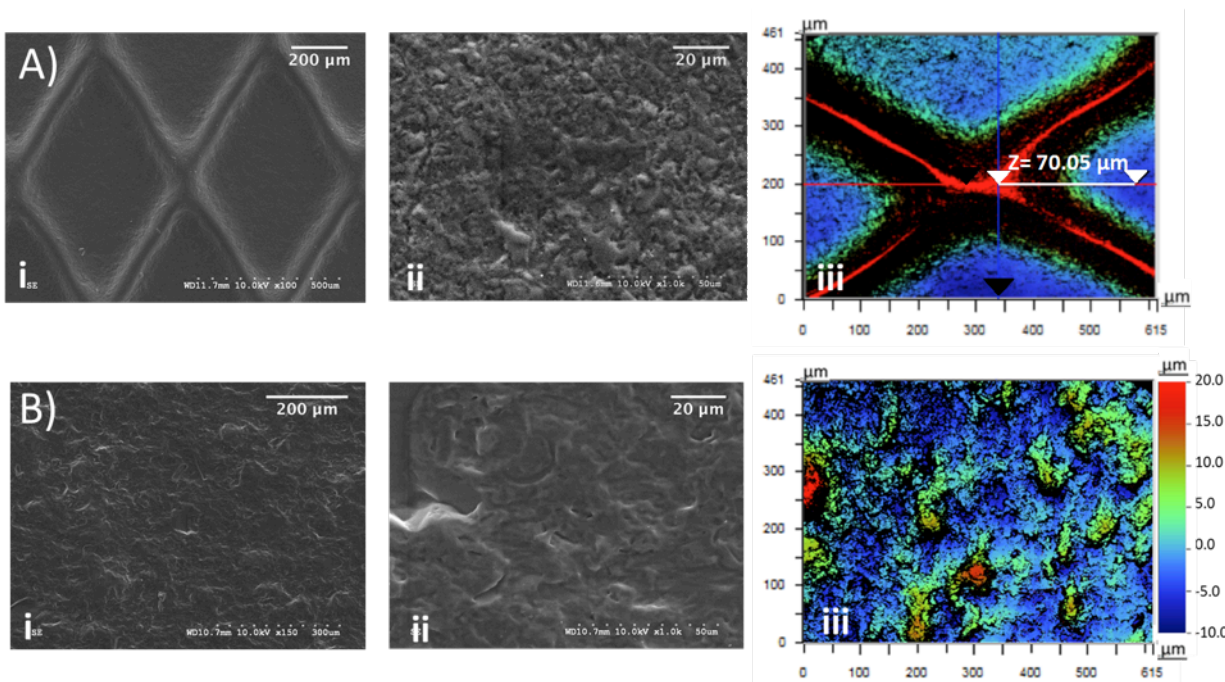


Figure 4.8 Both textured (A) and non-textured (B) surfaces of the pPVC substrate used in this chapter have a large scale of roughness. SEM and optical profilometry were used to image the surfaces.

There were no significant changes in the layer thickness of the coatings on silicon and gold substrates during 7 and 30-day storage in sterile PBS pH 7.4 (**Figure 4.7B**), which demonstrated the stability of the coating. Water contact angle on pPVC samples did not change within 7 days. After 30 days of storage in sterile PBS, a small increase was observed; however, it was statistically insignificant (Appendix C2).

Besides the oxidizing and cross linking of the catechol and amine groups that form the moisture-resistant bonds for anchoring onto the substrates, hydrophobic interactions between the polymer back bone and pPVC as well as pi-stacking between the catechol groups and the

aromatic rings of the plasticizer (TEHTM) can also be contributing forces between the coating and the substrate, as have been reported for other relevant materials.^{244–246}

Using SEM, some particles and aggregates in the size range of 300 nm to a few microns were observed sporadically on the surfaces of pPVC-PDA-DA51-cat (**Figure 4.9**). By comparing these images with pPVC-PDA surfaces, these structures seemed to be PDA assemblies, since DA51-cat did not form such microscopic structures by itself.

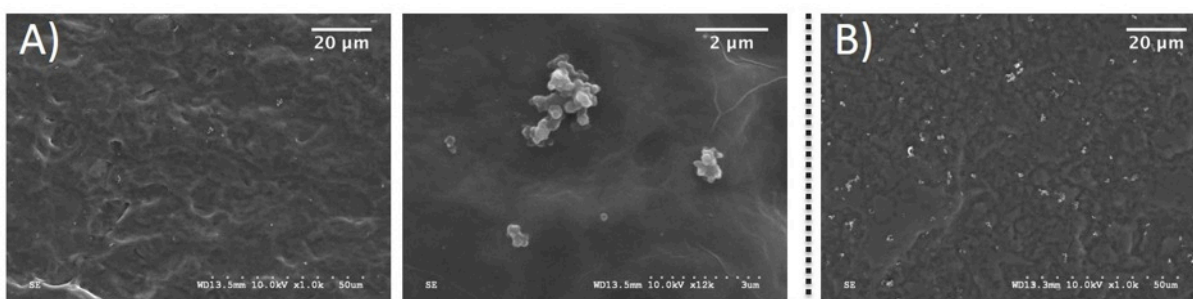


Figure 4.9 PDA aggregates were sporadically observed on pPVC surfaces (A). Shaking the samples during coating increased the amount of aggregates (B). In all the experiments, PDA coating was performed under static conditions.

A solution of pPVC in THF (1/240 w/w) was spin coated on the quartz crystal microbalance (QCM) sensors, which formed a uniform 32 ± 5 nm layer. The pPVC-coated sensors were placed in the flow chamber, and PBS with a flow of 0.1 mL/min was pumped over the surface. No loss of the mass was observed, which proved the stability of the spin-coated pPVC. Then, a 10 mg/mL solution of DA51 in MOPS buffer was pumped over the pPVC-coated sensors and no deposition of polymer was observed, while a flow of 10 mg/mL of DA51-cat solution in MOPS buffer caused a stable shift in the frequency of quartz crystal ($\Delta f \sim -80$ Hz) within one hour which proved development of a coating of DA51-cat on the pPVC material (**Figure 4.10**).

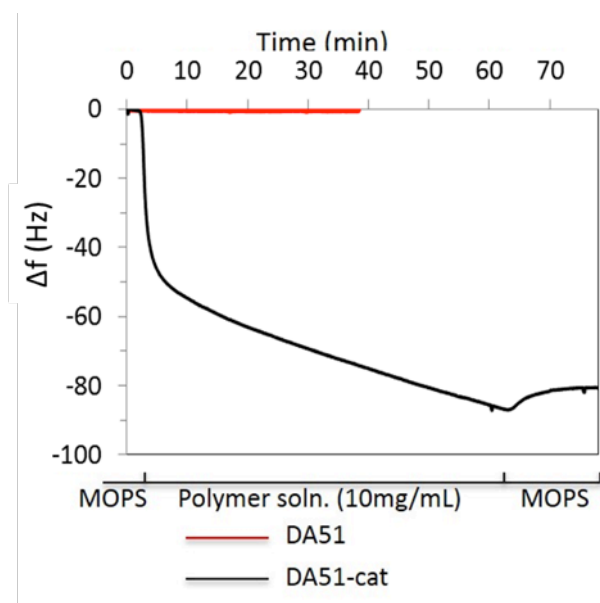


Figure 4.10 DA51-cat (black trace) could deposit on pPVC-coated sensors ($\sim 1300 \text{ ng/cm}^2$) within 1 h of flow under basic conditions (MOPS buffer, pH 8.5) while DA51 (red trace) did not show any interaction with the surfaces.

pPVC-coated sensors were additionally coated with DA51-cat or PDA-DA51-cat according to the procedure described above for silicon wafers, gold-coated silicon wafers and pPVC. A single layer of DA51-cat without an additional PDA adhesion layer decreased the water contact angle to 55° (**Figure 4.11**). On the other hand, as shown before, the DA51-cat single layer could not coat the commercial pPVC samples. The decrease in water contact angle resulting from the PDA layer was also different on spin-coated pPVC versus commercial pPVC (**Figure 4.11**). The spin-coated pPVC layer formed a smooth layer (a $32 \pm 5 \text{ nm}$ layer), but it was as hydrophobic as the commercial pPVC. Therefore, the surface roughness (**Figure 4.8**) can be one factor in the failure of the single layer in coating commercial pPVC.

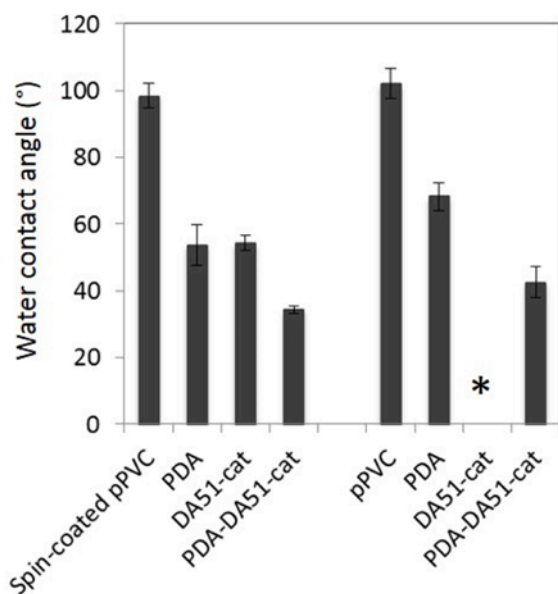


Figure 4.11 Static water contact angles on the bare and coated substrates. pPVC refers to platelet bag coupons. Spin-coated pPVC was prepared by dissolving pPVC coupons in THF and spin coating the solution on the QCM sensors. *DA51-cat failed to coat pPVC surfaces uniformly.

4.2.3 Fibrinogen adsorption

QCM-D (QCM with dissipation monitoring) measurements were used to evaluate the antifouling properties of different coatings against fibrinogen. Fibrinogen is known to strongly adsorb on hydrophobic surfaces.²⁴⁷ Both platelets and bacteria have fibrinogen-binding receptors, and adsorbed fibrinogen on surfaces can promote subsequent platelet/bacterial adhesion.^{51,248}

The pPVC-coated sensors were additionally coated with DA51-cat or PDA-DA51-cat according to the procedure described above. Samples were placed in the QCM-D device. After a stable baseline was reached by flowing PBS over the sensor surface, a 1 mg/mL solution of fibrinogen in PBS was passed over the surface for 30 minutes followed by a 10-minute PBS wash to remove any loosely attached fibrinogen. The frequency change of the quartz crystal on the coated or noncoated sensor surface before and after exposure to fibrinogen (after the 10-min PBS wash) correlates with the amount of adsorbed protein. Using the Sauerbrey equation²⁴⁹, the

amount of adsorbed fibrinogen on the untreated sensor-pPVC was calculated to be 1947 ± 30 ng/cm^2 , while PDA-DA51-cat coating on pPVC decreased the fibrinogen adsorption to as low as 5 % of the control (152 ± 62 ng/cm^2) (**Figure 4.12**).

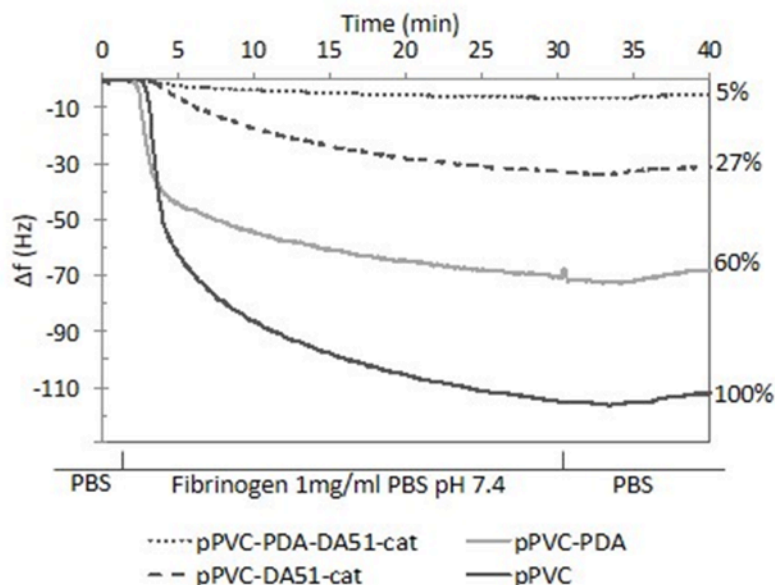


Figure 4.12 QCM traces (the third overtones) showing the shift in frequency (Δf) of the quartz crystal versus time in response to fibrinogen adsorption on untreated or treated pPVC-coated sensors. After obtaining a stable PBS baseline, the fibrinogen solution (1 mg/mL) was pumped over the sensors for 30 minutes followed by a 10-minute PBS wash to remove loosely bound proteins. The difference between the frequency at time 0 and 40 minute was used to find Δf . This value for the modified samples was compared with the untreated sample, pPVC-coated sensor, set as 100 %.

The single layer of DA51-cat without an additional PDA adhesion layer, however, decreased fibrinogen adsorption only to 30 % of the control. This confirms the partial success of single layer coating for the spin-coated pPVC, consistent with the change in water contact angle as discussed above.

Compared to the control sensors (with pPVC layer), PDA-coated samples revealed fibrinogen adsorption of around 60 % of the control. Previous studies have also shown that polydopamine coatings do not introduce antifouling properties to substrates. For example,

equivalent or higher bacterial adhesion on polydopamine-coated polycarbonate²⁵⁰ and stainless steel²⁵¹ substrates have been reported compared to the bare ones. Also, the same level of fibroblast cell adhesion on a bare glass substrate and PDA-coated one²³⁰ has been observed. The PDA layer, however, has been reported to attenuate the inflammatory responses to quantum dots and poly(L-lactic acid)²⁵² and to enhance biocompatibility of gold nanoparticles²⁵³ and graphene quantum dots.²⁵⁴

The PDA layer offered an active layer on pPVC surfaces for the anchoring of DA51-cat effectively and the resulting PDA-DA51-cat coating introduced strong antifouling properties to pPVC against fibrinogen.

4.2.4 Bacterial resistance

Although QCM-D measurements provide a quick method for the evaluation of antifouling properties of coatings, previous studies have shown that a single protein adsorption challenge cannot validate the non-fouling properties of a surface against bacteria or cells.¹⁷²

S. epidermidis, a normal skin flora microorganism, is one of the most commonly isolated bacterial strains from platelet bags as it may be introduced into the bag during blood collection or processing. This bacterial strain can form a biofilm in platelet concentrates and also has a slow growth rate that makes its detection during sampling of the cell suspension from the bag more challenging.

S. epidermidis is also well known for biofilm formation on surgical implants but interestingly was not considered an opportunistic pathogen until the widespread use of medical devices in recent decades.²⁵⁵ The bacteria in biofilm structures generally show high resistance to the common treatment effective against planktonic populations²⁵⁶ and the complications

associated with them result in a financial burden for biomedical devices and food processing equipment.²⁵⁷

To evaluate the antifouling character of the developed coating against *S. epidermidis* and platelets, the PDA-DA51-cat coating was used, which had shown promising results in protecting pPVC surfaces against fibrinogen adsorption.

Samples of the control pPVC (cuts from the platelet bag material) and the coated ones were horizontally placed in 24-well plates and covered with a 1×10^6 CFU/mL inoculum of SE10002, a biofilm-positive *S. epidermidis*, in tryptic soy broth (TSB) enriched with 0.5 % glucose (TSBG). TSBG is a bacterial growth medium that promotes biofilm formation. After a 32-h incubation period at 37 °C with 70 rpm shaking, samples were gently washed and fluorescently labeled with Syto 9, a green fluorescent nucleic acid dye. Syto 9 stains both live and dead bacteria. **Figure 4.13** shows that the polymer-coated samples could resist bacterial adhesion under the challenging conditions of high bacterial concentration in an ideal culture medium at 37 °C. This condition supported biofilm formation on the control pPVC surfaces (**Figure 4.13A**) on which extracellular matrix was observed as well (marked by arrows on **Figure 4.14A**).

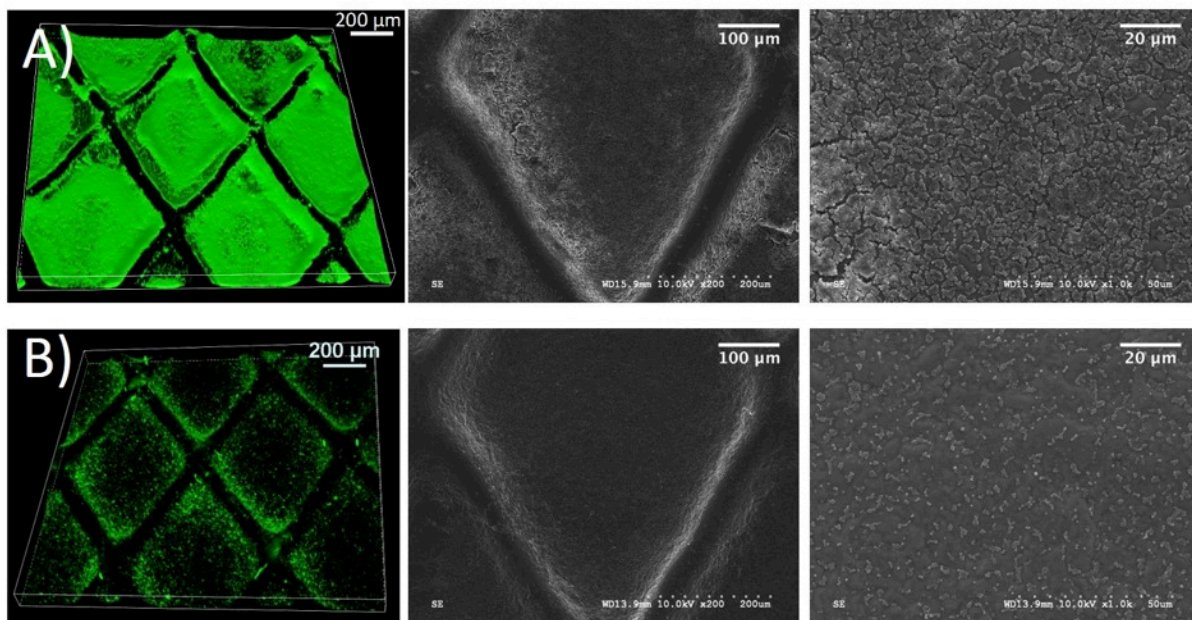


Figure 4.13 Fluorescent 3D confocal images (left-hand panels) and SEM images of control pPVC (A) and pPVC-PDA-DA51-cat (B) after 32-h incubation with SE11002, a biofilm-positive *S. epidermidis* strain, at 37 °C showed less bacterial adhesion and biofilm formation on the modified samples. The bacteria were stained with Syto 9 for fluorescence microscopy. Images are representative of three separate bacterial cultures.

To quantify the difference between the control and coated samples, small coupons of pPVC were cut and coated on both sides with PDA-DA51-cat. The coupons were put vertically in a bacterial inoculum of SE10003, a biofilm negative *S. epidermidis* strain, in 96-well plates for 4 h at 37 °C. The attached bacteria were released by sonication and quantified via serial dilution and spotting on agar plates. The PDA-DA51-cat-coated samples could decrease the bacterial adhesion to as low as 7 % of the control pPVC coupons (**Figure 4.14B**). This method of quantification could not be applied for the long-term incubation tests because the release of the adhered bacteria (mostly in biofilm structure) was not complete under the sonication condition.

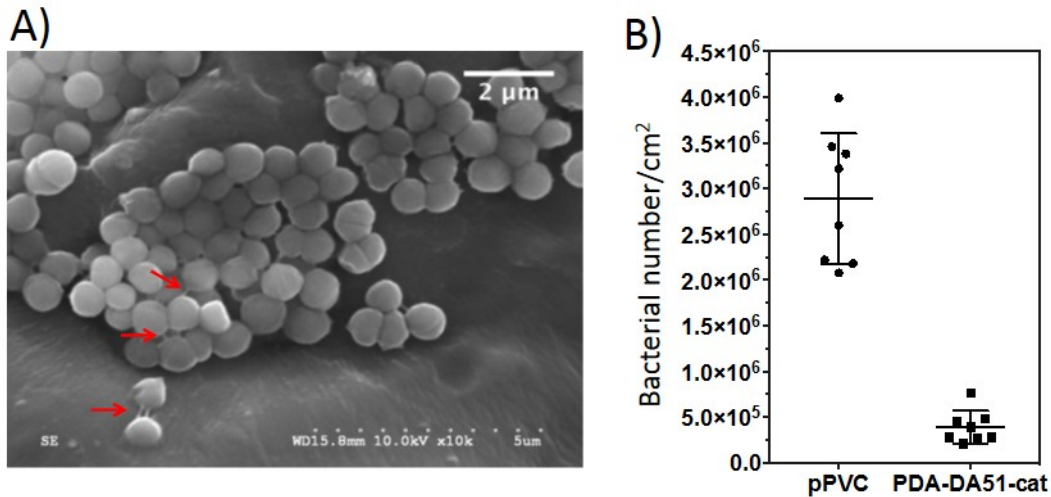


Figure 4.14 A) A cluster of SE10002, a biofilm-positive *S. epidermidis* strain, on the untreated pPVC samples with appearance of extracellular matrix (marked with arrows). B) Number of the released bacteria from pPVC coupons (CFUs/cm²) after 4-h incubation with SE11003, a biofilm-negative *S. epidermidis* strain.

As shown before pPVC has one textured face and one non-textured face. For imaging experiments, each side was evaluated independently; **Figure 4.13** and Appendix C3 represent the textured surfaces and the non-textured ones, respectively; the PDA-DA51-cat layer resisted bacterial adhesion on both faces of the substrates. In the dislodging method, the pPVC coupons (with one textured and one non-textured face) were positioned vertically in the bacteria media so the bacteria were dislodged from both surfaces.

For both imaging and quantification (dislodging method) experiments, the applied conditions were different from blood bank storage conditions. By using a rich culture media, 37 °C and high concentration of bacteria inoculum, the developed coating was challenged to a higher degree compared to the relevant clinical conditions.

The widespread emergence of antibiotic resistance encourages approaches that combat the initial phases of biofilm formation, ie., physicochemical interactions between bacteria and

surfaces.⁷⁶ In this regard, antifouling coatings such as PDA-DA51-cat that can be easily applied to any substrate are promising developments.

4.2.5 Biocompatibility with platelets

Mini platelet bags (Appendix C4) were fabricated for platelet storage tests. pPVC coupons were cut and then sealed together from three sides using a heat sealer. To modify the bags with the polymer coating, they were filled with dopamine solution, clamped on the top, and placed horizontally under static conditions. After 10 h, the bags were emptied, washed thoroughly, and filled with DA51-cat solution and placed on a rocking shaker at 10 rpm. After 24 h, the bags were washed.

Control and modified pPVC minibags were filled with 3 mL of platelet-rich plasma. After 24 h storage on a platelet agitator at 22 °C, 4 coupons from the lower faces were cut and evaluated for platelet adhesion. Fluorescent images of the platelets labeled by CD42a-FITC conjugated antibody demonstrated the much lower adhesion of platelets to the pPVC with PDA-DA51-cat coating (**Figure 4.15A, iii**) compared to the control samples (**Figure 4.15A, i and ii**). Both fluorescence and SEM images showed that the platelet aggregation and activation was not uniform across the surfaces of the control pPVC mini bag pieces. Around 30 % of the area scanned by the microscopes showed aggregates of activated platelets while other areas did not (**Figure 4.15B, ii**). This non-uniformity may be due to the design of the minibags and the way platelets move in them during agitation or chemical non-uniformity in the plane of the surfaces. The platelet adhesion level on the treated samples (pPVC-PDA-DA51-cat) was uniform across the samples (**Figure 4.15A, iii and 4.15B, iii**) and much lower compared to the controls. In SEM images of these samples, the white spots on the coated samples are mostly PDA aggregates

(compare with **Figure 4.9**). In higher magnification images (**Figure 4.15C and 4.15D**), these sporadic structures can be distinguished from the platelets. These aggregates did not act as starting points for platelet adhesion and activation.

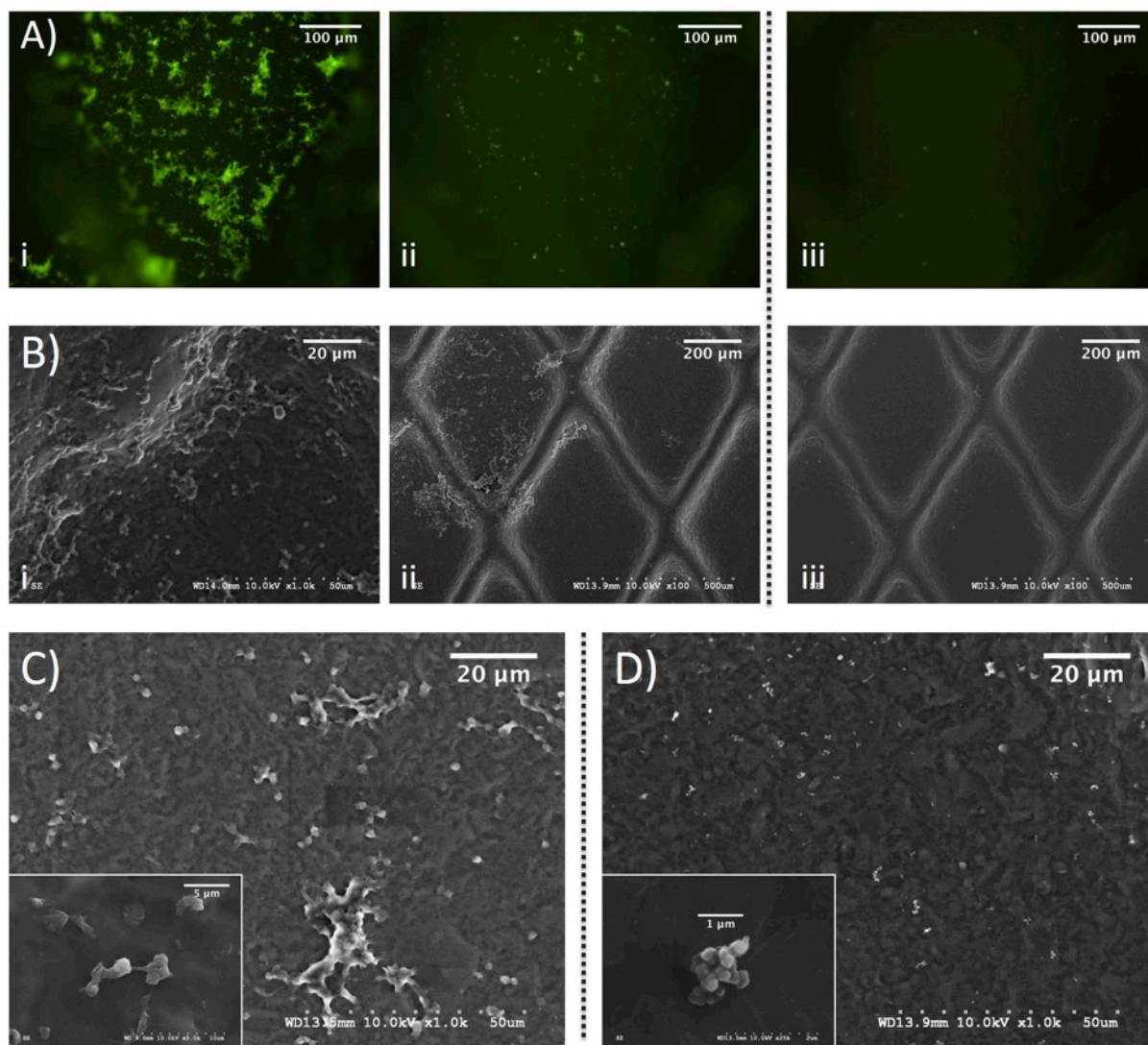


Figure 4.15 Fluorescent images (A) and SEM images (B) of the surfaces of the minibags made of pPVC (i and ii) and pPVC-PDA-DA51-cat (iii) after incubation with platelet-rich plasma for 1 day at 22 °C. Platelets were labeled with CD42a-FITC conjugated antibody for fluorescent images. Platelet adhesion on different scanned area of pPVC samples was not uniform as seen in Ai and Aii as well as SEM images (Bi and Bii). High aggregation and activation of platelets (C) was observed on some areas of pPVC, but not uniformly (Bii). Platelet adhesion was minimal on the modified substrates (Aiii and Biii). White spots seen in higher magnification images of pPVC-PDA-DA51-cat (D) were polymer aggregates as seen in the samples without any contact with platelets (**Figure 4.9**).

A high degree of platelet activation and spreading on PDA-coated stainless steel has been reported before²⁵⁸. Similar results were observed on the silicon wafers coated with a PDA layer (data not shown). Further, in the protein adsorption challenge, the PDA layer could not inhibit fibrinogen adsorption effectively on spin-coated pPVC. Therefore, the antifouling effect against platelet and bacteria is correlated with the biocompatible hydrophilic PDMA layer.

The potential release of any non-anchored and non-crosslinked dopamine seemed a concern; however, previous studies have demonstrated the biological safety of dopamine *in vitro* and *in vivo* with concentrations as high as 100 µg/mL.^{252,259}

A limitation of this study is that it was not performed under the standard conditions of blood banking. As noted above, levels of platelet adhesion varied across the control samples (**Figure 4.15**) and a similar variation was observed in the level of bacterial adhesion on pPVC coupons (**Figure 4.14B**). However, the modified samples showed little variation. Using the standard sized (commercial) platelet storage bags stored under blood banking conditions, and evaluating of their surfaces could be an improvement to this study. Further, with such a setup, the quality of platelets stored in the modified bags versus the control bags could be evaluated by measuring various *in vitro* markers. This data could be used to demonstrate if the developed coating preserves platelet quality and therefore extends the shelf-life of the stored platelets or not. However, doing a series of the relevant experiments in the commercial platelet storage bags requires a large volume of donated platelets (200 mL for each bag), which was not justified at this stage of study.

Although the number of studies on the development of antifouling surfaces based on polyacrylamides is relatively low^{128,131,133,260}, their established biocompatibility makes them a promising candidate for the development of antifouling coatings for biomaterials.

Polyacrylamides have been used as cell-free hydrogels for cartilage regeneration, as subdermal fillers for cosmetic or treatment purposes, and as transurethral and transanal submucosal hydrogels in urinary and anal incontinence.^{261–263}

PDA-DA51-cat showed high resistance against bacterial and platelet adhesion and has a potential to reduce the risk of missed bacterial detection during sampling and prevent the formation of biofilms on bag surfaces. However, it cannot kill the bacteria. As a result of all the preventive measures during the collection and processing of platelets, the bacterial concentration is generally low in the platelet bags. To kill bacteria (if any) in the platelet storage bags, AMPs were added to the developed coating, which will be discussed in the next section.

4.3 Results and Discussion: Bactericidal Coating

4.3.1 DA51-E6-cat: synthesis, coating, and characterization

To add AMPs to the developed polymeric system, the amine groups on DA51-cat were first reacted with an amine-to-sulfhydryl crosslinker, *N*-(β -maleimidopropoxy)succinimide ester (BMPS), to give DA51-L-cat, L for linker (**Figure 4.16A**). Around 6 % of the APMAAs were conjugated to BMPS estimated from ¹H NMR spectrum through integration of the maleimide protons at 6.88 ppm (**Figure 4.16B**) and the methyl group of APMA at 0.93 ppm. DA51-L-cat was further reacted with E6 (**Figure 4.17A**). E6 (Sequence: RRWRIVVIRVRRC) (**Table 4.1**) is an AMP with a cysteine on the C-terminus. E6 was reduced with TCEP prior to mixing with DA51-L-cat.

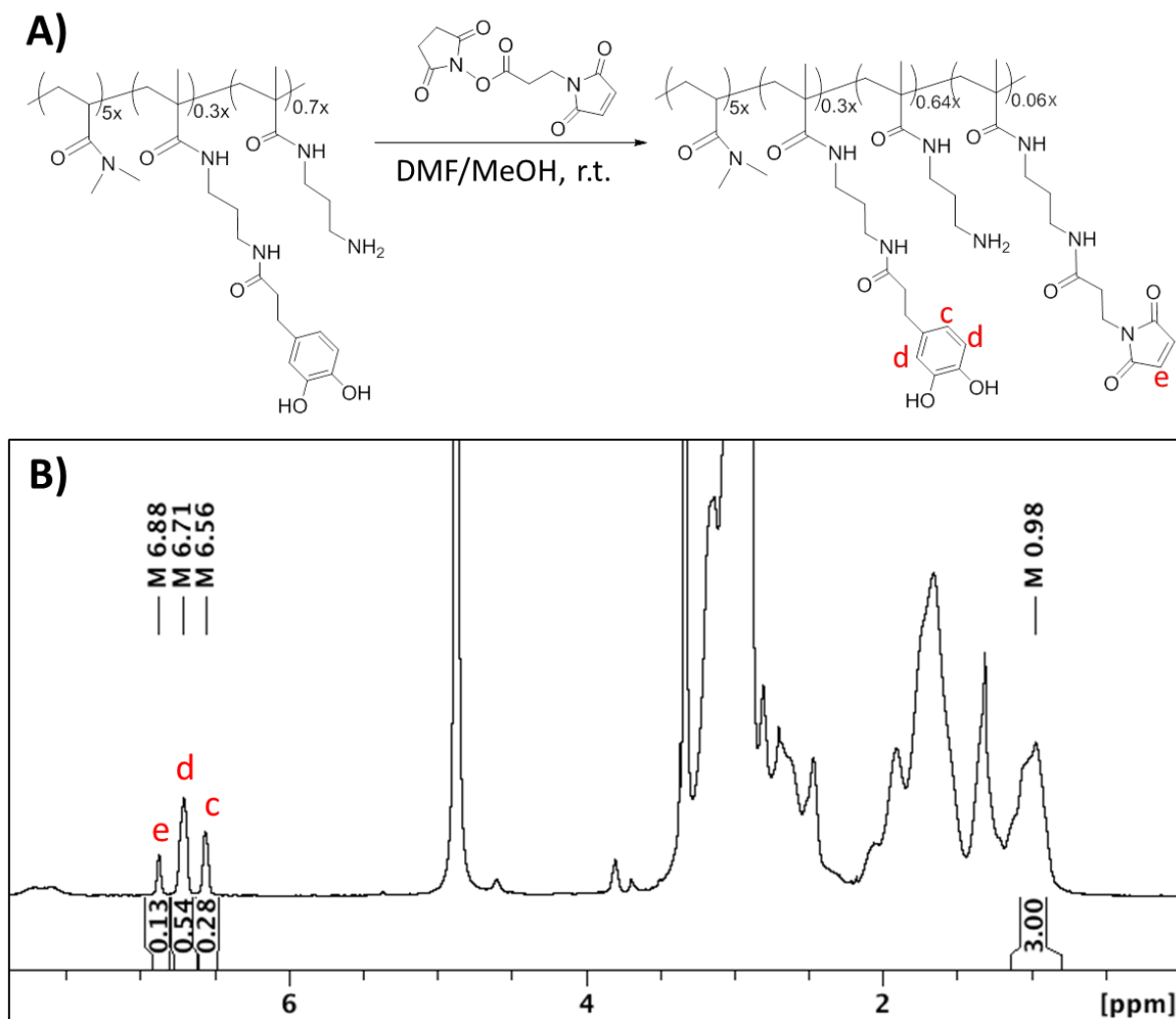


Figure 4.16 A) The scheme of conjugation of DA51-cat to an amine-to-sulphydryl crosslinker, BMPS. B) ^1H NMR spectrum of DA51-L-cat in d_4 -methanol.

The conjugation of E6 was confirmed by disappearance of the maleimide double bond peak at 6.88, and observing some peptide peaks in the zoomed regions (**Figure 4.17B**). ^1H NMR spectrum of E6 is shown in Appendix C5 for comparison. With a molar ratio of 5:1 for DMA:APMA monomers and $\sim 28\%$ conjugation of APMA to catechol and $\sim 6\%$ conjugation of APMA to E6, the density of catechol and E6 was respectively around 5 mol % and 1 mol %, equivalent to roughly 40 catechol groups and 6-8 E6 per a 100 kDa polymer chain.

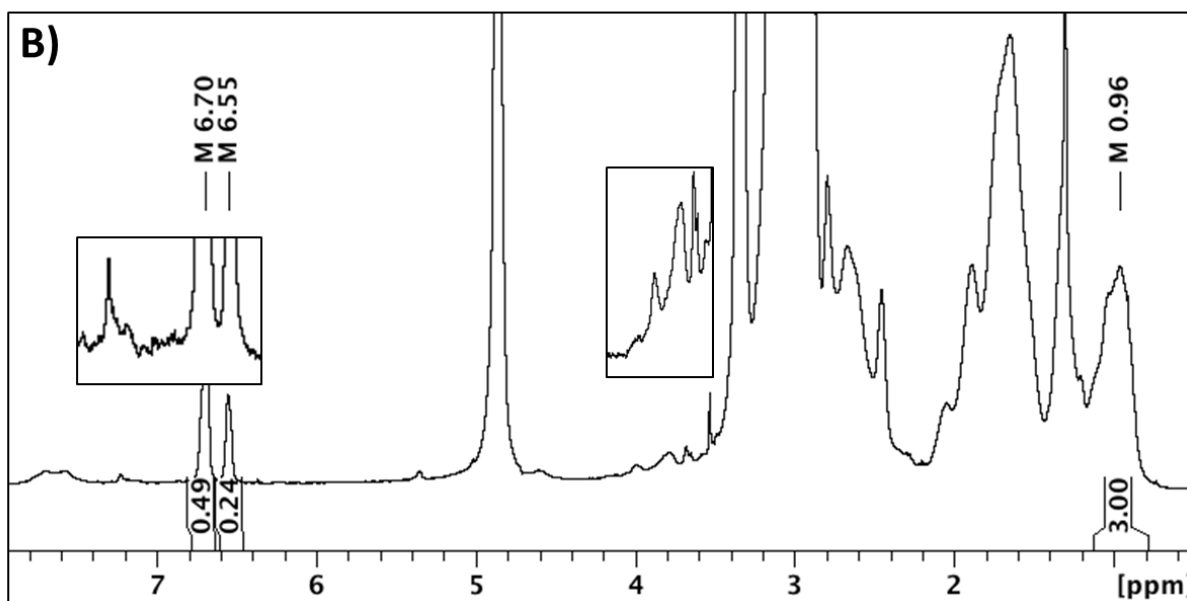
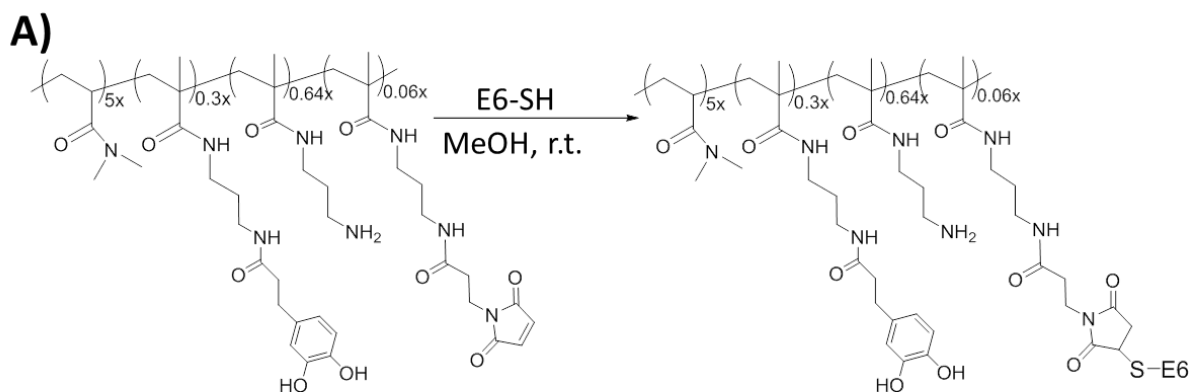


Figure 4.17 A) The scheme of conjugation of DA51-L-cat to a cysteine-containing AMP, E6. B) ^1H NMR spectrum of DA51-E6-cat in d_4 -methanol.

Table 4.1 The structures of amino acids present in E6. E6 sequence is RRWRIVVIRVRRC.

R	Arginine (Arg)	
W	Tryptophan (Trp)	
I	Isoleucine (Ile)	
V	Valine (Val)	
C	Cysteine (Cys)	

The ratio of the conjugation of amines to the linker and consequently AMPs could be increased by adding *N,N*-diisopropylethylamine in the reaction solution. However, a high percentage of the peptide and linker negatively affected the water solubility of the polymer system.

For a proof of concept, PDA-DA51-E6-cat was coated on silicon wafer surfaces by the same two-step procedure explained for PDA-DA51-cat. The thickness of PDA-DA51-E6-cat was 18.4 ± 0.6 nm versus 14.8 ± 0.7 nm for PDA-DA51-cat. The thickness of the DA51-E6-cat coating on silicon wafers was 5.9 ± 0.3 nm versus 3.2 ± 0.3 nm for DA51-cat on the substrate. The higher thickness of E6-containing coating can be attributed to the charged and hydrophobic character of E6 that contributes to the formation of more and larger aggregates.

Silicon wafers coated with PDA-DA51-E6-cat were studied by TOF-SIMS for confirmation of E6 presence and distribution on the surfaces. A TOF-SIMS spectrum of silicon wafers coated with PDA-DA51-cat was collected as a negative control for comparison.

TOF-SIMS provides high mass resolution of ~ 5000 m/ Δ m and high surface sensitivity with a ~ 2 nm sampling depth.²⁶⁴ These features make TOF-SIMS suitable for studying proteins on surfaces, including their conformation and orientation. For example, when the conformation of a protein changes, the amino acid side chains that are in the TOF-SIMS sampling region will be different and this change can be detected.²⁶⁵ Further, by rastering the ion beam over the sample and collecting sufficient data, an image with a high lateral resolution (as low as 100 nm) can be obtained.

Positive and negative ion TOF-SIMS spectra of the silicon wafer samples coated with either PDA-DA51-E6-cat or PDA-DA51-cat were collected. One characteristic difference between these two coatings is the presence of a sulfhydryl group in the E6-containing coating as

E6 carries one cysteine. **Figure 4.18A** shows negative ion TOF-SIMS spectrum of Si-PDA-DA51-E6-cat. The two most abundant isotopes of sulfur were detected at 31.9707 u (Reference: 31.972071 u) and 33.9666 u (Reference: 33.967867 u). Their relative abundance was 443 (^{32}S) and 19 (^{34}S), that gave an abundance ratio of ~ 23 . The abundance of sulfur isotopes in nature is 95.02 % for ^{32}S and 4.21 % for ^{34}S , which gives the similar abundance ratio of 22.6. As seen in **Figure 4.18B**, some sulfur (^{32}S) peak with very low intensity was detected in the negative control sample (Si-PDA-DA51-cat) that could be due to contamination.

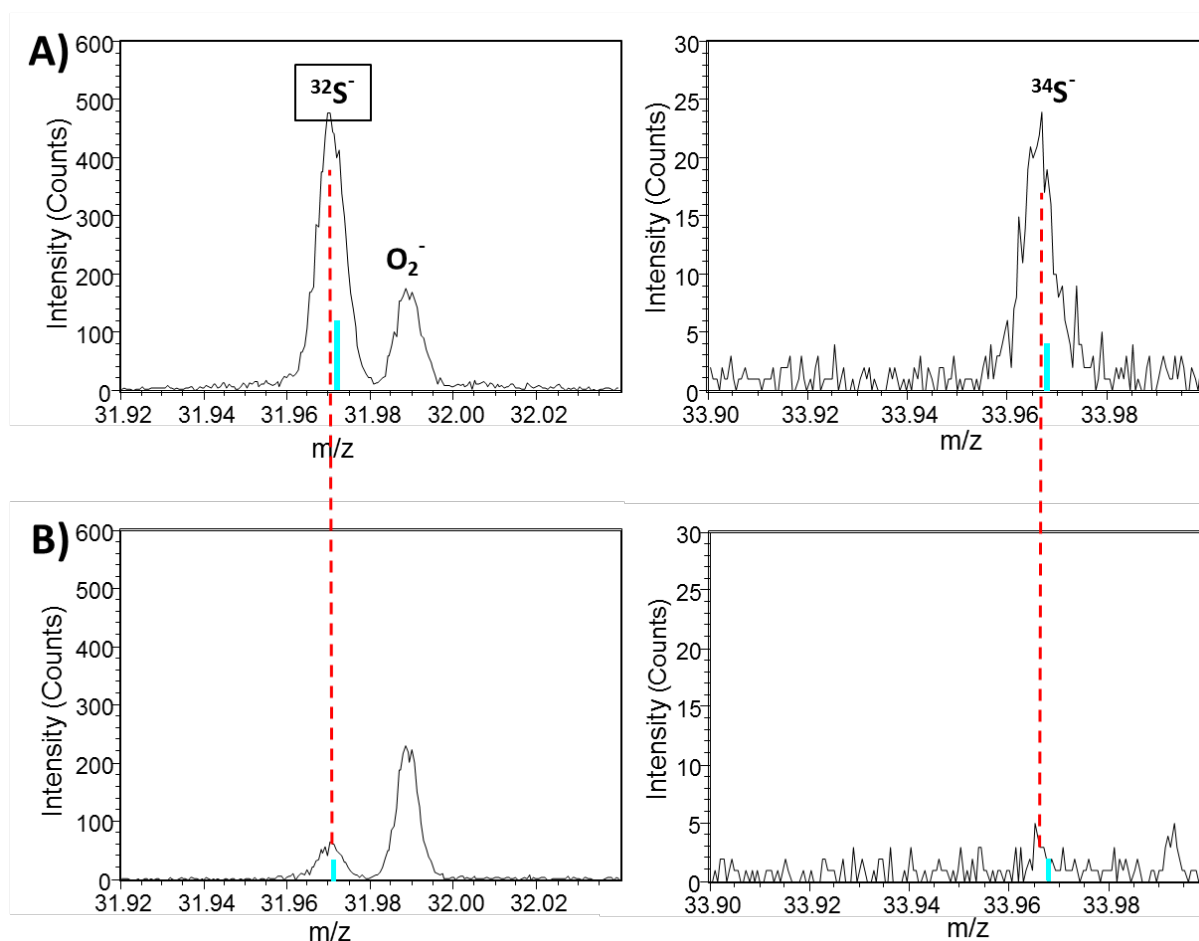


Figure 4.18 The negative ion TOF-SIMS spectra of the silicon wafer samples coated with PDA-DA51-E6-cat (A) and PDA-DA51-cat (B). The theoretical positions of two most abundant sulfur isotopes (^{32}S and ^{34}S) are marked with turquoise lines by the software.

The mapping of ^{32}S (Figure 4.19A, i) shows the uniform distribution of E6 across $400 \times 400 \mu\text{m}$ scanned areas of the Si-PDA-DA51-E6-cat sample. The total ions collected from the sample are also shown (Figure 4.19A, ii). Essentially the same counts of ions were collected from both samples: PDA-DA51-E6-cat (3,014,241) and PDA-DA51-cat (3,019,735). The ion count of sulfur on PDA-DA51-E6-cat was 7108 versus 846 on the negative control sample, PDA-DA51-cat.

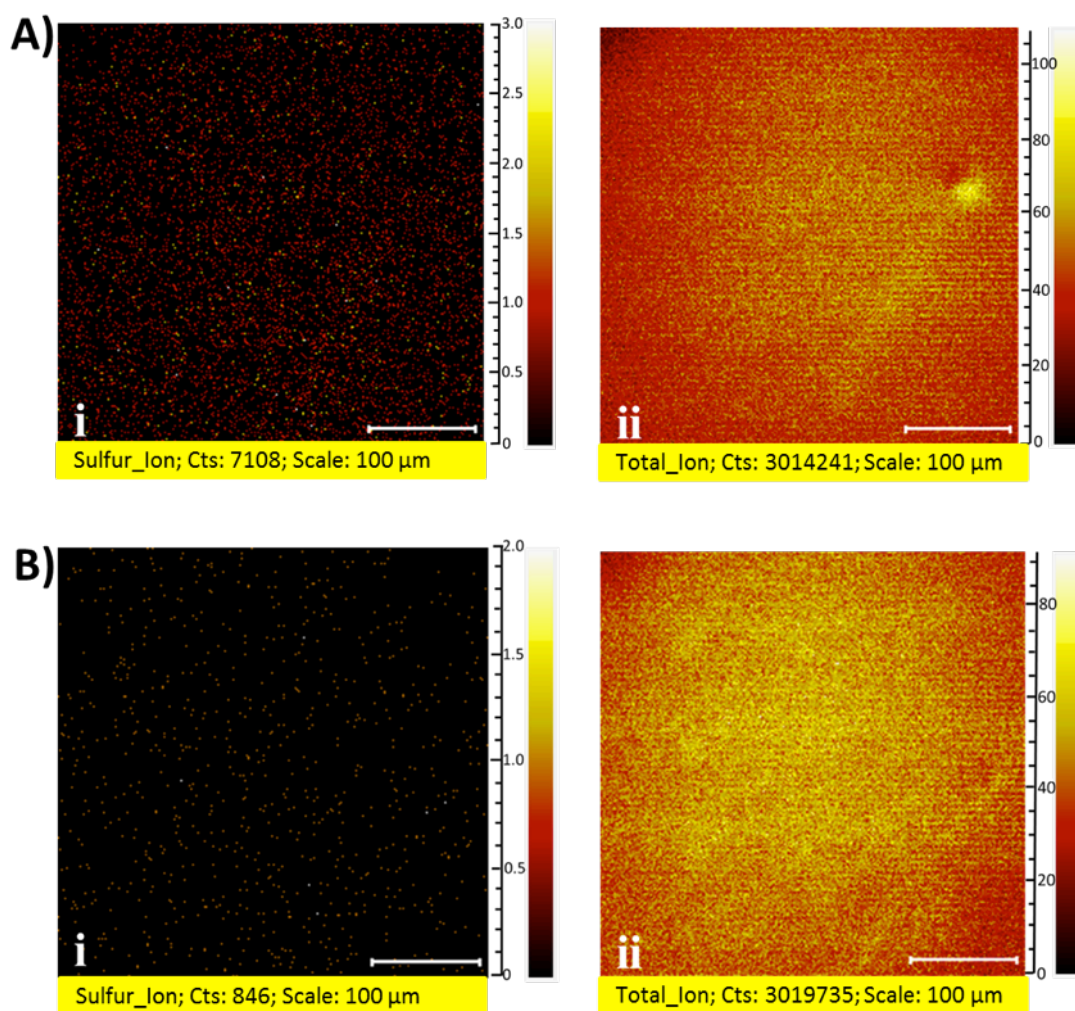


Figure 4.19 TOF-SIMS ion maps of ^{32}S on silicon wafers coated with PDA-DA51-E6-cat (Ai) and PDA-DA51- cat (Bi). The corresponding total ions maps are shown in Aii and Bii. In each image a $400 \times 400 \mu\text{m}$ area was sampled and the total collected ions were kept similar for the samples. The scale bar marks 100 μm .

The other amino acids of E6 were studied by positive ion TOF-SIMS. The characteristic peaks of arginine²⁶⁶ at 43.0290 u (CH_3N_2^+ , Reference: 43.02960 u) (**Figure 4.20**), 73.0624 ($\text{C}_2\text{H}_7\text{N}_3^+$, Reference: 73.06395 u) (**Figure 4.21**), and 127.0985 ($\text{C}_5\text{H}_{11}\text{N}_4^+$, Reference: 127.09830 u) (**Figure 4.21**) were detected in the samples coated with PDA-DA51-E6-cat, while they were absent in PDA-DA51-cat coated samples (**Figure 4.20** and **Figure 4.21**).

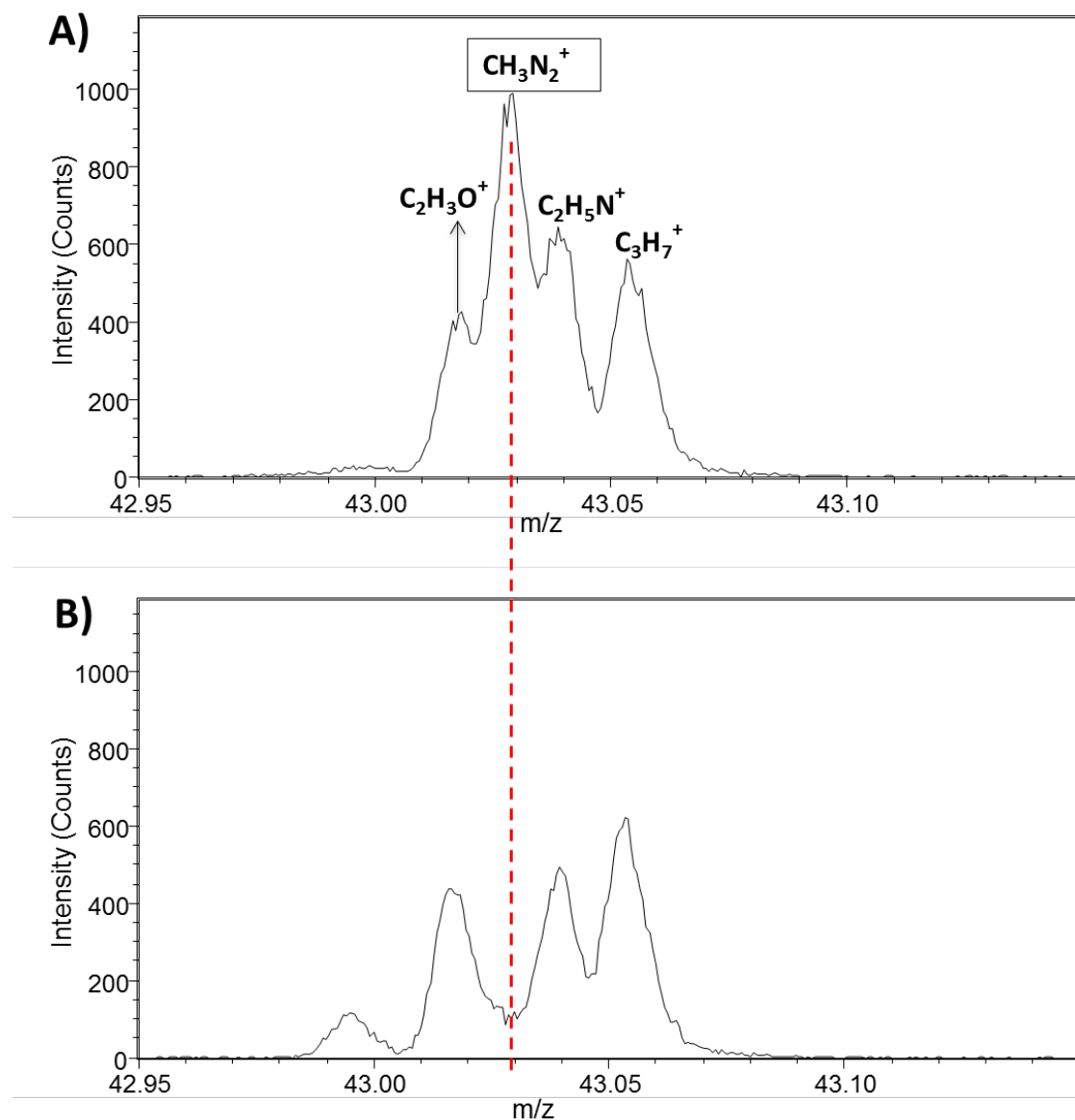


Figure 4.20 The positive ion TOF-SIMS spectra of the silicon wafer samples coated with PDA-DA51-E6-cat (A) and PDA-DA51-cat (B). The characteristic peak of arginine at 43.0290 was detected in the PDA-DA51-E6-cat samples.

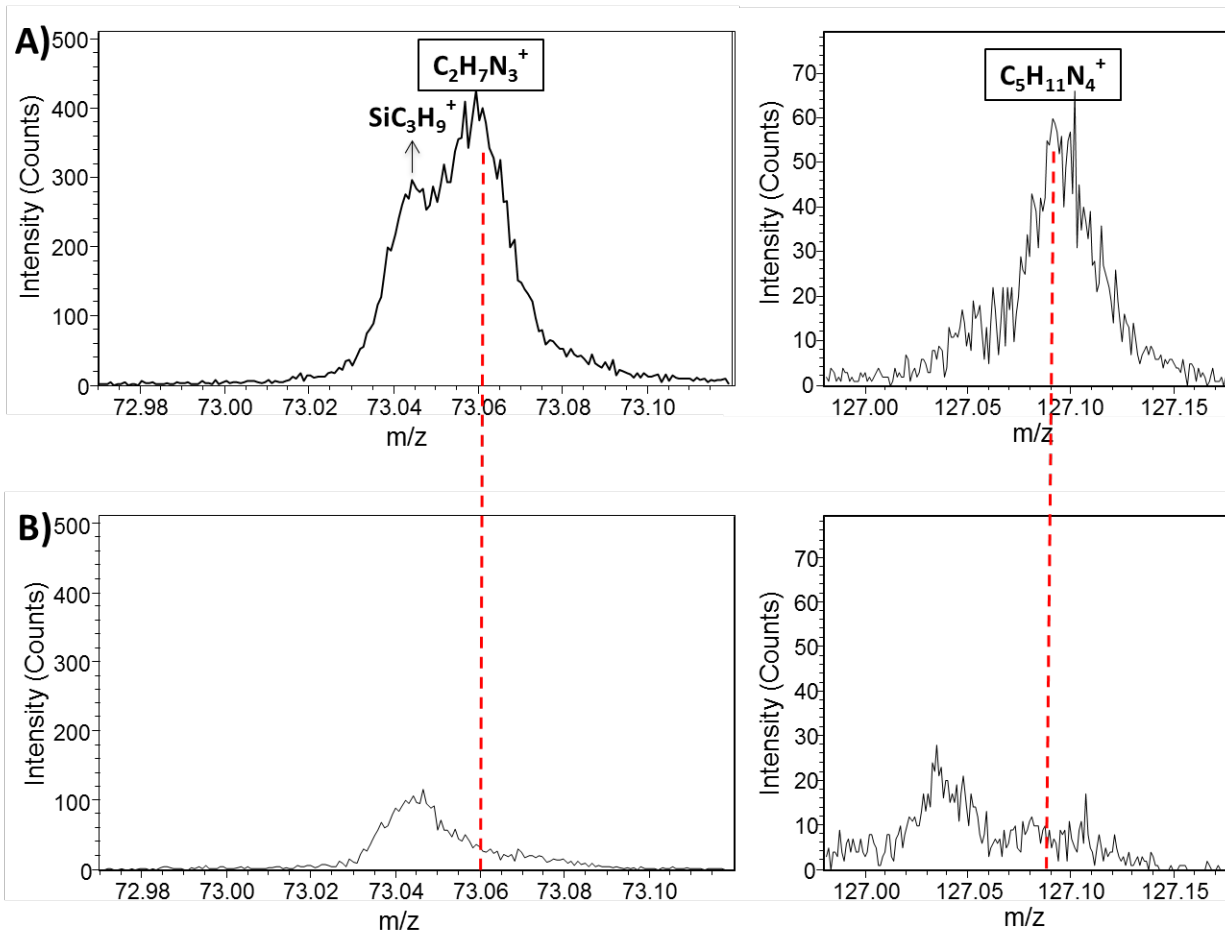


Figure 4.21 The positive ion TOF-SIMS spectra of the silicon wafer samples coated with PDA-DA51-E6-cat (A) and PDA-DA51-cat (B). The characteristic peaks of arginine at 73.0624 and 127.0985 were detected in the PDA-DA51-E6-cat samples.

Similarly, the characteristic peak of isoleucine at 86.0965 ($C_5H_{12}N^+$, Reference: 86.09691 u) was observed on Si-PDA-DA51-E6-cat samples but not on Si-PDA-DA51-cat (**Figure 4.22**). The characteristic peaks of valine and tryptophan were not distinguishable due to overlap or low intensity, however.

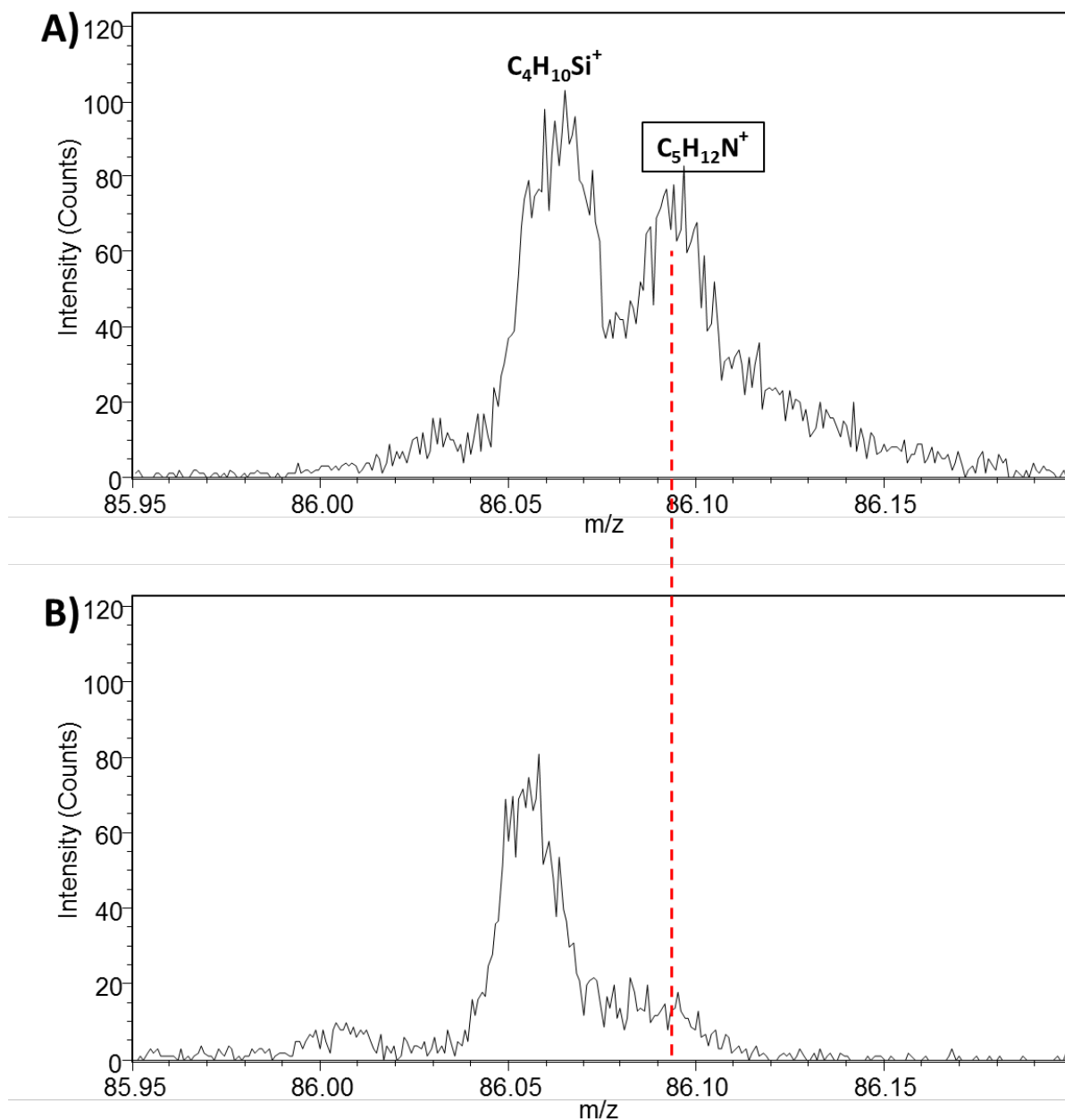


Figure 4.22 The positive ion TOF-SIMS spectra of the silicon wafer samples coated with PDA-DA51-E6-cat (A) and PDA-DA51-cat (B). The characteristic peak of isoleucine at 86.0965 was detected in the PDA-DA51-E6-cat samples.

As seen in Chapter 2, ATR-FTIR is not sufficiently surface sensitive on the scale in which we are interested. Further, its detection limit is relatively high (>1 %). AFM provides surface sensitivity as well as high lateral resolution for studying specific molecules (here E6) on

surfaces. However, functionalization of the tip to make it specific for the target molecule (E6) is required.

Here, both the negative control (PDA-DA51-cat) and PDA-DA51-E6-cat are composed of C, N, and O. E6 has a characteristic sulfur atom but it was not detected by XPS probably because it had a lower concentration than the detection limit of XPS (in the range of parts per thousand) whereas TOF-SIMS has detection limits in the range of ppm to ppb. Static TOF-SIMS (no depth profiling) only samples the outermost 2 nm of the surfaces. Its very high mass resolution (>8000 m/ Δ m at ^{28}Si here) gives it superb chemical specificity. These characteristics of TOF-SIMS made the characterization of low concentrations of AMPs on the coated silicon wafers possible, which was not readily possible with other techniques. TOF-SIMS proved the presence of E6 in the outermost layer of silicon wafers coated with PDA-DA51-E6-cat. The peptide was uniformly distributed across the 400×400 μm samples studied on three different scanned samples.

4.3.2 PDA-DA51-E6-cat: bactericidal activity

To demonstrate the bactericidal activity of the AMP-containing coating, silicon wafer samples coated with PDA-DA51-E6-cat were incubated with 1×10^6 CFU/mL of SE11003 in sterile PBS (not culture medium) at 37 °C for 4 h. Si-PDA-DA51-cat and untreated silicon wafers were incubated under the same conditions for comparison. After the incubation period, the samples were gently washed with sterile PBS and stained using LIVE/DEAD Bac Light Bacterial Viability Kit. This kit contains Syto 9 and a red fluorescent nucleic acid stain, propidium iodide (PI). As mentioned earlier, Syto 9 can stain both live and dead bacteria. PI, on the other hand, can only penetrate the bacteria with damaged membranes, and reduces the Syto 9

fluorescence in these cells. Therefore, the bacteria with damaged membranes will stain red while those with intact membrane will remain green.

Figure 4.23 shows control and coated surfaces under the fluorescence microscope with green (A) and red (B) filter. Almost no bacteria adhered on the silicon wafer with PDA-DA51-cat coating, which again confirmed the strong antifouling properties of this coating (**Figure 4.23, Aii and Bii**). The charged and hydrophobic character of E6 compromised the antifouling property of the coating and attracted some bacteria on the surfaces of Si-PDA-DA51-E6-cat. However, this coating could kill the majority of the adhered bacteria (**Figure 4.23, Biii**). Some bacteria were also observed under the green filter, which means the presence of some live bacteria. It should be noted that for control silicon wafer samples in this test, the natural silicon oxide thin layer was not removed to promote bacterial adhesion.

The presence of more bacteria on the Si-PDA-DA51-E6-cat samples compared to the Si-PDA-DA51-cat as well as the death of some of these bacteria confirmed that E6 was present in the outermost layer of the coating and could interact with the bacterial membrane and disturb their consistency.

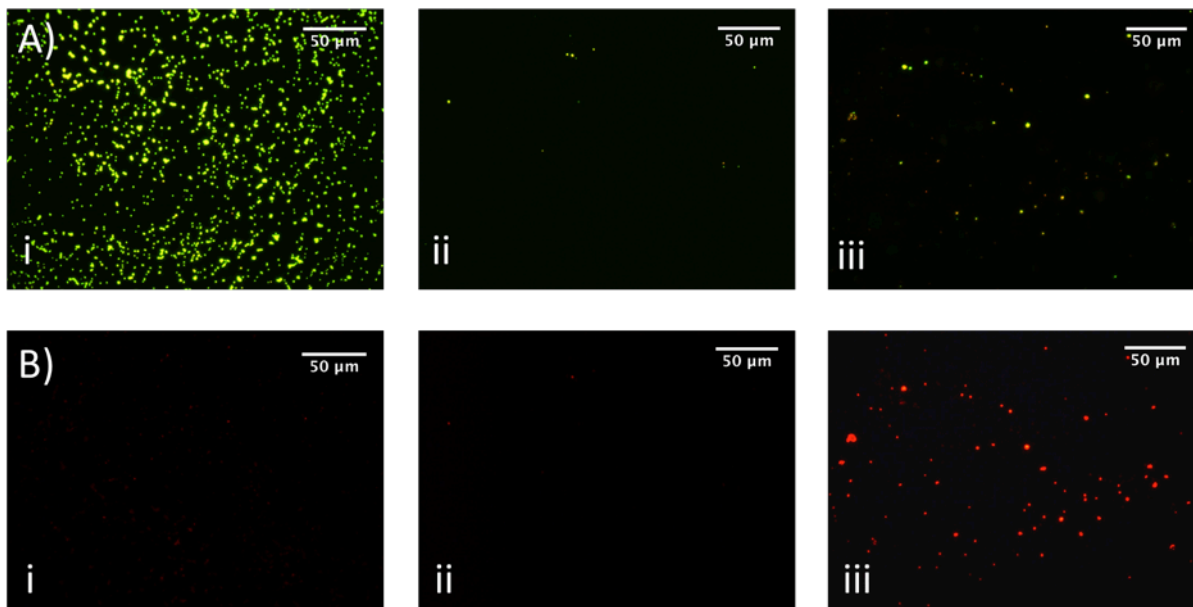


Figure 4.23 Fluorescent images of the untreated silicon wafer (i), silicon wafer coated with PDA-DA51-cat (ii) and silicon wafer coated with PDA-DA51-E6-cat (iii) with green filter (A) and red filter (B). Live and dead bacteria are stained green and red, respectively.

The bacterial inoculum in this experiment had a high concentration (10^6 CFU/mL), which can explain why not all the bacteria on the surfaces were dead. The clinically relevant bacterial concentration in platelet storage bags is much lower (10-100 bacteria per donation).²⁶⁷

As discussed in Chapter 3, tuning the concentration of AMP on the surface is important to make a balance between the bactericidal activity and antifouling properties of the surface. The synthesis of the polymeric system DA51-E6-cat in solution (not on the surface), provides the advantage of an easy control over the concentration of linker and AMP and further their definitive characterization before coating. It was mentioned above that a high concentration of AMP reduced the water solubility of the polymeric systems, which is one factor to be considered in the conjugation of the linker and the AMP to the polymer. The concentration of AMP in our system (6-8 E6 per every 100 kDa chains) was able to preserve the antifouling property of the polymer after coating on the surfaces as well as showing bactericidal activity.

As stated above, pPVC is widely used in medical applications. The demonstrated low-fouling coating (PDA-DA51-cat) and bactericidal coating (PDA-DA51-E6-cat) can be introduced to this material without any distinguishable change of its physical, mechanical and chemical properties so it may prove advantageous in other applications as well.

4.4 Conclusions

A dual layer coating consisting of an anchoring PDA film and an antifouling PDMA component introduced an antifouling character to platelet storage bag material that strongly reduced binding of fibrinogen, bacteria and platelets. The method of coating could be scaled up since the high gas permeability of the platelet bag material let the oxidation process occur inside the bags successfully, resulting in a covalently cross-linked stable coating. For inorganic substrates (silicon wafer and gold were tested), only a one-step coating of DA51-cat was required for a uniform, stable layer. Some of the free amine groups on the DA51-cat polymer were conjugated to AMPs. For a proof of concept, this polymer was coated on a silicon wafer and proved to have bactericidal activity.

The mild conditions needed for the surface reaction, which required neither organic solvent nor heat, are advantageous for the coating of the materials with leachable or easily decomposable ingredients. Heat sterilization may prove challenging in the presence of mobile coating elements but gamma radiation or other lower temperature methods could be applied. The presence of amine groups on DA51-cat also makes further modification with other compounds possible, and consequently has the potential to introduce new properties to the materials. Overall, this general approach provides a powerful, flexible method for protecting common commercial biomaterials from a wide variety of undesirable biological reactions. The ability to apply these coatings by a

simple process to inner surfaces inaccessible to externally applied agents or manipulations gives them a clear advantage over more demanding compatibilizing procedures.

4.5 Methods and Materials

pPVC and all ATRP reagents were introduced in Chapter 2, Section 2.5. PBS at pH 7.4 (10mM), 2-(*N*-morpholino)ethanesulfonic acid (MES, 10mM) buffer at pH 4.5, and MOPS sodium buffer at pH 8.5 (100mM) were used in this study. All chemicals were purchased from Sigma-Aldrich and used as received unless stated otherwise. EDC and BMPS were from Thermo Fisher Scientific. THF (99.9 %) was from Omnisolve. E6 (Sequence: RRWRIVVIRVRR) was designed by the Hancock lab, UBC, Vancouver and synthesized by CanPeptide Inc.

Dialysis was performed in regenerated cellulose tubes from Sigma-Aldrich (D7884, MWCO of 1000 and 3500 Da). Gold QSX sensors were purchased from Biolin Scientific Inc. LIVE/DEAD Bac Light Bacterial Viability Kit, L7012 was purchased from Thermo Fisher Scientific. The commercially available 25 % glutaraldehyde solution was diluted to 2.5 % using distilled water before use. IOSTest CD42a-FITC conjugated antibody purchased from Beckman Coulter Inc. was diluted to 1 % with PBS before use. Fibrinogen from bovine plasma (type I-S, 65-85 % protein, Sigma-Aldrich F8630) was used for protein adsorption tests.

^1H and ^{13}C NMR spectra were recorded on a Bruker Avance 400 MHz NMR spectrometer. Peaks are reported in ppm referenced to the deuterated solvent signal. GPC-MALLS/RI and TOF-SIMS were introduced in Chapter 2, Section 2.5. Mass calibration for positive mode was carried out using H, CH₃ and C₂H₅. Mass calibration for negative mode was carried out using CH, O, OH, and C₂H peaks. Three-dimensional topography of *rough* and *smooth* surfaces was studied with a Wyko NT1100 optical profiler (Veeco Inc.).

4.5.1 Development of antifouling coating on platelet bag surfaces

4.5.1.1 Synthesis of the hydrophilic polymer system (DA51)

A statistical copolymer of DMA and APMA (DMA:APMA, 5:1) was synthesized by ATRP and named DA51. Purified water (using a Millipore water purification system) degassed with four cycles of freeze-vacuum-thaw and the DMA aliquot degassed with argon flow for 20 minutes were transferred along with other chemicals to a glove box filled with argon. DMA (2 g, 20 mmol) and APMA·HCl (720 mg, 4 mmol) were dissolved in water (19 mL). CuCl (15 mg, 0.15 mmol) was mixed with 1, 1, 4, 7, 10, 10-hexamethyl triethylene tetramine (HMTETA) (88 μ L, 0.32 mmol) in water (1 mL) and added to the monomer solution along with CuCl₂ (2 mg, 0.015 mmol). Methyl 2-chloropropionate (2 μ L, 0.018 mmol) was used to initiate the polymerization. The reaction was stopped after 20 h by exposing the solution to air and dialyzed (MWCO 1000 Da) against distilled water for 3 days with water changes every 12 h.

$M_n = 97000$ kDa, Polydispersity (M_w/M_n) = 1.17.

4.5.1.2 Functionalization of the polymers with catecholic groups

To functionalize the polymers with catecholic groups (mussel-inspired chemistry), DA51 (100 mg, 0.001 mmol for a 100 kDa polymer, equivalent to ca. 0.14 mmol amine groups) and DHHA (77 mg, 0.42 mmol, ca. 3:1 molar ratio to amine groups of DA51) were dissolved in a 1:1 mixture of methanol and MES buffer (15 mL). EDC (28 mg, 0.14 mmol, ca. 1:1 molar ratio to amine groups of DA51) was added to the solution to activate the carboxylic group of DHHA. The mixture was stirred at room temperature for 1 h. The reaction was dialyzed against methanol (MWCO 1000 Da) for 24 h and the solvent was replaced every 8 h. After rotary evaporation 110 mg of DA51-cat was obtained.

4.5.1.3 Coating of the mussel-inspired polymeric system on substrates

Substrates, including silicon wafers (1 x 0.7 cm), gold-coated silicon wafers (1 x 0.7 cm) and pPVC (1.1 x 1.1 cm) coupons, were placed in sterile tissue culture dishes (35 mm diameter) containing a solution of dopamine·HCl (1 mg/mL) in phosphate buffer pH 8.5 (3.5 mL) for 10 h at room temperature under static conditions. Afterwards samples were immersed in milliQ water for 3 h and washed under running distilled water for 30 seconds. These PDA-coated samples as well as pristine uncoated samples were immersed in a solution of DA51-cat (10 mg/mL) in MOPS buffer pH 8.5 and kept for 24 h under static conditions. Samples were stored in milliQ water for 3 h and then washed as above.

For the preparation of double-side coated pPVC coupons, each 0.4 × 0.9 cm sample was placed vertically in 310 µl of the coating solution in a 96-well plate. Other steps proceeded as above.

4.5.1.4 Characterization

After drying, the thickness of the coatings (for gold and silicon wafer substrates) was measured on a variable angle spectroscopic ellipsometer as explained in Chapter 2, Section 2.5. Static water contact angles measurements were carried out as in Chapter 2, Section 2.5. Each reported water contact angle and thickness is the mean from at least three substrates and the value for each substrate is the average value measured on 3 to 5 locations. Any possible morphology changes on surfaces were investigated by SEM. The samples were gold coated before imaging using an Edwards S150A sputter coater with gold deposition rate of 15 nm/minute for 30 seconds.

4.5.2 *In vitro* evaluation of the modified surfaces

4.5.2.1 Fibrinogen adsorption on the samples

Coating QCM sensors with pPVC: Cut pieces of pPVC were dissolved in THF (1/240 w/w) and spin coated on gold QCM sensors at 2500 rpm. The backs of the sensors were wiped gently with a THF-wet tissue afterward. The pPVC-coated sensors were coated with PDA-DA51-cat or DA51-cat as described above.

Evaluation of fibrinogen adsorption: QCM-D (Q-Sense E1, Biolin Scientific) was used for evaluation of fibrinogen adsorption on surfaces. The coated sensors were placed into the titanium flow chamber (QFM 401, Q-Sense, internal volume of 40 μ L). PBS was pumped over the sensor surface until the baseline equilibrium was reached. Then, the fibrinogen solution in PBS (1 mg/mL) was pumped into the flow chamber for 30 minutes, followed by a PBS rinse for 10 minutes. The flow rate used for all steps was 0.1 mL/ min, and the temperature was set to 25 °C.

Considering the low dissipation value, the Sauerbrey equation²⁴⁹ was used to determine the mass of fibrinogen adsorbed on the surface. According to this equation ($\Delta m = C \times \Delta f$), the change in mass (Δm) is correlated with the mass sensitivity constant of the quartz crystal ($C = -17.7 \text{ ng}\cdot\text{cm}^{-2}\cdot\text{Hz}^{-1}$) and the change in the frequency (Δf) normalized for the overtone. The changes in frequency reported here are extracted from the third overtones.

4.5.2.2 Evaluation of bacterial adhesion

Two different strains of *S. epidermidis* isolated from contaminated clinical platelet units by the Ramirez-Arcos lab at the Canadian Blood Services research laboratory in Ottawa were used in this study. One strain, SE10002, can form a biofilm in TSBG while the other strain, SE11003, is biofilm negative.

TSBG was prepared by dissolving 30 g of the powder in 1 litre of distilled water and sterilizing by autoclaving. Concentrated glucose solution was added to the cooled media after filtration with a 0.2 µm syringe filter under aseptic conditions.

To prepare TSB agar plates, TSB powder (30 g) and agar (12 g) were dissolved in 1 L of distilled water and autoclaved. When the solution cooled down enough to be handled, it was divided among the agar plates in a sterile safety cabinet; ~20-25 mL of media was poured in each 10 cm plate.

The bacterial strains were transferred from frozen stocks into TSBG at 37 °C without shaking. After 8-10 h, the bacteria were subcultured in TSBG for another 8-10 h. The OD of the culture was read at 595 nm and a bacterial inoculum containing 1×10^6 CFU/mL was prepared in TSBG, knowing that an optical density of 0.1 represents 1×10^8 CFU/mL of the bacteria. The final concentration of bacteria was verified by serial dilution and spotting on an agar plate.

Imaging of adhered bacteria: Control and modified pPVC coupons 1.1×1.1 cm were washed with 70 % ethanol, followed by five sterile PBS washes, then fitted in the bottom of a sterile 24-well plate. One milliliter of 1×10^6 CFU/mL of SE10002 inoculum was added to each well and incubated at 37 °C for 32 h with 70 rpm shaking (coupons were horizontally positioned, just as platelet bags are positioned on shakers in blood banks). Each coupon was then gently rinsed by immersion in sterile PBS four times. Each sample was halved with a blade; one half was covered with Syto 9 solution. Syto 9, one of the stains of the Live/Dead kit, was diluted prior to use by dissolving 3 µL of the stain in 1 mL of distilled water. After 20 minutes, the sample was gently immersed in water and observed after drying under a Nikon C2+ Eclipse Ti-E confocal laser scanning microscope (Nikon Instruments Inc.) with an FITC filter.

The other half of each pPVC coupon was prepared for SEM imaging as in Chapter 2, Section 2.5.2.1.

Dislodging and counting the released bacteria: Control and modified pPVC coupons were washed before use as stated above. Each 0.4×0.9 cm coupon was placed vertically in one well of a 96-well plate filled with 320 μL of 1×10^6 CFU/mL of SE11003 inoculum.

After a 4-h incubation at 37°C without shaking, each coupon was consecutively immersed gently in sterile PBS five times then transferred to a sterile 0.6 mL Eppendorf safe-lock tube containing 500 μL of sterile PBS and sonicated for 10 minutes (details as in Chapter 2, Section 2.5.2.1). The detached bacteria were serially diluted in PBS to give concentrations from 10^2 to 10^{-6} CFU/mL and 10 μL of each concentration was spotted on agar plates in triplicate and counted after incubation for about 15 h at 37°C .

4.5.2.3 Evaluation of platelet adhesion

Minibag preparation: Two 5×4.2 cm pPVC coupons were cut and then sealed together from three sides using a heat sealer. Textured faces of the coupons were positioned inside the bag. The mini bags were filled with 3.5 mL of dopamine solution, closed using a clean clamp 5 mm from the top, and placed horizontally under static conditions. This volume of solution was enough to coat both top and bottom faces. After 10 h, the bags were emptied, washed with 5 cycles of filling and emptying distilled water. After the last wash, the bags filled with water were put on a rocking shaker at 10 rpm. After 3 h bags were washed with water again 5 times.

The mini bags were rinsed once with MOPS buffer then filled with DA51-cat solution and placed on a rocking shaker at 10 rpm. After 24 h, the bags were washed as in the previous step.

Platelet preparation: Platelet-rich plasma was prepared as described in Chapter 2, Section 2.5.2.2.

Imaging of adhered platelets: The minibags were filled with 3 mL of platelet-rich plasma (around 4×10^8 platelets/mL), closed with the clamps as before and put in a 22 °C platelet incubator with agitation at 70 cycles per minute. After 24 h, the outer walls of the bags were washed with PBS, minibags were emptied and the section 5 mm below the clamp (10 mm from the top) was cut off. Four coupons, each 1×0.7 cm were cut from the lower surface of each bag. They were washed gently three times in PBS and immersed in the 2.5 % glutaraldehyde solution for 1 h. After washing with water, the coupons were halved and one half was incubated with a solution of monoclonal CD42a-FITC-conjugated antibody (see above for preparation) at 37 °C for 1 h. At the end of the incubation, the samples were rinsed with distilled water, air dried, and studied by fluorescence microscopy with an FITC filter (Axioskop 2 plus, Carl Zeiss Microimaging Inc.). The other half was prepared for SEM imaging as described above for the bacteria. Platelets tended to expand and merge into the structure of the plastic. In order to avoid leaching of plasticizer, which would reduce the quality of the images, 85% and 100% ethanol were not used for these samples.

4.5.3 Development of bactericidal coating

4.5.3.1 Synthesis and coating of the bactericidal polymers (DA51-E6-cat)

To functionalize DA51-cat with the crosslinker BMPS, DA51-cat (130 mg, 0.0012 mmol for a 106 kDa polymer, equivalent to ca. 0.13 mmol free (not reacted with catechol) amine groups) was dissolved in 25 mL of methanol. BMPS (24 mg, 0.09 mmol) was completely dissolved in a minimal amount of DMF and added to the DA51-cat solution. The solution was

stirred at room temperature for 2 h then it was dialyzed against methanol (MWCO 1000 Da) for 24 h and the solvent was replaced every 8 h. A sample was taken and evaporated for NMR spectroscopy. Based on NMR results, 6 % of the total APMA was conjugated to the BMPS, which means around 8-9 % of the free amines had reacted with the linker.

E6 (20mg, 0.0113 mmol, ca. 1:1 molar ratio to the conjugated BMPS) was dissolved in 5 mL methanol. TCEP (1.6 mg, 0.006 mmol) was dissolved in a minimal amount of distilled water and added to the E6 solution and mixed for 5 minutes. The peptide solution was added to the above DA51-L-cat solution (138mg DA51-L-cat in methanol) and stirred for 2 h at room temperature. The solution was dialyzed against methanol (MWCO 3500 Da) for 24 h and the solvent was replaced every 8 h. After rotary evaporation 148 mg of DA51-E6-cat was obtained.

To develop DA51-E6-cat and PDA-DA51-E6-cat on silicon wafers, the same protocol as Section 4.5.1.3 was used. In cases where any insolubility was observed in the solution of DA51-E6-cat in MOPS buffer, the solution was filtered before adding to the substrates.

4.5.3.2. Imaging of live/dead bacteria on the surfaces: Untreated control silicon wafers and modified silicon wafers 0.7×0.7 cm were washed with five sterile PBS washes, then put horizontally in the bottom of a sterile 24-well plate. Untreated control silicon wafers were only washed with methanol and no further treatment (flame or oxygen plasma) was applied in order to preserve the natural silicon oxide layer on the substrate. One milliliter of 1×10^6 CFU/mL of SE11003 inoculum in PBS was added to each well and incubated at 37 °C for 4 h without shaking. Samples were then gently rinsed by immersion in sterile PBS three times. Syto 9 (1.5 μ L) and PI (1.5 μ L) were mixed in 1 mL of distilled water. Each sample was covered with

around 150 μL of this solution. After 20 minutes, the sample was gently immersed in PBS and observed after air drying under the fluorescence microscope.

CHAPTER 5: Effect of Texture of Platelet Bags on Bacterial and Platelet Adhesion

5.1 Introduction

As described in Chapter 1, in spite of the improvements in the safety of platelet transfusion, missed detection of bacterial contamination and the resulting adverse reactions or even fatalities are still reported.^{5,8,9} *S. epidermidis* is one of the most commonly isolated contaminant in blood products, mainly introduced into blood banking during donation.^{6,268} It has been shown that *S. epidermidis* strains slowly grow²⁶⁹ and form a biofilm in platelet concentrates.^{23,270} Slow growth and the strong tendency of *S. epidermidis* to adhere to surfaces can decrease the number of planktonic bacteria, leading to missed pathogen detection and false-negative bacterial tests.^{23,24}

In order to fabricate a platelet storage bag with the desired mechanical and physical properties as well as sufficient gas permeability, manufacturers use a high percentage of plasticizer (~ 40 %) in a mixture with PVC. Surfaces of these bags are further textured to prevent the inside faces from blocking during heat sterilization or blood processing. Some providers of platelet bags use one textured (denoted *rough* here) and one non-textured face (denoted *smooth*) inside the bags, such as Terumo 80440 bags while other providers use textured surfaces for both inside faces, such as MacoPharma TDV8006XU, Fenwal PL2410, and Pall platelet bags as part of the CP2D/AS-3 Triple Blood Bag system. This chapter investigates whether platelet adhesion and bacterial adhesion and biofilm formation differ on *rough* versus *smooth* faces when either is on the bottom. It is of interest if using one *rough* face positioned above a *smooth* face decreases the risk of adhesion and biofilm formation of *S. epidermidis*, decreasing the risk of its missed detection.

Sections 5.2 presents some characterization results on the morphology and chemical identity of the platelet storage bags used by the Canadian Blood Services in the past five years. Then it focuses on the comparison of platelet and bacterial adhesion on the *rough* surfaces of the platelet bags, in particular *rough* surface of the Terumo 80440 bag, versus its *smooth* surface. The topography of Terumo 80440 bag surfaces is studied in detail and correlated with their biocompatibility. Section 5.3 includes the Conclusions followed by Methods and Materials in Section 5.4.

5.2 Results and Discussion

5.2.1 Topography of platelet bag surfaces

The Terumo 80440 platelet bag included in the Trima Accel automated blood collection set (TerumoBCT) is currently used by the Canadian Blood Services for the storage of apheresis platelets, named A15 here. MacoPharma TDV8006XU is currently used for the storage of pooled platelets derived from buffy coats, named P15 here. Fenwal PL2410 was used before P15 bags for the storage of pooled platelets, named F1 here.

All bags have hydrophobic surfaces exhibiting water contact angles around 95° on A15 and P15, and around 80° on F1 surfaces (**Table 5.1**). Both inside faces of P15 and F1 are *rough* while A15 has one *rough* and one *smooth* face inside the bag (**Figure 5.1**). The axes (D_1 and D_2 , **Figure 5.1**) of the diamond patterns on *rough* surfaces of the bags were measured and recorded in **Table 5.1**. The rim heights of the patterns were measured to be $105 \pm 7 \mu\text{m}$ for A15, $70 \pm 5 \mu\text{m}$ for P15, and $76 \pm 6 \mu\text{m}$ for F1 using a profilometer (**Table 5.1**).

Table 5.1 Some physicochemical characteristics of the platelet storage bags studied in Chapter 5.

Material	Diamond size ^{a*} (axes in μm)	Rim height ^b (μm)	Water contact angle ^c ($^\circ$)
A15-Smooth	N.A.	N.A.	99 ± 2
A15-Rough	602×1030	105 ± 7	
P15	577×1013	70 ± 5	95 ± 3
F1	725	76 ± 6	82 ± 2

^a Measured on SEM images. *The axes of the diamonds (D_1 and D_2) are marked in **Figure 5.1**. ^b Measured using profilometer. ^c Determined by placing a water droplet of $3 \mu\text{L}$ on the surface and measuring the angle.

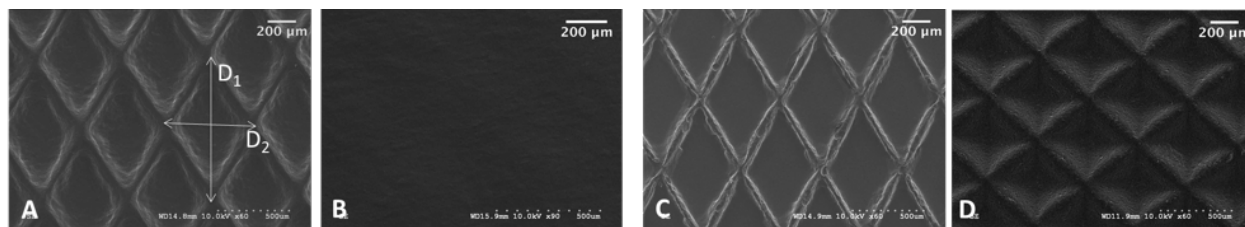


Figure 5.1 A15 bag has one textured (*rough*) face (A) and one *smooth* face (B) while both inside faces of P15 (C) and F1 (D) are *rough*.

Optical profilometry was used to confirm the rim heights of the bags and observe the morphology of the center of the diamond patterns (**Figure 5.2**). For all these samples, A15-rough, P15 and F1, surfaces had a roughness of micrometer scale.

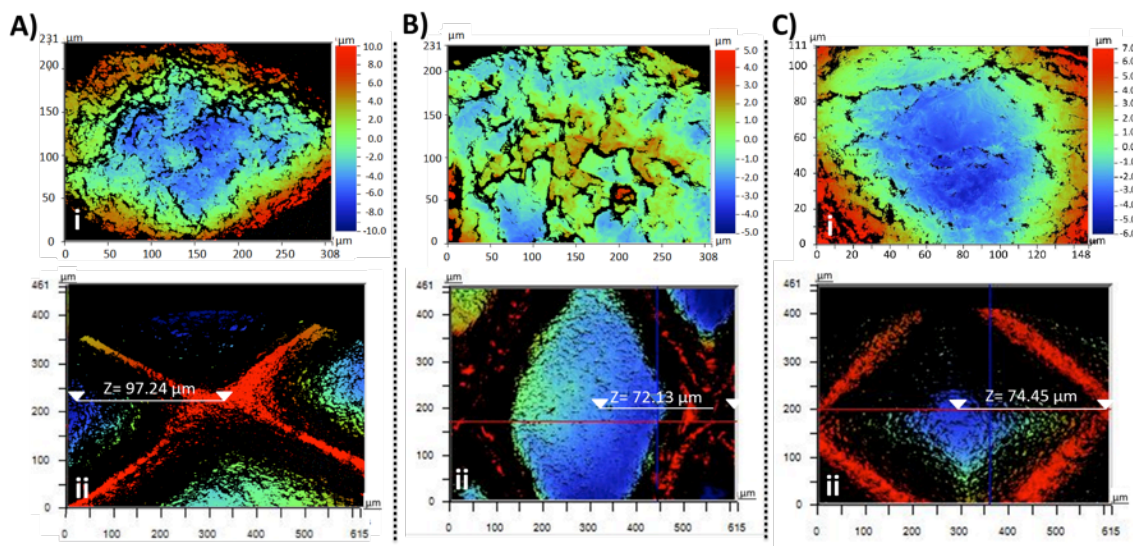


Figure 5.2 Optical profilometry of A15-rough (A), P15 (B) and F1 (C) showed a micrometer-scale of roughness of these surfaces. Top line shows the central parts of the diamonds.

Sections of $111 \times 148 \mu\text{m}$ of A15-rough and A15-smooth were studied by optical profilometry (this was the smallest possible size for scanning by this method) (**Figure 5.3**). The average roughness (R_a ; arithmetic mean distance between the peak and adjacent valley) was $3.47 \mu\text{m}$ in this area for A15-rough surfaces (**Figure 5.3A, i**). It should be noted that this value varies depending on the positions of the cross sections. In order to avoid overestimating the roughness of the sample, extreme features of the surfaces were neglected but nonetheless micrometer-scale roughness was obtained (**Figure 5.3A, ii and iii**).

R_a was found to be $604 \pm 101 \text{ nm}$ on $111 \times 148 \mu\text{m}$ sections of A15-smooth (**Figure 5.3B, i**). Y- and X-cross section profiles (**Figure 5.3B, ii and iii**) demonstrated that the roughness scale on the *smooth* surface was limited to a few micrometers so AFM was used for higher sensitivity; AFM analysis showed that R_a and R_{max} , the largest peak-to-valley height, were $17 \pm 1 \text{ nm}$ and $128 \pm 13 \text{ nm}$, respectively, in a $10 \times 10 \mu\text{m}$ scanned area (**Figure 5.4A**), and $122 \pm 9 \text{ nm}$ (R_a) and $1322 \pm 125 \text{ nm}$ (R_{max}) in a $40 \times 40 \mu\text{m}$ scanned area (**Figure 5.4B**). Analysis of the inner part of

the diamonds by AFM on the *rough* surfaces was not possible because the scale of surface structure was too large to be measured by this sensitive method.

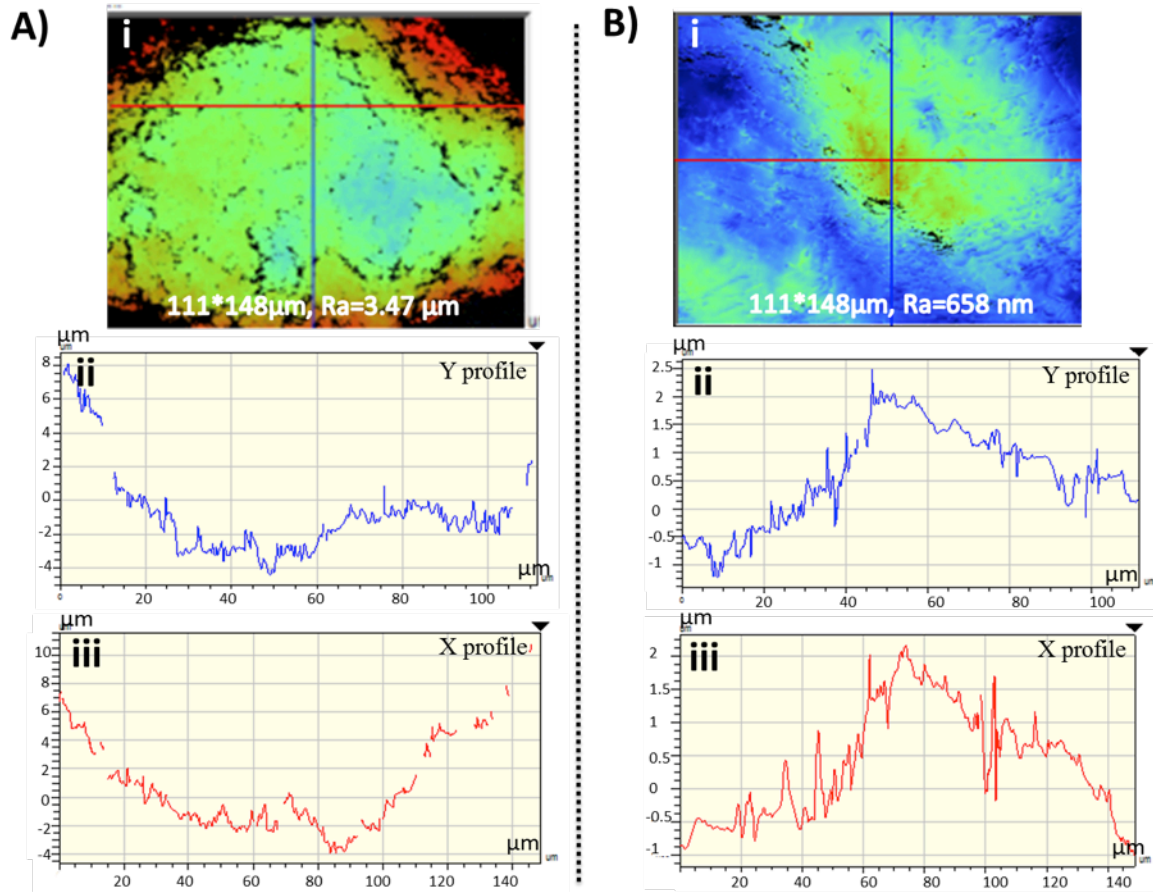


Figure 5.3 For comparison, the same surface areas ($111 \times 148 \mu\text{m}$) of central part of the diamond in A15-rough (Ai) and A15-smooth (Bi) were studied by optical profilometer (scale color bars are not shown; more details in the corresponding profiles) and gave R_a $3.47 \mu\text{m}$ and 658 nm , respectively. Y-cross section profile (Aii) and X-cross section profile (Aiii) on A15-rough. Both profiles varied largely depending on their positions. The depressions and defects of the surface were intentionally avoided in order not to overestimate the R_a . Y-cross section profile (Bii) and X-cross section profile (Biii) on A15-smooth (note scale differences).

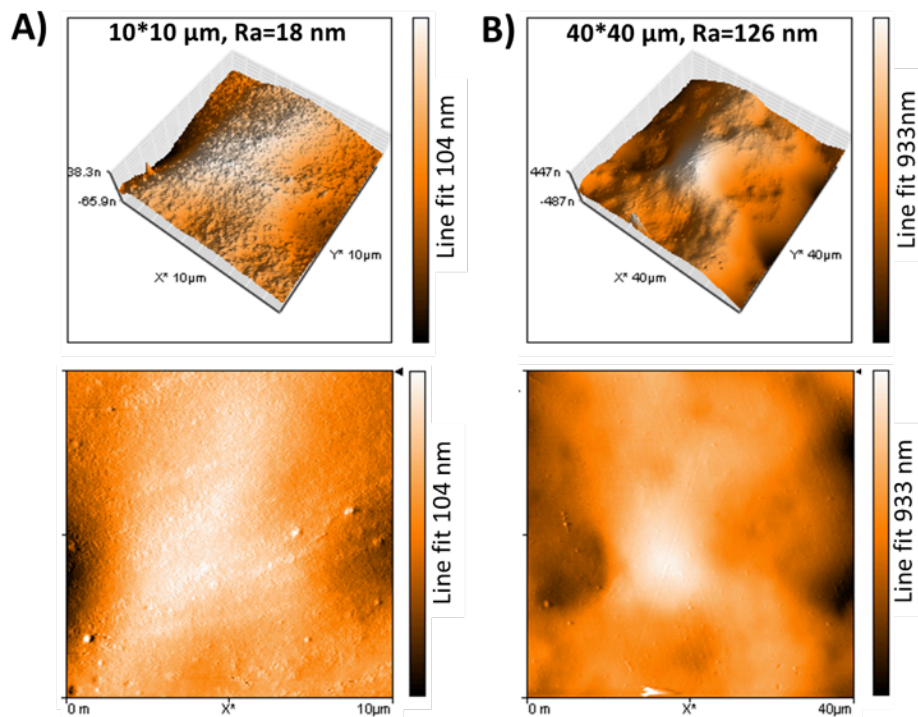


Figure 5.4 Surface topography of $10 \times 10 \mu\text{m}$ (A) and $40 \times 40 \mu\text{m}$ (B) of A15-smooth obtained by atomic force microscopy.

5.2.2 Chemical composition of platelet bags

As explained in Chapter 1, surface properties of biomaterials, including chemical properties and morphology, affect the biocompatibility of materials. The main compositions of A15, P15 and F1 were investigated by NMR and ATR-FTIR spectroscopy to understand if their chemical compositions were similar.

A15 and P15 lost around 30 % of their weight after 3 days of storage in hexane, and became brittle which confirmed the loss of plasticizer.

Figure 5.5 shows ^1H NMR and ^{13}C NMR spectra of the hexane extract of P15. As NMR spectra of A15 and P15 matched, only the NMR spectrum of P15 is reported here. The structure of the extract was characterized to be BTHC by NMR. Some characteristic peaks of DEHP at

7.56 and 7.75 ppm were also detected but with very low concentration, around 2 % of BTHC (molar ratio).

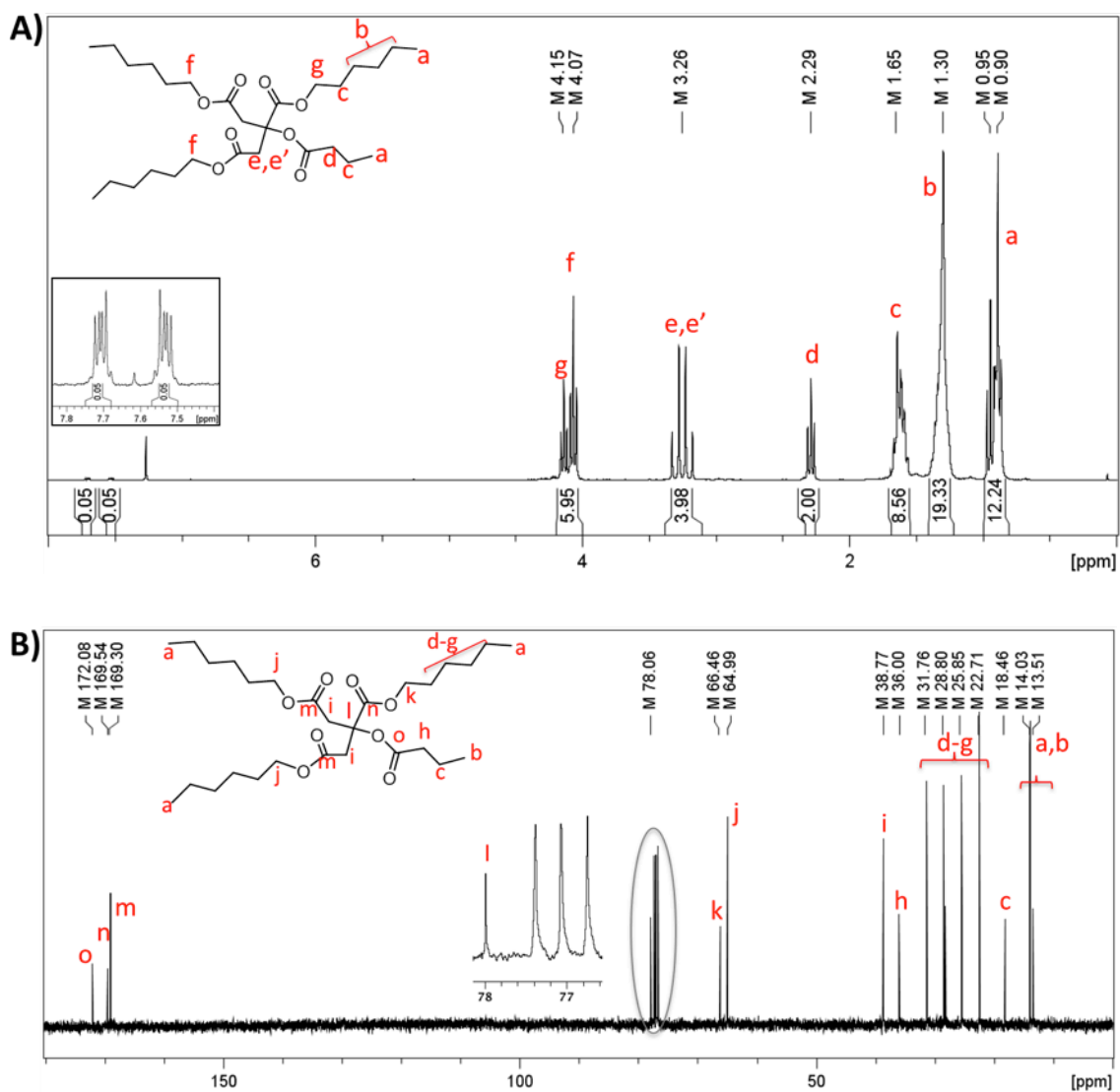


Figure 5.5 ^1H NMR (A) and proton-decoupled ^{13}C NMR (B) spectra of the hexane extract of P15 in CDCl_3 .

A15 and P15 were both completely soluble in THF. ^1H NMR spectrum of P15 (and A15) in THF confirmed the presence of PVC and BTHC as the main components of these bags (Figure 5.6).

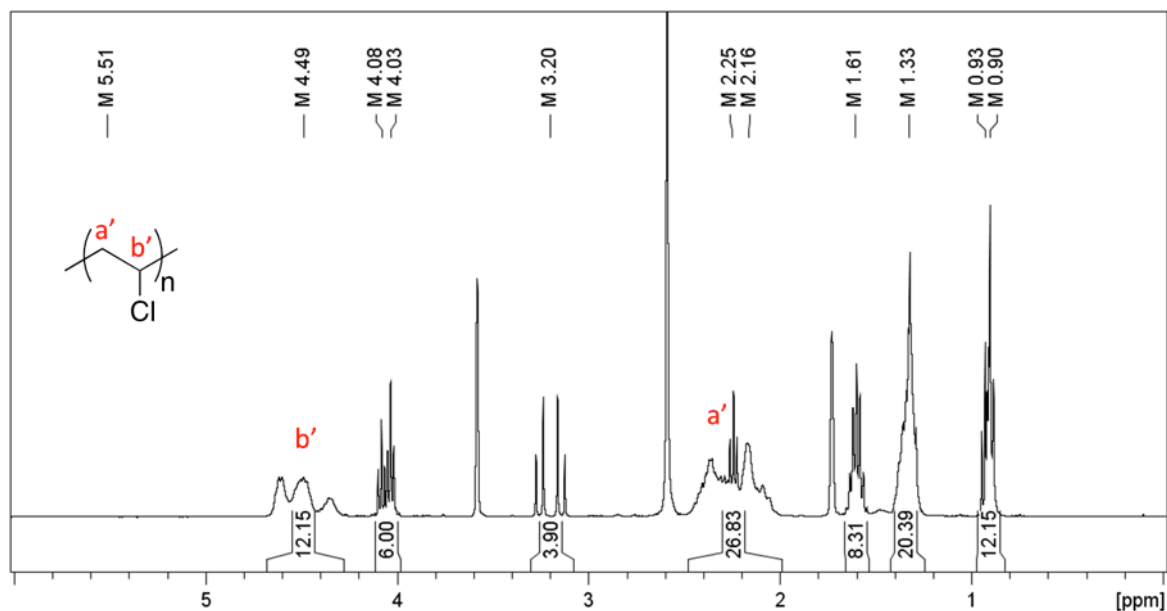


Figure 5.6 ^1H NMR spectrum of P15 in d_8 -THF. The BTHC peaks are assigned in Figure 5.5A.

The mass of F1 did not change in hexane and only a few milligrams were extracted from a 30 mg F1 piece even after 7 days of storage in hexane. F1 became more flexible as a result of exposure to hexane. Further, F1 did not dissolve in THF.

Figure 5.7A shows the ATR-FTIR spectrum of F1. The peak at 1740 cm^{-1} suggested the presence of a carbonyl group. However, it did not look to be a major component by comparing its intensity to the CH stretch at $\sim 2900\text{ cm}^{-1}$. For comparison, please see the ATR-FTIR spectrum of P15 in **Figure 5.7B**.

F1 swelled considerably in chloroform. Some pieces of F1 were sonicated in chloroform and the extract was used for NMR spectroscopy. The ^1H NMR spectrum showed some peaks at 6.55 and 7.07 ppm (**Figure 5.8**). These peaks were broad which suggested a polymeric identity for the compound (not similar to the sharp resolved aromatic peaks of TEHTM in the composition of the platelet bags studied in Chapter 2, Figure 2.6). The integration and position of the peaks were close to polystyrene or a derivative of it. The high integration of protons upfield

(~ 0.5-2 ppm) suggested a high number of olefinic protons, which was in agreement with the strong relative intensity of ATR-FTIR peaks at ~2900 cm^{-1} .

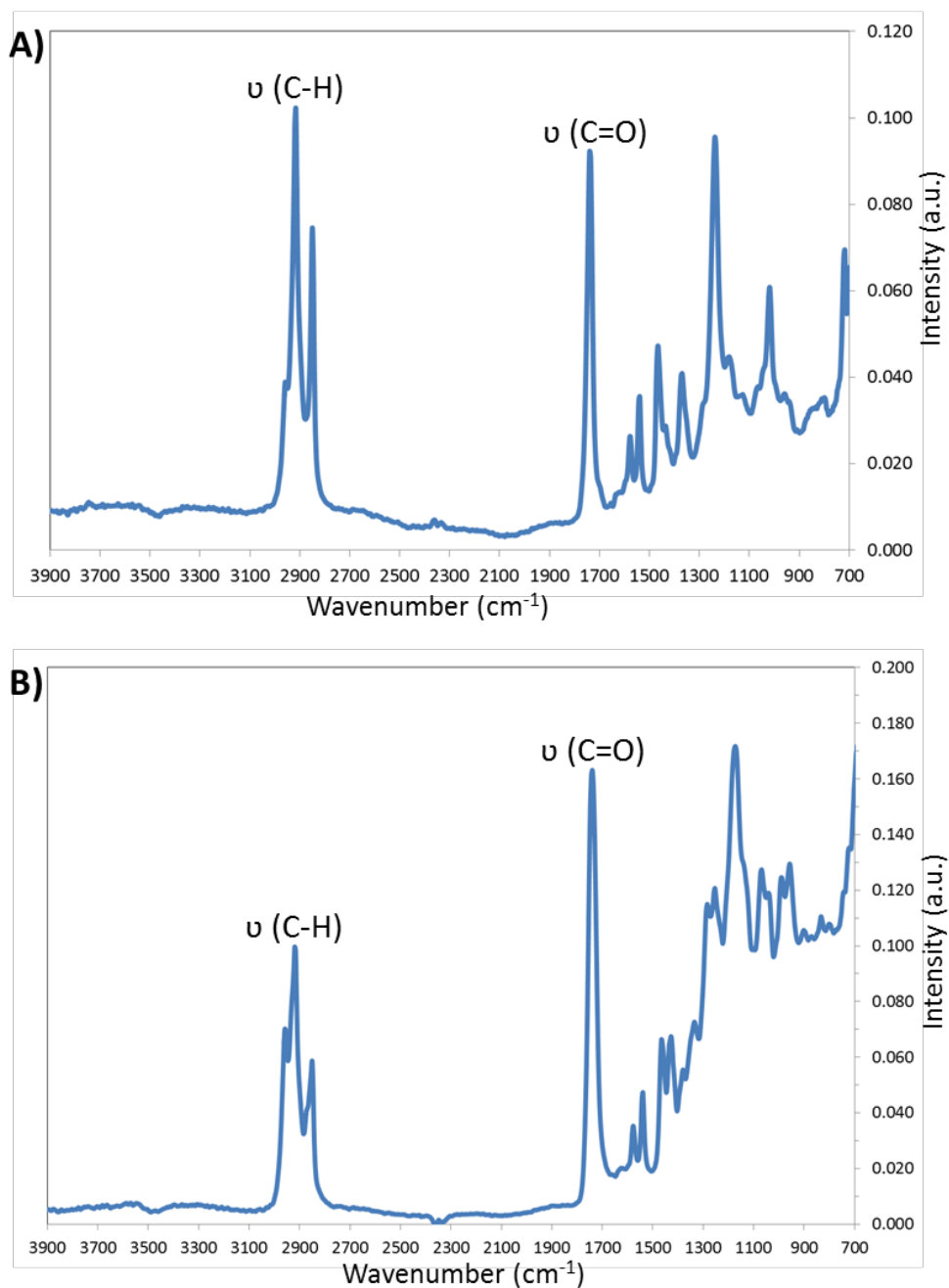


Figure 5.7 ATR-FTIR spectra of F1 (A) and P15 (B). The peak at ~ 1740 cm^{-1} suggested the presence of a carbonyl group.

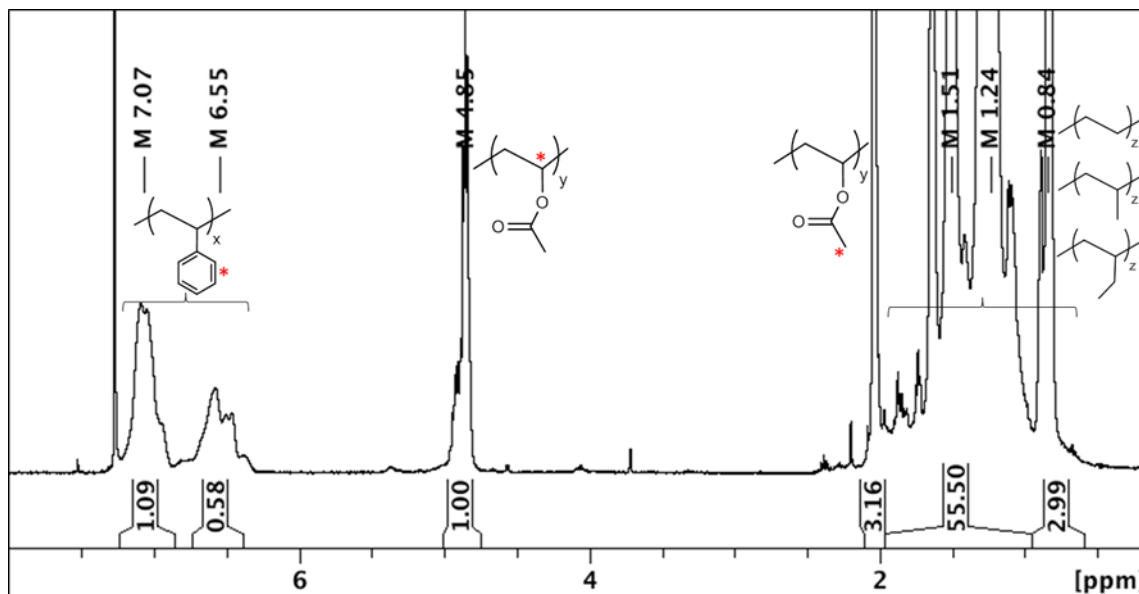


Figure 5.8 ^1H NMR spectrum of F1. The olefinic part of polymer can be made of polyethylene, polypropylene and/or polybutylene. The final structure is not definite.

The behaviour of F1 in hexane and THF as well as its NMR and ATR-FTIR spectra did not match the characteristics of commonly used plasticized PVC platelet bags.

A patent file by Baxter (1992) explained the invention of a plastic composition with an antihemolytic effect. This bag formulation had a non-PVC part made of a copolymer of ethylene and butylene units with terminal blocks of polystyrene, in a mixture with DEHP or some citrate esters as hemolysis suppressants.²⁷¹ The olefin and polystyrene parts could explain our collected ATR-FTIR and NMR data from F1 (**Figure 5.7A** and **Figure 5.8**). However, as seen before, DEHP and citrate plasticizers could be easily extracted with hexane, while F1 lost very little mass upon storage in hexane. Further, some characteristic peaks of DEHP and citrate plasticizers were absent in the NMR spectrum, therefore F1 does not have the same formulation as this invention. On the other hand, the carbonyl peak in ATR-FTIR spectrum of F1 and the 4.85 ppm peak in the NMR spectrum remained unassigned.

Another patent file by Baxter (1979) described an autoclavable plastic formulation for medical uses that was free of liquid plasticizers.²⁷² The formulation had two or three components: 1. polypropylene, 2. a copolymer made of a central block of ethylene and butylene copolymer with terminal blocks of polystyrene, and (optional) 3. polyethylene or poly(ethylene-vinyl acetate) as a softening agent. Polyvinyl acetate can nicely explain the unassigned peaks in the ATR-FTIR and NMR spectra (**Figure 5.7A and Figure 5.8**). The solid state ¹³C CP-MAS (cross polarization- magic-angle spinning) NMR of F1 was acquired and showed that the major peaks in the NMR spectrum of the extract (**Figure 5.8**) were consistent with the solid state F1 (plastic itself) spectral data (Appendix D1).

In summary, the main components of both A15 and P15 platelet storage bags are PVC and BTHC, while F1 mainly consists of polyolefins, polystyrene (in a block copolymer structure with polyolefins), and polyvinyl acetate. The definite composition and ratios of the components in F1 are not known, however.

5.2.3 Bacterial adhesion

To compare bacterial adhesion on the different surfaces, A15-rough, P15, F1 and A15-smooth coupons were incubated with 1×10^6 CFU/mL of SE10002, a biofilm former *S. epidermidis* strain, under accelerated growth conditions in TSBG medium at 37 °C without shaking. The samples were incubated horizontally in the bacterial medium. For A15-rough, P15 and F1, the *rough* side was facing up (exposed to the medium) and for A15-smooth, the *smooth* side was facing up. After an incubation period of 24 h, a consistent and thorough washing step was used to minimize variability and eliminate loosely attached bacteria as much as possible. The adhered bacteria were labeled with Syto9, a green fluorescent dye, and studied by

fluorescence microscopy and confocal fluorescence microscopy (for *rough* surfaces). The imaging showed that bacterial adhesion was significantly higher on all the *rough* surfaces than on A15-smooth samples (**Figure 5.9**).

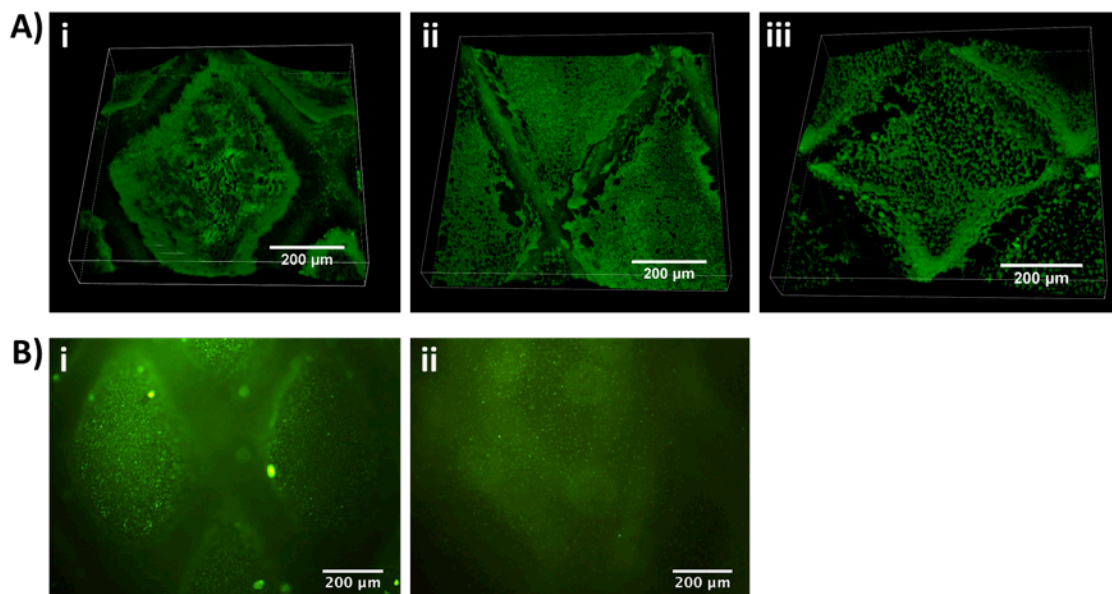


Figure 5.9 Fluorescent 3D confocal images of A15-rough (Ai), P15 (Aii) and F1 (Aiii), and fluorescent images of A15-rough (Bi) and A15-smooth (Bii) after 24-h incubation with SE10002. The images revealed less bacterial adhesion on A15-smooth compared to the *rough* surfaces. For A15-smooth (Bii), the textures of the back side can be seen showing through. For confocal 3D images (A), stacks of 35 slices (A15-rough) or 27 slices (P15 and F1), each 3 µm thick, were scanned. Bacteria were stained with Syto 9, a green fluorescent dye.

To study the effect of morphology on the bacterial adhesion, A15-rough and A15-smooth were studied further. The chemical details of these two surfaces are the same, so the biocompatibility differences can be attributed to the difference in morphology with more confidence.

A15-rough and A15-smooth coupons were incubated with two bacterial strains, SE10002 and SE11003, a biofilm-negative *S. epidermidis*, and studied by SEM after 24 h of incubation under the accelerated conditions as above. Consistent with the fluorescence microscopy imaging results, SEM imaging showed that for both strains, bacterial adhesion was significantly higher on

A15-rough samples than on A15-smooth samples (**Figure 5.10**). SE10002 clearly tended to form biofilm structures on A15-rough samples (**Figure 5.10, Bi**). Bacterial clusters were observed on A15-smooth samples, but no obvious biofilm structures were observed (**Figure 5.10, Bii**).

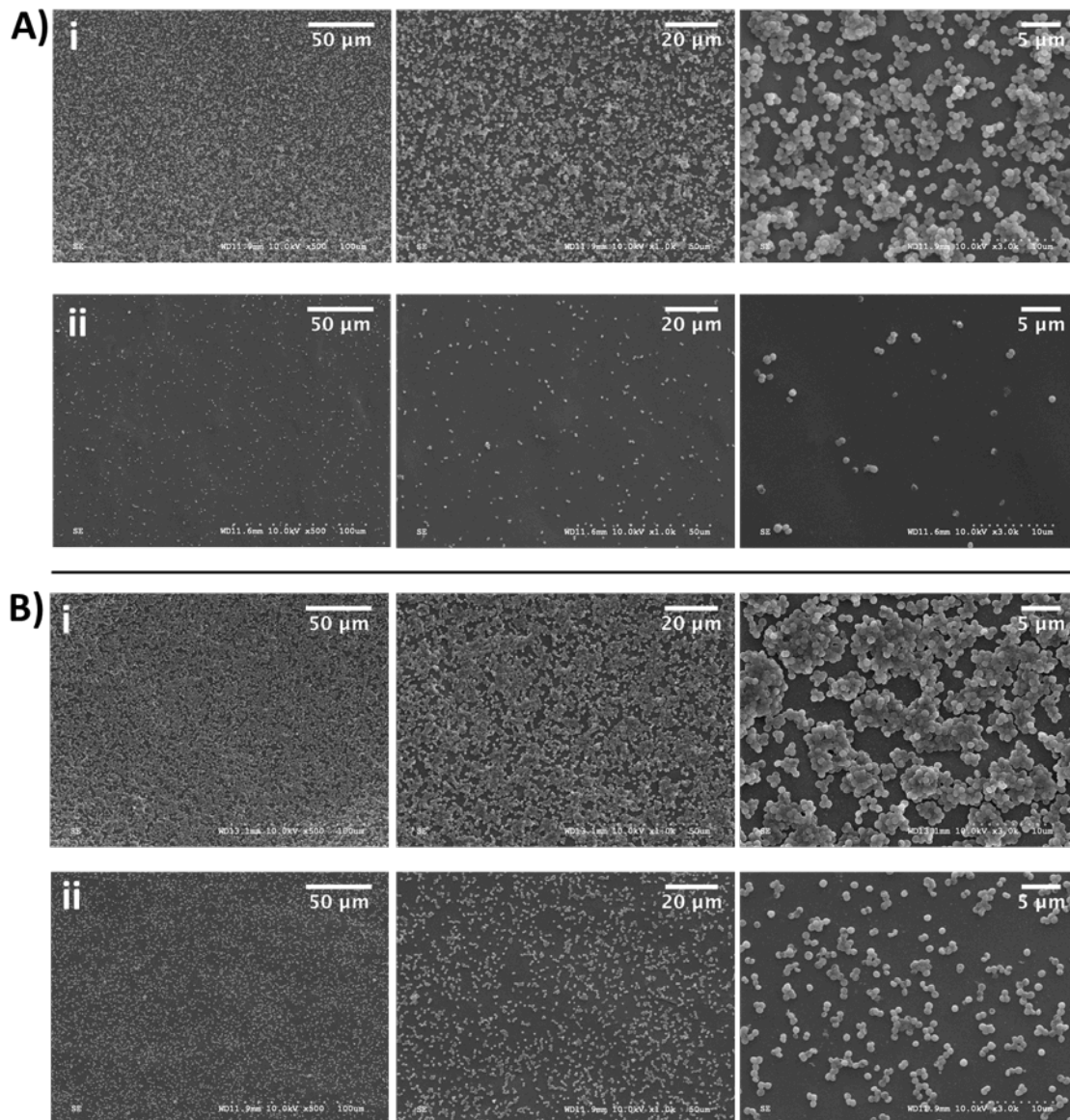


Figure 5.10 SEM images of A15-rough (i) and A15-smooth (ii) after 24-h incubation with biofilm-negative SE11003 (A) and biofilm-positive SE10002 (B) revealed less bacterial adhesion and biofilm formation on A15-smooth.

To quantify the difference between the surfaces, some minibags were fabricated. Like the commercial Terumo bags, these minibags were made with one *smooth* and one *rough* surface. For each experimental repeat, one minibag was set in a way that the *rough* face was on the bottom, named A15-rough, and in the other one, the *smooth* face was on the bottom, named A15-smooth. To quantify the differences between the surfaces, bacterial strains were incubated in the home-made minibags. **Figure 5.11** summarizes the numbers of bacteria dislodged by sonication. For SE11003, the number of bacteria per unit area (CFU numbers/cm²) dislodged from A15-rough surfaces was 15 times higher than the number from A15-smooth. For SE10002, the difference became smaller (8 times), but was significant ($p < 0.01$). Fluorescence microscopy of the samples before and after sonication showed that for the SE10002 strain, not all of the bacteria detached from the surface. In particular, some biofilm structures and clusters remained in the corners of the diamonds upon sonication. Detachment of the bacteria from *smooth* surfaces, however, was complete under the same conditions, so the actual difference between the surfaces for SE10002 is higher than the value reported by our method of quantification (**Figure 5.11**).

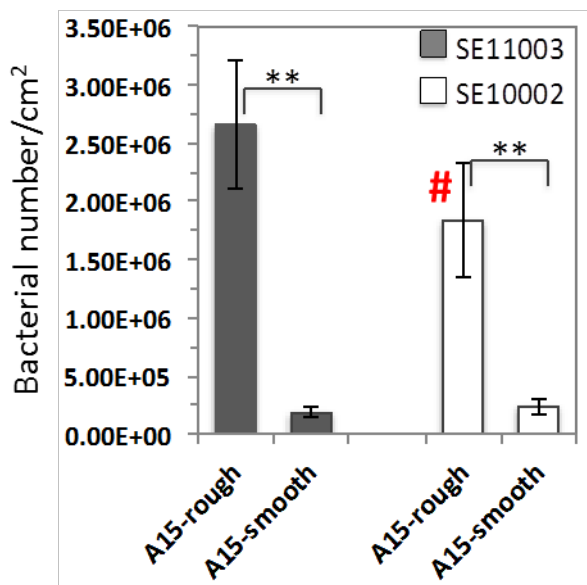


Figure 5.11 Number of the released bacteria from platelet bag cuts (CFU number/cm²). Gray and white bars represent biofilm-negative SE11003 and biofilm-positive SE10002 strains,

respectively. # The release of SE10002 from A15-rough was not complete during sonication and some bacteria were left on the surface. Bars reflect the mean \pm SD of 5 separate bacteria cultures. ** P<0.01.

These minibags do not reproduce platelet storage conditions of temperature, shear, bag dimensions or sample volume because it would waste resources; they simply represent the bacterial interaction with the relevant surfaces. Bacterial adhesion is not significantly affected by shear levels characteristic of platelet storage conditions^{273–275} so the static conditions were used. However, platelet interactions with similar surfaces were tested under blood bank conditions and support using this simplified model as a proof of concept.

Plasma proteins or platelets were not included in these bacterial adhesion experiments. A preliminary experiment was done in both platelet-poor plasma and platelet-rich plasma diluted 1:1 with the biofilm forming strain in TSBG and both showed obviously enhanced bacterial binding to A15-rough compared to A15-smooth. Quantification of the numbers of platelets and bacteria was uncertain so it was not pursued.

The differences between bacterial adhesion on *rough* surfaces (A15-rough, P15 and F1) and A15-smooth surfaces can be primarily explained by the different surface areas. The *rough* surfaces provide a larger total surface area than *smooth* surfaces. However, in more detailed studies of A15-rough and A15-smooth samples in **Figure 5.10**, it can be seen that other parameters besides total surface area must play a role, since larger bacterial clusters and biofilm structures tend to form on *rough* surfaces (**Figure 5.10B**).

It has been shown that surface roughness on the scale of bacterial size promotes their adhesion by increasing the contact area between the material and bacteria and by protecting the bacteria from shear forces.⁸² In other words, smoothness leads to reduced bacterial attachment and biofilm formation, and some studies have reported R_a values $\leq 0.2 \mu\text{m}$ as a threshold for

maximum inhibition of bacterial adhesion.⁷⁸ Dairy standard DIN 11 480 has considered surfaces with average roughness less than 0.8 μm hygienic enough for dairy product packaging.⁷⁹ Taylor *et al.* have demonstrated that an increase in surface roughness between 0.04 and 1.24 μm significantly enhances bacterial adhesion⁸⁰ while Medilanski *et al.* observed that bacterial adhesion was minimal at $\text{Ra}=0.16 \mu\text{m}$.⁸¹

One can expect that there is no definite roughness that defines a gold standard for reduction of all types of bacterial adhesion but the limited roughness of the A15-smooth sample and its very low bacterial surface adhesion align with the findings discussed above. The roughness on A15-smooth surfaces is too small (**Figure 5.3B and Figure 5.4**) for bacteria to fit in, thus reducing the contact area of bacteria with the material surfaces and hence, their adhesion. At the other extreme, both bacterial strains could adhere strongly on the A15-rough surfaces (**Figure 5.10**), and in the case of SE10002 could form biofilm structures. These biofilm structures did not completely detach during sonication. Whether due to the protective effect of the rims of the diamond texture and roughness during washing and sonication, or the micro-roughness of the area providing more contact points, these observations suggest that the bacteria can strongly adhere to the *rough* surfaces and may be missed during sampling for a bacterial screening test. On the contrary, for A15-smooth samples, bacteria have a higher chance to stay in a planktonic state and allow a positive result.

Generally, bacteria tend to settle in grooves, scratches, and depressions because of the increased contact area with the walls, protection from environmental disturbances or possible chemistry changes in the area.^{81,276} Such defects on *rough* surfaces that are likely a result of the texturing process can serve as preferential starting points for bacterial attachment and biofilm formation on A15-rough, P15 and F1 surfaces. The diamond rims (105 μm in A15, $\sim 70 \mu\text{m}$ in

P15 and F1) are too big/wide for the bacteria to sense them as roughness. However, some studies have shown that bacterial attachment and biofilm formation on surfaces change with changes in the dimension of peaks and valleys even when they are much bigger than the dimensions of bacteria.^{277,278}

There are other studies that have shown that the creation of regular nano-scale and micro-scale patterns on surfaces reduce bacterial adhesion and biofilm formation in comparison with flat surfaces.^{82,279} These data, which are in conflict to some extent, as well as the previous referred studies, have all been obtained from elaborately engineered materials that are designed for studying the effect of roughness and topography.²⁸⁰ They all emphasize that bacterial attachment is a complex process with numerous controlling factors. Physicochemical parameters of the substrate (e.g. topography²⁸¹ and surface chemistry²⁸²) are critical.

In this study, the *S. epidermidis* strain was used as one of the most common sources of platelet contamination with a slow growth rate and biofilm forming character. Bacterial characteristics are among the factors affecting the bacteria-material interaction.⁷⁶ However, many studies have shown that the effect of roughness on bacterial adhesion followed the same overall trend independent of the bacterial species including Gram-positive or -negative bacteria.^{80,82,277,279,283,284} It is expected that higher adherence of bacteria on *rough* surfaces compared to *smooth* surfaces to be valid for other Gram-positive and also Gram-negative bacteria.

5.2.4 Platelet adhesion and quality

Three ABO-matched pooled platelet units were mixed and split among four platelet storage bags: two commercial A15 bags that were positioned with different orientation during storage, a

commercial P15 bag, and a commercial F1 bag. The bags were stored under blood bank storage conditions (horizontally positioned on platelet agitators in a 22 °C incubator). Platelet adhesion on the lower surface of the commercial bags was evaluated on day 7 of storage. Similar to the bacteria, platelets adhered more on the *rough* samples compared to the A15-*smooth* surfaces. Images showed that platelet attachment and aggregation occurred on *rough* surfaces (**Figure 5.12**). This experiment was performed only twice because of limitations in the resources.

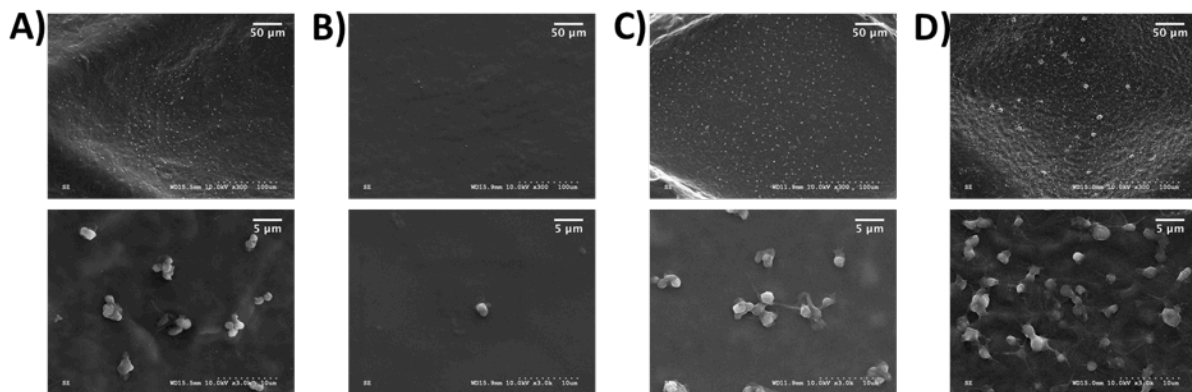


Figure 5.12 SEM images of A15-rough (A), A15-smooth (B), P15 (C) and F1 (D) after 7 days of incubation with pooled platelets under blood bank storage conditions revealed less platelet adhesion on A15-smooth compared to all the *rough* surfaces.

In a continuation of these experiments, commercial A15 bags were studied in detail. For each batch of experiments, two platelet concentrates were pooled and split into two commercial A15 bags. The bags were placed in a 22 °C platelet incubator on agitators, oriented either with the *rough* or *smooth* surface at the bottom. Sampling from these bags was done aseptically in a biosafety cabinet on days 2, 5, and 7 of storage.

The quality of the platelets stored as above was analyzed on days 2, 5, and 7 of storage (**Figure 5.13**). A decrease in the level of glucose, an increase in the level of lactate and the following decrease in pH level are signs of the platelets under stress and activation. Comparing the levels of glucose, lactate and pH, there were no differences between the two bags.

CD62P is a glycoprotein expressed on the surfaces of platelets upon activation. The expression level of CD62P (CD62P %) can be used as a marker for platelet activation level. The increase in CD62P level in a response to ADP (an agonist for platelet activation) can be used as a marker for the response capacity of platelets (Δ CD62P %).

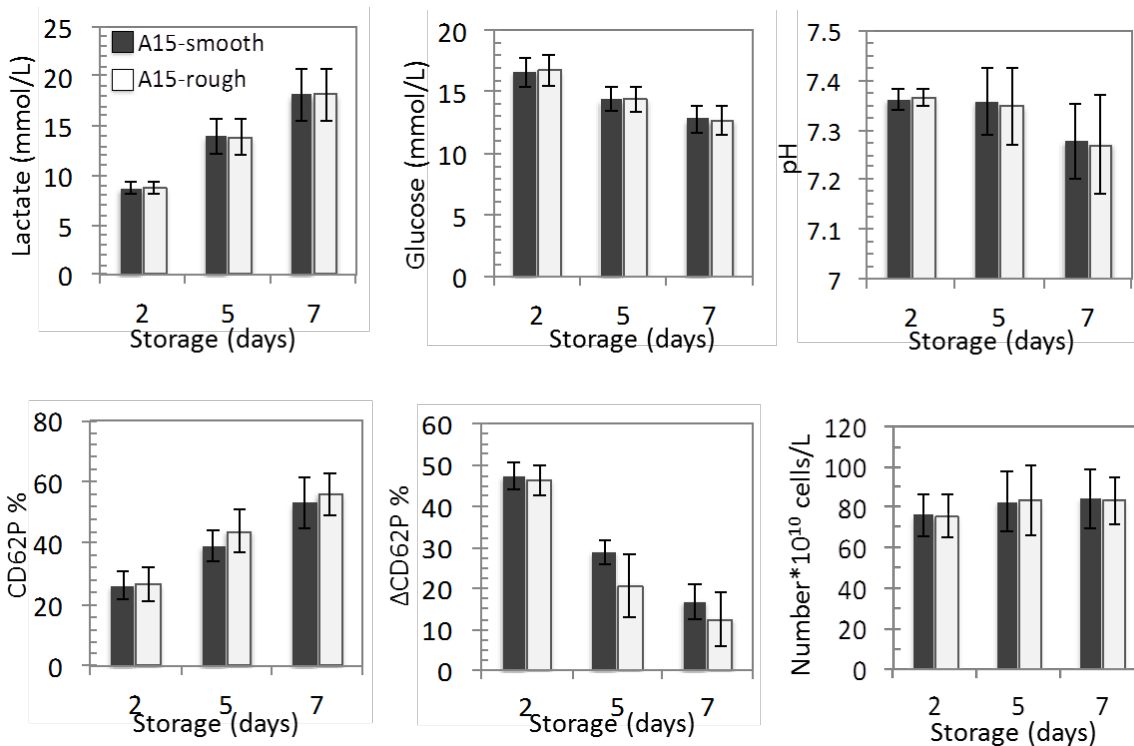


Figure 5.13 Evaluation of platelet quality after 2, 5, and 7 days of storage in the A15 bags under blood bank storage conditions. Black and white bars represent A15-smooth and A15-rough bags. *In vitro* platelet quality measures reported here are lactate, glucose, pH, CD62P percentage (a marker of activation), Δ CD62P % (activation level in response to ADP), and platelet count. Bars reflect the mean \pm SD of 5 separate experiments.

Figure 5.13 shows that the levels of platelet activation and response to ADP showed some consistent differences between A15-smooth and A15-rough bags but applying the Bonferroni statistics²⁸⁵ the observed difference was not significant. These experiments were repeated 5 times and the bags were cut and opened in three batches on day 7 for surface imaging. As seen before, the level of platelet adhesion and aggregation was higher on A15-rough surfaces.

It is noteworthy that although the *rough* surface in A15-smooth samples is on top, platelets still adhered on this surface, however, to a much less degree than when it is positioned on the bottom (A15-rough samples).

Compared to bacterial adhesion, there has been less research on platelet adhesion on surfaces with different topography. Milner *et al.* have shown that molding submicron pillars (height of the pillars and separation between them were between 400 and 900 nm) on polyurethane surfaces could decrease platelet adhesion.²⁸⁶ They hypothesized that this roughness decreased the contact area between the platelet and polyurethane as the contact points became limited to the top of the pillars. They expected that this would decrease the possibility of interaction between the adsorbed fibrinogen and platelets.²⁸⁶ Fibrinogen plays a key role in adhesion of platelets to biomaterials with various topographies and less fibrinogen-platelet interaction results in less adhesion or weak attachments that can be released by lower shear force.^{247,287}

The scale of roughness and the resulting low platelet adhesion on A15-smooth samples (**Figure 5.12**) nicely align with the data referred above.²⁸⁶ Tsunoda *et al.* also observed that smoother surfaces had lower platelet adhesion and better hemocompatibility.⁸³ Micrometer-scale patterns on polyurethane surfaces similar to shark skin patterns, on the other hand, were reported to reduce bacterial and platelet adhesion on polyurethane surfaces, but the effect was correlated to super hydrophobicity of these surfaces that is not related to our substrate and study.²⁸⁸ One of the relevant early works showed that under a flow condition, platelet adhesion increased on a rough hydrophobic surface when compared with the same smooth surface.⁸⁴

The preliminary results of the platelet storage test in the different commercial bags showed the higher platelet adhesion on A15-rough, P15 and F1 samples compared to A15-smooth

samples. The imaging results showed that platelet adhesion was higher on F1 than on P15 and A15-rough. However this difference cannot be correlated to the difference in their morphology at this stage. The chemical identities of these bags are different; that might play a role in the platelet activation and adhesion, for example by providing insufficient gas exchange.⁸⁵

The stored platelets in A15-rough and A15-smooth had similar pH and metabolite concentrations during the storage period; however, they showed consistently different but not significant response capacity to ADP (Δ CD62P %) on day 7 of storage (**Figure 5.13**). Imaging showed that platelets adhered more on *rough* surfaces. These strongly attached platelets appear mostly activated and could stimulate activation of the bulk platelets and affect their quality.

Blood centers recommend that a platelet unit should be mixed thoroughly prior to transfusion,²⁸⁹ which may stimulate the release of the activated platelets into the bulk. Based on our observations, this recommendation might deserve further studies and reconsideration.

Importantly, it has been well established that adhered platelets themselves, combined with surface-bound plasma proteins such as fibrinogen, promote bacterial attachment to the material and biofilm formation can result.^{248,290} Biofilm-forming bacteria are more pathogenic and virulent compared to planktonic ones; detachment of bacterial clusters from the biofilms and their inhomogeneous distribution in analyzed samples should be of concern.²⁹¹ Placing the *smooth* surface on the bottom during platelet storage decreases the possibility of formation of such aggregates, which in turn decreases the chance of missed bacterial detection during sampling as well as any adverse effect on the quality of transfused platelets. It is noteworthy that the *smooth* faces of the P15 and F1 bags (outer faces of the bags) do not have the required smoothness (submicron roughness) for suppression of bacterial and platelet adhesion. This work

suggests it might be worth flipping one face of the current bags but if so consideration ought to be given to further smoothing of the current “smooth” surfaces of these bags.

The presence of a *smooth* surface that resists bacterial adhesion can increase the chance of bacteria staying in a planktonic state and being sampled during the screening. This is particularly valuable for countries that, besides the regular sampling from the day 1 platelets, require a point-of-care bacterial detection testing²⁶⁷ before the transfusion so another sample is taken directly from the bag for bacterial screening before transfusing it.

As mentioned in Chapter 1, in most countries including Canada, a 10 mL sample is taken from the platelet bags 24-48 hours after the donation. The sample is transferred into the BacT/ALERT 3D medium bottle. The bottles are incubated in the BacT/ALERT 3D culture system for 6 days after the blood collection time to detect any bacterial growth.

In pooled platelet bags that are currently stored in P15 bags in Canada, the sample is taken from a small pouch bag which is filled at the same time that the P15 bag is filled. The topography of this bag was found to be different from the P15 bag so it was studied and found to be quite rough, too (**Figure 5.14**).

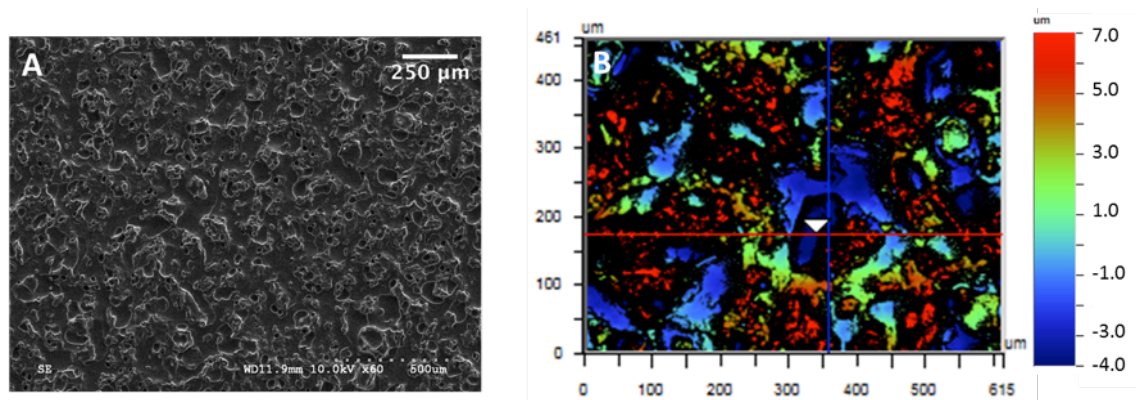


Figure 5.14 SEM imaging (A) and optical profilometry (B) of the pouch bag of P15 revealed roughness of the surfaces of this bag to be in micrometer scale.

5.3 Conclusions

A textured surface is essential in bag fabrication to prevent the inside faces from blocking (adhering) during sterilization or filling processes. The current results on the effect of texture on bacterial and platelet adhesion may encourage more fabrication of bags with only one textured surface inside and positioning it above a smooth (with submicron roughness) non-textured surface. Further research on the fabrication of bags with more carefully designed topography would also be welcome. To the best of our knowledge, there have been only a few studies on the development of new platelet bag systems without such texture,^{292,293} and more data would be useful. This chapter for the first time demonstrated biocompatibility differences between the *smooth* and *rough* surfaces of platelet storage bags and raised awareness of the relevance of properties of the platelet bag surfaces to platelet and bacterial adhesion. These features potentially could impact the safety and quality of platelet concentrates for transfusion.

5.4 Methods and Materials

5.4.1 Topography of platelet bag surfaces

SEM was used to study the diamond textures of the *rough* surfaces. The height of the rims (h) was determined using a Tencor Alpha-step 200 Profilometer (Tencor). Three-dimensional topography of *rough* and *smooth* surfaces was investigated with a Wyko NT1100 optical profiler (Veeco Inc.). Surface topography of the *smooth* sides of A15 bags was further studied by AFM (Nanosurf EasyScan 2) in non-contact mode with a commercial silicon AFM tip (CT170R, NanoScience instrument) having a 50 N/m spring constant. The data, collected from 14 scanned areas, was analyzed using NanoSurf software.

5.4.2 Bacterial adhesion

Bacterial inoculum preparation: SE10002 and SE11003 were introduced in Chapter 4, Section 4.5.2.2. Both strains are able to form biofilms in platelet concentrates, but under growth conditions using TSBG, only SE10002 forms biofilms. The bacteria inocula (1×10^6 CFU/mL) were prepared in TSBG as reported in Chapter 4, Section 4.5.2.2.

Imaging of adhered bacteria: In each experimental repeat, three 1.1×1.1 cm coupons of A15, P15, F1 were immersed in 70 % ethanol for 10 minutes and washed five times with sterile PBS. Each coupon was fitted in the bottom of one well of a sterile 24-well plate. Coupons were placed with the *rough* surface facing up for A15-rough, P15 and F1 samples, and with the *smooth* surface facing up for the A15-smooth sample. One milliliter of 1×10^6 CFU/mL of bacteria inoculum (in TSBG) was added to each well and incubated at 37 °C for 24 h without shaking. Each coupon was thoroughly rinsed by consecutive immersion in 5 sterile PBS vials, one minute in each. For fluorescence microscopy, samples were stained with Syto 9 as explained in Chapter 4, Section 4.4.5.2. The coupons were covered with the diluted stain for 20 minutes then rinsed with distilled water and analyzed with fluorescence microscope or confocal laser scanning microscope.

For comparison of A15-rough and A15-smooth surfaces, the samples were incubated with SE10002 and SE11003 as above. After 24 h, the samples were washed as above and fixed for SEM imaging as in Chapter 2, Section 2.5.2.1.

Dislodging and counting the released bacteria: To prepare minibags for this study, 5×4.2 cm coupons were cut from A15 bags and three sides sealed using a heat sealer. Like the Terumo bags, the minibags were made with one *smooth* and one *rough* surface.

For sterilization, each minibag was filled with 3.5 mL of 70 % ethanol, closed with a sterile clamp and kept for 10 minutes, followed by five consecutive cycles of wash with sterile PBS pH 7.4. Bags were filled with 3.5 mL of 1×10^6 CFU/mL bacteria inoculum in TSBG, clamped with sterile clamps 5 mm from the top, and placed in a second clean container in a 37 °C incubator under static conditions (no shaking). For each experimental repeat, one minibag was set in a way that the *rough* face was on the bottom, named A15-rough, and in the other one, the *smooth* face was on the bottom, named A15-smooth.

After 24 h of incubation at 37 °C without shaking, the external walls of the bags were gently wiped with a 70 % ethanol pad followed by five sterile PBS washes. Clamps were removed, and the section 5 mm below the clamp position (10mm from the top section) was cut off with sterile scissors. The bags were emptied and three coupons of 1×0.7 cm were cut from the lower surface of each bag. To remove loosely adhered bacteria, each coupon was consecutively immersed in 5 sterile PBS vials, one minute in each. Each sample was then transferred to a sterile 1.5 mL Eppendorf safe-lock tube containing 1 mL of sterile PBS and was sonicated for 30 minutes (details as in Chapter 2, Section 2.5.2.1). The detached bacteria were subjected to a 10-fold serial dilution to give concentrations from 10^{-2} to 10^{-6} and 10 μ l of each dilution was spotted on TSB agar plates in triplicate and counted after incubation for about 15 h at 37 °C.

5.4.3 Evaluation of platelet quality

5.4.3.1 Platelet concentrate preparation: This study was approved by the research ethics board of Canadian Blood Services and informed consent obtained from healthy volunteers prior to whole blood donation. Whole blood collection was carried out by the NetCad using standard

operating procedures. Platelet concentrates were prepared 22 h after blood collection (defined as day 1) and the buffy-coat fractions of blood from four individual donors pooled for each platelet unit.

5.4.3.2 Platelet quality in the A15 bags under blood bank storage conditions

Three ABO-matched platelet units for the 4 bag experiments, and two platelet units for the 2 bag experiments (A15-rough and A15-smooth) were pooled and split into the commercial bags. The bags were placed in a platelet incubator at 22 °C. For A15 bags, one was oriented with the *rough* surface at the bottom, and the other with the *smooth*.

Sampling from the bags for platelet quality tests was done aseptically in a biosafety cabinet on days 2, 5, and 7 of storage. For each sample, the platelet count was determined by a hematology analyzer (Advia 120, Siemens). Metabolite levels (glucose and lactate) and pH were measured with a blood gas analyzer (Gem Premier 3000, Instrumentation Laboratories, Bedford, MA). Platelet activation and response to ADP was assessed by the expression level of P-selectin (CD62P) on the platelet surface as previously published by the Devine lab.¹⁶ The bag label was facing up on A15-smooth bags and down for A15-rough bags.

5.4.4 Platelet adhesion

Evaluation of platelet adhesion on surfaces of the platelet bags under blood bank storage conditions

On the day 7 of storage, the bags were emptied and 10 coupons of 1 × 0.7 cm were cut from both surfaces of each bag at similar positions. Each coupon was consecutively immersed in

5 vials of sterile PBS, one minute in each. To fix the surface-adhered platelets, samples were immersed in glutaraldehyde solution (prepared as above) for one hour then washed with water.

For SEM imaging, fixed samples were treated with 30 and 60 % ethanol, stored in a desiccator and gold coated before imaging.

CHAPTER 6: Conclusions and Future Work

6.1 Conclusions and Summary

The work presented in this dissertation has focused on an important but little considered element in transfusion medicine, namely the surface properties of platelet storage bags. In spite of the large surface area to which platelets are exposed and sheared against during storage in a blood bank, there has been surprisingly little work done on this subject. Platelets are the most valuable of the blood products for transfusion but their storage lasts only 5 to 7 days, about half their lifetime in the circulation. The effects of platelet-material interactions seemed to be relevant, particularly given the likelihood of bacterial growth and biofilm formation in bags during the room temperature storage required for platelets.

The major contribution of this work is raising awareness about the relevance of the surface properties of platelet storage bags to platelet transfusion safety and quality, and initiating some work in this regard. Chemical properties and morphology of biomaterials are known to affect their biocompatibility. This dissertation studied possible methods to improve the biocompatibility of platelet storage bags and to decrease bacterial adhesion and biofilm formation on platelet bag surfaces. The following results and conclusions were obtained:

- Copolymers and homopolymers made of DMA, APMA and MPDSAH were grafted from surfaces of platelet bag material, pPVC, using SI-ATRP. The mild aqueous conditions used for the development of polymers were advantageous for the substrates containing leachable or decomposable ingredients such as plasticizers.
- Water contact angles on pPVC surfaces were changed from $\sim 100^\circ$ on pPVC to as low as $\sim 40^\circ$ on the coated surfaces. Compared to commonly used inorganic surfaces in the literature such as silicon wafers, rough, non-reflective and multi-ingredient pPVC surfaces are

challenging to characterize. XPS (with some limitations) and AFM analyses were used for further characterization of these surfaces. AFM analysis could be applied for the measurement of L_e and estimate of σ of polymer chains on pPVC surfaces (205 nm (L_e) and 0.12 chains/nm² (σ) for 182 kDa grafted PDMA chains). ATR-FTIR spectroscopy, cleavage of polymers from surfaces and some control samples (omitting some essential polymerization steps) confirmed the presence of some polymer in the bulk of pPVC likely due to the penetrability and compatibility of this material with the monomers. Further the control experiments suggested growth of polymers from sources other than the immobilized initiators.

- AMPs carrying a cysteine on their C terminal were conjugated to DA51 polymer chains via some amine-to-sulphydryl cross linkers. A fluorometric method based on the reaction of arginine with PAQ was manipulated for the estimation of the amount of AMPs on pPVC surfaces. This value varied among surfaces and was found to be difficult to reproduce in different batches. Omitting the 'linker conjugation' step, strongly adhered AMPs were still observed on these surfaces, which challenged the AMP-linker conjugation as the only source of the presence of AMPs on surfaces.
- The developed PDMA brush system on pPVC could inhibit the adhesion of a Gram-positive bacterium, *S. aureus*, on surfaces to as low as 5% of controls. DA copolymers showed lower antifouling properties compared to PDMA, with DA51 showing the best results among them, 70% decrease in bacterial adhesion. PDMA and DA51 both showed biocompatibility with platelets and resisted platelet adhesion. Adding AMP to DA51 coatings ($8 \pm 1 \mu\text{g}/\text{cm}^2$) increased the level of platelet adhesion and activation on surfaces. Poor control over reproducibility and tuning the properties of polymer brushes and the amount of conjugated

AMPs was a limitation.

- Development of polymer brushes inside the platelet bags required cutting and opening the bags for exposure to the allylamine plasma step but other steps could be easily performed inside the bags after resealing.
- Gamma irradiation sterilization of platelet storage bags seemed to be compatible with polymer coatings on pPVC.
- Taking a different approach, pPVC surfaces were coated with DA51 using mussel-inspired chemistry. DA51 (~ 100 kDa) was conjugated to some catechol groups (5 mol %, 40 groups per chain). DA51-cat was satisfactorily coated on gold and silicon wafers during a one-step immersion and on pPVC during a two-step procedure (PDA-DA51) under oxidative aqueous conditions at room temperature. pPVC was spin coated on QCM sensors and coated with PDA-DA51. Measured by QCM, the PDA-DA51 coating could decrease fibrinogen adsorption to 5 % of adsorption on control pPVC, while this value was 60 % for a single PDA coating and 27 % for a single DA51 coating. PDA-DA51 coating could significantly inhibit adhesion of platelets and two clinically isolated *S. epidermidis* strains on surfaces of pPVC.
- DA51-cat-E6, DA51 (100 kDa) conjugated with catechol and an AMP (1 mol %, 6-8 E6 per chain), were coated on silicon wafers for a proof of concept. The presence of AMP in the outermost layer was confirmed and mapped by TOF-SIMS. The immobilized peptides in this coating were shown to be bactericidal. An advantage of this bactericidal coating was the simplicity of tuning the polymer properties such as M_n , amount of conjugated peptides and catechol in solution before coating them on surfaces.
- Due to the gas permeability of platelet storage bags, coating of pPVC with PDA-DA51-cat

was successfully and easily performed inside the bags, which was an advantage of this method.

- Currently used platelet bags in Canada are made of PVC plasticized with BTHC, however, they have differing topographies. While texturing is required to prevent surfaces sticking (blocking) before filling, A15 bags have only one textured face inside them while both faces of P15 bags are textured. Bacterial and platelet adhesion was significantly higher on all the textured surfaces than on the non-textured surface of A15 bags, which encourages the further development of platelet storage bags with only one textured surface inside and positioning it above the non-textured *smooth* surface.

6.2 Future Work

The following may be recommended for future studies:

- Considering the lower platelet adhesion on modified surfaces (e.g. PDMA polymer brushes or DA51-cat) than on control pPVC samples, hydrophilic polymer coatings might preserve the platelet quality for a longer time. Modification of commercial platelet bags with these coatings and evaluation of platelet quality markers can be a next step for this study, which will shed light on the possibility of prolonging the shelf life of stored platelets by such modifications. It should be noted that our lab experience showed that performing platelet quality tests in some fabricated mini platelet bags (in order to use less donated platelets) was not an appropriate model for such evaluations so a large scale trial would need to be approved and organized with the Canadian Blood Services.
- Although the developed polymeric systems are known as biocompatible polymers, any release of the polymeric coating into the platelet bulk during storage should be evaluated.

This is more critical for the polymer brush coating where the penetration of polymers into the bulk of pPVC without covalent coupling to the pPVC was suspected.

- We observed that gamma irradiation sterilization was compatible with the modified platelet bags. A common method of platelet bag sterilization is autoclaving (steam sterilization). Whether the polymer coatings decompose or become buried into the bulk of pPVC under these conditions is valuable to study as thermal and photo degradation of polyacrylamide to the monomers can be a health concern. If other sterilization methods (gamma irradiation and ethylene oxide) were not available or appropriate, using other biocompatible polymeric systems with greater stability against degradation, e.g. polyvinylpyrrolidinone, could be a solution.
- Comparison of the rate of bacterial missed detection in bags with one textured surface versus those with both surfaces textured, as well as in bags with hydrophilic coatings versus controls (if significantly different) could encourage more systematic studies on the design of platelet bag morphology and their chemical composition. Textures in platelet bags are required to prevent the inside faces from blocking. Research on the methods other than patterning (e.g. by changing the material or perhaps just using brush coatings) can be a next step for the improvement of platelet storage bags. Ongoing discussions about the safety of PVC plastic itself, the way it is made and disposed of can be another reason to encourage such studies.

References:

- (1) Guyton, A. C.; Hall, J. E. *Textbook of Medical Physiology, Eleventh Edition*; Elsevier Inc., 2006.
- (2) British Committee for Standards in Haematology. Guidelines for the Use of Platelet Transfusions. *Br. J. Haematol.* **2003**, *122*, 10–23.
- (3) Vassallo, R. R.; Murphy, S. A Critical Comparison of Platelet Preparation Methods. *Curr. Opin. Hematol.* **2006**, *13*, 323–330.
- (4) Hoffmeister, K. M.; Felbinger, T. W.; Falet, H.; Denis, C. V.; Bergmeier, W.; Mayadas, T. N.; von Andrian, U. H.; Wagner, D. D.; Stossel, T. P.; Hartwig, J. H. The Clearance Mechanism of Chilled Blood Platelets. *Cell* **2003**, *112*, 87–97.
- (5) Brecher, M. E.; Blajchman, M. A.; Yomtovian, R.; Ness, P.; Aubuchon, J. P. Addressing the Risk of Bacterial Contamination of Platelets within the United States: A History to Help Illuminate the Future. *Transfusion* **2013**, *53*, 221–231.
- (6) Walther-Wenke, G.; Schrezenmeier, H.; Deitenbeck, R.; Geis, G.; Burkhart, J.; Hochsmann, B.; Sireis, W.; Schmidt, M.; Seifried, E.; Gebauer, W.; Liebscher, U. M.; Weinauer, F.; Muller, T. H. Screening of Platelet Concentrates for Bacterial Contamination: Spectrum of Bacteria Detected, Proportion of Transfused Units, and Clinical Follow-Up. *Ann. Hematol.* **2010**, *89*, 83–91.
- (7) Palavecino, E. L.; Yomtovian, R. A.; Jacobs, M. R. Bacterial Contamination of Platelets. *Transfus. Apher. Sci.* **2010**, *42*, 71–82.
- (8) Kou, Y.; Pagotto, F.; Hannach, B.; Ramírez-Arcos, S. Fatal False-Negative Transfusion Infection Involving a Buffy Coat Platelet Pool Contaminated with Biofilm-Positive *Staphylococcus epidermidis*: A Case Report. *Transfusion* **2015**, *55*, 2384–2389.
- (9) Perpoint, T.; Lina, G.; Poyart, C.; de Barbeyrac, B.; Traineau, R.; Jeanne, M.; Vandenesch, F.; Etienne, J. Two Cases of Fatal Shock after Transfusion of Platelets Contaminated by *Staphylococcus aureus*: Role of Superantigenic Toxins. *Clin. Infect. Dis.* **2004**, *39*, e106-9.
- (10) Devine, D. V.; Serrano, K. The Platelet Storage Lesion. *Clin. Lab. Med.* **2010**, *30*, 475–487.
- (11) Tomasulo, P.; Su, L. Is It Time for New Initiatives in the Blood Center And/or the Hospital to Reduce Bacterial Risk of Platelets? *Transfusion* **2011**, *51*, 2527–2533.
- (12) Solheim, B. G.; Seghatchian, J. The Six Questions of Pathogen Reduction Technology: An Overview of Current Opinions. *Transfus. Apher. Sci.* **2008**, *39*, 51–57.
- (13) Ruane, P. H.; Edrich, R.; Gampp, D.; Keil, S. D.; Leonard, R. L.; Goodrich, R. P. Photochemical Inactivation of Selected Viruses and Bacteria in Platelet Concentrates Using Riboflavin and Light. *Transfusion* **2004**, *44*, 877–885.
- (14) Goodrich, R. P.; Gilmour, D.; Hovenga, N.; Keil, S. A Laboratory Comparison of Pathogen Reduction Technology Treatment and Culture of Platelet Products for Addressing Bacterial Contamination Concerns. *Transfusion* **2009**, *49*, 1205–1216.

- (15) Cardo, L. J.; J, S.; Mendez, J.; Reddy, H.; Goodrich, R. P. Pathogen Inactivation of *Trypanosoma Cruzi* in Plasma and Platelet Concentrates Using Riboflavin and Ultraviolet Light. *Transfus. Apher. Sci.* **2007**, *37*, 131–137.
- (16) Schubert, P.; Coupland, D.; Culibrk, B.; Goodrich, R. P.; Devine, D. V. Riboflavin and Ultraviolet Light Treatment of Platelets Triggers p38MAPK Signaling: Inhibition Significantly Improves *in Vitro* Platelet Quality after Pathogen Reduction Treatment. *Transfusion* **2013**, *53*, 3164–3173.
- (17) Thorpe, T. C.; Wilson, M. L.; Turner, J. E.; DiGuisseppi, J. L.; Willert, M.; Mirrett, S.; Reller, L. B. BacT/Alert: An Automated Colorimetric Microbial Detection System. *J. Clin. Microbiol.* **1990**, *28*, 1608–1612.
- (18) Pietersz, R. N. I.; Reesink, H. W.; Panzer, S.; Oknaian, S.; Kuperman, S.; Gabriel, C.; Rapaille, A.; Lambermont, M.; Deneys, V.; Sondag, D.; Ram, S.; Goldman, M.; Delage, G.; Bernier, F.; Germain, M.; Vuk, T.; Georgsen, J.; Morel, P.; Naegelen, C.; Bardiaux, L.; Cazenave, J.; Dreier, J.; Vollmer, T.; Knabbe, C.; Seifried, E.; Hourfar, K.; Lin, C. K.; Spreafico, M.; Raffaele, L.; Berzuini, A.; Prati, D.; Satake, M.; Korte, D. De; Meer, P. F. Van Der; Kerkhoffs, J. L.; Blanco, L. Bacterial Contamination in Platelet Concentrates. *Vox Sang.* **2014**, *106*, 256–283.
- (19) Fang, C. T.; Chambers, L. A.; Kennedy, J.; Strupp, A.; Fucci, M. C. H.; Janas, J. A.; Tang, Y.; Hapip, C. A.; Lawrence, T. B.; Dodd, R. Y. Detection of Bacterial Contamination in Apheresis Platelet Products: American Red Cross Experience, 2004. *Transfusion* **2005**, *45*, 1845–1852.
- (20) Benjamin, R. J.; Mintz, P. D. Bacterial Detection and Extended Platelet Storage: The next Step Forward. *Transfusion* **2005**, *45*, 1832–1835.
- (21) Vuong, C.; Otto, M. *Staphylococcus epidermidis* Infections. *Microbes Infect.* **2002**, *4*, 481–489.
- (22) Goldman, M.; Delage, G.; Beauregard, P.; Pruneau-Fortier, D.; Ismail, J. A Fatal Case of Transfusion-Transmitted *Staphylococcus epidermidis* Sepsis. *Transfusion* **2001**, *41*, 1075–1076.
- (23) Ali, H.; Greco-Stewart, V. S.; Jacobs, M. R.; Yomtovian, R. A.; Rood, I. G. H.; de Korte, D.; Ramírez-Arcos, S. Characterization of the Growth Dynamics and Biofilm Formation of *Staphylococcus epidermidis* Strains Isolated from Contaminated Platelet Units. *J. Med. Microbiol.* **2014**, *63*, 884–891.
- (24) Murphy, W. G.; Foley, M.; Doherty, C.; Tierney, G.; Kinsella, A.; Salami, A.; Cadden, E.; Coakley, P. Screening Platelet Concentrates for Bacterial Contamination: Low Numbers of Bacteria and Slow Growth in Contaminated Units Mandate an Alternative Approach to Product Safety. *Vox Sang.* **2008**, *95*, 13–19.
- (25) Blass, C. R. *The Role of Poly(vinyl Chloride) in Healthcare*; Rapra Technology Limited, 2001.
- (26) Wallvik, J.; Akerblom, O. Platelet Concentrates Stored at 22 °C Need Oxygen. The Significance of Plastics in Platelet Preservation. *Vox Sang.* **1983**, *45*, 303–311.
- (27) Guidance for FDA Reviewers: Premarket Notification Submissions for Empty Containers

- for the Collection and Processing of Blood and Blood Components, Accessed Nov. 2016 <http://www.fda.gov/BiologicsBloodVaccines/GuidanceComplianceRegulatoryInformation/Guidances/Blood/ucm076749.htm>.
- (28) Scientific Committee on Emerging and Newly-Identified Health Risks. *Opinion on the Safety of Medical Devices Containing DEHP- Plasticized PVC or Other Plasticizers on Neonates and Other Groups Possibly at Risk (2015 Update)*; 2015.
 - (29) Ball, P. Poison Plastic? *Nat. Mater.* **2007**, *6*, 96–News & Views.
 - (30) FDA Public Health Notification: PVC Devices Containing the Plasticizer DEHP, Accessed Oct. 2016. <http://www.fda.gov/MedicalDevices/Safety/AlertsandNotices/PublicHealthNotifications/UCM062182>.
 - (31) Health Canada Expert Advisory Panel. *Summary of the 2002 Report of the Health Canada Expert Advisory Panel on DEHP in Medical Devices*; 2002.
 - (32) Kambia, K.; Dine, T.; Azar, R.; Gressier, B.; Luyckx, M.; Brunet, C. Comparative Study of the Leachability of Di(2-ethylhexyl) Phthalate and Tri(2-ethylhexyl) Trimellitate from Haemodialysis Tubing. *Int. J. Pharm.* **2001**, *229*, 139–146.
 - (33) Kambia, K.; Dine, T.; Gressier, B.; Dupin-Spriet, T.; Luyckx, M.; Brunet, C. Evaluation of the Direct Toxicity of Trioctyltrimellitate (TOTM), Di(2-Ethylhexyl) Phthalate (DEHP) and Their hydrolysis Products on Isolated Rat Hepatocytes. *Int. J. Artif. Organs* **2004**, *27*, 971–978.
 - (34) ter Veld, M. G. R.; Schouten, B.; Louisse, J.; van Es, D. S.; van der Saag, P. T.; Rietjens, I. M. C. M.; Murk, A. J. Estrogenic Potency of Food-Packaging-Associated Plasticizers and Antioxidants as Detected in ER α and ER β Reporter Gene Cell Lines. *J. Agric. Food Chem.* **2006**, *54*, 4407–4416.
 - (35) Estep, T. N.; Pedersen, R. A.; Miller, T. J.; Stupar, K. R. Characterization of Erythrocyte Quality during the Refrigerated Storage of Whole Blood Containing Di-(2-Ethylhexyl) Phthalate. *Blood* **1984**, *64*, 1270–1276.
 - (36) Bicalho, B.; Serrano, K.; dos Santos Pereira, A.; Devine, D. V.; Acker, J. P. Blood Bag Plasticizers Influence Red Blood Cell Vesiculation Rate without Altering the Lipid Composition of the Vesicles. *Transfus. Med. Hemotherapy* **2015**, *43*, 19–26.
 - (37) Rock, G.; Labow, R. S.; Tocchi, M. Distribution of Di(2-Ethylhexyl) Phthalate and Products in Blood and Blood Components. *Environ. Health Perspect.* **1986**, *65*, 309–316.
 - (38) Turner, V. S.; Mitchell, S. G.; Kang, S. K.; Hawker, R. J. A Comparative Study of Platelets Stored in Polyvinyl Chloride Containers Plasticised with Butyryl Trihexyl Citrate or Triethylhexyl Trimellitate. *Vox Sang.* **1995**, *69*, 195–200.
 - (39) Bhaskaran Nair, C. S.; Vidya, R.; Ashalatha, P. M. Studies on the Storage of Pooled Platelets in Non DOP PVC Containers. *Int. J. Pharma Bio Sci.* **2014**, *5*, 520–531.
 - (40) Gorman, S. P.; McGovern, J. G.; David Woolfson, A.; Adair, C. G.; Jones, D. S. The Concomitant Development of Poly(vinyl Chloride)-Related Biofilm and Antimicrobial Resistance in Relation to Ventilator-Associated Pneumonia. *Biomaterials* **2001**, *22*, 2741–2747.

- (41) Triandafillu, K.; Balazs, D. J.; Aronsson, B.-O.; Descouts, P.; Tu Quoc, P.; van Delden, C.; Mathieu, H. J.; Harms, H. Adhesion of *Pseudomonas aeruginosa* Strains to Untreated and Oxygen-Plasma Treated Poly(vinyl Chloride) (PVC) from Endotracheal Intubation Devices. *Biomaterials* **2003**, *24*, 1507–1518.
- (42) Hong, J.; Ekdahl, K. N.; Reynolds, H.; Larsson, R.; Nilsson, B. A New *in Vitro* Model to Study Interaction between Whole Blood and Biomaterials. Studies of Platelet and Coagulation Activation and the Effect of Aspirin. *Biomaterials* **1999**, *20*, 603–611.
- (43) Lamba, N. M. K.; Courtney, J. M.; Gaylor, J. D. S.; Lowe, G. D. O. *In Vitro* Investigation of the Blood Response to Medical Grade PVC and the Effect of Heparin on the Blood Response. *Biomaterials* **2000**, *21*, 89–96.
- (44) McLeod, A. G.; Walker, I. R.; Zheng, S.; Hayward, C. P. Loss of Factor VIII Activity during Storage in PVC Containers due to Adsorption. *Haemophilia* **2000**, *6*, 89–92.
- (45) Yin, H. Q.; Zhao, X. B.; Courtney, J. M.; Blass, C. R.; West, R. H.; Lowe, G. D. Blood Interactions with Plasticized Poly(vinyl Chloride): Relevance of Plasticizer Selection. *J. Mater. Sci. Mater. Med.* **1999**, *10*, 527–531.
- (46) Kim, S. W.; Petersen, R. V.; Lee, E. S. Effect of Phthalate Plasticizer on Blood Compatibility of Polyvinyl Chloride. *J. Pharm. Sci.* **1976**, *65*, 670–673.
- (47) Zhao, X. B.; Courtney, J. M. Blood Response to Plasticized Poly(vinyl Chloride): Dependence of Fibrinogen Adsorption on Plasticizer Selection and Surface Plasticizer Level. *J. Mater. Sci. Mater. Med.* **2003**, *14*, 905–912.
- (48) Nilsson, B.; Ekdahl, K. N.; Mollnes, T. E.; Lambris, J. D. The Role of Complement in Biomaterial-Induced Inflammation. *Mol. Immunol.* **2007**, *44*, 82–94.
- (49) Vogler, E. A.; Siedlecki, C. A. Contact Activation of Blood-Plasma Coagulation. *Biomaterials* **2009**, *30*, 1857–1869.
- (50) Ekdahl, K. N.; Huang, S.; Nilsson, B.; Teramura, Y. Complement Inhibition in Biomaterial- and Biosurface-Induced Thromboinflammation. *Semin. Immunol.* **2016**, *28*, 268–277.
- (51) Gorbet, M. B.; Sefton, M. V. Biomaterial-Associated Thrombosis: Roles of Coagulation Factors, Complement, Platelets and Leukocytes. *Biomaterials* **2004**, *25*, 5681–5703.
- (52) Thevenot, P.; Hu, W.; Tang, L. Surface Chemistry Influences Implant Biocompatibility. *Curr. Top. Med. Chem.* **2008**, *8*, 270–280.
- (53) Yebra, D. M.; Kiil, S.; Dam-Johansen, K. Antifouling Technology—past, Present and Future Steps towards Efficient and Environmentally Friendly Antifouling Coatings. *Prog. Org. Coatings* **2004**, *50*, 75–104.
- (54) Malaisamy, R.; Berry, D.; Holder, D.; Raskin, L.; Lepak, L.; Jones, K. L. Development of Reactive Thin Film Polymer Brush Membranes to Prevent Biofouling. *J. Memb. Sci.* **2010**, *350*, 361–370.
- (55) Brash, J. L. Exploiting the Current Paradigm of Blood-Material Interactions for the Rational Design of Blood-Compatible Materials. *J. Biomater. Sci. Polym. Ed.* **2000**, *11*, 1135–1146.

- (56) Anderson, J. M.; Rodriguez, A.; Chang, D. T. Foreign Body Reaction to Biomaterials. *Semin. Immunol.* **2008**, *20*, 86–100.
- (57) Shen, M.; Garcia, I.; Maier, R. V.; Horbett, T. A. Effects of Adsorbed Proteins and Surface Chemistry on Foreign Body Giant Cell Formation, Tumor Necrosis Factor Alpha Release and Procoagulant Activity of Monocytes. *J. Biomed. Mater. Res. A* **2004**, *70*, 533–541.
- (58) Anderson, J. M.; Bonfield, T. L.; Ziats, N. P. Protein Adsorption and Cellular Adhesion and Activation on Biomedical Polymers. *Int. J. Artif. Organs* **1990**, *13*, 375–382.
- (59) Nath, N.; Hyun, J.; Ma, H.; Chilkoti, A. Surface Engineering Strategies for Control of Protein and Cell Interactions. *Surf. Sci.* **2004**, *570*, 98–110.
- (60) Tegoulia, V. A.; Rao, W.; Kalambur, A. T.; Rabolt, J. F.; Cooper, S. L. Surface Properties, Fibrinogen Adsorption, and Cellular Interactions of a Novel Phosphorylcholine-Containing Self-Assembled Monolayer on Gold. *Langmuir* **2001**, *17*, 4396–4404.
- (61) Benesch, J.; Svedhem, S.; Svensson, S. C.; Valiokas, R.; Liedberg, B.; Tengvall, P. Protein Adsorption to Oligo(ethylene Glycol) Self-Assembled Monolayers: Experiments with Fibrinogen, Heparinized Plasma, and Serum. *J. Biomater. Sci. Polym. Ed.* **2001**, *12*, 581–597.
- (62) Liu, L.; Elwing, H. Complement Activation on Solid Surfaces as Determined by C3 Deposition and Hemolytic Consumption. *J. Biomed. Mater. Res.* **1994**, *28*, 767–773.
- (63) Liu, L.; Elwing, H. Complement Activation on Thiol-Modified Gold Surfaces. *J. Biomed. Mater. Res.* **1996**, *30*, 535–541.
- (64) Tang, L.; Liu, L.; Elwing, H. B. Complement Activation and Inflammation Triggered by Model Biomaterial Surfaces. *J. Biomed. Mater. Res.* **1998**, *41*, 333–340.
- (65) Ostuni, E.; Chapman, R. G.; Holmlin, R. E.; Takayama, S.; Whitesides, G. M. A Survey of Structure-Property Relationships of Surfaces that Resist the Adsorption of Protein. *Langmuir* **2001**, *17*, 5605–5620.
- (66) Chen, S.; Li, L.; Zhao, C.; Zheng, J. Surface Hydration: Principles and Applications toward Low-Fouling/nonfouling Biomaterials. *Polymer (Guildf)*. **2010**, *51*, 5283–5293.
- (67) Barbosa, J. N.; Barbosa, M. A.; Aguas, A. P. Adhesion of Human Leukocytes to Biomaterials: An *in Vitro* Study Using Alkanethiolate Monolayers with Different Chemically Functionalized Surfaces. *J. Biomed. Mater. Res. A* **2003**, *65*, 429–434.
- (68) Stanford, M. F.; Munoz, P. C.; Vroman, L. Platelets Adhere Where Flow Has Left Fibrinogen on Glass. *Ann. N. Y. Acad. Sci.* **1983**, *416*, 504–512.
- (69) Gluszko, P.; Rucinski, B.; Musial, J.; Wenger, R. K.; Schmaier, A. H.; Colman, R. W.; Edmunds, L. H. J.; Niewiarowski, S. Fibrinogen Receptors in Platelet Adhesion to Surfaces of Extracorporeal Circuit. *Am. J. Physiol.* **1987**, *252*, H615-21.
- (70) Vroman, L. Possible Relationships and Interactions among Events in Clotting, Platelet Adhesion, Immune Surface Reactions and Granulocyte Adhesion. *J. Theor. Biol.* **1983**, *105*, 541–543.
- (71) Tsai, W. B.; Grunkemeier, J. M.; Horbett, T. A. Human Plasma Fibrinogen Adsorption and Platelet Adhesion to Polystyrene. *J. Biomed. Mater. Res.* **1999**, *44*, 130–139.

- (72) Cox, D.; Kerrigan, S. W.; Watson, S. P. Platelets and the Innate Immune System: Mechanisms of Bacterial-Induced Platelet Activation. *J. Thromb. Haemost.* **2011**, *9*, 1097–1107.
- (73) van Oss, C. J. Long-Range and Short-Range Mechanisms of Hydrophobic Attraction and Hydrophilic Repulsion in Specific and Aspecific Interactions. *J. Mol. Recognit.* **2003**, *16*, 177–190.
- (74) Hermansson, M. The DLVO Theory in Microbial Adhesion. *Colloids Surfaces B Biointerfaces* **1999**, *14*, 105–119.
- (75) Pidhatika, B.; Möller, J.; Benetti, E. M.; Konradi, R.; Rakhmatullina, E.; Mühlebach, A.; Zimmermann, R.; Werner, C.; Vogel, V.; Textor, M. The Role of the Interplay between Polymer Architecture and Bacterial Surface Properties on the Microbial Adhesion to Polyoxazoline-Based Ultrathin Films. *Biomaterials* **2010**, *31*, 9462–72.
- (76) Katsikogianni, M.; Missirlis, Y. F. Concise Review of Mechanisms of Bacterial Adhesion to Biomaterials and of Techniques Used in Estimating Bacteria-Material Interactions. *Eur. Cells Mater.* **2004**, *8*, 37–57.
- (77) Curtis, A.; Wilkinson, C. Topographical Control of Cells. *Biomaterials* **1997**, *18*, 1573–1583.
- (78) Quirynen, M.; Bollen, C. M.; Papaioannou, W.; Van Eldere, J.; van Steenberghe, D. The Influence of Titanium Abutment Surface Roughness on Plaque Accumulation and Gingivitis: Short-Term Observations. *Int. J. Oral Maxillofac. Implants* **1996**, *11*, 169–178.
- (79) Flint, S. H.; Brooks, J. D.; Bremer, P. J. Properties of the Stainless Steel Substrate, Influencing the Adhesion of Thermo-Resistant Streptococci. *J. Food Eng.* **2000**, *43*, 235–242.
- (80) Taylor, R. L.; Verran, J.; Lees, G. C.; Ward, A. J. P. The Influence of Substratum Topography on Bacterial Adhesion to Polymethyl Methacrylate. *J. Mater. Sci. Mater. Med.* **1998**, *9*, 17–22.
- (81) Medilanski, E.; Kaufmann, K.; Wick, L. Y.; Wanner, O.; Harms, H. Influence of the Surface Topography of Stainless Steel on Bacterial Adhesion. *Biofouling* **2002**, *18*, 193–203.
- (82) Hsu, L. C.; Fang, J.; Borca-Tasciuc, D. A.; Worobo, R. W.; Moraru, C. I. Effect of Micro- and Nanoscale Topography on the Adhesion of Bacterial Cells to Solid Surfaces. *Appl. Environ. Microbiol.* **2013**, *79*, 2703–2712.
- (83) Tsunoda, N.; Kokubo, K. I.; Sakai, K.; Fukuda, M.; Miyazaki, M.; Hiyoshi, T. Surface Roughness of Cellulose Hollow Fiber Dialysis Membranes and Platelet Adhesion. *ASAIO J* **1999**, *45*, 418–423.
- (84) Zingg, W.; Neumann, W.; Strong, A.; Hum, O.; Absolom, D. Platelet Adhesion to Smooth and Rough Hydrophobic and Hydrophilic Surfaces under Conditions of Static Exposure and Laminar Flow. *Biomaterials* **1981**, *2*, 156–158.
- (85) Ezuki, S.; Kanno, T.; Ohto, H.; Herschel, L.; Ito, T.; Kawabata, K.; Seino, O.; Ikeda, K.; Nollet, K. E. Survival and Recovery of Apheresis Platelets Stored in a Polyolefin Container with High Oxygen Permeability. *Vox Sang.* **2008**, *94*, 292–298.

- (86) Brittain, W. J.; Minko, S. A Structural Definition of Polymer Brushes. *J. polym. Sci., Part A Polym. Chem.* **2007**, *45*, 3505–3512.
- (87) Milner, S. T. Polymer Brushes. *Science* **1991**, *251*, 905–914.
- (88) Milner, S.; Witten, T.; Cates, M. Theory of the Grafted Polymer Brush. *Macromolecules* **1988**, *21*, 2610–2619.
- (89) Alexander, S. Adsorption of Chain Molecules with a Polar Head a Scaling Description. *J. Phys.* **1977**, *38*, 983–987.
- (90) de Gennes, P. G. Conformations of Polymers Attached to an Interface. *Macromolecules* **1980**, *13*, 1069–1075.
- (91) Fleer, G. J.; Cohen-Stuart, M. A.; Scheutjens, J. M. H. M.; Cosgrove, T.; Vincent, B. *Polymers at Interfaces, First Edition*; Chapman & Hall, 1993.
- (92) Zhao, B.; Brittain, W. J. Polymer Brushes: Surface-Immobilized Macromolecules. *Prog. Polym. Sci.* **2000**, *25*, 677–710.
- (93) Moh, L. C. H.; Losego, M. D.; Braun, P. V. Solvent Quality Effects on Scaling Behavior of Poly(methyl Methacrylate) Brushes in the Moderate- and High-Density Regimes. *Langmuir* **2011**, *27*, 3698–3702.
- (94) Guzonas, D.; Boils, D.; Hair, M. L. Surface Force Measurements of Polystyrene-Block-Poly(ethylene Oxide) Adsorbed from a Nonselective Solvent on Mica. *Macromolecules* **1991**, *24*, 3383–3387.
- (95) Parsonage, E.; Tirrell, M.; Watanabe, H.; Nuzzo, R. G. Adsorption of poly(2-Vinylpyridine)- Poly(Styrene) Block Copolymers from Toluene Solutions. *Macromolecules* **1991**, *24*, 1987–1995.
- (96) Zdyrko, B.; Luzinov, I. Polymer Brushes by The “grafting To” method. *Macromol. Rapid Commun.* **2011**, *32*, 859–869.
- (97) Yockell-Lelièvre, H.; Desbiens, J.; Ritcey, A. M. Two-Dimensional Self-Organization of Polystyrene-Capped Gold Nanoparticles. *Langmuir* **2007**, *23*, 2843–2850.
- (98) Liu, G.; Cheng, H.; Yan, L.; Zhang, G. Study of the Kinetics of the Pancake-to-Brush Transition of Poly(*N*-Isopropylacrylamide) Chain. *J. Phys. Chem. B* **2005**, *109*, 22603–22607.
- (99) Taylor, W.; Jones, R. A. L. Producing High-Density High-Molecular-Weight Polymer Brushes by a “Grafting To” Method from a Concentrated Homopolymer Solution. *Langmuir* **2010**, *26*, 13954–13958.
- (100) Mansky, P.; Liu, Y.; Huang, E.; Russell, T. P.; Hawker, C. Controlling Polymer-Surface Interactions with Random Copolymer Brushes. *Science* **1997**, *275*, 1458–1460.
- (101) Iyer, K. S.; Zdyrko, B.; Malz, H.; Pionteck, J.; Luzinov, I. Polystyrene Layers Grafted to Macromolecular Anchoring Layer. *Macromolecules* **2003**, *36*, 6519–6526.
- (102) Barbey, R.; Lavanant, L.; Paripovic, D.; Schüwer, N.; Sugnaux, C.; Tugulu, S.; Klok, H.-A. Polymer Brushes via Surface-Initiated Controlled Radical Polymerization: Synthesis, Characterization, Properties, and Applications. *Chem. Rev.* **2009**, *109*, 5437–5527.

- (103) Olivier, A.; Meyer, F.; Raquez, J.-M.; Damman, P.; Dubois, P. Surface-Initiated Controlled Polymerization as a Convenient Method for Designing Functional Polymer Brushes: From Self-Assembled Monolayers to Patterned Surfaces. *Prog. Polym. Sci.* **2012**, *37*, 157–181.
- (104) Matyjaszewski, K.; Xia, J. Atom Transfer Radical Polymerization. *Chem. Rev.* **2001**, *101*, 2921–2990.
- (105) Pyun, J.; Kowalewski, T.; Matyjaszewski, K. Synthesis of Polymer Brushes Using Atom Transfer Radical Polymerization. *Macromol. Rapid Commun.* **2003**, *24*, 1043–1059.
- (106) Ejaz, M.; Yamamoto, S.; Ohno, K.; Tsujii, Y.; Fukuda, T. Controlled Graft Polymerization of Methyl Methacrylate on Silicon Substrate by the Combined Use of the Langmuir-Blodgett and Atom Transfer Radical Polymerization Techniques. *Macromolecules* **1998**, *31*, 5934–5936.
- (107) Choukourov, A.; Biederman, H.; Slavinska, D.; Hanley, L.; Grinevich, A.; Boldyryeva, H.; Mackova, A. Mechanistic Studies of Plasma Polymerization of Allylamine. *J. Phys. Chem. B* **2005**, *109*, 23086–23095.
- (108) Zou, Y.; Kizhakkedathu, J. N.; Brooks, D. E. Surface Modification of Polyvinyl Chloride Sheets via Growth of Hydrophilic Polymer Brushes. *Macromolecules* **2009**, *42*, 3258–3268.
- (109) Akeroyd, N.; Klumperman, B. The Combination of Living Radical Polymerization and Click Chemistry for the Synthesis of Advanced Macromolecular Architectures. *Eur. Polym. J.* **2011**, *47*, 1207–1231.
- (110) Leckband, D.; Sheth, S.; Halperin, A. Grafted Poly(ethylene Oxide) Brushes as Nonfouling Surface Coatings. *J. Biomater. Sci. Polym. Ed.* **1999**, *10*, 1125–1147.
- (111) Brooks, D. E.; Haynes, C. a; Hritcu, D.; Steels, B. M.; Müller, W. Size Exclusion Chromatography Does Not Require Pores. *Proc. Natl. Acad. Sci. U. S. A.* **2000**, *97*, 7064–7067.
- (112) Halperin, A. Polymer Brushes That Resist Adsorption of Model Proteins: Design Parameters. *Langmuir* **1999**, *15*, 2525–2533.
- (113) Halperin, A.; Fragneto, G.; Schollier, A.; Sferrazza, M. Primary versus Ternary Adsorption of Proteins onto PEG Brushes. *Langmuir* **2007**, *23*, 10603–10617.
- (114) Unsworth, L. D.; Sheardown, H.; Brash, J. L. Protein Resistance of Surfaces Prepared by Sorption of End-Thiolated Poly(ethylene Glycol) to Gold: Effect of Surface Chain Density. *Langmuir* **2005**, *21*, 1036–1041.
- (115) Roosjen, A.; Kaper, H. J.; van der Mei, H. C.; Norde, W.; Busscher, H. J. Inhibition of Adhesion of Yeasts and Bacteria by Poly(ethylene Oxide)-Brushes on Glass in a Parallel Plate Flow Chamber. *Microbiology* **2003**, *149*, 3239–3246.
- (116) Roosjen, A.; Busscher, H. J.; Norde, W.; van der Mei, H. C. Bacterial Factors Influencing Adhesion of *Pseudomonas aeruginosa* Strains to a Poly(ethylene Oxide) Brush. *Microbiology* **2006**, *152*, 2673–2682.
- (117) Roosjen, A.; van der Mei, H. C.; Busscher, H. J.; Norde, W. Microbial Adhesion to

- Poly(ethylene Oxide) Brushes: Influence of Polymer Chain Length and Temperature. *Langmuir* **2004**, *20*, 10949–10955.
- (118) Nejadnik, M. R.; van der Mei, H. C.; Norde, W.; Busscher, H. J. Bacterial Adhesion and Growth on a Polymer Brush-Coating. *Biomaterials* **2008**, *29*, 4117–4121.
- (119) Jin, J.; Huang, F.; Hu, Y.; Jiang, W.; Ji, X.; Liang, H.; Yin, J. Immobilizing PEO-PPO-PEO Triblock Copolymers on Hydrophobic Surfaces and Its Effect on Protein and Platelet: A Combined Study Using QCM-D and DPI. *Colloids Surfaces B Biointerfaces* **2014**, *123*, 892–899.
- (120) Nejadnik, M. R.; Engelsman, A. F.; Saldarriaga Fernandez, I. C.; Busscher, H. J.; Norde, W.; van der Mei, H. C. Bacterial Colonization of Polymer Brush-Coated and Pristine Silicone Rubber Implanted in Infected Pockets in Mice. *J. Antimicrob. Chemother.* **2008**, *62*, 1323–1325.
- (121) Kawai, F. Microbial Degradation of Polyethers. *Appl. Microbiol. Biotechnol.* **2002**, *58*, 30–38.
- (122) Branch, D. W.; Wheeler, B. C.; Brewer, G. J.; Leckband, D. E. Long-Term Stability of Grafted Polyethylene Glycol Surfaces for Use with Microstamped Substrates in Neuronal Cell Culture. *Biomaterials* **2001**, *22*, 1035–1047.
- (123) Garay, R. P.; El-Gewely, R.; Armstrong, J. K.; Garratty, G.; Richette, P. Antibodies against Polyethylene Glycol in Healthy Subjects and in Patients Treated with PEG-Conjugated Agents. *Expert Opin. Drug Deliv.* **2012**, *9*, 1319–1323.
- (124) Rossegger, E.; Schenk, V.; Wiesbrock, F. Design Strategies for Functionalized Poly(2-Oxazoline)s and Derived Materials. *Polymers* **2013**, *5*, 956–1011.
- (125) Hoogenboom, R. Poly(2-Oxazoline)s: A Polymer Class with Numerous Potential Applications. *Angew. Chem. Int. Ed.* **2009**, *48*, 7978–7994.
- (126) Konradi, R.; Pidhatika, B.; Mühlebach, A.; Textor, M. Poly-2-Methyl-2-Oxazoline: A Peptide-like Polymer for Protein-Repellent Surfaces. *Langmuir* **2008**, *24*, 613–616.
- (127) Wang, C. H.; Fan, K. R.; Hsiue, G. H. Enzymatic Degradation of PLLA-PEOz-PLLA Triblock Copolymers. *Biomaterials* **2005**, *26*, 2803–2811.
- (128) Fundeanu, I.; van der Mei, H. C.; Schouten, A. J.; Busscher, H. J. Polyacrylamide Brush Coatings Preventing Microbial Adhesion to Silicone Rubber. *Colloids Surf. B. Biointerfaces* **2008**, *64*, 297–301.
- (129) Fundeanu, I.; Klee, D.; Schouten, A. J.; Busscher, H. J.; van der Mei, H. C. Solvent-Free Functionalization of Silicone Rubber and Efficacy of PAAm Brushes Grafted from an Amino-PPX Layer against Bacterial Adhesion. *Acta Biomater.* **2010**, *6*, 4271–4276.
- (130) Fundeanu, I.; van der Mei, H. C.; Schouten, A. J.; Busscher, H. J. Microbial Adhesion to Surface-Grafted Polyacrylamide Brushes after Long-Term Exposure to PBS and Reconstituted Freeze-Dried Saliva. *J. Biomed. Mater. Res. A* **2010**, *94*, 997–1000.
- (131) Liu, Q.; Singh, A.; Lalani, R.; Liu, L. Ultralow Fouling Polyacrylamide on Gold Surfaces via Surface-Initiated Atom Transfer Radical Polymerization. *Biomacromolecules* **2012**, *13*, 1086–1092.

- (132) Zou, Y.; Lai, B. F. L.; Kizhakkedathu, J. N.; Brooks, D. E. Inhibitory Effect of Hydrophilic Polymer Brushes on Surface-Induced Platelet Activation and Adhesion. *Macromol. Biosci.* **2010**, *10*, 1432–1443.
- (133) Lai, B. F. L.; Creagh, A. L.; Janzen, J.; Haynes, C. A.; Brooks, D. E.; Kizhakkedathu, J. N. The Induction of Thrombus Generation on Nanostructured Neutral Polymer Brush Surfaces. *Biomaterials* **2010**, *31*, 6710–6718.
- (134) Haraguchi, K.; Kubota, K.; Takada, T.; Mahara, S. Highly Protein-Resistant Coatings and Suspension Cell Culture Thereon from Amphiphilic Block Copolymers Prepared by RAFT Polymerization. *Biomacromolecules* **2014**, *15*, 1992–2003.
- (135) Cheng, G.; Li, G.; Xue, H.; Chen, S.; Bryers, J. D.; Jiang, S. Zwitterionic Carboxybetaine Polymer Surfaces and Their Resistance to Long-Term Biofilm Formation. *Biomaterials* **2009**, *30*, 5234–5240.
- (136) Cheng, G.; Zhang, Z.; Chen, S.; Bryers, J. D.; Jiang, S. Inhibition of Bacterial Adhesion and Biofilm Formation on Zwitterionic Surfaces. *Biomaterials* **2007**, *28*, 4192–4199.
- (137) Smith, R. S.; Zhang, Z.; Bouchard, M.; Li, J.; Lapp, H. S.; Brotske, G. R.; Lucchino, D. L.; Weaver, D.; Roth, L. a; Coury, A.; Biggerstaff, J.; Sukavaneshvar, S.; Langer, R.; Loose, C. Vascular Catheters with a Nonleaching Poly-Sulfobetaine Surface Modification Reduce Thrombus Formation and Microbial Attachment. *Sci. Transl. Med.* **2012**, *4*, 153ra132.
- (138) Hirota, K.; Murakami, K.; Nemoto, K.; Miyake, Y. Coating of a Surface with 2-Methacryloyloxyethyl Phosphorylcholine (MPC) Co-Polymer Significantly Reduces Retention of Human Pathogenic Microorganisms. *FEMS Microbiol. Lett.* **2005**, *248*, 37–45.
- (139) Bertal, K.; Shepherd, J.; Douglas, C. W. I.; Madsen, J.; Morse, A.; Edmondson, S.; Armes, S. P.; Lewis, A.; MacNeil, S. Antimicrobial Activity of Novel Biocompatible Wound Dressings Based on Triblock Copolymer Hydrogels. *J. Mater. Sci.* **2009**, *44*, 6233–6246.
- (140) Yang, W. J.; Cai, T.; Neoh, K. G.; Kang, E. T.; Teo, S. L. M.; Rittschof, D. Barnacle Cement as Surface Anchor For “clicking” of Antifouling and Antimicrobial Polymer Brushes on Stainless Steel. *Biomacromolecules* **2013**, *14*, 2041–2051.
- (141) Takahashi, N.; Iwasa, F.; Inoue, Y.; Morisaki, H.; Ishihara, K.; Baba, K. Evaluation of the Durability and Antiadhesive Action of 2-Methacryloyloxyethyl Phosphorylcholine Grafting on an Acrylic Resin Denture Base Material. *J. Prosthet. Dent.* **2014**, *112*, 194–203.
- (142) Jiang, H.; Wang, X. B.; Li, C. Y.; Li, J. S.; Xu, F. J.; Mao, C.; Yang, W. T.; Shen, J. Improvement of Hemocompatibility of Polycaprolactone Film Surfaces with Zwitterionic Polymer Brushes. *Langmuir* **2011**, *27*, 11575–11581.
- (143) Kim, J. C.; Kim, M.; Jung, J.; Kim, H.; Kim, I. J.; Kim, J. R.; Ree, M. Biocompatible Characteristics of Sulfobetaine-Containing Brush Polymers. *Macromol. Res.* **2012**, *20*, 746–753.
- (144) Cheng, G.; Xue, H.; Zhang, Z.; Chen, S.; Jiang, S. A Switchable Biocompatible Polymer

- Surface with Self-Sterilizing and Nonfouling Capabilities. *Angew. Chem. Int. Ed.* **2008**, *47*, 8831–8834.
- (145) Zhang, S. F.; Rolfe, P.; Wright, G.; Lian, W.; Milling, A. J.; Tanaka, S.; Ishihara, K. Physical and Biological Properties of Compound Membranes Incorporating a Copolymer with a Phosphorylcholine Head Group. *Biomaterials* **1998**, *19*, 691–700.
- (146) Zha, Z.; Ma, Y.; Yue, X.; Liu, M.; Dai, Z. Self-Assembled Hemocompatible Coating on Poly (Vinyl Chloride) Surface. *Appl. Surf. Sci.* **2009**, *256*, 805–814.
- (147) Weber, N.; Wendel, H. P.; Ziemer, G. Hemocompatibility of Heparin-Coated Surfaces and the Role of Selective Plasma Protein Adsorption. *Biomaterials* **2002**, *23*, 429–439.
- (148) Lee, J. H.; Kim, K. O.; Ju, Y. M. Polyethylene Oxide Additive-Entrapped Polyvinyl Chloride as a New Blood Bag Material. *J. Biomed. Mater. Res.* **1998**, *48*, 328–334.
- (149) Khorasani, M. T.; Mirzadeh, H. Effect of Oxygen Plasma Treatment on Surface Charge and Wettability of PVC Blood bag—*In Vitro* Assay. *Radiat. Phys. Chem.* **2007**, *76*, 1011–1016.
- (150) Asadinezhad, A.; Novák, I.; Lehocký, M.; Sedlařík, V.; Vesel, A.; Junkar, I.; Sába, P.; Chodák, I. A Physicochemical Approach to Render Antibacterial Surfaces on Plasma-Treated Medical-Grade PVC: Irganox Coating. *Plasma Process. Polym.* **2010**, *7*, 504–514.
- (151) Lai, B. F. L.; Zou, Y.; Brooks, D. E.; Kizhakkedathu, J. N. The Influence of Poly-*N*-[(2,2-Dimethyl-1,3-Dioxolane)methyl]acrylamide on Fibrin Polymerization, Cross-Linking and Clot Structure. *Biomaterials* **2010**, *31*, 5749–5758.
- (152) Gao, G.; Lange, D.; Hilpert, K.; Kindrachuk, J.; Zou, Y.; Cheng, J. T. J.; Kazemzadeh-Narbat, M.; Yu, K.; Wang, R.; Straus, S. K.; Brooks, D. E.; Chew, B. H.; Hancock, R. E. W.; Kizhakkedathu, J. N. The Biocompatibility and Biofilm Resistance of Implant Coatings Based on Hydrophilic Polymer Brushes Conjugated with Antimicrobial Peptides. *Biomaterials* **2011**, *32*, 3899–3909.
- (153) Xiao, D.; Zhang, H.; Wirth, M. Chemical Modification of the Surface of Poly(dimethylsiloxane) by Atom-Transfer Radical Polymerization of Acrylamide. *Langmuir* **2002**, *18*, 9971–9976.
- (154) Zou, Y.; Lam, A.; Brooks, D. E.; Phani, S.; Kizhakkedathu, J. N. Bending and Stretching Actuation of Soft Materials through Surface-Initiated Polymerization. *Angew. Chem. Int. Ed.* **2011**, *50*, 5116–5119.
- (155) Kizhakkedathu, J. N.; Janzen, J.; Le, Y.; Kainthan, R. K.; Brooks, D. E. Poly (Oligo (Ethylene Glycol) Acrylamide) Brushes by Surface Initiated Polymerization: Effect of Macromonomer Chain Length on Brush Growth and Protein Adsorption from Blood Plasma. *Langmuir* **2009**, *25*, 3794–3801.
- (156) Yu, K.; Kizhakkedathu, J. N. Synthesis of Functional Polymer Brushes Containing Carbohydrate Residues in the Pyranose Form and Their Specific and Nonspecific Interactions with Proteins. *Biomacromolecules* **2010**, 3073–3085.
- (157) Folarin, O. M.; Sadiku, E. R. Thermal Stabilizers for Poly(vinyl Chloride): A Review. *Int. J. Phys. Sci.* **2011**, *6*, 4323–4330.

- (158) Dong, X.; Gusev, A.; Hercules, D. M. Characterization of Polysiloxanes with Different Functional Groups by Time-of-Flight Secondary Ion Mass Spectrometry. *J. Am. Soc. Mass Spectrom.* **1998**, *9*, 292–298.
- (159) Kala, S. V.; Lykissa, E. D.; Lebovitz, R. M. Detection and Characterization of Poly(dimethylsiloxane)s in Biological Tissues by GC/AED and GC/MS. *Anal. Chem.* **1997**, *69*, 1267–1272.
- (160) Reyes-Labarta, J.; Herrero, M.; Tiemblo, P.; Mijangos, C.; Reinecke, H. Wetchemical Surface Modification of Plasticized PVC. Characterization by FTIR-ATR and Raman Microscopy. *Polymer* **2003**, *44*, 2263–2269.
- (161) Gubala, V.; Gandhiraman, R. P.; Volcke, C.; Doyle, C.; Coyle, C.; James, B.; Daniels, S.; Williams, D. E. Functionalization of Cycloolefin Polymer Surfaces by Plasma-Enhanced Chemical Vapour Deposition: Comprehensive Characterization and Analysis of the Contact Surface and the Bulk of Aminosiloxane Coatings. *Analyst* **2010**, *135*, 1375–1381.
- (162) Puleo, D. A.; Kissling, R. A.; Sheu, M.-S. A Technique to Immobilize Bioactive Proteins, Including Bone Morphogenetic Protein-4 (BMP-4), on Titanium Alloy. *Biomaterials* **2002**, *23*, 2079–2087.
- (163) Howarter, J. a; Youngblood, J. P. Optimization of Silica Silanization by 3-Aminopropyltriethoxysilane. *Langmuir* **2006**, *22*, 11142–11147.
- (164) Xiao, S. J.; Textor, M.; Spencer, N. D.; Wieland, M.; Keller, B.; Sigrist, H. Immobilization of the Cell-Adhesive Peptide Arg-Gly-Asp-Cys (RGDC) on Titanium Surfaces by Covalent Chemical Attachment. *J. Mater. Sci. Mater. Med.* **1997**, *8*, 867–872.
- (165) Lacik, I.; Chovancova, A.; Uhelska, L.; Preusser, C.; Hutchinson, R. A.; Buback, M. PLP-SEC Studies into the Propagation Rate Coefficient of Acrylamide Radical Polymerization in Aqueous Solution. *Macromolecules* **2016**, *49*, 3244–3253.
- (166) Goodman, D.; Kizhakkedathu, J. N.; Brooks, D. E. Evaluation of an Atomic Force Microscopy Pull-off Method for Measuring Molecular Weight and Polydispersity of Polymer Brushes: Effect of Grafting Density. *Langmuir* **2004**, *20*, 6238–6245.
- (167) Kizhakkedathu, J. N.; Norris-Jones, R.; Brooks, D. E. Synthesis of Well-Defined Environmentally Responsive Polymer Brushes by Aqueous ATRP. *Macromolecules* **2004**, *37*, 734–743.
- (168) Kizhakkedathu, J. N.; Janzen, J.; Le, Y.; Kainthan, R. K.; Brooks, D. E. Poly(oligo(ethylene Glycol)acrylamide) Brushes by Surface Initiated Polymerization: Effect of Macromonomer Chain Length on Brush Growth and Protein Adsorption from Blood Plasma. *Langmuir* **2009**, *25*, 3794–3801.
- (169) Tang, F.; Zhang, L.; Zhang, Z.; Cheng, Z.; Zhu, X. Cellulose Filter Paper with Antibacterial Activity from Surface-Initiated ATRP. *J. Macromol. Sci. Part A* **2009**, *46*, 989–996.
- (170) Lee, S. B.; Koepsel, R. R.; Morley, S. W.; Matyjaszewski, K.; Sun, Y.; Russell, A. J. Permanent, Nonleaching Antibacterial Surfaces. 1. Synthesis by Atom Transfer Radical Polymerization. *Biomacromolecules* **2004**, *5*, 877–882.
- (171) Huang, J.; Murata, H.; Koepsel, R. R.; Russell, A. J.; Matyjaszewski, K. Antibacterial

- Polypropylene via Surface-Initiated Atom Transfer Radical Polymerization. *Biomacromolecules* **2007**, *8*, 1396–1399.
- (172) Jiang, S.; Cao, Z. Ultralow-Fouling, Functionalizable, and Hydrolyzable Zwitterionic Materials and Their Derivatives for Biological Applications. *Adv. Mater.* **2010**, *22*, 920–932.
- (173) Zou, Y.; Kizhakkedathu, J. N.; Brooks, D. E. Surface Modification of Polyvinyl Chloride Sheets via Growth of Hydrophilic Polymer Brushes. *Macromolecules* **2009**, *42*, 3258–3268.
- (174) Bicak, N.; Ozlem, M. Graft Copolymerization of Butyl Acrylate and 2-Ethyl Hexyl Acrylate from Labile Chlorines of Poly(vinyl Chloride) by Atom Transfer Radical Polymerization. *J. Polym. Sci. Part A Polym. Chem.* **2003**, *41*, 3457–3462.
- (175) Aouachria, K.; Belhaneche-Bensemra, N. Miscibility of PVC/PMMA Blends by Vicat Softening Temperature, Viscometry, DSC and FTIR Analysis. *Polym. Test.* **2006**, *25*, 1101–1108.
- (176) Butt, H.-J.; Cappella, B.; Kappl, M. Force Measurements with the Atomic Force Microscope: Technique, Interpretation and Applications. *Surf. Sci. Rep.* **2005**, *59*, 1–152.
- (177) Zou, Y.; Rossi, N. A. A.; Kizhakkedathu, J. N.; Brooks, D. E. Barrier Capacity of Hydrophilic Polymer Brushes To Prevent Hydrophobic Interactions: Effect of Graft Density and Hydrophilicity. *Macromolecules* **2009**, *42*, 4817–4828.
- (178) Turgman-Cohen, S.; Genzer, J. Computer Simulation of Concurrent Bulk- and Surface-Initiated Living Polymerization. *Macromolecules* **2012**, *45*, 2128–2137.
- (179) Kang, C.; Crockett, R.; Spencer, N. D. The Influence of Surface Grafting on the Growth Rate of Polymer Chains. *Polym. Chem.* **2016**, *7*, 302–309.
- (180) Koylu, D.; Carter, K. R. Stimuli-Responsive Surfaces Utilizing Cleavable Polymer Brush Layers. *Macromolecules* **2009**, *42*, 8655–8660.
- (181) Goodman, D.; Kizhakkedathu, J. N.; Brooks, D. E. Attractive Bridging Interactions in Dense Polymer Brushes in Good Solvent Measured by Atomic Force Microscopy. *Langmuir* **2004**, *20*, 2333–2340.
- (182) Yang, X.; Li, N.; Constantinesco, I.; Yu, K.; Kizhakkedathu, J. N.; Brooks, D. E. Choline Phosphate Functionalized Cellulose Membrane: A Potential Hemostatic Dressing Based on a Unique Bioadhesion Mechanism. *Acta Biomater.* **2015**, *40*, 212–225.
- (183) Teraoka, I. *Polymer Solutions: An Introduction to Physical Properties*; John Wiley & Sons, Inc., 2002.
- (184) Ulman, A. *An Introduction to Ultrathin Organic Films: From Langmuir-Blodgett to Self-Assembly*; Academic Press: San Diego, 1991.
- (185) Zasloff, M. Magainins, a Class of Antimicrobial Peptides from *Xenopus* Skin: Isolation, Characterization of Two Active Forms, and Partial cDNA Sequence of a Precursor. *Proc. Natl. Acad. Sci. U. S. A.* **1987**, *84*, 5449–5453.
- (186) Modrzakowski, M. C.; Spitznagel, J. K. Bactericidal Activity of Fractionated Granule Contents from Human Polymorphonuclear Leukocytes: Antagonism of Granule Cationic

- Proteins by Lipopolysaccharide. *Infect. Immun.* **1979**, *25*, 597–602.
- (187) Elsbach, P.; Weiss, J.; Franson, R. C.; Beckerdite-Quagliata, S.; Schneider, A.; Harris, L. Separation and Purification of a Potent Bactericidal/permeability-Increasing Protein and a Closely Associated Phospholipase A2 from Rabbit Polymorphonuclear Leukocytes. Observations on Their Relationship. *J. Biol. Chem.* **1979**, *254*, 11000–11009.
- (188) Lehrer, R. I.; Selsted, M. E.; Szklarek, D.; Fleischmann, J. Antibacterial Activity of Microbicidal Cationic Proteins 1 and 2, Natural Peptide Antibiotics of Rabbit Lung Macrophages. *Infect. Immun.* **1983**, *42*, 10–14.
- (189) Brown, K.; Hancock, R. Cationic Host Defense (Antimicrobial) Peptides. *Curr. Opin. Immunol.* **2006**, *18*, 24–30.
- (190) Hale, J. D. F.; Hancock, R. E. W. Alternative Mechanisms of Action of Cationic Antimicrobial Peptides on Bacteria. *Expert Rev. Anti. Infect. Ther.* **2007**, *5*, 951–959.
- (191) Ingham, A. B.; Moore, R. J. Recombinant Production of Antimicrobial Peptides in Heterologous Microbial Systems. *Biotechnol. Appl. Biochem.* **2007**, *47*, 1–9.
- (192) Hilpert, K.; Elliott, M.; Jenssen, H.; Kindrachuk, J.; Fjell, C. D.; Körner, J.; Winkler, D. F. H.; Weaver, L. L.; Henklein, P.; Ulrich, A. S.; Chiang, S. H. Y.; Farmer, S. W.; Pante, N.; Volkmer, R.; Hancock, R. E. W. Screening and Characterization of Surface-Tethered Cationic Peptides for Antimicrobial Activity. *Chem. Biol.* **2009**, *16*, 58–69.
- (193) Brogden, K. A. Antimicrobial Peptides: Pore Formers or Metabolic Inhibitors in Bacteria? *Nat. Rev. Microbiol.* **2005**, *3*, 238–250.
- (194) Nicolas, P. Multifunctional Host Defense Peptides: Intracellular-Targeting Antimicrobial Peptides. *FEBS J.* **2009**, *276*, 6483–6496.
- (195) Nguyen, L. T.; Haney, E. F.; Vogel, H. J. The Expanding Scope of Antimicrobial Peptide Structures and Their Modes of Action. *Trends Biotechnol.* **2011**, *29*, 464–472.
- (196) Matsuzaki, K. Why and How Are Peptide-Lipid Interactions Utilized for Self-Defense? Magainins and Tachyplesins as Archetypes. *Biochim. Biophys. Acta* **1999**, *1462*, 1–10.
- (197) Costa, F.; Carvalho, I. F.; Montelaro, R. C.; Gomes, P.; Martins, M. C. L. Covalent Immobilization of Antimicrobial Peptides (AMPs) onto Biomaterial Surfaces. *Acta Biomater.* **2011**, *7*, 1431–1440.
- (198) Aumsuwan, N.; Danyus, R. C.; Heinhorst, S.; Urban, M. W. Attachment of Ampicillin to Expanded Poly(tetrafluoroethylene): Surface Reactions Leading to Inhibition of Microbial Growth. *Biomacromolecules* **2008**, *9*, 1712–1718.
- (199) Campoccia, D.; Montanaro, L.; Speziale, P.; Arciola, C. R. Antibiotic-Loaded Biomaterials and the Risks for the Spread of Antibiotic Resistance Following Their Prophylactic and Therapeutic Clinical Use. *Biomaterials* **2010**, *31*, 6363–6377.
- (200) Cademartiri, R.; Anany, H.; Gross, I.; Bhayani, R.; Griffiths, M.; Brook, M. A. Immobilization of Bacteriophages on Modified Silica Particles. *Biomaterials* **2010**, *31*, 1904–1910.
- (201) Hosseinidoust, Z.; Van de Ven, T. G. M.; Tufenkji, N. Bacterial Capture Efficiency and Antimicrobial Activity of Phage-Functionalized Model Surfaces. *Langmuir* **2011**, *27*,

5472–5480.

- (202) Page, K.; Wilson, M.; Parkin, I. P. Antimicrobial Surfaces and Their Potential in Reducing the Role of the Inanimate Environment in the Incidence of Hospital-Acquired Infections. *J. Mater. Chem.* **2009**, *19*, 3819–3831.
- (203) Appendini, P.; Hotchkiss, J. H. Immobilization of Lysozyme on Food Contact Polymers as Potential Antimicrobial Films. *Packag. Technol. Sci.* **1997**, *10*, 271–279.
- (204) Siedenbiedel, F.; Tiller, J. C. Antimicrobial Polymers in Solution and on Surfaces: Overview and Functional Principles. *Polymers* **2012**, *4*, 46–71.
- (205) Kugel, A.; Staflien, S.; Chisholm, B. J. Antimicrobial Coatings Produced by “tethering” Biocides to the Coating Matrix: A Comprehensive Review. *Prog. Org. Coatings* **2011**, *72*, 222–252.
- (206) Campoccia, D.; Montanaro, L.; Arciola, C. R. A Review of the Biomaterials Technologies for Infection-Resistant Surfaces. *Biomaterials* **2013**, *34*, 8533–8554.
- (207) Knetsch, M. L. W.; Koole, L. H. New Strategies in the Development of Antimicrobial Coatings: The Example of Increasing Usage of Silver and Silver Nanoparticles. *Polymers* **2011**, *3*, 340–366.
- (208) Hegstad, K.; Langsrud, S.; Lunestad, B. T.; Scheie, A. A.; Sunde, M.; Yazdankhah, S. P. Does the Wide Use of Quaternary Ammonium Compounds Enhance the Selection and Spread of Antimicrobial Resistance and Thus Threaten Our Health? *Microb. Drug Resist.* **2010**, *16*, 91–104.
- (209) Haynie, S. L.; Crum, G. A.; Doele, B. A. Antimicrobial Activities of Amphiphilic Peptides Covalently Bonded to a Water-Insoluble Resin . These Include : Antimicrobial Activities of Amphiphilic Peptides Covalently Bonded to a Water-Insoluble Resin. *Antimicrob. Agents Chemother.* **1995**, *39*, 301–307.
- (210) Bagheri, M.; Beyermann, M.; Dathe, M. Immobilization Reduces the Activity of Surface-Bound Cationic Antimicrobial Peptides with No Influence upon the Activity Spectrum. *Antimicrob. Agents Chemother.* **2009**, *53*, 1132–1141.
- (211) Bagheri, M.; Beyermann, M.; Dathe, M. Mode of Action of Cationic Antimicrobial Peptides Defines the Tethering Position and the Efficacy of Biocidal Surfaces. *Bioconjug. Chem.* **2012**, *23*, 66–74.
- (212) Glinel, K.; Jonas, A. M.; Jouenne, T.; Leprince, J.; Galas, L.; Huck, W. T. S. Antibacterial and Antifouling Polymer Brushes Incorporating Antimicrobial Peptide. *Bioconjug. Chem.* **2009**, *20*, 71–77.
- (213) Blin, T.; Purohit, V.; Leprince, J.; Jouenne, T.; Glinel, K. Bactericidal Microparticles Decorated by an Antimicrobial Peptide for the Easy Disinfection of Sensitive Aqueous Solutions. *Biomacromolecules* **2011**, *12*, 1259–1264.
- (214) Basu, A.; Mishra, B.; Leong, S. S. J. Immobilization of Polybia-MPI by Allyl Glycidyl Ether Based Brush Chemistry to Generate a Novel Antimicrobial Surface. *J. Mater. Chem. B* **2013**, *1*, 4746–4755.
- (215) Li, X.; Li, P.; Saravanan, R.; Basu, A.; Mishra, B.; Lim, S. H.; Su, X.; Tambyah, P. A.;

- Leong, S. S. J. Antimicrobial Functionalization of Silicone Surfaces with Engineered Short Peptides Having Broad Spectrum Antimicrobial and Salt-Resistant Properties. *Acta Biomater.* **2014**, *10*, 258–266.
- (216) Li, Y.; Santos, C. M.; Kumar, A.; Zhao, M.; Lopez, A. I.; Qin, G.; McDermott, A. M.; Cai, C. “Click” immobilization on Alkylated Silicon Substrates: Model for the Study of Surface Bound Antimicrobial Peptides. *Chem. Eur. J.* **2011**, *17*, 2656–2665.
- (217) Gao, G.; Yu, K.; Kindrachuk, J.; Brooks, D. E.; Hancock, R. E. W.; Kizhakkedathu, J. N. Antibacterial Surfaces Based on Polymer Brushes: Investigation on the Influence of Brush Properties on Antimicrobial Peptide Immobilization and Antimicrobial Activity. *Biomacromolecules* **2011**, *12*, 3715–3727.
- (218) Gao, G.; Cheng, J. T. J.; Kindrachuk, J.; Hancock, R. E. W.; Straus, S. K.; Kizhakkedathu, J. N. Biomembrane Interactions Reveal the Mechanism of Action of Surface-Immobilized Host Defense IDR-1010 Peptide. *Chem. Biol.* **2012**, *19*, 199–209.
- (219) Yeaman, M. R.; Yount, N. Y.; Waring, A. J.; Gank, K. D.; Kupferwasser, D.; Wiese, R.; Bayer, A. S.; Welch, W. H. Modular Determinants of Antimicrobial Activity in Platelet Factor-4 Family Kinocidins. *Biochim. Biophys. Acta Biomembr.* **2007**, *1768*, 609–619.
- (220) Tang, Y.; Yeaman, M. R.; Selsted, M. E. Antimicrobial Peptides from Human Platelets. *Infect. Immun.* **2002**, *70*, 6524–6533.
- (221) Mohan, K. V. K.; Rao, S. S.; Atreya, C. D. Evaluation of Antimicrobial Peptides as Novel Bactericidal Agents for Room Temperature-Stored Platelets. *Transfusion* **2010**, *50*, 166–173.
- (222) Bosch-Marcé, M.; Seetharaman, S.; Kurtz, J.; Mohan, K. V. K.; Wagner, S. J.; Atreya, C. D. Leukoreduced Whole Blood-Derived Platelets Treated with Antimicrobial Peptides Maintain in Vitro Properties during Storage. *Transfusion* **2014**, *54*, 1604–1609.
- (223) Bosch-Marcé, M.; Mohan, K. V. K.; Gelderman, M. P.; Ryan, P. L.; Russek-Cohen, E.; Atreya, C. D. Preclinical Safety Evaluation of Human Platelets Treated with Antimicrobial Peptides in Severe Combined Immunodeficient Mice. *Transfusion* **2014**, *54*, 569–576.
- (224) Kubicek-Sutherland, J. Z.; Lofton, H.; Vestergaard, M.; Hjort, K.; Ingmer, H.; Andersson, D. I. Antimicrobial Peptide Exposure Selects for *Staphylococcus aureus* Resistance to Human Defence Peptides. *J. Antimicrob. Chemother.* **2017**, *72*, 115–127.
- (225) Smith, R. E.; MacQuarrie, R. A Sensitive Fluorometric Method for the Determination of Arginine Using 9,10-Phenanthrenequinone. *Anal. Biochem.* **1978**, *90*, 246–255.
- (226) Indurthi, V. S. K.; Leclerc, E.; Vetter, S. W. Interaction between Glycated Serum Albumin and AGE-Receptors Depends on Structural Changes and the Glycation Reagent. *Arch. Biochem. Biophys.* **2012**, *528*, 185–196.
- (227) Tanabe, S.; Sakaguchi, T. Reaction of Guanidines with α -Diketones. V. Mechanism of the Fluorescence Reaction of Monosubstituted Guanidines with 9,10-Phenanthraquinone. *Chem. Pharm. Bull.* **1978**, *26*, 337–342.
- (228) Ishihara, K. Advanced Bioinspired Phospholipid Polymer Biomaterials for Making High Performance Artificial Organs. *Sci. Technol. Adv. Mater.* **2000**, *1*, 131–138.

- (229) Waite, J. H.; Tanzer, M. L. Polyphenolic Substance of *Mytilus Edulis*: Novel Adhesive Containing L-Dopa and Hydroxyproline. *Science* **1981**, *212*, 1038–1040.
- (230) Lee, H.; Dellatore, S. M.; Miller, W. M.; Messersmith, P. B. Mussel-Inspired Surface Chemistry for Multifunctional Coatings. *Science* **2007**, *318*, 426–430.
- (231) Waite, J. H.; Qin, X. Polyphosphoprotein from the Adhesive Pads of *Mytilus Edulis*. *Biochemistry* **2001**, *40*, 2887–2893.
- (232) Silverman, H. G.; Roberto, F. F. Understanding Marine Mussel Adhesion. *Mar. Biotechnol.* **2007**, *9*, 661–681.
- (233) Wu, J.; Zhang, L.; Wang, Y.; Long, Y.; Gao, H.; Zhang, X.; Zhao, N.; Cai, Y.; Xu, J. Mussel-Inspired Chemistry for Robust and Surface-Modifiable Multilayer Films. *Langmuir* **2011**, *27*, 13684–13691.
- (234) Liebscher, J.; Mrówczyński, R.; Scheidt, H. A.; Filip, C.; Haidade, N. D.; Turcu, R.; Bende, A.; Beck, S. Structure of Polydopamine: A Never-Ending Story? *Langmuir* **2013**, *29*, 10539–10548.
- (235) Xu, L. Q.; Pranantyo, D.; Neoh, K. G.; Kang, E. T.; Teo, S. L. M.; Fu, G. D. Synthesis of Catechol and Zwitterion-Bifunctionalized Poly(ethylene Glycol) for the Construction of Antifouling Surfaces. *Polym. Chem.* **2016**, *7*, 493–501.
- (236) Yang, W.; Sundaram, H. S.; Ella, J.-R.; He, N.; Jiang, S. Low-Fouling Electrospun PLLA Films Modified with Zwitterionic Poly(sulfobetaine Methacrylate)-Catechol Conjugates. *Acta Biomater.* **2016**, *40*, 92–99.
- (237) Wei, Q.; Achazi, K.; Liebe, H.; Schulz, A.; Noeske, P.-L. M.; Grunwald, I.; Haag, R. Mussel-Inspired Dendritic Polymers as Universal Multifunctional Coatings. *Angew. Chem. Int. Ed.* **2014**, *53*, 11650–11655.
- (238) Wei, Q.; Becherer, T.; Noeske, P.-L. M.; Grunwald, I.; Haag, R. A Universal Approach to Crosslinked Hierarchical Polymer Multilayers as Stable and Highly Effective Antifouling Coatings. *Adv. Mater.* **2014**, *26*, 2688–2693.
- (239) Dalsin, J. L.; Lin, L.; Tosatti, S.; Vörös, J.; Textor, M.; Messersmith, P. B. Protein Resistance of Titanium Oxide Surfaces Modified by Biologically Inspired mPEG-DOPA. *Langmuir* **2005**, *21*, 640–646.
- (240) Park, J. Y.; Yeom, J.; Kim, J. S.; Lee, M.; Lee, H.; Nam, Y. S. Cell-Repellant Dextran Coatings of Porous Titania Using Mussel Adhesion Chemistry. *Macromol. Biosci.* **2013**, *13*, 1511–1519.
- (241) Kang, S. M.; Hwang, N. S.; Yeom, J.; Park, S. Y.; Messersmith, P. B.; Choi, I. S.; Langer, R.; Anderson, D. G.; Lee, H. One-Step Multipurpose Surface Functionalization by Adhesive Catecholamine. *Adv. Funct. Mater.* **2012**, *22*, 2949–2955.
- (242) Meddikeri, R. R.; Tosatti, S.; Schuler, M.; Chessari, S.; Textor, M.; Richards, R. G.; Harris, L. G. Reduced Medical Infection Related Bacterial Strains Adhesion on Bioactive RGD Modified Titanium Surfaces: A First Step toward Cell Selective Surfaces. *J. Biomed. Mater. Res. Part A* **2008**, *84*, 425–435.
- (243) Sundaram, H. S.; Han, X.; Nowinski, A. K.; Ella-Menye, J.-R.; Wimbish, C.; Marek, P.;

- Senecal, K.; Jiang, S. One-Step Dip Coating of Zwitterionic Sulfobetaine Polymers on Hydrophobic and Hydrophilic Surfaces. *ACS Appl. Mater. Interfaces* **2014**, *6*, 6664–6671.
- (244) Yu, J.; Kan, Y.; Rapp, M.; Danner, E.; Wei, W.; Das, S.; Miller, D. R.; Chen, Y.; Waite, J. H.; Israelachvili, J. N. Adaptive Hydrophobic and Hydrophilic Interactions of Mussel Foot Proteins with Organic Thin Films. *Proc. Natl. Acad. Sci. U. S. A.* **2013**, *110*, 15680–15685.
- (245) Dreyer, D. R.; Miller, D. J.; Freeman, B. D.; Paul, D. R.; Bielawski, C. W. Elucidating the Structure of Poly(dopamine). *Langmuir* **2012**, *28*, 6428–6435.
- (246) You, I.; Kang, M.; Byun, Y.; Lee, H. Enhancement of Blood Compatibility of Poly (Urethane) Substrates by Mussel-Inspired Adhesive Heparin Coating. *Bioconjug. Chem.* **2011**, *22*, 1264–1269.
- (247) Nonckreman, C. J.; Fleith, S.; Rouxhet, P. G.; Dupont-Gillain, C. C. Competitive Adsorption of Fibrinogen and Albumin and Blood Platelet Adhesion on Surfaces Modified with Nanoparticles and/or PEO. *Colloids Surf. B. Biointerfaces* **2010**, *77*, 139–149.
- (248) Herrmann, M.; Lai, Q. J.; Albrecht, R. M.; Mosher, D. F.; Proctor, R. a. Adhesion of *Staphylococcus aureus* to Surface-Bound Platelets: Role of Fibrinogen/Fibrin and Platelet Integrins. *J. Infect. Dis.* **1993**, *167*, 312–322.
- (249) Buttry, D. a; Ward, M. D. Measurement of Interfacial Processes at Electrode Surfaces with the Electrochemical Quartz Crystal Microbalance. *Chem. Rev.* **1992**, *92*, 1355–1379.
- (250) Sileika, T. S.; Kim, H.-D.; Maniak, P.; Messersmith, P. B. Antibacterial Performance of Polydopamine-Modified Polymer Surfaces Containing Passive and Active Components. *ACS Appl. Mater. Interfaces* **2011**, *3*, 4602–4610.
- (251) Yang, W. J.; Cai, T.; Neoh, K. G.; Kang, E. T.; Dickinson, G. H.; Teo, S. L.-M.; Rittschof, D. Biomimetic Anchors for Antifouling and Antibacterial Polymer Brushes on Stainless Steel. *Langmuir* **2011**, *27*, 7065–7076.
- (252) Hong, S.; Kim, K. Y.; Wook, H. J.; Park, S. Y.; Lee, K. D.; Lee, D. Y.; Lee, H. Attenuation of the in Vivo Toxicity of Biomaterials by Polydopamine Surface Modification. *Nanomedicine* **2011**, *6*, 793–801.
- (253) Liu, X.; Cao, J.; Li, H.; Li, J.; Jin, Q.; Ren, K.; Ji, J. Mussel-Inspired Polydopamine: A Biocompatible and Ultrastable Coating for Nanoparticles in Vivo. *ACS Nano* **2013**, *7*, 9384–9395.
- (254) Nurunnabi, M.; Khatun, Z.; Nafiujjaman, M.; Lee, D.; Lee, Y. Surface Coating of Graphene Quantum Dots Using Mussel Inspired Polydopamine for Biomedical Optical Imaging. *ACS Appl. Mater. Interfaces* **2013**, *5*, 8246–8253.
- (255) Hall-Stoodley, L.; Costerton, J. W.; Stoodley, P. Bacterial Biofilms: From the Natural Environment to Infectious Diseases. *Nat. Rev. Microbiol.* **2004**, *2*, 95–108.
- (256) Schachter, B. Slimy Business- the Biotechnology of Biofilms. *Nat. Biotechnol.* **2003**, *21*, 361–365.
- (257) Chmielewski, R. A. N.; Frank, J. F. Biofilm Formation and Control in Food Processing

- Facilities. *Compr. Rev. Food Sci. Food Saf.* **2003**, *2*, 22–32.
- (258) Luo, R.; Tang, L.; Zhong, S.; Yang, Z.; Wang, J.; Weng, Y.; Tu, Q.; Jiang, C.; Huang, N. In Vitro Investigation of Enhanced Hemocompatibility and Endothelial Cell Proliferation Associated with Quinone-Rich Polydopamine Coating. *ACS Appl. Mater. Interfaces* **2013**, *5*, 1704–1714.
- (259) Hong, S.; Na, Y. S.; Choi, S.; Song, I. T.; Kim, W. Y.; Lee, H. Non-Covalent Self-Assembly and Covalent Polymerization Co-Contribute to Polydopamine Formation. *Adv. Funct. Mater.* **2012**, *22*, 4711–4717.
- (260) Lilge, I.; Schönherr, H. Control of Cell Attachment and Spreading on Poly(acrylamide) Brushes with Varied Grafting Density. *Langmuir* **2016**, *32*, 838–847.
- (261) Kitamura, N.; Yokota, M.; Kurokawa, T.; Gong, J. P.; Yasuda, K. In Vivo Cartilage Regeneration Induced by a Double-Network Hydrogel: Evaluation of a Novel Therapeutic Strategy for Femoral Articular Cartilage Defects in a Sheep Model. *J. Biomed. Mater. Res. A* **2016**, *104*, 2159–2165.
- (262) Pallua, N.; Wolter, T. P. A 5-Year Assessment of Safety and Aesthetic Results after Facial Soft-Tissue Augmentation with Polyacrylamide Hydrogel (Aquamid): A Prospective Multicenter Study of 251 Patients. *Plast. Reconstr. Surg.* **2010**, *125*, 1797–1804.
- (263) Altman, D.; Hjern, F.; Zetterström, J. Transanal Submucosal Polyacrylamide Gel Injection Treatment of Anal Incontinence: A Randomized Controlled Trial. *Acta Obstet. Gynecol. Scand.* **2016**, *95*, 528–533.
- (264) Wagner, M. S.; Castner, D. G. Analysis of Adsorbed Proteins by Static Time-of-Flight Secondary Ion Mass Spectrometry. *Appl. Surf. Sci.* **2004**, *231–232*, 366–376.
- (265) Tidwell, C. D.; Castner, D. G.; Golledge, S. L.; Ratner, B. D.; Meyer, K.; Hagenhoff, B.; Benninghoven, A. Static Time-of-Flight Secondary Ion Mass Spectrometry and X-Ray Photoelectron Spectroscopy Characterization of Adsorbed Albumin and Fibronectin Films. *Surf. Interface Anal.* **2001**, *31*, 724–733.
- (266) Wagner, M. S.; Castner, D. G. Characterization of Adsorbed Protein Films by Time-of-Flight Secondary Ion Mass Spectrometry with Principal Component Analysis. *Langmuir* **2001**, *17*, 4649–4660.
- (267) McDonald, C. P. Transfusion Risk Reduction: Testing for Bacteria. *ISBT Sci. Ser.* **2013**, *8*, 73–79.
- (268) Jacobs, M. R.; Good, C. E.; Lazarus, H. M.; Yomtovian, R. A. Relationship between Bacterial Load, Species Virulence, and Transfusion Reaction with Transfusion of Bacterially Contaminated Platelets. *Clin. Infect. Dis.* **2008**, *46*, 1214–1220.
- (269) Brecher, M. E.; Means, N.; Jere, C. S.; Heath, D.; Rothenberg, S.; Stutzman, L. C. Evaluation of an Automated Culture System for Detecting Bacterial Contamination of Platelets: an Analysis with 15 Contaminating Organisms. *Transfusion* **2001**, *41*, 477–482.
- (270) Greco, C.; Martincic, I.; Gusinjac, A.; Kalab, M.; Yang, A.-F.; Ramírez-Arcos, S. *Staphylococcus epidermidis* Forms Biofilms under Simulated Platelet Storage Conditions. *Transfusion* **2007**, *47*, 1143–1153.

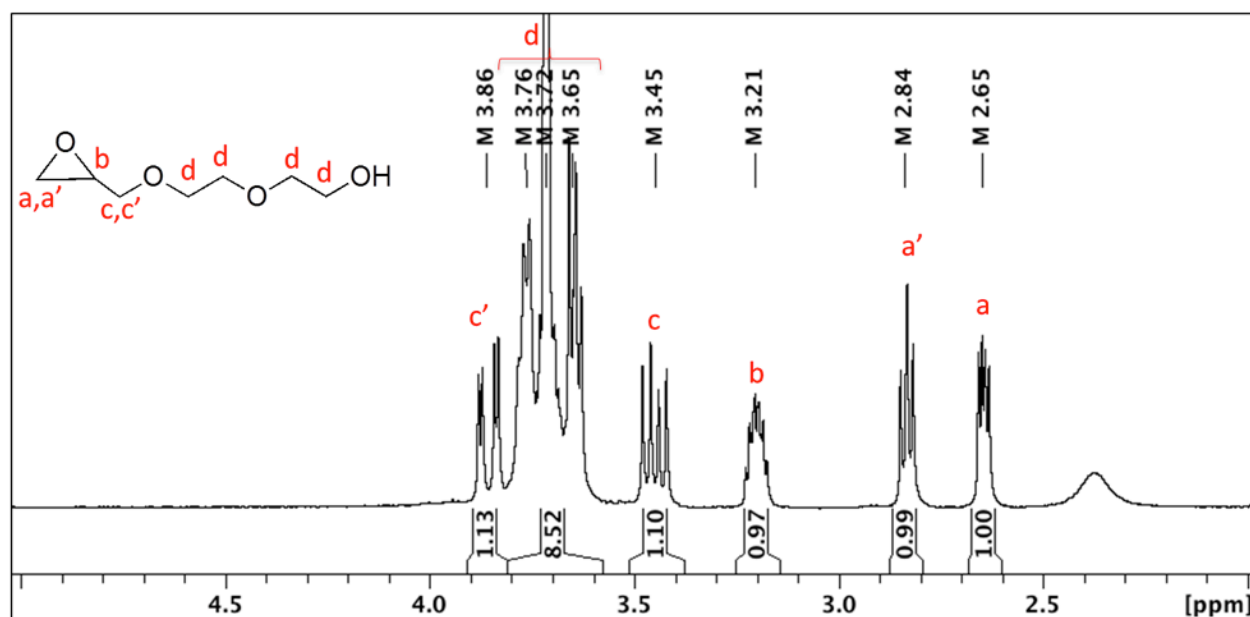
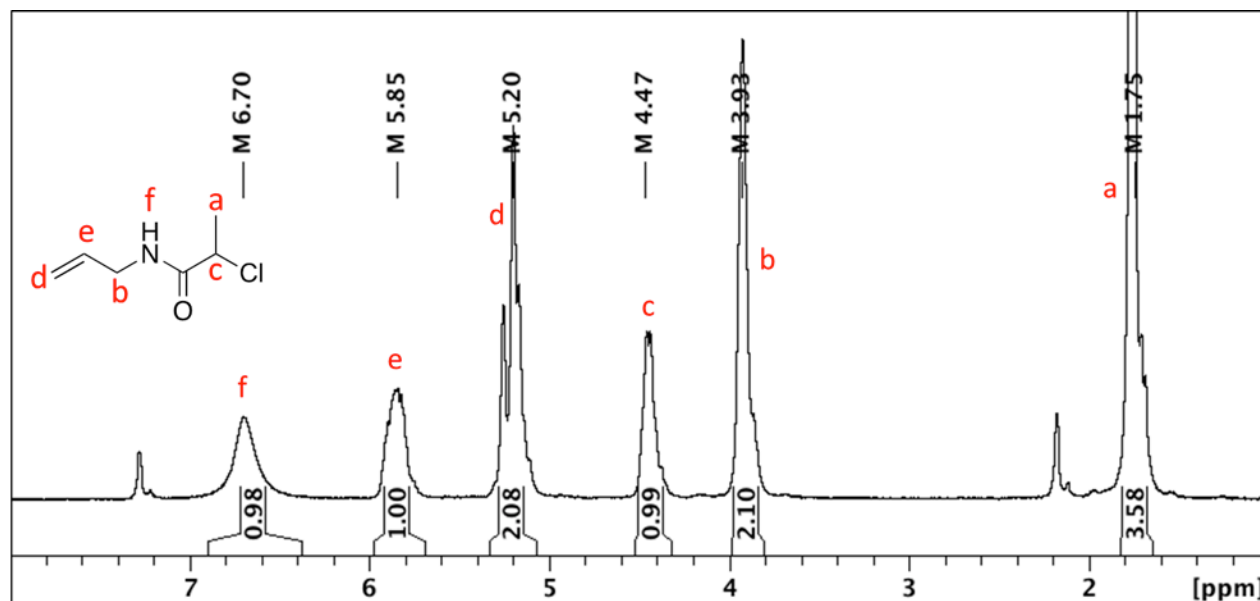
- (271) Patel, I. Plastic Composition with Anti-Hemolytic Effect. United States Patent, US 5167657, Dec. 1, 1992.
- (272) Gajewski, H. M.; Measell, E.; Laurin, D. G.; Czuba, L. F. Clear, Autoclavable Plastic Formulation Free of Liquid Plasticizers. United States Patent, US 4140162, Feb. 20, 1979.
- (273) Lecuyer, S.; Rusconi, R.; Shen, Y.; Forsyth, A.; Vlamakis, H.; Kolter, R.; Stone, H. A. Shear Stress Increases the Residence Time of Adhesion of *Pseudomonas aeruginosa*. *Biophys. J.* **2011**, *100*, 341–350.
- (274) Mercier-Bonin, M.; Duviau, M.; Ellero, C. Dynamics of Detachment of *Escherichia coli* from Plasma-Mediated Coatings under Shear Flow. *Biofouling* **2012**, *28*, 37–41.
- (275) Paris, T.; Skali-Lami, S.; Block, J.-C. Effect of Wall Shear Rate on Biofilm Deposition and Grazing in Drinking Water Flow Chambers. *Biotechnol. Bioeng.* **2007**, *97*, 1550–1561.
- (276) Scheuerman, T. R.; Camper, A. K.; Hamilton, M. A. Effects of Substratum Topography on Bacterial Adhesion. *J. Colloid Interface Sci.* **1998**, *208*, 23–33.
- (277) Perni, S.; Prokopovich, P. Micropatterning with Conical Features Can Control Bacterial Adhesion on Silicone. *Soft Matter* **2013**, *9*, 1844–1851.
- (278) Gu, H.; Hou, S.; Yongyat, C.; De Tore, S.; Ren, D. Patterned Biofilm Formation Reveals a Mechanism for Structural Heterogeneity in Bacterial Biofilms. *Langmuir* **2013**, *29*, 11145–11153.
- (279) Perera-Costa, D.; Bruque, J. M.; Gonzalez-Martin, M. L.; Gomez-Garcia, A. C.; Vadillo-Rodriguez, V. Studying the Influence of Surface Topography on Bacterial Adhesion Using Spatially Organized Microtopographic Surface Patterns. *Langmuir* **2014**, *30*, 4633–4641.
- (280) Truong, V. K.; Lapovok, R.; Estrin, Y. S.; Rundell, S.; Wang, J. Y.; Fluke, C. J.; Crawford, R. J.; Ivanova, E. P. The Influence of Nano-Scale Surface Roughness on Bacterial Adhesion to Ultrafine-Grained Titanium. *Biomaterials* **2010**, *31*, 3674–3683.
- (281) Wu, Y.; Zitelli, J. P.; TenHuisen, K. S.; Yu, X.; Libera, M. R. Differential Response of Staphylococci and Osteoblasts to Varying Titanium Surface Roughness. *Biomaterials* **2011**, *32*, 951–960.
- (282) Katsikogianni, M. G.; Missirlis, Y. F. Interactions of Bacteria with Specific Biomaterial Surface Chemistries under Flow Conditions. *Acta Biomater.* **2010**, *6*, 1107–1118.
- (283) Bagherifard, S.; Hickey, D. J.; de Luca, A. C.; Malheiro, V. N.; Markaki, A. E.; Guagliano, M.; Webster, T. J. The Influence of Nanostructured Features on Bacterial Adhesion and Bone Cell Functions on Severely Shot Peened 316L Stainless Steel. *Biomaterials* **2015**, *73*, 185–197.
- (284) Puckett, S. D.; Taylor, E.; Raimondo, T.; Webster, T. J. The Relationship between the Nanostructure of Titanium Surfaces and Bacterial Attachment. *Biomaterials* **2010**, *31*, 706–713.
- (285) Gordi, T.; Khamis, H. Simple Solution to a Common Statistical Problem: Interpreting Multiple Tests. *Clin. Ther.* **2004**, *26*, 780–786.

- (286) Milner, K. R.; Snyder, A. J.; Siedlecki, C. A. Sub-Micron Texturing for Reducing Platelet Adhesion to Polyurethane Biomaterials. *J. Biomed. Mater. Res. A* **2006**, *76*, 561–570.
- (287) Corum, L. E.; Hlady, V. The Effect of Upstream Platelet-Fibrinogen Interactions on Downstream Adhesion and Activation. *Biomaterials* **2012**, *33*, 1255–1260.
- (288) May, R. M.; Magin, C. M.; Mann, E. E.; Drinker, M. C.; Fraser, J. C.; Siedlecki, C. A.; Brennan, A. B.; Reddy, S. T. An Engineered Micropattern to Reduce Bacterial Colonization, Platelet Adhesion and Fibrin Sheath Formation for Improved Biocompatibility of Central Venous Catheters. *Clin. Transl. Med.* **2015**, *4*, 9.
- (289) Circular of Information for the Use of Human Blood Components- Pooled Platelets LR CPD, Apheresis Platelets by Canadian Blood Services, Accessed Dec. 2016 https://blood.ca/sites/default/files/Pooled_Platelets_LR_CPD_Apheresis_Platelets_0.pdf.
- (290) Fallgren, C.; Ljungh, A.; Shenkman, B.; Varon, D.; Savion, N. Venous Shear Stress Enhances Platelet Mediated Staphylococcal Adhesion to Artificial and Damaged Biological Surfaces. *Biomaterials* **2002**, *23*, 4581–4589.
- (291) Stoodley, P.; Wilson, S.; Hall-Stoodley, L.; Boyle, J. D.; Lappin-Scott, H. M.; Costerton, J. W. Growth and Detachment of Cell Clusters from Mature Mixed-Species Biofilms. *Appl. Environ. Microbiol.* **2001**, *67*, 5608–5613.
- (292) Nicola, T.; Pott, H. Heat Sterilizable Laminated Film for Use in Blood Bags or Medical Pump Membranes, German Patent, DE19728686, April 15, 1999.
- (293) Nakamura, Y. Multiple Bag. United States Patent, US 5330462 A, July 19, 1994.

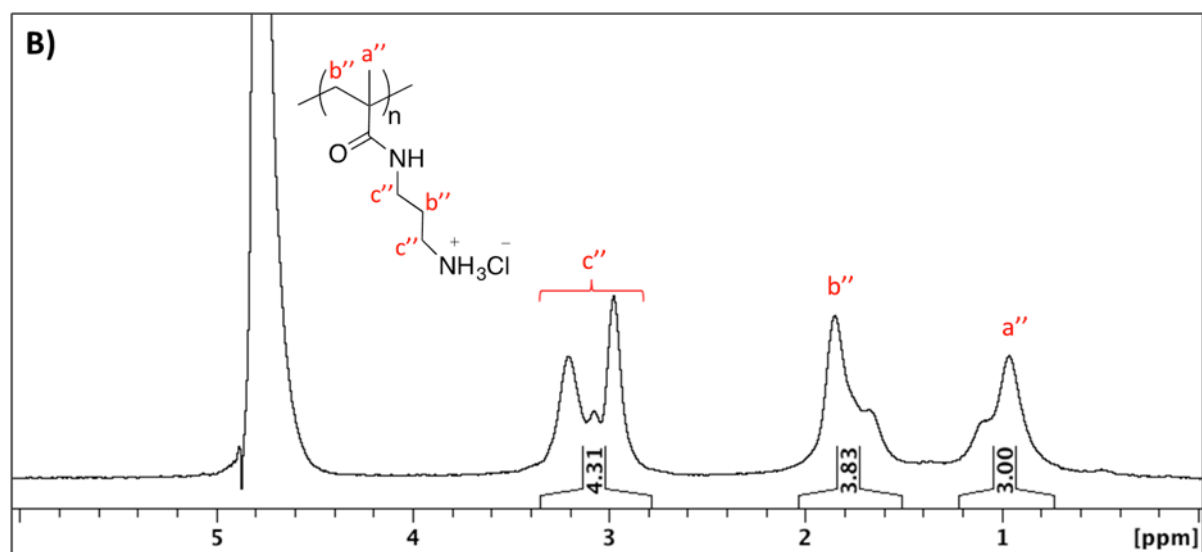
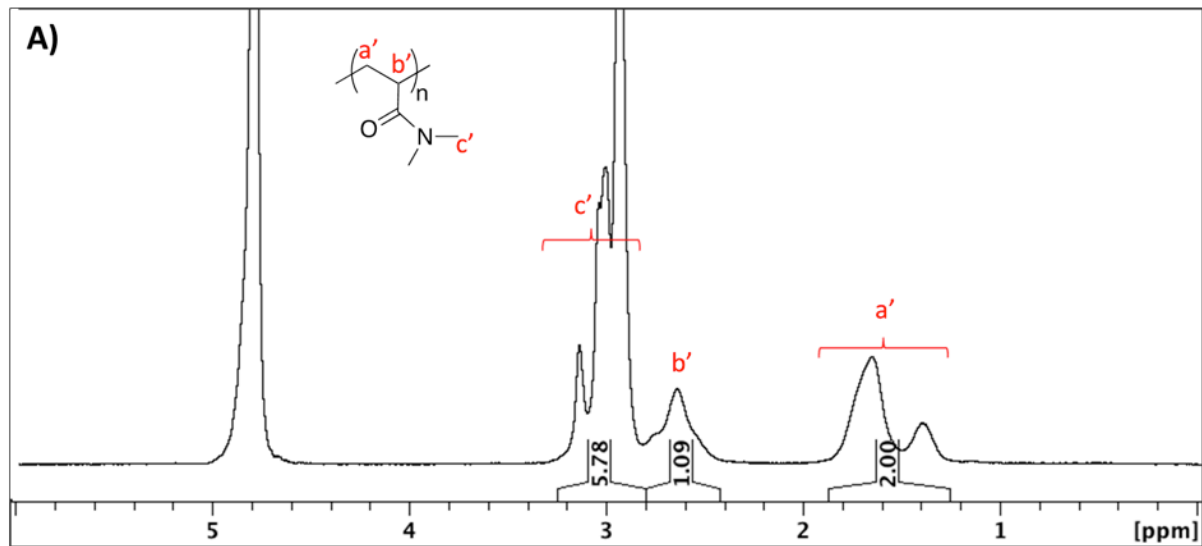
APPENDICES

Appendix A

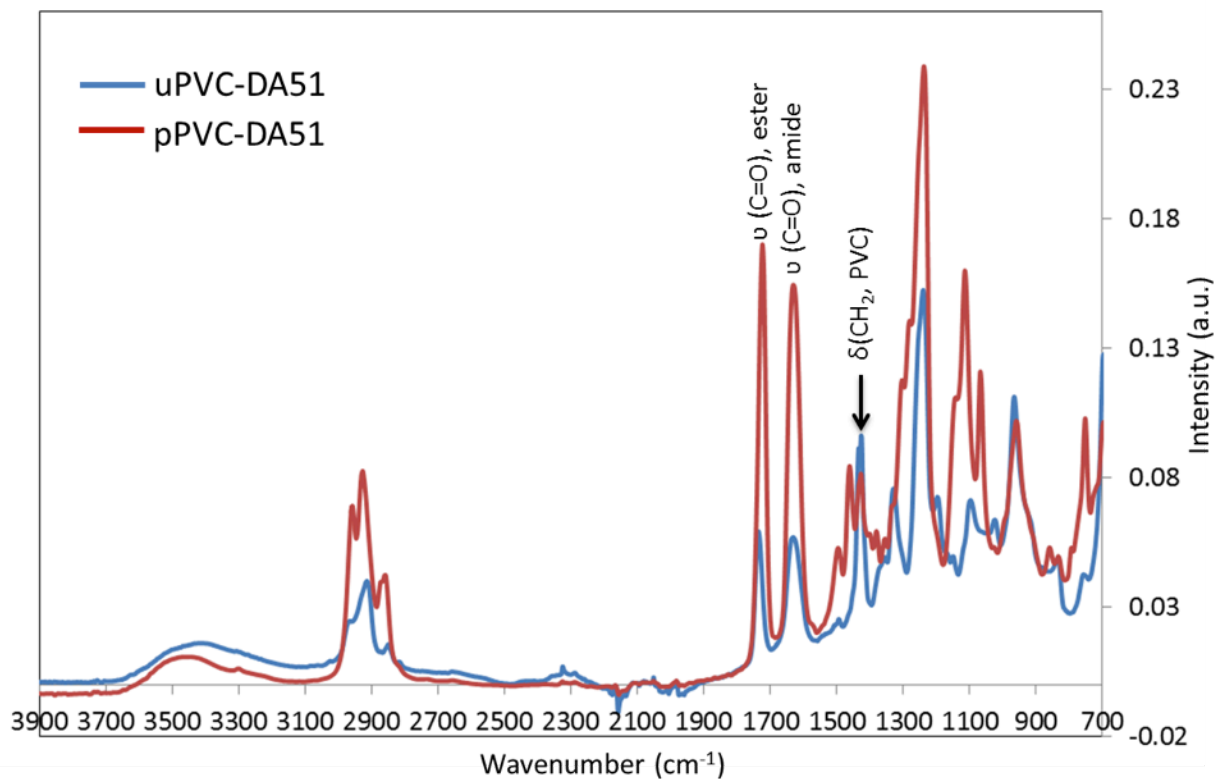
1. The ^1H NMR spectra of the intermediates of SI-ATRP initiators in CDCl_3 .



2. The ^1H NMR spectra of PDMA (A) and PAPMA (B).



3. ATR-FTIR spectra of uPVC and pPVC coupons modified with DA51 polymer brushes under similar conditions. CH₂ vibration of PVC at 1426 cm⁻¹ (used as a reference peak) has relatively similar intensities in the both spectrum.

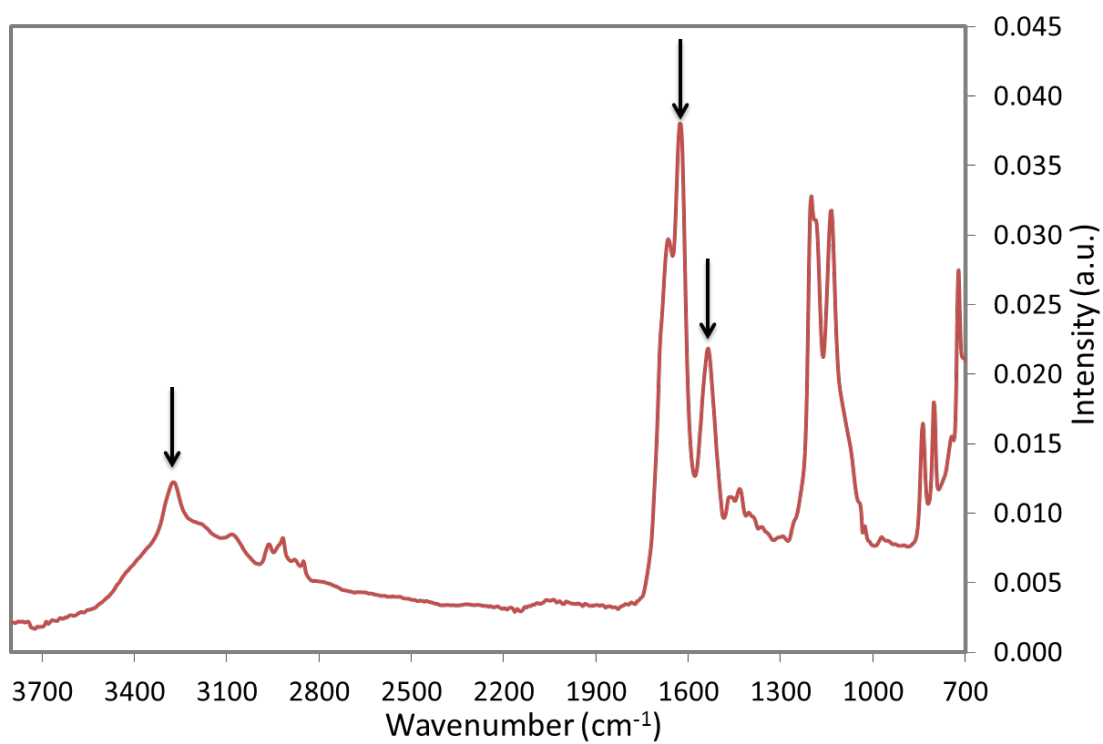


Appendix B

1. Determination of peptide amount on the surfaces using two different methods. Please see Section 3.2.2 for the uncertainty in measurements.

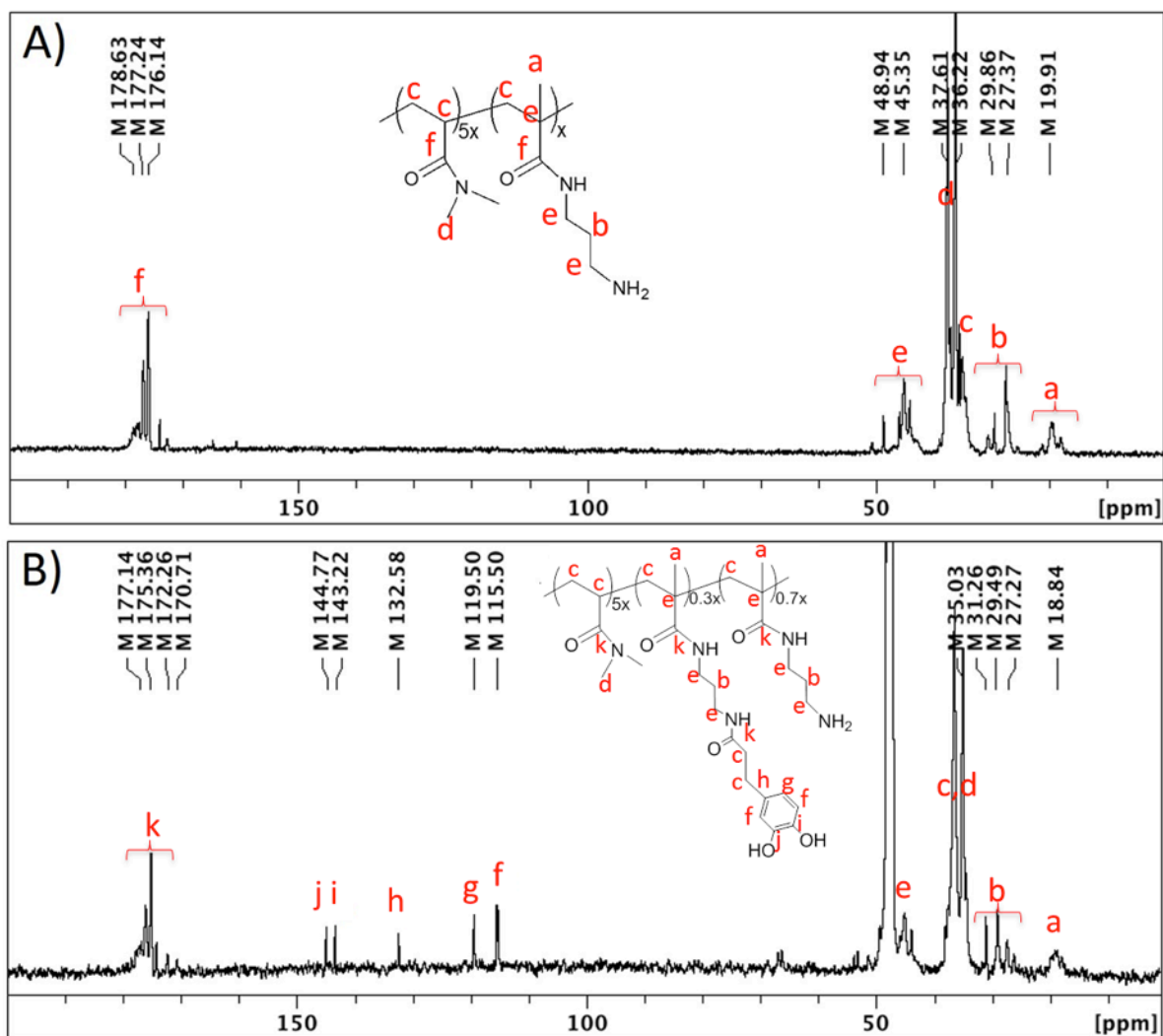
Sample	Peptide concentration ($\mu\text{g}/\text{cm}^2$)	
	Based on the increase in dry thickness	Based on fluorometry
1	1.7 (1010cys)	2.2
2	2.5 (1010cys)	2.8
3	1.8 (Tet-26)	2.1

2. The ATR-FTIR spectrum of Tet-26

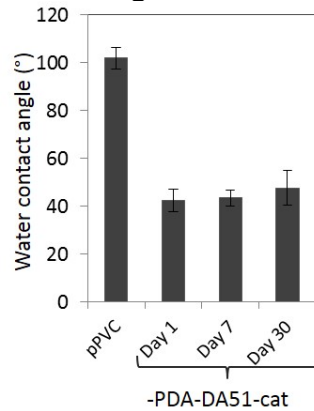


Appendix C

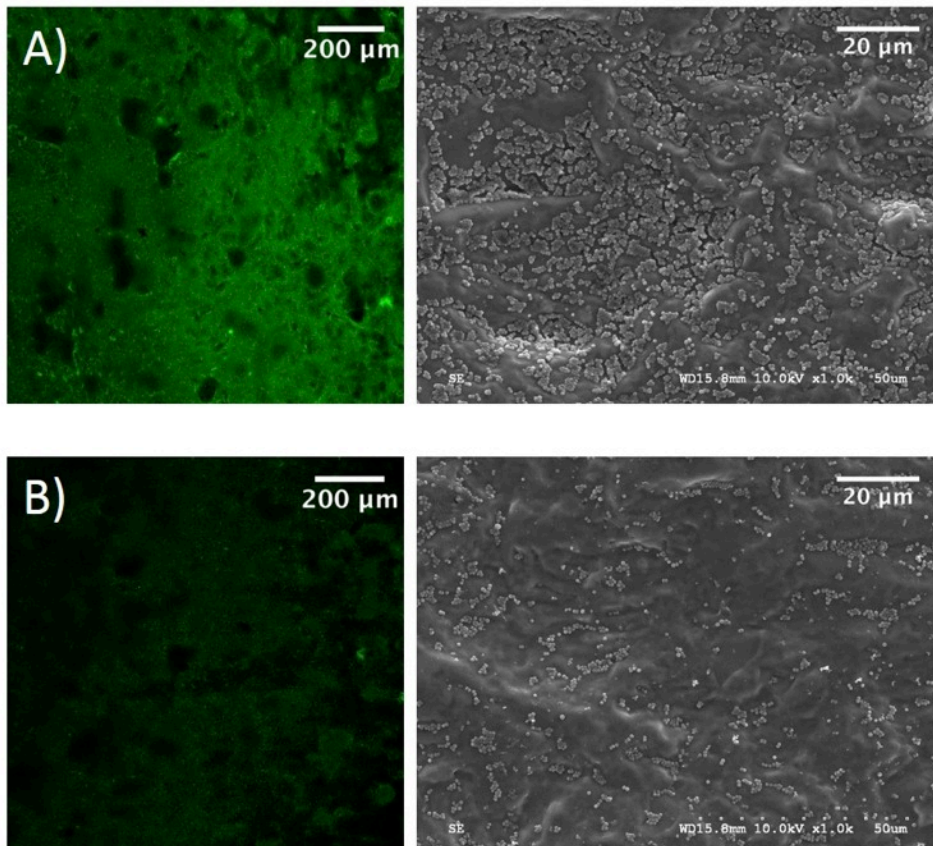
1. The proton-decoupled ^{13}C NMR spectra of DA51 in D_2O (A) and DA51-cat in d_4 -methanol (B).



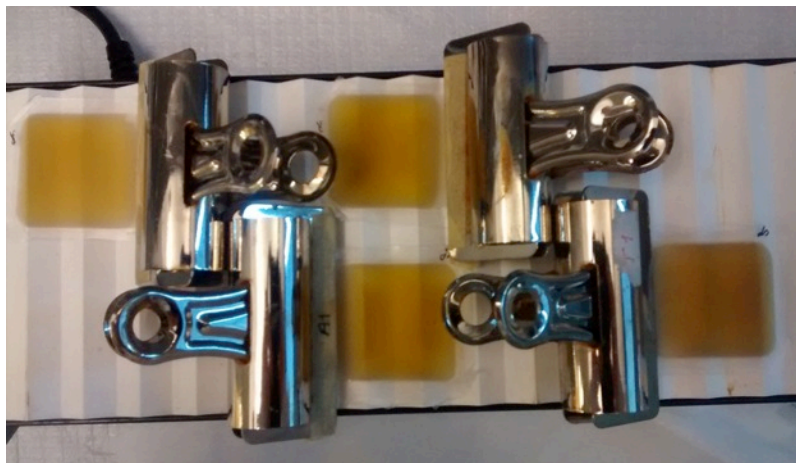
2. pPVC coupons coated with PDA-DA51-cat were stored in sterile PBS. The samples were evaluated for water contact angle after 7 and 30 days. After 30 days, a small increase in water contact angle was observed, which was not statistically significant.



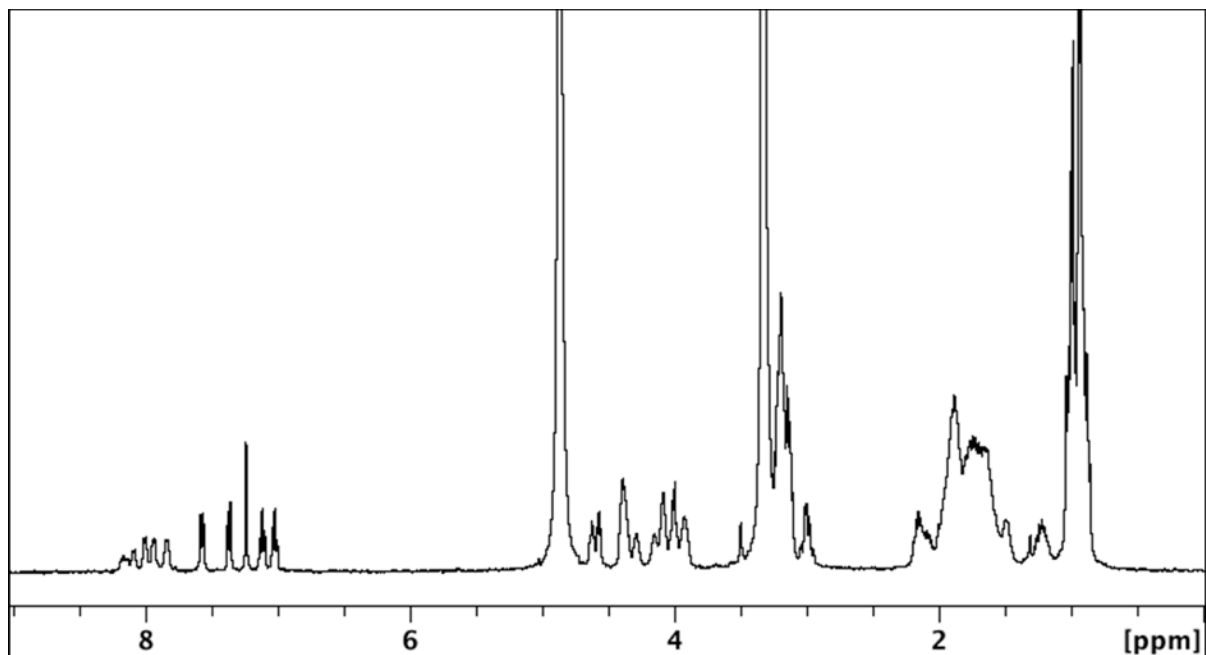
3. Fluorescent (left-hand panels) and SEM images of non-textured surfaces of control pPVC (A) and pPVC-PDA-DA51-cat (B) after 32-h incubation with SE11002, a biofilm-positive *S. epidermidis* strain, at 37 °C. Similar to the textured surfaces, less bacterial adhesion and biofilm formation was observed on the modified samples. The bacteria were stained with Syto 9 for fluorescence microscopy.



4. The photo shows mini bags filled with DA51-cat solution after 24 h shaking on a rocking shaker. DA51-cat solution is colorless before oxidation under basic conditions. To fabricate these mini bags, two pPVC coupons (each 5×4.2 cm) were thermally sealed together from three sides. Textured faces of the coupons were positioned inside the bags. The bag opening was closed with the clamp.



5. The ^1H NMR spectrum of E6 in d_4 -methanol



Appendix D

1. The ^{13}C CP-MAS NMR data of F1 platelet bag was acquired on a Bruker 400 MHz Avance spectrometer running with xwinnmr 2.6. The MAS speed was set at 4 kHz. The contact time to establish cross polarization was set to be 2 ms. Total number of scans was 15000 with a recycle delay of 5 seconds. The NMR spectrum of adamantane was used as an external ^{13}C standard for solids NMR.

